Characterisation of *l(3)IX-14*, a novel mitotic mutant in *Drosophila melanogaster*

Brian McHugh

9757816

A dissertation submitted to the University of Edinburgh in conformity with the requirements for the degree of Doctor of Philosophy.

Declaration

I hereby declare that the material contained within this thesis was composed by myself, being a member of the research group led by Dr. Margarete Heck, and that the work was performed by me. Other contributions have been clearly stated in the text.

Brian McHugh.

To my parents, Bernard and Katharina.

"If we knew what it was we were doing, it would not be called research, would it?"
Albert Einstein.

"We're in it for the truth...."
Margarete M.S. Heck, personal communication.

Abstract

Mitotic chromosome formation is vital in eukaryotic cells to avoid such hazards as sister-chromatid entanglement and cleavage of trailing chromatin at cytokinesis, although much of the precise mechanics of this process remains unclear. *Drosophila melanogaster* has much to contribute to this area, due to its excellent cytology and well characterized genetics.

I have characterised alleles of the late larval lethal mutation *l(3)IX-14*, which was previously observed to disrupt mitotic and polytene chromosome structure. Mitotic chromosomes from homozygous mutant larval neuroblasts appear hypercondensed in length and surrounded by a halo of loosely condensed chromatin. Polytene chromosomes from homozygous mutant larval salivary glands also display a chromatin packaging problem and lack the characteristic banding patterns normally observed in wild type polytene chromosomes. Further phenotypic chracterisation of the ICR-170 induced allele $l(3)IX\text{-}14^{1}$ has shown that several other cell division processes are defective, mainly the duplication of centrosomes and the establishment of a bipolar mitotic spindle. BrdU labeling of larval brains has indicated that replication may be proceeding at a slower rate than in wild type. Also, despite the almost normal level of cells committed to mitosis, the mitotic index of *l(3)IX-14* is low, and elevated levels of TUNEL labeling has suggested that many cells are switching to an apoptotic pathway.

I have cloned a novel full length cDNA for the putative *IX-14* gene by inverse PCR, utilising a P-element allele of *l(3)IX-14* . The surrounding genomic region has also been characterised in detail, and I have determined that the P insertion site is 40 bp upstream of the putative *IX-14* gene. Northern blot analysis using the cDNA from this gene reveals a message of 3.6 kb present in wild type and heterozygous larvae but absent in homozygous mutants. The predicted *IX-14* gene product is 684 amino acids in length containing a well conserved zinc-metalloprotease motif, and has homologues in several higher eukaryotes, but not in lower eukaryotes or prokaryotes. RNAi of IX-14 in cultured *Drosophila* cells has given similar phenotypes to those observed in the late larval lethal alleles, providing further evidence that this novel metalloprotease is responsible for the phenotypes observed.

I conclude from this that the novel zinc-metalloprotease IX-14 discovered in *Drosophila melanogaster* appears to be playing a crucial role in controlling several aspects of mitosis, from chromosome condensation to spindle formation. This presents an unprecedented role for this type of protease in the cell cycle.

Acknowledgements

I would like to sincerely thank my supervisor Dr. Margarete Heck for her guidance, patience, and numerous glasses of strong drink over the last three years. I would also like to thank Maurizio Gatti for kindly providing the *l(3)IX-14* mutant line on which I have based my thesis, and the Wellcome Trust for funding my Prize Studentship.

Many members of the Heck laboratory deserve special mention. Past members Sue Ann Krause, Alison Wilkie and Liping Lu all had significant input into the preliminary characterisation of *l(3)IX-14*, and present members Sharron Vass, Neville Cobbe, Marie-Louise Loupart, Victor Simossis and Emanuela Giacometti have provided me with much appreciated technical assistance and discussion along the way (not to mention entertainment!). In addition, Sharron Vass was extremely helpful in setting up the IX-14 RNAi experiments.

I would also like to thank members of the Earnshaw laboratory for their help, especially Mar Carmena and Ciaran Morrison, and Professor William Earnshaw himself for his scientific advice and allowing me to surf down a snow-laden hillside in his 15-foot canoe.

Finally, I would like to thank my family, friends, and Zoë Popper for their encouragement and support.

Table of Contents

List of Figures

Note: Page number refers to the text page immediately before the figure.

CHAPTER 1

CHAPTER 3

CHAPTER 4

CHAPTER 5

CHAPTER 6

CHAPTER 7

List of Tables

Abbreviations

BrdU	5-bromo-2'-deoxyuridine
BSA	Bovine Serum Albumin
Bub	Budding uninhibited by benomyl
C-terminus	Carboxyl terminus
CCD	Charged Coupled Device
CDK	Cyklin Dependant Kinase
CENP	Centromere Binding Protein
CHO	Chinese Hamster Ovary
CLAP	Chymostatin, leupeptin, antipain and pepstatin A
DAPI	4',6-diamidino-2-phenylindole
Df	Deficiency
DTT	Dithiothreitol
EBR	Ephrussi-Beadle Ringer's buffer
ECL	Enhanced Chemiluminescence
EDTA	Ethylenediaminetetraacetate, disodium salt
EGTA	Ethyleneglycol-bis(β-amino ethyl ether)-N,N,N',N'-tetraacetate
EMS	Ethyl methylsulfonate
EST	Expressed Sequence Tag
γ-TuRC	γ-tubulin ring complex
GFP	Green Fluorescent Protein
HEPES	N-([2-hydroxyethyl]piperazine-N'-[2-ethanesulfonic acid])
HRP	Horseradish peroxidase
INCENP	Inner Centromere Binding Protein
LB	Luria-Bertani medium
MAP	Microtubule-Associated Protein
Mad	Mitotic arrest deficient
MCAK	Mitotic centromere-associated Kinesin
MI	Mitotic Index
MT	Microtubule
MTOC	Microtubule Organising Center
N-terminus	Amino-terminus
NGS	Normal Goat Serum
ORC	Origin Recognition Complex
PAGE	Polyacrylamide Gel Electrophoresis
PBS	Phophate Buffered Saline
PCR	Polymerase Chain Reaction
PFA	Paraformaldehyde
PMSF	Phenylmethylsulfonylfluoride
RFC	Replication Factor C
SAR	Scaffold Attachment Region
SCC	Sister Chromatid Cohesion
SDS	Sodium Dodecyl Sulphate
SMC	Structural Maintenance of Chromosomes
SSPE	Sodium chloride and sodium phosphate buffer with EDTA
TAE	Tris acetate buffer with EDTA
TBE	Tris borate buffer with EDTA
TE	Tris buffer with EDTA
topoII	DNA topoisomerase II
UV	Ultraviolet

Notes

In the text, '*Drosophila*' should be taken to signify '*Drosophila melanogaster*' unless otherwise specified. I have used the nomenclature *l(3)IX-14*, *IX-14* and IX-14 to signify *Drosophila* mutants, genes and proteins respectively.

Introduction

Part I: An overview of the components of eukaryotic cell division

One of the conditions that defines any living organism is its ability to faithfully reproduce the genetic material that it contains. In order to achieve this, all cells must undergo a complex series of events culminating in the reproduction and equal segregation of DNA (arranged into chromosomes) into each new daughter cell. This process, termed the cell cycle, has classically been subdivided into four sections: S-phase (when the process of DNA replication occurs), M-phase (when the process of mitosis occurs, resulting in segregation of the duplicated genome), and the two intervening Gap phases termed G1 and G2 respectively. This review will concentrate on the events that take place during M-phase, with respect mainly to the formation of mitotic chromosomes from interphase chromatin and the cellular machinery used to segregate them to each new daughter cell.

All eukaryotic cells utilise a microtubule-based spindle to physically segregate their replicated chromosomes to opposite poles of the cell during mitosis. This fascinating process requires a great deal of components and is monitored by a series of checkpoints. Due to its complexity, I intend to describe many of the features of this process in some detail. However, before attempting this, a general summary of the more well-characterised events must be given.

A Summary of Eukaryotic Mitosis

The events described in this summary are depicted in Figure 1.1. At the initiation of mitosis, the nuclear envelope surrounding the condensing interphase chromatin breaks down, and microtubules (MTs) begin to grow out in all directions from organelles termed the Micrtotubule Organising Centers (MTOCs) - centrosomes

Figure 1.1 - Diagrammatic representation of eukaryotic mitosis

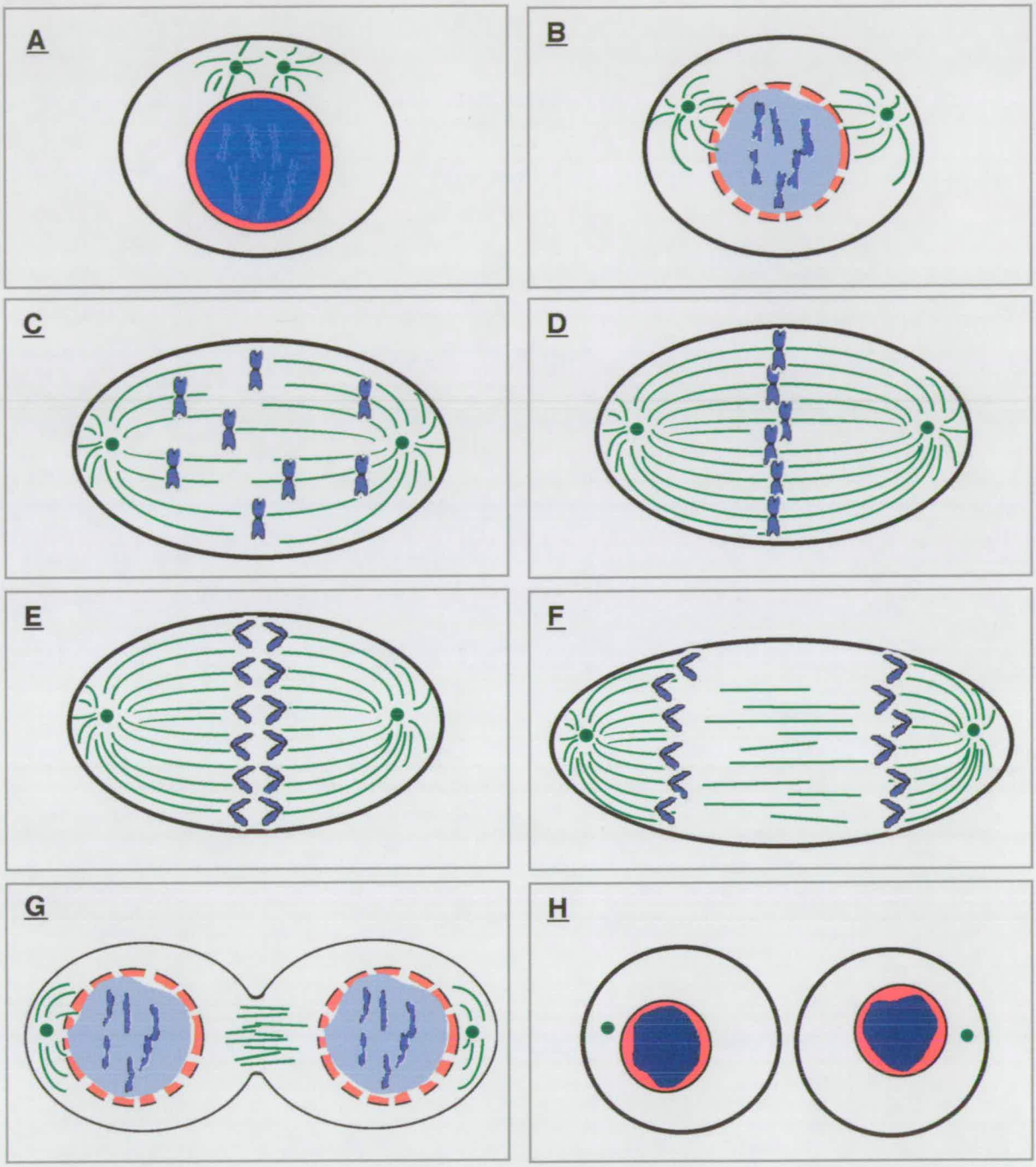

Figure 1.1 Diagrammatic representation of eukaryotic mitosis. DNA/mitotic chromosomes are shown in blue, microtubules in light green and centrosomes as dark green circles. Cell membrane is drawn as black lines, whereas nuclear membrane is shown as patches of red. A summary of mitosis is presented in the text (see page 1), referring to the relevant panels shown above.

in animal cells or spindle pole bodies in yeast (Figure 1.1, A-B). Centrosomes exist as single cytoplasmic structures containing a pair of centrioles during interphase, but replicate once usually during S phase and proceed to migrate to opposite sides of the nucleus at the onset of metaphase (Figure 1:1, B-C). Correct positioning of each centrosome is achieved by astral MTs which grow out from the organelles until they encounter the cytoplasmic membrane. Other out-growing MTs become attached to the by-now paired, condensed mitotic chromosomes at discrete structures known as kinetochores (Figure 1.1, C). Once these microtubules (henceforth known as kinetochore fibres) have attached, positioning of the condensed chromosomes midway between the two spindle poles (a process termed 'congression') is initiated. It is the balance of both 'poleward' and 'away from the pole' forces acting during congression provided by the dynamic nature of the microtubules themselves and the action of MT-associated motors, which results in the alignment of mitotic chromosomes at the equator midway between poles (Figure 1.1, D). The balance of 'poleward' and 'away from the pole' forces also appears to serve to maintain the chromosome alignment at the metaphase plate. Once all chromosomes have been aligned and monitored by a mitotic checkpoint, the physical cohesion that is imposed on replicated sister chromatids during replication is dissolved and the poleward forces generated by kinetochore fibers and motors result in the movement of sister chromatids to opposite poles (Figure 1.1, E-F). Following this separation, nuclear membranes form *de novo* around the segregated genomes - concurrently, the splitting of the cellular cytoplasm into two daughter cells is achieved by the action of the cleavage furrow (Figure 1.1, G-H). The final result is two new daughter cells containing a full genomic complement and a single centrosome (Figure 1.1, H).

Initiation of Mitosis

The initiation of mitosis is controlled by a complex set of regulatory feedback loops. The activity of Cdk1-cyclin B which governs the G2-M transition is itself

dependent on the balance between opposing inhibitory kinases of the Wee1/Mik1/Myt1 family and the activating phosphatase Cdc25 (reviewed in (Nurse, 1990)). Cdc25 is in turn regulated by phosphorylation by Polo kinase (Kumagi and Dunphy, 1996; Abrieu *et al.*, 1998; Qian *et al.*, 1998), an intriguing protein with multiple regulatory roles throughout mitosis (reviewed in Glover *et al.*, 1998). What activates Polo kinase remains unclear. Once activated, Cdk1 enters a positive feedback loop whereby it promotes further activation of Cdc25 and the cell is then committed to enter mitosis.

Several events take place concurrently after the onset of metaphase has been initiated. These include the condensation of replicated chromatin into mitotic chromosomes, nucleation of MTs from opposing MTOCs, and dissolution of the nuclear lamins. Nuclear lamins have a dynamic and essential role in maintaining nuclear integrity during interphase and then become reorganised during mitosis; these details are outside the scope of this introduction but are reviewed in (Moir *et al.*, 2000). The complicated logistics of chromosome condensation are discussed in detail in Part II of this Introduction. What follows in Part I therefore is an analysis of the various cellular machinery required during metaphase, with regard mainly to elements that I have studied during the course of my thesis work.

The Role of Centrosomes

Centrosomes are discrete cytoplasmic cellular organelles approximately 1 μm^3 in size that are directly responsible for the nucleation of spindle MTs during mitosis and interphase, and function as the MTOC of higher eukaryotic cells. Each centrosome consists of a pair of cylindrical centrioles that are surrounded by a mass of pericentriolar material (see Figure 1.2). After being duplicated and transported to opposite sides of the nucleus, each centrosome functions as a pole of the spindle during mitosis. Centrosomes have long been the subject of interest, having first been identified in the late 19th century by Boveri and van Benedin. Along with the DNA

contained within the nucleus, they are the only other organelle of the cell that must undergo a precise duplication which will result in the inheritance of a complete centrosome in each new daughter cell. Exactly how this duplication is achieved still remains unclear, although several processes that occur during this period have been studied intensely. Amongst these are the duplication of the paired centrioles that lie at the heart of each centrosome.

Centrioles are composed of cylindrical arrays of nine triplets of microtubules, and lie perpendicular to one another with the 'daughter' centriole dissecting the axis of the 'mother' (see Figure 1.2). It is now believed that (in animal cells at any rate) centrioles may provide a framework upon which other factors that nucleate MTs are organised. This was shown by studies such as Bobinnec *et al.* (Bobinnec *et al.*, 1998) who found that direct disruption of the polyglutamylated tubulin (found only in centrioles and possibly acting as a stabilising factor) by specific antibodies caused the disassembly of centrioles and resulted in the dispersal of other MT-nucleating material throughout the cytoplasm. Importantly, this disruption was not permanent, as after the eventual degradation of the antibodies, centrioles were able to reform and their ability to focus MT-nucleating material was restored. However, formation of a functional mitotic spindle can and does occur in the absence of centrosomes in some systems, e.g. in unfertilised *Sciara coprophila* oocytes (de Saint Phalle and Sullivan, 1998), female meiosis in *Drosophila* (Theurkauf and Hawley, 1992) and mitosis in higher plants (Smirnova and Bajer, 1992), where it appears that spindles can grow out from the chromosomes themselves. However, these spindles appear unfocused and can show positioning defects. More recent studies on Ganglion Mother Cells (GMCs) in *Drosophila* brains in the centrosome mutant *asterless* (*asl*) have highlighted a similar phenomenon (Bonaccorsi *et al.*, 2000). This centrosome-independent pathway may represent a back-up system for spindle formation in these cells, although since these mutants are lethal at the larval/pupal stage this mechanism presumably cannot fully compensate for the centrosomal defect in all proliferating cells. Nevertheless, it

Figure 1.2 Centrosome and centriole structure

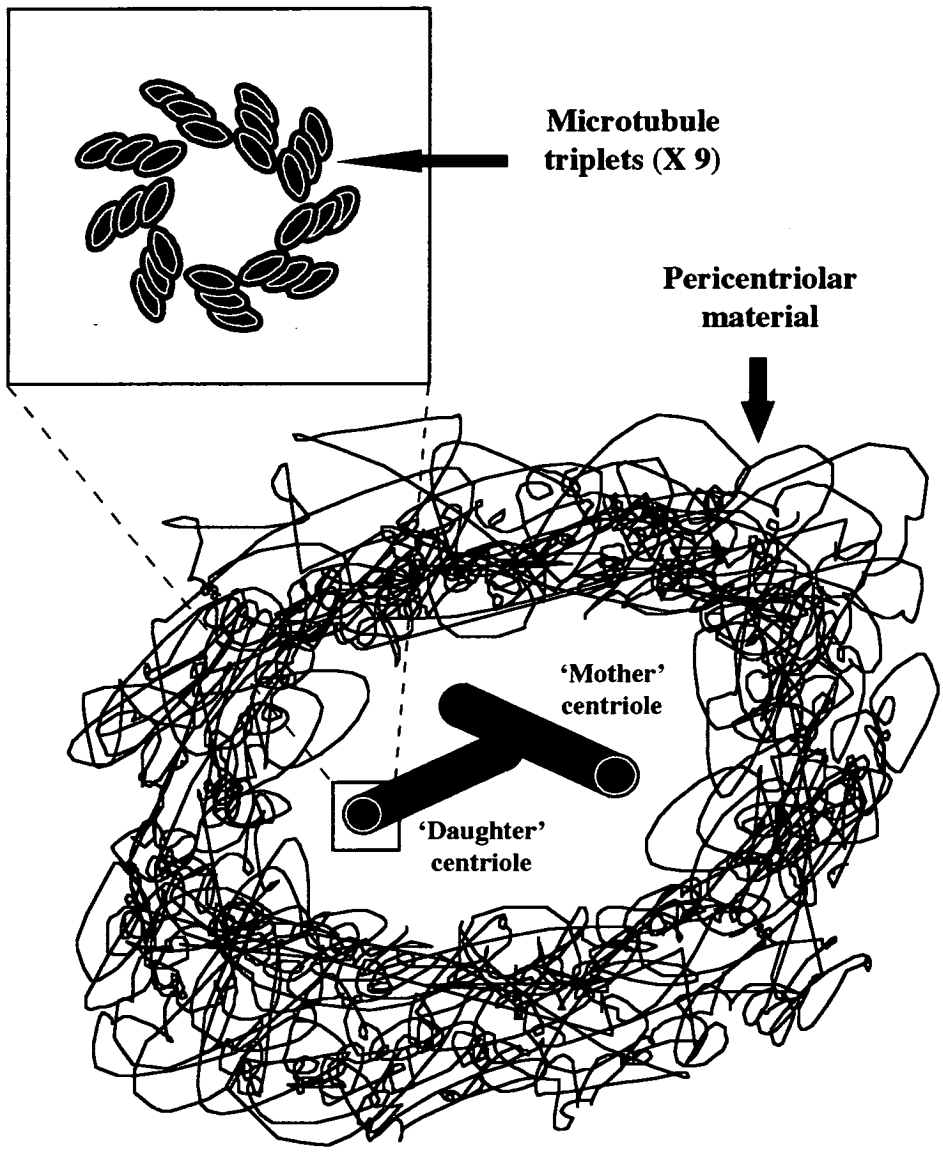

Figure 1.2 Centrosome and centriole structure. The mother and daughter centrioles are shown surrounded by an amorphous mass of pericentriolar material, known to contain components required for microtubule nucleation, e.g. γ-tubulin and pericentrin. The inset shows a cross-section of a single centriole, based on EM data.

highlights the existence of a mechanism for establishing a bi-polar spindle that is normally eclipsed by the stronger MT nucleating influence of the centrosome.

Although centriole replication remains poorly understood, there are some prime candidates likely to be involved. Recently, γ-tubulin disruption was shown to cause MTOC duplication defects in *Paramecium* (Ruiz *et al.*, 1999). As γ -tubulin is found not only surrounding the centriole pairs in an amorphous mass, but inside the cylindrical centrioles themselves (Fuller *et al.*, 1995), this is extremely significant. One idea is that γ -tubulin may provide a physical template on which the duplicated centriole can be modeled, but this has not been tested. *Chlamydomonas reinhardtii* has also been used as a genetic tool to dissect this process (yeast, which would otherwise be ideal, does not have a structural analogue of a centrosome, although its spindle pole body is functionally analogous). One new discovery using this system is the UNI3 gene which encodes a new member of the tubulin superfamily, δ-tubulin (Dutcher and Trabuco, 1998). This protein appears to be responsible for the addition of the third microtubule to each developing triplet in the centriole barrel, although duplication of the entire structure does still occur.

Other factors involved in the control of centrosome duplication have been found from *in vitro* studies in eukaryotic systems. *Xenopus laevis* egg extract studies have helped implicate the action of the cyclin-dependent kinase Cdk2, which serves to drive major transitions in the cell cycle such as the G1 to S phase transition, in promoting the duplication of centrosomes. This was shown by injecting a small protein inhibitor of the Cdk2-cyclin A and Cdk2-cyclin E complexes which resulted in blockage of centrosome replication, apparently by preventing centriole duplication (Lacey *et al.*, 1999). A parallel study by Matsumoto *et al.* (1999) using CHO cells achieved a similar result. Conversely, multiple rounds of centrosome duplication was achieved in a study by Hinchcliffe *et al.* (Hinchcliffe *et al.*, 1999) by falsely prolonging S phase in the *Xenopus* system. Additionally, they were able to demonstrate localisation of cyclin E to centrosomes, further implicating Cdk2 as

playing a direct role in the duplication process. Clearly the details of centriole duplication are only beginning to emerge, with Cdk2-cyclin E being implicated as controlling centrosome duplication, and proteins such as γ and δ tubulin apparently playing a more direct role in the assembly of new centrioles within the centrosome.

Microtubule Growth and Spindle Formation

While the centriole pair residing at the heart of the centrosome has been shown to be essential for MT organisation, it appears not to be directly involved in their nucleation. This role is fulfilled by elements contained within the mass of surrounding pericentriolar material (Gould and Borisy, 1977), using the centrioles as a scaffold for organisation. Well characterised elements such as g-tubulin, pericentrin and NuMA (for *Nu*clear/*M*itotic *A*pparatus protein), have all been found to be localised in this region (Archer and Solomon, 1994; Merdes *et al.*, 1996; Oakley and Oakley, 1989). In its MT nucleating role, g-tubulin is organised into a roughly 25 nm diameter complex termed the g-tubulin ring complex (γ -TuRC), first found in *Drosophila* centrosomes (Moritz *et al.*, 1995) and shown to be sufficient to nucleate MTs (Zheng *et al.*, 1995). Another component required for MT nucleation, pericentrin, had previously been identified in the *Xenopus* egg extract system (Doxsey *et al.*, 1994). It was then shown that both g-tubulin and pericentrin can combine to form a lattice-like structure in *Xenopus* egg extracts (Dictenberg *et al.*, 1998) which may represent a higher order structure responsible for MT nucleation. Lastly, the action of NuMA, a large nuclear protein that becomes relocated to spindle poles during mitosis by the dynein/dynactin complex, appears to be necessary for focusing MTs into spindle poles (Merdes *et al.*, 2000; Merdes *et al.*, 1996).

The mitotic spindle is composed largely of microtubules (MTs), themselves composed of heterodimers of α and β tubulin. These dimers become organised into a 25 nm diameter MT by an as yet poorly understood process. It is known however that

the β-tubulin subunit must bind GTP for MT polymerisation to occur and several studies have now shown the importance of GTPases such as RAN and GTPase Activating Proteins (GAPs) such as CYK-4 in the regulation of MT growth (Ohba *et al.*, 1999) (Jantsch-Plunger *et al.*, 2000). The binding of GTP allows the rapid polar growth of MTs in what is termed the 'plus end' direction, i.e. with β -tubulin as the outward facing molecule. MT growth can also occur in the opposite, or 'minus end' direction, although this is far slower than plus-end directed growth. Most importantly for the action of the mitotic spindle, MTs are also capable of rapid depolymerisation from the ends, resulting in their shrinkage. This inherent dynamic instability is the underlying principle behind the rearrangement of MTs from their stable configuration in interphase to the more fluid structure seen in mitosis. Only recently have several factors involved in this change in stability been characterised. Several Microtubule-Associated Proteins (MAPs) have been shown to be regulatory proteins involved in the stability of MTs (using mostly the *in vitro Xenopus* egg extract system). MAP4, XMAP215 (called Msps in *Drosophila*) and XMAP310 have all been shown to cause an increase in polymer mass when added to MTs (reviewed in (Andersen, 2000)), despite their divergence at the molecular level. They do this by effectively shifting the equilibrium towards MT polymerisation, resulting in an overall stability. Conversely, factors such as Stathmin/Op18 are known to destabilize MTs by pushing the equilibrium in the opposite direction, towards 'catastrophe' (Marklund *et al.*, 1996) (Belmont and Mitchison, 1996). The mechanistics of destabilisation are also unclear, although proteins such as Stathmin/Op18 may infer decreased stability to the MT perhaps by simply binding to one or more tubulin dimers.

Centromere and kinetochore structure

MTs growing out from centrosomes eventually encounter a condensed chromosome, and some become attached at to a proteinaceous plate structure termed

the kinetochore, which is assembled at region of the chromosome called the centromere. Centromeres exist at the primary constriction of a mitotic chromosome where the attachment between replicated sister chromatids is strongest. They are specialised regions of heterochromatin, composed mostly of highly repetitive DNA sequence and contain a variety of associated proteins. The centromere has two vital functions: First, it serves as the primary site of cohesion between replicated sister chromatids as mentioned above - this will be discussed in more detail in a following section. Secondly it is the assembly point for the kinetochore, which provides the means of attaching mitotic chromosomes to spindle MTs, and also functions in a signaling checkpoint that prevents premature entry into anaphase.

Kinetochores assemble at active centromeres of mitotic chromosomes, and have been shown by EM to have a tri-laminar structure of an outer kinetochore plate 35 - 40 nm thick, a central zone 15 - 35 nm thick and an inner plate which is associated with the underlying centromeric chromatin (see Figure 1.3). This assembled structure is then capped by a fibrous corona whose filaments reach outwards to a length of roughly 100 - 300 nm from the kinetochore (these measurements are based on electron micrographs of vertebrate cells, reviewed in (Rieder and Salmon, 1998)). Assembly of active kinetochores onto the centromeric heterochromatin requires various protein components, namely CENP-A, CENP-B and CENP-C. CENP-A, a histone H3 variant present only at centromeres, has been shown to associate with (or at a minimum is in very close proximity to) the repetitive DNA which is normally present at the region defining the inner kinetochore plate (Vafa and Sullivan, 1997; Warburton *et al.*, 1997). CENP-B and CENP-C are both DNA-binding proteins which bind to the centromeric heterochromatin and inner kinetochore plate respectively, again shown by immuno-EM staining (Cooke *et al.*, 1990; Saitoh *et al.*, 1992). Intriguingly, CENP-B does not appear to be an essential protein, as shown by three independent gene knock-out studies in mice (Hudson *et al.*, 1998; Kapoor *et al.*, 1997; Perez-Castro *et al.*, 1998). These papers report that CENP-B null mice are viable and do not appear to

Figure 1.3 - Basic structure of the eukaryotic kinetochore

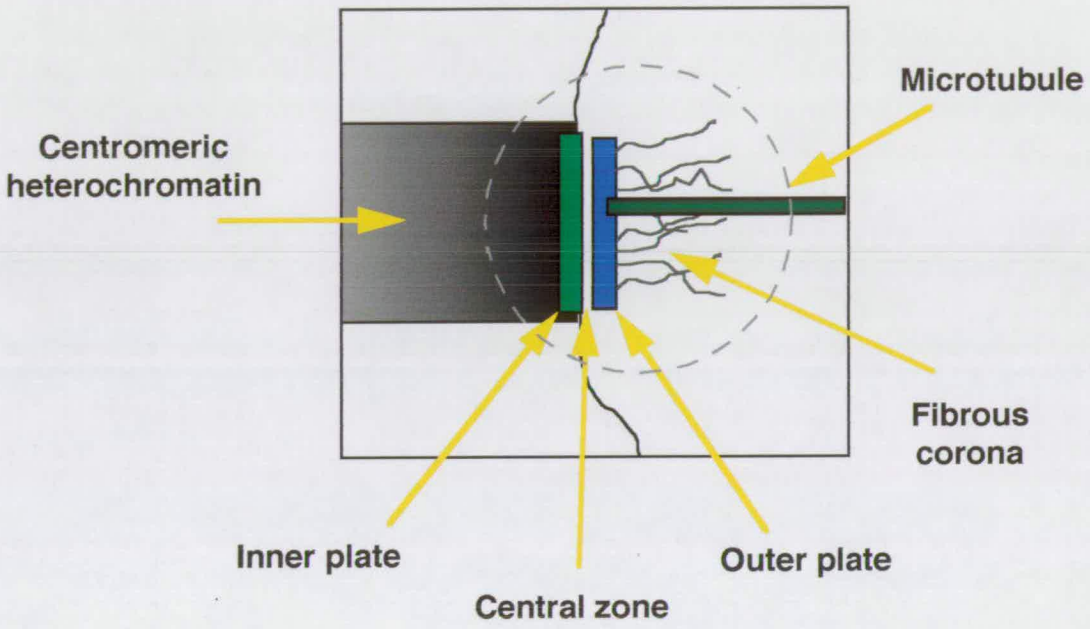

Figure 1.3 Basic structure of the eukaryotic kinetochore. The trilaminar kinetochore structure is shown within the grey dashed circle, assembled onto the block of heterochromatic DNA that exists at mammalian centromeres. A kinetochore microtubule is shown terminating at the outer kinetochore plate.

have any mitotic or meiotic defects (although Hudson *et al.* do note a reduced body weight). Conversely, similar studies with CENP-C have demonstrated that this protein is essential. Conditional lethal experiments in the chicken DT40 cell line have shown that a CENP-C null background caused mitotic arrest followed by apoptosis (Fukagawa and Brown, 1997), and gene knock-out mice were shown to be lethal at the early embryo stage (Kalitsis *et al.*, 1998). In fact the requirement for CENP-C had been predicted before these mutational studies, based on findings relating to CENP-C kinetochore function. Antibody injection studies had shown that if CENP-C function was impaired, the size of the kinetochore was reduced and the timing of the metaphase to anaphase transition was disrupted (Tomkiel *et al.*, 1994). Following this it was seen that CENP-C was required to recruit the motor protein cytoplasmic dynein to the kinetochore (Wordeman *et al.*, 1996), an important observation as it is believed that cytoplasmic dynein most likely functions as one of the forces contributing to chromosome movement to the poles.

Cytoplasmic dynein has been known to be a kinetochore component for over a decade (Pfaar *et al.*, 1990; Steuer *et al.*, 1990), and it has been implicated in the capture of kinetochore MTs and the movement of chromosomes along them as it is a minus-end directed motor. Additionally, its rate of movement *in vitro* emulates that of chromosomes attached to kinetochore MTs (Rieder and Salmon, 1998). However, mutational studies have shown that chromosomes are still able to attach and move along spindle MTs when dynein activity is compromised in antibody injection experiments in vertebrates (Vaisberg *et al.*, 1993), or in *Drosophila* lines with mutated dynein (Robinson *et al.*, 1999; Starr *et al.*, 1998). Furthermore, a recent study on dynein localisation in grasshopper spermatocytes has demonstrated that the association of dynein may be more transient than previously suspected (King *et al.*, 2000). Clearly there must therefore be other MT-associated motors located at the kinetochore which act in concert with cytoplasmic dynein, and the best candidate currently known is CENP-E. First described as a kinetochore component in 1991 (Yen *et al.*, 1991),

CENP-E is a large kinesin-related MT motor protein and was first demonstrated to have minus-end directed motor function in a study using mitotic HeLa cells (Thrower *et al.*, 1995). However, these results have now been superseded by subsequent work examining the role of CENP-E in the *Xenopus* egg extract system (Wood *et al.*, 1997), showing that it had *plus*-end directed motor function, using *Xenopus* CENP-E tethered to a coverslip in a MT-gliding assay . A variety of studies of CENP-E deficiency by different methods such as antibody injection and immunodepletion in *Xenopus* egg extracts (Schaar *et al.*, 1997; Wood *et al.*, 1997), and antisense-mediated inhibition in HeLa cells (Yao *et al.*, 2000) have shown that chromosomes fail to align during metaphase and as a result are spread out over the spindle. This demonstrates the essential requirement for CENP-E in coordinating chromosome movement, presumably by driving attached chromosomes to the plus ends of MTs.

Lastly, several other proteins have also been found to be associated with the kinetochore. These include the chromosomal passenger proteins INCENP and Aurora-like kinase Airk-2, the kinesin-like protein Mitotic centromere-associated Kinesin (MCAK) and the Zw10/Rod complex. INCENP has a dynamic localisation throughout mitosis, appearing first along chromosome arms, then concentrating at the kinetochore, and is finally deposited at the central spindle during cytokinesis. This localisation is critical to it's role during mitosis, as mutants of INCENP have been shown to have defects in both chromosome segregation and cytokinesis (Cutts *et al.*, 1999; Mackay *et al.*, 1998). INCENP also binds to Airk-2, which has a similar localisation pattern, and targets it to the central spindle where it also functions in cytokinesis (Adams *et al.*, 2000). MCAK was shown to localise to kinetochores in CHO cells (Wordeman and Mitchison, 1995) and may function in coordinating the onset of sister chromatid separation (Maney *et al.*, 1998), whereas a recent series of publications on Zw10 and Rod in *Drosophila* and human cells demonstrate its role in the mitotic checkpoint in these systems (Basto *et al.*, 2000; Savoian *et al.*, 2000; Chan *et al.*, 2000). Also present are members of the Mad (*M*itotic *a*rrest *d*eficient) and Bub (*B*udding

*u*ninhibited by *b*enomyl) protein families, namely Mad2, Bub1, Bub3, and BubR1 a kinase related to both Bub1 and Mad3. These have been shown to function in the kinetochore attachment checkpoint that prevents the metaphase to anaphase transition from occurring until all chromosomes are aligned and have achieved bi-orientation (reviewed in Hardwick *et al.*, 1998).

Kinetochore MT capture and Congression

As plus-end directed growth occurs from the centrosomes, MTs eventually come into contact with condensed mitotic chromosomes, and proceed to attach normally to a kinetochore that happens to be facing the nearest pole (illustrated in Figure 1.4, panels A and B). MT attachment to the outer kinetochore plate appears to depend upon the actions of cytoplasmic dynein and CENP-E (described above), which both localise to the fibrous corona of the kinetochore, and aid in the physical capturing of plus-end growing Mts. Kinetochore capture immediately initiates poleward movement (Figure 1.4, panel C), again most likely via the minus-end directed motor action of dynein, although recent work in *Drosophila* spermatocytes has shown that Zw10 is also required for this process (Savoian *et al.*, 2000).

Eventually, the other kinetochore of the condensed chromosome becomes attached to MTs emanating from the opposite pole (Figure 1.4, panel D). Once MT attachment has occurred at both kinetochores of a chromatid pair, termed bi-orientation, the process of congression can begin. Congression involves the movement of paired sister chromatids to the spindle equator, midway between the two poles formed by the centrosomes. This is achieved by a combination of forces generated not only by MTs attached to kinetochores but also those acting on the chromosome arms themselves (thin black arrows in Figure 1.4). This was demonstrated recently by the requirement of chromokinesins such as Xkid (for *Xenopus* Kinesin-like DNA binding protein - a homologue of the *Drosophila* Nod protein), which localises along mitotic

Figure 1.4 Congression

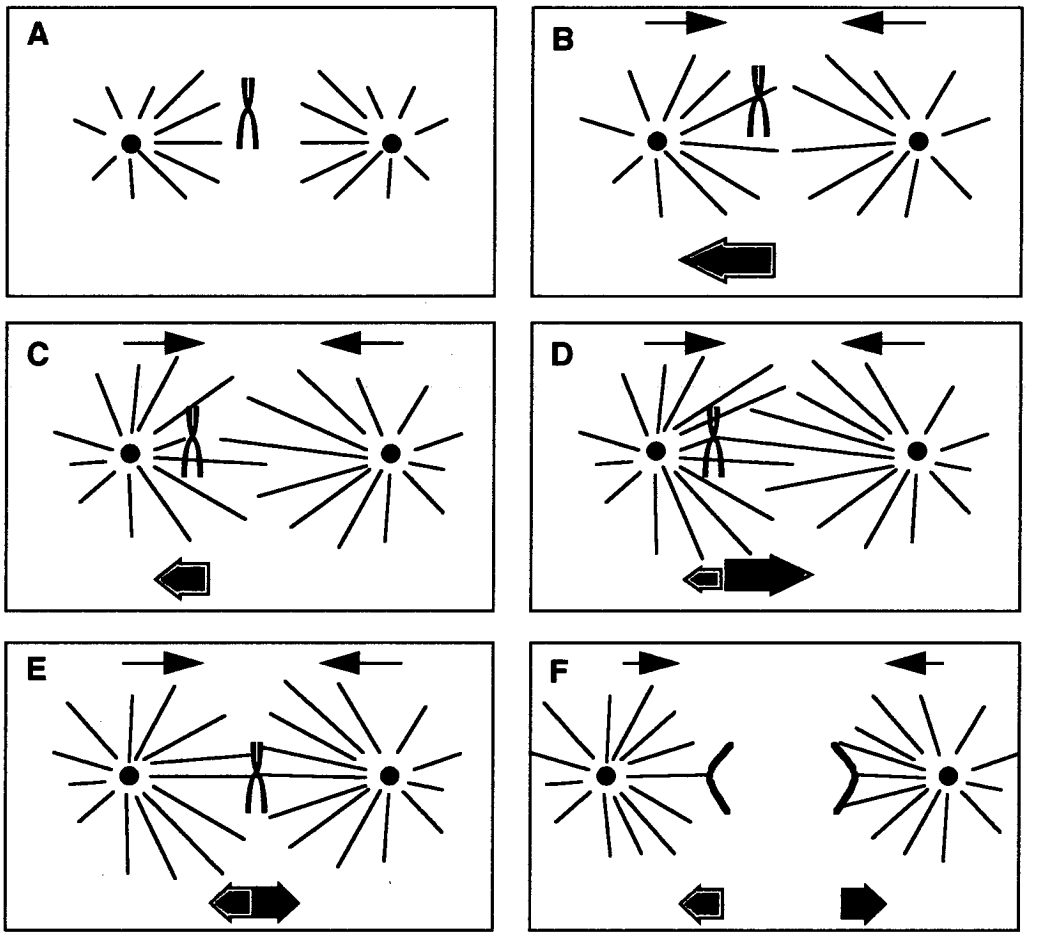

Figure 1.4 Congression. Spindle microtubules (green) growing out from opposite poles eventually encounter the kinetochore of a condensed mitotic chromosome (blue) (Panels A and B) which immediately moves towards one pole (Panel C). Once bi-orientation has occured (Panel D), the balance of forces at the kinetochore and chromosome arms positions the chromosome midway between the poles (Panel E). Separation of sister chromatids then occurs at anaphase (Panel F). Force generated by the kinetochores is indicated by red and blue arrows, the size of which reflect the amount of force generated. Polar ejection force acting on chromosome arms is indicated by thin black arrows.

chromosome arms and appears to be involved in the establishment and maintenance of chromosome alignment during metaphase (demonstrated in the *Xenopus* egg extract system (Funabiki and Murray, 2000; Antonio *et al.*, 2000). It appears to be the 'tug-of-war' between poleward and away-from-the-pole forces exerted through MTs binding at the kinetochore and those in contact with the chromosome arms that positions the attached chromosome pairs at the point where the balance of forces is equal, midway between the poles as shown in Figure 1.4, panel E (reviewed in (Rieder and Salmon, 1994)). Once chromosomes are aligned at this equator, termed the metaphase plate, a mitotic checkpoint is satisfied and the signal for the release of cohesion occurs. The process of movement of sister chromatids to opposite poles, i.e. anaphase, can then begin (Figure 1.4, panel F).

Sister chromatid separation and onset of anaphase

Control of sister chromatid separation is vital - if the cohesion between replicated sister chromatids was to dissolve too early, it would be essentially impossible for the cell to symmetrically segregate them to opposite poles and aneuploidy would most likely result. Cohesion between replicated sister chromatids, a process that occurs hand-in-hand with replication (Michaelis *et al.*, 1997), is only dissolved once the checkpoint conditions governing the positioning of chromosomes on the metaphase plate midway between the poles and the bipolar attachment of kinetochore MTs to each kinetochore are satisfied. The signal that these events have taken place is relayed by kinetochore components such as the Mad2, Bub1 and BubR1 proteins (Hardwick, 1998; Craig *et al.*, 1999; Rieder and Salmon, 1998) and the Zw10/ROD complex (Basto *et al.*, 2000; Chan *et al.*, 2000), which appear to monitor MT attachment and MT tension at the kinetochore respectively. The tension of attached MT kinetochores has been elegantly demonstrated by laser ablation studies, showing that release of MT attachment at one kinetochore of a mitotic chromosome results in the

Figure 1.5 Dissolution of cohesion at the metaphase to anaphase transition

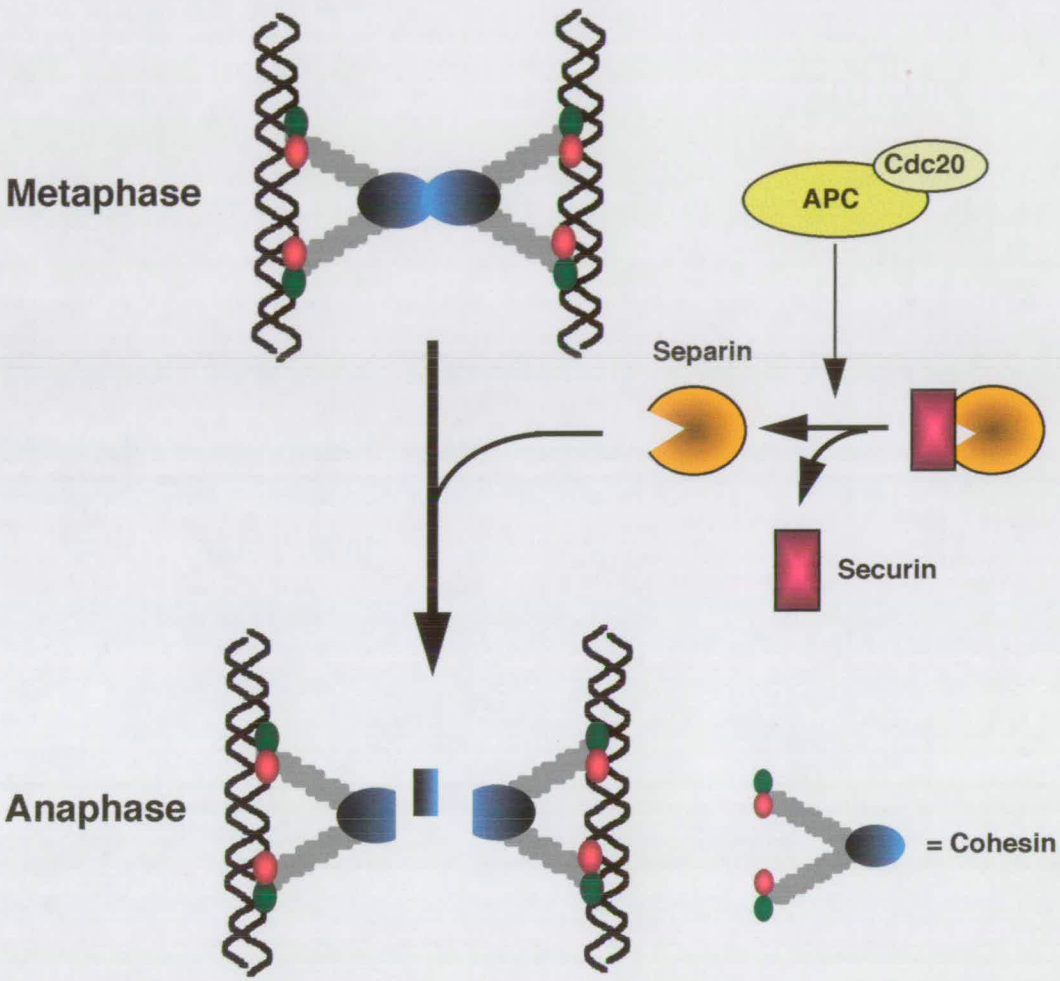

Figure 1.5 Dissolution of cohesion at the metaphase to anaphase transition. In this model, adapted from Nasmyth *et al.* (2000), Cohesin is recruited to specific sites on chromatin post replication and acts to hold the sister chromatids together. At the onset of anaphase, the Separin protease, normally sequestered by Securin, is released by the action of the Anaphase Promoting Complex (APC). Separin is known to cleave 2 sites of the Cohesin subunit Scc1, resulting in dissolution of cohesion between chromatids.

abrupt and rapid movement of the entire chromosome to the opposite pole (McNeill and Berns, 1981).

The tension present at the kinetochore implies that sister chromatids must be actively held together until the signal to proceed into anaphase is given. Only recently however has direct evidence for specific proteins responsible for cohesion been found. Previous suggestions for sister chromatid cohesion were based on the physical intertwining of sister chromatid DNA during replication (Murray and Szostak, 1985), relying on increased topoII activity to decatenate the molecules at anaphase. However, although topoII has been shown to be essential for cell division, it is not apparently needed to release sister chromatid cohesion as inhibitors of the enzyme added during metaphase do not block separation of sister chromatids (Downes *et al.*, 1991). It is now believed that cohesion is mediated by a multisubunit complex situated mainly, but not exclusively, at the centromeres, termed the 'cohesin' complex (reviewed in Nasmyth *et al.*, 2000 and discussed in more detail in Part II of this Introduction).

Crucial to the release of cohesion is the cohesin subunit Scc1 (also called Mcd1 and Rad21), which is required to be degraded at the metaphase-anaphase transition in order for sister chromatids to separate in yeast (Guacci *et al.*, 1997; Michaelis *et al.*, 1997). This degradation is mediated by the 'separin' endopeptidase Esp1, whose actions are inhibited until required by formation of a complex with the 'securin' protein Pds1 (Ciosk *et al.*, 1998). At the metaphase-anaphase transition, Pds1 is targeted for degradation by the Anaphase Promoting Complex in response to action by Cdc20 (Shirayama *et al.*, 1999), thus releasing Esp1 and promoting Scc1 cleavage (see Figure 1.5). This in turn allows sister chromatids to migrate to opposite poles by the driving force of the mitotic spindle and kinetochore motors, and the process of forming new daughter cells around the segregated genetic material can begin.

Part II: Mitotic chromosome formation

Chromosome condensation is vital in eukaryotic cells:

Chromosome condensation has long been known to be a vital process for the survival of eukaryotic cells. As far back as the 1880's, Flemming made observations concerning the fact that chromosomes (which he called the 'spireme threads') could only be seen just before the cell divided and seemed to disappear afterwards (Flemming, 1879). He postulated that this sudden visibility of chromosomes reflected a process of condensation that made them thicker and thus easier to see under the microscope. Considerably more is now known about the process of mitotic chromosome condensation but even so, many of the details (particularly at the molecular level) remain unclear. However the gaps in our knowledge have been fast closing especially in the last two decades, due to vast improvements in fluorescence and electron microscopy. Another large contributor had been the development of powerful *in vitro* methods, such as the *Xenopus laevis* egg extract system, which allows great insight into the biochemistry of the process.

The need for chromosome condensation becomes obvious when one considers the length of the starting material. The DNA contained in a human cell would stretch roughly two meters if laid end-to-end. This is extensively compacted even in interphase and is dispersed throughout the nucleus. However, during the process of cell division the genome must be packaged into a more convenient form that will allow the equal division of the replicated genome to each new daughter cell. This highly packaged form of DNA and associated proteins, the mitotic chromosome, makes this precise handling possible and helps to avoid such hazards as sister-chromatid entanglement and cleavage of trailing chromatin at cytokinesis. The condensation process must occur in a precise and ordered fashion, as demonstrated by the repeatable binding pattern of numerous chromosome-associated proteins, and the characteristic

banding pattern of chromatin itself as illustrated for example in g-banded mammalian chromosomes.

The birth of the scaffold hypothesis

The first level of DNA packaging begins with the class of proteins named histones. Histones are highly conserved proteins throughout eukaryotes, and serve as a core structure around which the naked DNA molecule is wound, resulting in a 10 nm chromatin fibre. Approximately 200 bp of the DNA molecule wraps roughly twice around an octamer of positively charged histone subunits (composed of two copies each of histones H2A, H2B, H3 and H4) to form a disc-shaped nucleosome (McGhee and Felsenfeld, 1980; Richmond *et al.*, 1984)). Packaging of the DNA molecule in this fashion gives rise to a "beads-on-a-string" structure approximately 10 nm thick. A second level of compaction is then brought about most likely by the addition of Histone H1, which is thought to organise this fibre into a regular repeating array to form a 30 nm fiber (Koshland and Strunnikov, 1996).

Chromatin is thought to exist in the 30 nm fibre state during interphase, and whilst this 40x level of compaction makes chromatin more manageable to organise in the nucleus during interphase, it falls significantly short of explaining the 10,000-fold degree of condensation required to form a mitotic chromosome in higher eukaryotes. Basic chromatin structure appears to be similar in both mitotic and interphase chromatin (Paulson and Langmore, 1989), although it has been shown that both histones H1 and H3 are hyperphosphorylated in mitosis (Bradbury, 1992; Mueller *et al.*, 1985; Gurley *et al.*, 1975). Indeed, mitosis-specific phosphorylation of histone H3 has been shown to be vital for correct mitotic chromosome condensation (Wei *et al.*, 1999).

However, the requirement for non-histone proteins in higher order chromosome architecture and condensation has become clear only within the last 25

years. A major step forward was the development of techniques for isolating pure mitotic chromosomes from synchronised cells. Using this technique, Paulson and Laemmli (1977) were able to demonstrate the existence of a scaffold-like core structure surrounded by a halo of DNA when histones were removed from mitotic chromosomes by high salt extraction. Significantly, this structure closely resembled the shape of the mitotic chromosome with paired chromatids connected at a central region resembling the centromere. On close inspection of the DNA halo, very few free DNA ends were observed - the observed loops of chromatin generally returned to a position on the scaffold adjacent to their point of origin. The authors therefore hypothesised that in mitotic cells, chromatin is folded into large loops of up to 100 kb and anchored to a core scaffold composed of non-histone proteins. More evidence for this came from experiments using similar chromosome preparation techniques showing that the "scaffold" could still be isolated when almost all (over 99.9%) of the DNA had been removed by treatment with micrococcal nuclease prior to complete histone removal (Adolph *et al.*, 1977). These results have given rise to what is known as the "radial loop model", or "scaffold hypothesis" of mitotic chromosome condensation, where non-histone proteins play a major role in forming the proteinaceous scaffold upon which chromatin fibre loops are anchored, providing the framework for the final levels of compaction. Many of the non-histone scaffold components have now been identified, as detailed in the sections below, thus contributing significantly to the understanding of the condensation process.

Further evidence for the scaffold hypothesis was provided by the discovery of *cis* elements present in DNA that possibly facilitated the tethering of chromatin loops. Certain sequences known as Scaffold Attachment Regions (SARs) have been shown to be bound with high affinity to the chromosome scaffold (Mirkovitch *et al.*, 1984). These sequences appeared to be spaced approximately 100 kb apart on average, correlating roughly with the loop sizes from the electron micrograph experiments described above. SARs were seen to be similar at the structural level, as they were

predominantly composed of repeated AT-rich elements of over 200 bp and generally contained long stretches of homopolymeric dT (Gasser, 1992). It has been possible to identify several domains within SARs (including a possible topoisomerase II binding site) that are thought to act as several interacting subfragments which have a reduced binding activity on an individual basis (Laemmli *et al.*, 1992). Several observations have implicated SARs as having an important role in chromosome condensation. Fluorescent probes that detect AT-rich regions produced a staining pattern on mitotic chromosomes consistent with the idea that SARs are positioned along the chromosomal axis, in a prime position to provide attachment sites for chromatin loops (Saitoh and Laemmli, 1994). Furthermore, it has been shown that synthetic peptides containing multiple AT hooks (so-called MATH proteins) specifically bind to SARs, and result in disruption of chromosome condensation (Girard *et al.*, 1998; Strick and Laemmli, 1995). For example, the MATH20 peptide (containing 20 hooks) was able to significantly disrupt normal chromosome condensation and was also seen to affect the formation of heterochromatin, demonstrated by the suppression of position effect variegation in the *Drosophila* eye (Girard *et al.*, 1998). Further recent work in *Drosophila* showed that similar MATH peptides were able to induce defined gain or loss-of-function phenotypes when fed to 3rd instar larvae (Janssen *et al.*, 2000). The authors have proposed that this occurs by displacement of other proteins at chromatin attachment regions by MATH20, with the result that their function in organising chromatin is impaired.

DNA topoisomerase II is a major scaffold protein

With the ability to purify the scaffold fraction from mitotic chromosomes, Laemmli and co-workers attempted to ascertain what non-histone components were present. When mitotic scaffolds were fractionated by SDS-PAGE, two major protein species, Sc1 and Sc2, were observed with molecular weights of 170 kDa and 135 kDa

respectively, as well as numerous other minor bands (Lewis and Laemmli, 1982). Further work with antibodies raised against Sc1 from chicken mitotic scaffolds showed that this protein was in fact DNA topoisomerase II (topo II). An anti-Sc1 antibody inhibited topo II function, and was seen to have the same binding pattern as anti-topo II antibodies to partial peptides generated from the intact protein (Earnshaw *et al.*, 1985; Gasser *et al.*, 1986). Topo II functions by creating double-stranded breaks in the DNA molecule and subsequently passing another strand through the gap. The function of topo II and its localisation at the base of loops in mitotic chromosomes supported the idea that it was involved in chromosome segregation and condensation (Earnshaw and Heck, 1985). Indeed, topo II mutants in *S. cerevisiae* were lethal at mitosis due to chromosome segregation defects (Holm *et al.*, 1985; Uemura and Yanagida, 1984; Uemura and Yanagida, 1986) and were later seen to have poorly condensed chromosomes (Uemura *et al.*, 1987). Furthermore, topo II has been demonstrated to bind efficiently to SARs (Adachi *et al.*, 1989), which would seem to lend support to a function as part of an anchoring complex for chromatin loops.

Topo II immunolocalisation on mitotic chromosomes in varying systems ranges from an axial distribution on the arms (Earnshaw *et al.*, 1985) to a more centromeric distribution (Taagepera *et al.*, 1993). It has been conclusively shown that topoII is necessary for the process of chromosome condensation in *Xenopus laevis* extracts (Adachi *et al.*, 1991; Hirano and Mitchison, 1993). In the study by Adachi *et al.*, immunodepletion of topoII from the extracts was shown to disrupt formation of mitotic chromosomes. Strangely, this was not seen to be the case when incubating HeLa nuclei in the same fashion. Additionally, in the Hirano and Mitchison study, topo II depletion from *Xenopus* mitotic egg extracts after condensation had occurred showed no apparent change from normal chromosome appearance. This suggests that topo II may not be involved in physically maintaining the structure of the condensed chromosome, yet it has been clearly shown to be a major element in chromosome scaffolds. Perhaps the requirement for topo II might be to resolve sister chromatid

entanglement either before or during the chromatin condensation process, shifting the catenation:decatenation equilibrium towards decatenation by allowing the immediate condensation of any untangled loops. However, when topo II was inactivated in *S. pombe* cells condensation was only reduced by a factor of three (Uemura *et al.*, 1987). Topo II function might therefore only be necessary for removing occasional chromatin tangles in *S. pombe*.

The SMC family of proteins

As mentioned above, two major proteins were recovered from purified mitotic scaffolds - Sc1 (170 kDa - shown to be topo II) and Sc2 (135 kDa). When Sc2 was cloned and sequenced it was found to be related to a new family of proteins called SMCs. The founding member of the SMC family, *smc1,* had been discovered in *S. cerevisiae* (Strunnikov *et al.*, 1993) and was originally described as a chromosome segregation defect affecting the stability of mini-chromosomes. However, the discovery of further *smc1*-like genes demonstrated that several of the mutants had an effect on chromosome condensation or dosage compensation, and so the family was renamed structural maintenance of chromosomes. Several SMCs from a range of species were found over a short space of time in 1994, when four separate laboratories reported genes with homology to *smc1* from *S. pombe*, *G. gallus*, *X. laevis*, and *C. elegans* (Chuang *et al.*, 1994; Hirano and Mitchison, 1994; Saitoh *et al.*, 1994; Saka *et al.*, 1994). Completion of the *S. cerevisiae* genome sequence allowed the further classification of SMCs into four sub-families - SMC1 through 4 - in which the sub-family members are more homologous to each other than to those in other groups (Koshland and Strunnikov, 1996). SMCs have now been found in all eukaryotes that have been analysed, and in several prokaryotes. Additionally, they have now been shown to have important roles not only in chromosome condensation and segregation but also in dosage compensation and recombinational repair (reviewed in Hirano,

1998). Work in recent years has increasingly demonstrated that SMCs function as components of multi-protein 'condensin' and 'cohesin' complexes (see below sections).

SMC proteins share significant structural similarity, in the form of a head-rod-tail configuration. They are generally around 1000 to 1200 amino acids is length, and contain globular amino and carboxy termini separated by a long α-helical coiled-coil domain (see Figure 1.6A). The coiled-coil region is conserved more on a structural rather than a sequence level, and appears to be necessary for dimerisation (Jessberger *et al.*, 1998). It also contains a small 'hinge' region which has been postulated to allow a scissors-like movement of the dimer. The head region contains a Walker A site, an NTP-binding region common to ATPases (Walker *et al.*, 1982). In addition, the C-terminus includes a conserved amino sequence known as a 'DA box', and this has been postulated to correspond to the second half of the NTP hydrolysis site (i.e. a Walker B site) (Saitoh *et al.*, 1995). A complete NTP hydrolysis site is then formed after the anti-parallel dimerisation of SMC molecules bringing their respective Walker A and B sites together. Homology between various SMCs is highest between the globular domains, commonly ~40% identity, with members of each sub-group generally being more homologous to each other than to members of other groups.

Based on the structure of these proteins, the function of SMCs was unclear at first. The NTP-binding domains originally provided a similarity to ATPases, and hinted at an enzymatic function. However, it had also been proposed that SMCs might be related to motor proteins, based on the similar head-rod-tail structure between the two types of proteins (Guacci *et al.*, 1993). In addition, a structural role was also proposed based on the observation that Sc2 was seen to be one of the major scaffold components (Saitoh *et al.*, 1994). The presence of NTP-binding sites also lead to speculation that SMCs could perhaps form a filamentous meshwork and help to provide a structure for the mitotic chromosome (Peterson, 1994).

The amino terminal NTP-binding site had been shown to be necessary for SMC function in studies on the DPY-27 gene product in *C. elegans*, where it is involved in dosage compensation (Chuang *et al.*, 1994). A DPY-27 construct containing a site-directed mutation in the N-terminal Walker A site was unable to rescue the mutant phenotype, whereas the wild type allele could. However, SMC ATPase activity was dependent on the presence of an NTP-B site in the molecule, as both sites are known to be required for NTP hydrolysis (Walker *et al.*, 1982). Phylogenetic data from a review by Saitoh *et al.* (1995) suggested that the C-terminal DA box was indeed equivalent to a Walker B site. However, in other ATPases these sites are in close proximity, whereas in all SMCs they are separated by almost the entire length of the protein. Two suggestions have been made to overcome this problem - the hinge region could allow the protein to bend back on itself and allow the Walker sites to come together and form the hydrolysis 'pocket'. Alternatively, antiparallel homo- or hetero-dimerisation would allow the A and B sites from separate proteins to form an active site. There is evidence that SMCs do indeed form anti-parallel dimers in prokaryotes, as seen by rotary shadowing of the *E.coli* SMC homologue MukB (Melby *et al.*, 1998), although a homodimer is formed in this case as there is only one SMC orthologue.

There is a growing body of evidence to suggest that SMCs do in fact function as hetero-dimers. SMC interactions have been demonstrated between groups 1 and 3 and groups 2 and 4 in *S. pombe*, *X. laevis*, *C. elegans* and *B. bovis* (reviewed in Cobbe and Heck, 2000; Heck, 1997). In all eukaryotic systems they are found in a complex together with other subunits, but the cellular process in which they are involved can vary. For example, the SMC group 1 and 3 partnership is involved in sister chromatid cohesion in yeast, as part of the so-called 'cohesin' complex. However, the same two SMC proteins in combination with different subunits in *B. bovis* are seen to function in DNA recombination and repair. There is a similar scenario for the group 2 and 4 pairing - mitotic chromosome condensation in *Xenopus* but

dosage compensation in *C. elegans*. Clearly SMCs are capable of contributing essential functions across a wide range of cellular processes, not just in chromosome condensation and segregation as was previously thought. The structural similarities of SMCs and their occurrence throughout the prokaryotic and eukaryotic kingdoms suggests that they may be descended from an ancestral chromatin modifying complex that has since evolved to function in the different processes described above. However, SMCs alone cannot accomplish these tasks - other non-SMC subunits play vital roles in forming the functional complexes of condensins and cohesins, as detailed below.

Condensins mediate chromosome condensation

The first evidence of multi-subunit condensation complexes containing SMCs was provided by the *Xenopus* egg extract system (Hirano and Mitchison, 1994). Chromosomes were assembled from sperm chromatin and mitotic egg extracts, then isolated by sedimentation. Analysis of the protein components from sedimentation revealed several higher molecular weight species present together with known components such as histones. Two of these proteins were shown to be the *Xenopus* homologues of *smc2* and *smc4*, termed XCAP-E and XCAP-C respectively. The proteins were isolated as a heterodimer and associated specifically with mitotic chromosomes (Hirano and Mitchison, 1994). Furthermore, immunodepletion experiments with antibodies to XCAP-C inhibited the final stages of chromosome condensation in the system. In the reciprocal experiment, localised de-condensation was observed when antibodies were added to already condensed chromosomes during mitosis. However, an important discovery in 1997 showed that XCAP-C and XCAP-E also form subunits of condensation-promoting complexes called 'condensins' (Hirano *et al.*, 1997). The two *Xenopus* SMCs co-precipitated in two complexes, one sedimenting at 8S, the other at 13S. The 8S complex was found to be composed of

Figure 1.6 Structure of the SMC protein and SMC-containing complexes

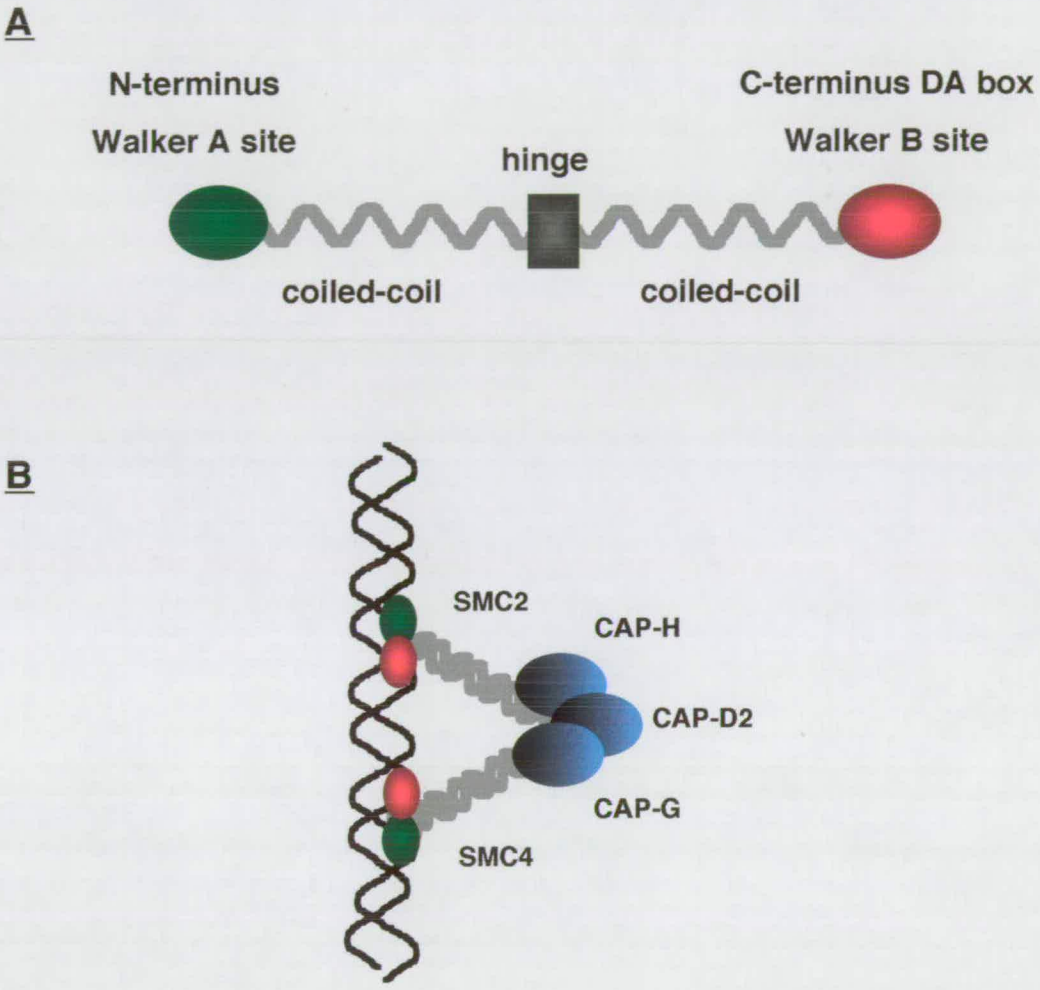

Figure 1.6 Structure of the SMC protein and SMC-containing complexes. **A**) SMC domain structure - globular head and tail regions, each containing one half of a functional ATPase domain, are separated by two long coiled-coil regions divided by a hinge region. **B**) Possible conformation of a condensin complex attached to chromatin, containing two antiparallel SMC molecules and three non-SMC subunits CAP-D2, CAP-G and CAP-H.

XCAP-C and XCAP-E only, and did not have any significant effect on condensation (this complex is possibly just residual dimers of XCAP-C and XCAP-E). However, the 13S complex was seen to contain both the 9S components plus 3 other non-SMC proteins - XCAP-D2, XCAP-G and XCAP-H (see Figure 1.6B) - and was shown by immunodepletion studies to be absolutely required for mitotic chromosome condensation *in vitro*. When the non-SMC subunits were cloned, XCAP-H was found to be homologous to the *barren* gene product, a *Drosophila* gene previously seen to have a disrupted chromosome segregation phenotype in embryos and shown to regulate topo II activity (Bhat *et al.*, 1996). Previously observed co-localisation of Sc1 and Sc2 on the scaffold had prompted the possibility of topo II interacting with condensation factors, e.g. SMCs. Supporting this is the finding that the *cut3* mutant from *S. pombe* (an SMC 4 group member) was found to be synthetic lethal in combination with a cold-sensitive topo II mutant (Saka *et al.*, 1994). Topo II's interaction with *barren*/XCAP-H would seem to lend support to this idea. However, Hirano observed no interaction between them in the *Xenopus* egg extract system and topo II and condensins were shown to be targeted to chromatin independently of one another. The possibility of the 13S condensin having affinity for specific sites on chromatin was also raised, perhaps binding to SARs, as localisation to the bases of chromatin loops could promote the condensing activity. Immunolocalisation of condensin SMCs has indeed detected staining along the chromosomal axis and at the centromeres, reflecting that of topoII (Hirano and Mitchison, 1994; Saitoh *et al.*, 1994). SMCs have also been shown to preferentially bind AT-rich sequences (Akhmedov *et al.*, 1999), correlating well with the predicted roles of SMCs at the bases of chromatin loops.

Although the various members of the condensin complex have been identified, their precise mode of action has not been fully determined. (Kimura and Hirano, 1997) provided evidence that the condensin complex may function by introducing positive supercoils to the loops of chromatin anchored to the scaffold, in turn leading to

accumulation of superhelical tension in the neighbouring DNA regions which would serve to compact the chromatin further. Further studies refined this idea and showed that condensin could reconfigure DNA into knots in the presence of DNA topoisomerase I (Kimura *et al.*, 1999), generating an ordered array of positive solenoidal supercoils. However, these studies were performed on plasmid DNA *in vitro*, using higher concentrations of condensins than would normally be present, allowing the DNA molecules to be completely saturated with the complex. Whether this activity is an accurate reflection of what occurs to chromatin during the condensation process is not known.

Cohesins are important for proper segregation of chromosomes

Alongside the discovery of the role of SMCs in chromosome condensation, over the last few years there has been much work on a similar SMC-containing complex that helps mediate the process of sister chromatid segregation, termed the cohesin complex. As was the case for the condensin complex, much of the pioneering work on cohesins has been done in the yeast and *Xenopus* systems. The cohesin complex is similar in basic structure to condensin - it is composed of five subunits, two of which are SMCs (this time from SMC subfamilies 1 and 3), demonstrated first in *S. cerevisiae* and *Xenopus* (Guacci *et al.*, 1997; Losada *et al.*, 1998; Michaelis *et al.*, 1997). Cohesins were also shown to include three non-SMC subunits. The first of these was the homologue of the *rad21* gene from *S. pombe*, although *rad21* itself had not previously been implicated as a cohesin subunit. Two groups independently identified the *S. cerevisiae rad21* homologue and named it *mcd1* (Guacci *et al.*, 1997; Guacci *et al.*, 1993) or *scc1* (Michaelis *et al.*, 1997). The *mcd1* mutant was identified in two screens, one for mutants defective in chromosome segregation (Guacci *et al.*, 1993),the other for interactors of *smc1* (Guacci *et al.*, 1997). The cohesion defect in *mcd1* cells was demonstrated by using FISH to a centromeric region of chromosome

XVI. One signal in wild type cells indicated that both sister chromatids were still being held together, whereas two signals in *mcd1* cells indicated that paired sister chromatids had segregated inappropriately. MCD1 was therefore concluded to be necessary for sister chromatid cohesion. In a parallel study, Michaelis *et al.* (1997) identified *scc1*, alongside *smc3* and another non-SMC subunit *scc2*, in a screen for mutants that showed sister chromatid separation in cells that lacked Anaphase Promoting Complex (APC) activity. Previous studies had shown that APC mutants failed to separate their chromatids, suggesting that the complex might function to dissolve the cohesion between sister chromatids to promote anaphase. Similar FISH results were obtained as for MCD1, and immunofluorescence studies of SCC1 on chromosome spreads from yeast showed that it dissociated from chromosomes in anaphase, correlating well with a role in sister chromatid cohesion.

Further evidence for a cohesin complex emerged when the *Xenopus* homologues of Smc1 and Smc3 were identified and shown to be subunits in a complex that was required for efficient cohesion of sister chromatids *in vitro* (Losada *et al.*, 1998). This complex - termed 14S cohesin by the authors - had no affect on condensation in these mutants despite containing SMC subunits. It seemed therefore that the proper condensation and cohesion of chromatids is mediated by complexes that appear similar but act independently of one another. However, recent data from analysis of an SMC4 condensin subunit mutant in *Drosophila* has shown that segregation defects do arise from condensation defects (Steffensen *et al.*, 2000). These defects could be explained by taking into account unresolved chromatin tangles caused by condensin deficiency that may prevent efficient segregation of sister chromatids, even though the cohesin subunits are unaffected.

The cohesin complex is thought to bring about sister chromatid cohesion primarily by association with centromeric regions of the paired chromatids, although binding at discrete sites along chromosome arms has also been observed in yeast (Blat and Kleckner, 1999; Megee *et al.*, 1999; Tanaka *et al.*, 1999). The complex has been

shown in yeast to associate with chromatin shortly before S phase (Michaelis *et al.*, 1997), and remains bound until the metaphase-anaphase transition, governed by the APC-mediated cleavage of the SCC1 subunit. The details of this dissolution of cohesion have been described in Part I of this Introduction.

The search for novel condensation factors

The above sections have summarised the current understanding of the known factors involved in mitotic chromosome formation. However, in order to finish this part of the Introduction I will discuss proteins that appear to play a role in mitotic chromosome condensation but have not been shown to interact with the above complexes. The role of Histone phosphorylation as a marker for the onset of mitosis is well documented (Gurley *et al.*, 1975), and it has also been shown to play an important role in the condensation process (Wei *et al.*, 1999). However, there are several other less well known proteins involved in condensation. Among these are the giant filamentous protein Titin (over 2 megadaltons), first known as a component of muscle sarcomeres, which controversially is thought it to play a structural role in assembling mitotic chromosomes (Machado and Andrew, 2000; Machado *et al.*, 1998). Another surprising finding is that the A-kinase-anchoring protein AKAP95 (which serves as a recruiting platform for a cAMP/Protein Kinase A complex onto chromosomes) also appears to regulate chromosome structure during mitosis in HeLA cells (Collas *et al.*, 1999). Furthermore, studies from our own laboratory have provided evidence that correct mitotic chromosome condensation is linked to replication timing, as shown by work on RFC4 and ORC2 in *Drosophila* (Loupart *et al.*, 2000; Krause *et al.*, submitted). I mention these here to stress that mitotic chromosome condensation does not depend purely on the SMC-containing complexes and topoII - there are clearly more proteins vital to this process waiting to be discovered.

Part III: Background to the *Drosophila melanogaster* mutant *l(3)IX-14*

Why use Drosophila melanogaster?

Drosophila melanogaster has been used successfully as a model organism for studying genetics for a century now. As a result of this, it is perhaps the best characterised genetic higher eukaryotic model system. The recent completion of the euchromatic *Drosophila* genome sequence in March of 2000 has served to underline its status as a versatile experimental organism. However, despite its contributions to pioneering work in many diverse fields over the years (such as developmental biology, neurobiology, population biology and behavioural studies), it seems that *Drosophila* has been somewhat under-used as a model for processes such as cell cycle events, and in particular that of investigating chromosome structure and condensation. This is indeed a great shame, as it fails to recognise two of the most useful aspects of *Drosophila* - its extremely well-characterised genetics, as mentioned above, but also its excellent cytology. As the first two parts of the Introduction have shown, previous studies on chromosome structure have often relied on the genetic analysis of the yeasts *Saccharomyces cerevisiae* and *Schizosaccharomyces pombe*, and on the convenient *in vitro* biochemistry provided by the *Xenopus laevis* egg extract system. However, *Drosophila* can provide an *in vivo* environment for analysing these events throughout the early stages of its life-cycle (see Figure 1.7), ranging from the rapid synchronised divisions of early embryogenesis to the differentiated mitotic and polytene tissues that exist in larvae. Its complement of four relatively large and easily identifiable mitotic chromosomes allows the necessary morphological study that can be lacking in yeast, and the existence of endoreduplicating polytene chromosomes in larval tissues provide even more opportunity for analysis. Coupled with the recent genome sequence and the advent of techniques such as dsRNA-mediated interference (RNAi) in both in embryos

Figure 1.7 Life cycle of *Drosophila melanogaster*

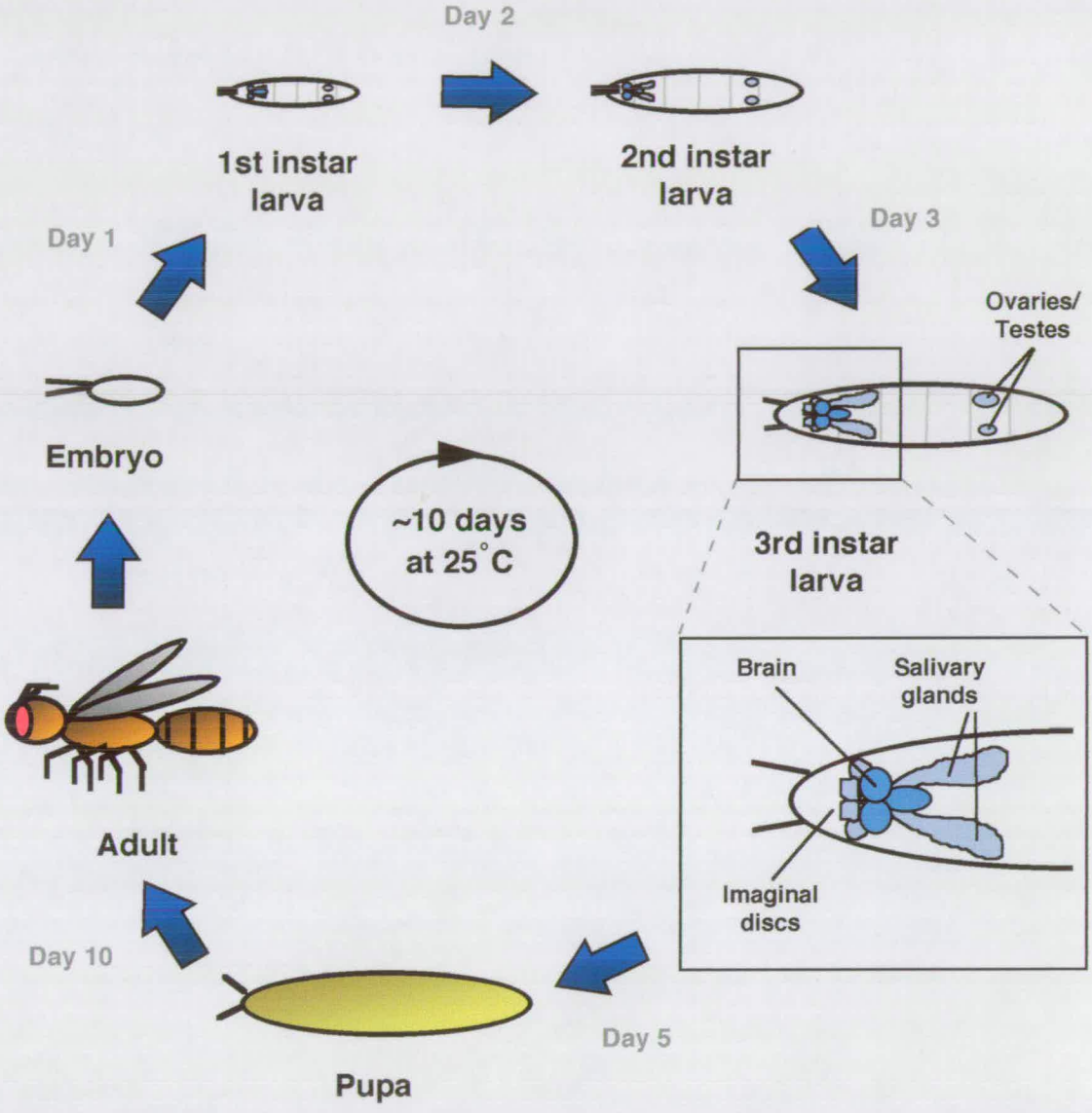

Figure 1.7 Life cycle of *Drosophila melanogaster*. After the *Drosophila* egg is laid, it takes approximately one day after fertilisation for the embryo to develop and hatch into a 1st instar larva. There are three larval molts, occurring after days 1, 2 and 4 for each instar resectively. Third instar larvae molt to form an immobile pupal case, inside which the body is completely remodelled. Four days later an adult fly ecloses from the pupal case. Larval tissue growth occurs mostly by endo-reduplication and increase in cell size (for example in the salivary glands, shown in inset of 3rd instar larva). Mitotic activity only occurs in tissues that will be used to form the adult fly, e.g. the brain and imaginal discs (see inset), histoblasts and gonads (ovaries or testes).

and in tissue culture cells, it would seem that there has never been a better time to use *Drosophila.*

A history of the Drosophila mitotic mutant l(3)IX-14^1

The work presented in this thesis focuses on the late larval lethal mutation *l(3)IX-14^1* and its various alleles. This mutant was first generated in a chemical mutagenesis screen (using ICR-170, which preferentially causes frame-shift mutations) in Alan Shearn's laboratory (Shearn and Garen, 1971) in an attempt to identify genes necessary for imaginal disc proliferation. *l(3)IX-14^1* was then characterised in greater detail by Maurizio Gatti and Bruce Baker, in a study that focused on mitotic mutants in *Drosophila* (Gatti and Baker, 1989). The authors postulated that mutations affecting mitosis could be identified in late 3rd instar larvae, on the premise that maternal contributions essential for embryogenesis would be depleted by then. As *Drosophila* larval tissues grow largely by endoreduplication, the only tissues that require mitosis are those that will later form structures in the adult, i.e. the brain, the histoblasts and the imaginal tissues. Defects in these proliferating tissues will then become apparent once the maternal products have been depleted during the second and third larval instars. The authors identified several genes from the Shearn and Garen mutagenesis screen with mitotic defects, including *l(3)IX-14^1* which they reported as having hypercondensed chromosomes and an increased mitotic index (i.e. the number of mitotic cells relative to the total number of cells present). This mutant line along with several others affecting chromosome condensation were then kindly given to this laboratory by Maurizio Gatti.

Further work on the *l(3)IX-14^1* mutation was initiated by Sue Ann Krause, a former Ph.D. student in the Heck laboratory who analysed mitotic chromosome architecture in the stocks received from M. Gatti (S.A. Krause, Ph.D. thesis 1999). Sue Ann reconfirmed the hypercondensed phenotype observed earlier by examining

neuroblast squashes from 3rd instar larval mutants (see Figure 1.8). However, she demonstrated that the mitotic index in *l(3)IX-14*^{1} appeared to decrease rather than increase as had previously been noted. It was also noted that a lower frequency of undercondensed chromosomes were observed in this mutant. Significantly, Sue Ann was able to generate a P element insertion allele of *l(3)IX-14*^{1} by local hopping of a nearby P element. This allele was termed *l(3)IX-14*^{4Y7}, and was to prove instrumental in the cloning of the putative *IX-14* gene.

Following on from this work an honours student in the laboratory, Alison Wilkie (1997) precisely excised the P element from *l(3)IX-14*^{4Y7} and reverted the lethality, thus confirming the P element insertion caused the mutation. She also generated two excision derivative alleles in the process by imprecise excision of the P element. Alison began the cloning of *IX-14* by inverse PCR amplification of a small flanking region of the P element insertion, and succeeded in cloning an approximately 700 bp genomic fragment which was then used to screen a *Drosophila* genomic library. More phenotypic analysis on the mitotic index of *l(3)IX-14*^{1} was performed by Liping Lu, a research assistant in the laboratory, quantifying the various chromosomal defects seen in *l(3)IX-14*^{1} mitotic neuroblasts (shown in Figure 1.8B). Liping also observed whether the mitotic index in wild type and *l(3)IX-14*^{1} neuroblasts would increase when the brains were incubated in colchicine, a microtubule-destabilising drug, which would prevent cell progression from metaphase to anaphase. The wild type mitotic index was seen to double on incubation with colchicine, indicating an accumulation of metaphase figures as expected. Interestingly, colchicine treatment also doubled the mitotic index in *l(3)IX-14*^{1} neuroblasts. This contrasts with the earlier reports of a mitotic arrest in *l(3)IX-14*^{1}- had this been the case, the mitotic index would not be expected to change significantly. This provided preliminary evidence that a defect in the cell cycle was occurring prior to mitosis in these mutants. It was at this point that I began my Ph.D. in the laboratory with the aim of characterising this interesting mutant further at both the molecular and phenotypic levels.

Figure 1.8 Mitotic chromosome phenotypes of *l(3)IX-14¹*

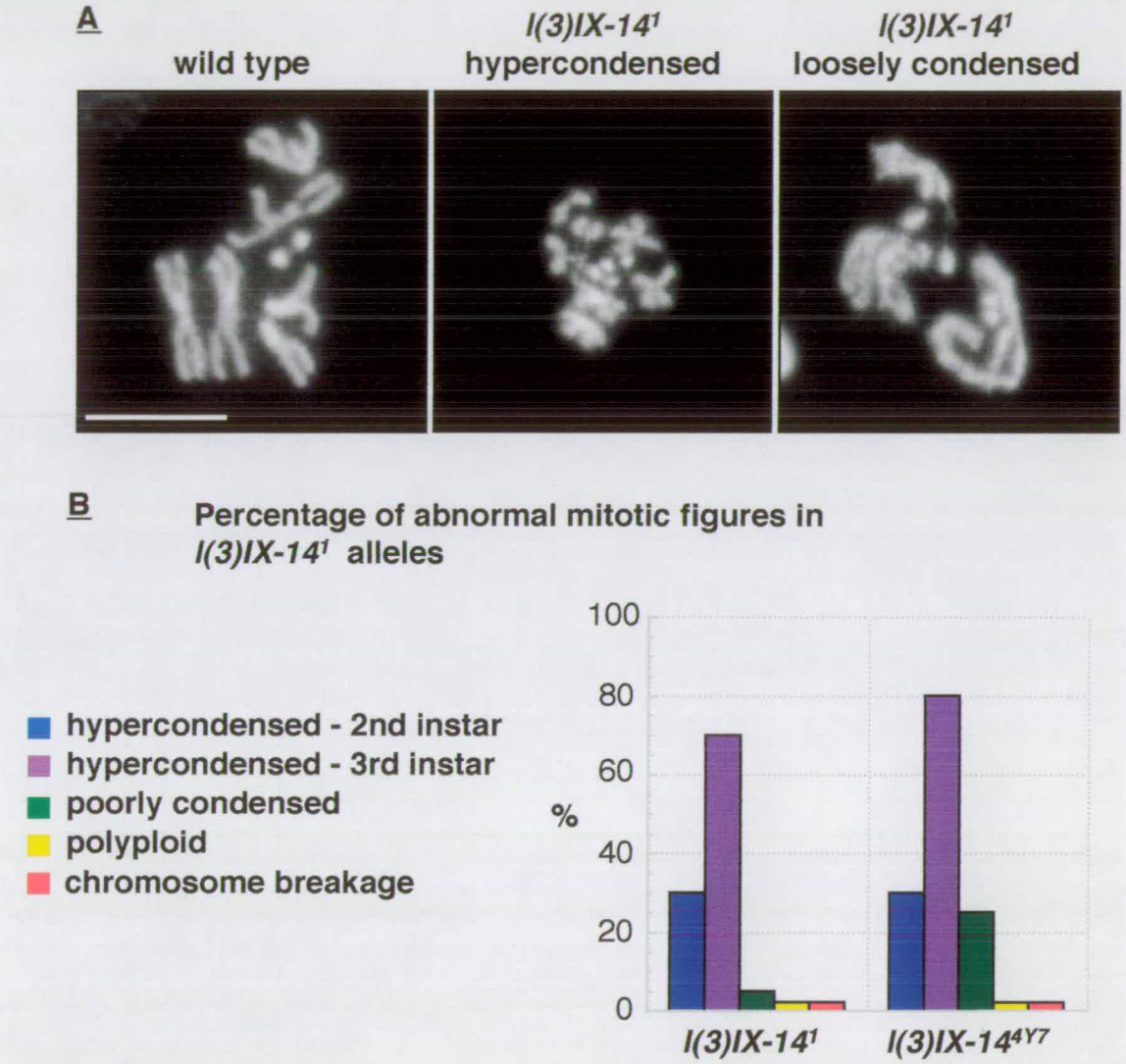

Figure 1.8 Mitotic chromosome phenotypes of *l(3)IX-14¹*. **A**) Mitotic chromosomes from 3rd larval instar neuroblast squashes, hypotonically swollen in 0.25X EBR and stained with DAPI. The primary chromosomal phenotype is shown in the middle panel and is seen in ~70% of mutant mitotic figures in all *l(3)IX-14¹* larval lethal alleles. The minor secondary phenotype of loosely condensed chromosomes is shown in the right panel. Scale bar = 5μm. **B**) Quantitation of the various chromosomal abnormalities observed in the ICR-170 induced *l(3)IX-14¹* allele and the P-element induced *l(3)IX-14⁴Y⁷* allele. The background levels of these abnormalities in wild type neuroblasts is less than 1%.

Chapter 2
Materials and Methods

Materials

Drosophila melanogaster stocks

Strain	Source
Canton S w^{1118} *l(3)ry100*/TM6B *l(3)P1532*/TM6B	Bloomington Stock Center
l(3)IX-14^{1}/TM6B *l(3)k43*/TM6B	A. Shearn, Baltimore
yw;D gl[3]/TM3,*Sb* (P,w^{+} KrGFP)	T. Kornberg, San Fransisco
l(3)IX-14^{4Y}/TM6B *l(3)IX-14*^{eB}/TM6B *l(3)IX-14*^{eG}/TM6B	S.A. Krause and A. Wilkie, Heck Laboratory, Edinburgh

Immunofluoresence reagents

Antibody	Source
rat monoclonal anti-BrdU	Harlan SeraLab
mouse monoclonal anti-α tubulin	Sigma
rabbit polyclonal anti-CP190 (Rb188) mouse monoclonal anti-CP190 (Bx63)	W. Whitfield, Dundee
rabbit polyclonal anti P-H3	Upstate Biotechnologies
rabbit polyclonal anti-INCENP	W. Earnshaw, Edinburgh
mouse monoclonal anti-lamin	P Fischer, New York
rabbit polyclonal anti-Bub1	C. Sunkel, Porto
Alexa secondary antibodies	Molecular Probes

Bacterial strain information

E. coli XL1-Blue (New England Biolabs)	*F' proAB lacI*^{q}*lacZΔM15 TN10(Tet*^{r}*)/recA1 endA1 gyrA96(Nal*^{r}*) thi1 hsdR17(*$r_k^- m_k^+$*) supE44 relA1 lac*
E. Coli BL-21	*F- ompT hsdSB (rB-mB-) gal dcm(DE3)*
E. coli ER2566 (New England Biolabs)	*F' lamda' fhuA2 [lon] ompT D(mcrC-mrr)114::IS10 R(mcr-73::miniTn10 TetS)2 R(zgb-210::Tn10) (TetS) endA1 [dcm]*

PCR, sequencing and RNAi primers*

Primer	Sequence (5' - 3')
PF2	CGACGGGACCACCTTATGTTAT
p32	TATACTTCGGTAAGCTTCGGGTTT
p561	GCAAGCATACGTTAAGTGGATGTCTC
T3	GAGCTCCATTCGCCC
T7	TTCGCGCGTTAATTGG
PM001	CGTTAGAACGCGGCTACAAT
BPUP1	CATTTTTGGGGCTTTCTCTTGA
BPLW2	CGCCAGCCGATTTTGTTTTGA
Ex1-Int1.Up	TGTTTTTATGGTTTTGCTGAATGA
Ex1-Int1.Lw	GAAAGGGCGGAGTAAGAGAAGAAG
BGEN2	ATGCTTTTCCGAATCTGGTAACAC
BGEN4	ATCATTCCCCACCACTATCACAT
BNG-GAP.Up	TCTTGCCCTTTTTGCCTTTGTTG
Pair7.Up	CCACATTTCCGGGCAGATA
Pair7.Lw	AAAAGGGTCCGTTGGTAGTCATTA
Pair2.Up	TGTTGGTTTATTTATTTTATTTTG
Pair2.Lw	GTACCATCACAGCATCAGG

RNAi primers - Underlined text denotes T7 polymerase binding site

T7-BMC01	TTAATACGACTCACTATAGGGAGAGG CGGAAAAGCAGCAAACA
T7-BMC09	TTAATACGACTCACTATAGGGAGAAG AGCCGCTTCCTGTTGAC
T7-BMC04	TTAATACGACTCACTATAGGGAGAGC CGGATGCGCACTTGGATGT
T7-BMC07	TTAATACGACTCACTATAGGGAGAGC GAGAAGACCGGCGACTGTG

*All primers were synthesised by MWG Biotech.

Common reagents and buffers

CLAP	1 mg/ml chymostatin, 1 mg/ml leupeptin, 1 mg/ml antipain, 1 mg/ml pepstatin A (all from Sigma)
BSA	30% stock solution, from Sigma
DAPI	from Sigma, used at 0.1 µg/ml
5x Dye for agarose gels	17.5% Ficoll 400, 100 mM EDTA, 2.5% SDS, 0.25% Bromophenol Blue, 0.25% Xylene Cyanol FF
EBR	130 mM NaCl, 4.7 mM KCl, 1.9 mM $CaCl_2$, 10 mM HEPES, pH 6.9
Hybridisation buffer	0.5 M $NaHPO_4$ pH 7.2, 7% SDS, 1 mM EDTA, 1% BSA
LB	1% Bacto-tryptone, 0.5% Bacto-yeast extract, 1% NaCl, pH 7.4
Mowiol	14% Mowiol, 28% Glycerol in PBS
PFA	16% Paraformaldehyde ampules from TAAB
PBS (Dulbecco's)	65 mM Na_2PO_4, 8.8 mM KH_2PO_4, 1.37 M NaCl, 2.7 mM KCl, pH 7.4
PBS-Tw	PBS + 0.1% Tween 20
PBS-Tx	PBS + 0.05% TritonX 100
5x SSPE	0.75 M NaCl, 50 mM NaH_2PO_4, 6 mM EDTA
SOB	2% Bacto-tryptone, 0.5% Bacto-yeast extract, 8.6 mM NaCl, 50 mM $MgCl_2$, 2.5 mM KCl, pH 7.4
SOC	SOB + 20 mM Glucose
Stop solution	40 mM Tris pH 8.0, 20 mM EDTA pH 8.0, 0.5% SDS, 200 µg/ml Salmon sperm DNA
TE	10 mM Tris-HCl, 1 mM EDTA
TAE	40 mM Tris-Acetate, 1 mM EDTA
TBE	45 mM Tris-Borate, 1 mM EDTA

Methods

2.1 Making electrocompetent cells

2 ml overnight culture of appropriate bacterium (e.g. BL21, XL-1 Blue) was grown with shaking at 37°C in SOB (per litre: 20 g Bacto-tryptone, 5 g Bacto-yeast extract, 8.6 mM NaCl, 2.5 mM KCl, pH 7.0). 0.5 ml of the overnight culture was then diluted into each of two 2 litre flasks containing 500 ml SOB. This larger culture was then grown with shaking at 37°C to an optical density (OD)600 of 0.8 (usually for 4 hours at least). The flask was then immediately chilled on ice for 15 - 30 minutes. All subsequent steps were performed on ice - it is important that the bacterial cells remain cold as their competence is affected otherwise.

The bacterial cells were harvested by centrifuging in sterile, chilled bottles for 15 minutes at 2500 rpm in a Beckman JLA 10.500 rotor at 4°C. As much of the supernatant was removed as possible, and the cells were then resuspended in 500 ml ice-cold 10% glycerol in distilled water (sterilised by autoclaving). The resuspended culture was centrifuged again at 2500 rpm for 15 minutes at 4°C, and the supernatant subsequently removed. Each pellet was resuspended in 4.5 ml 10% glycerol, and 200 µl aliquots were snap-frozen in 500 µl microfuge tubes by placing them in liquid nitrogen. The electrocompetent cells were finally stored at -80°C.

2.2 Electroporation

All electroporation was performed using a BioRad electroporator.

Tubes of competent cells (aliquots of 200 µl) were thawed on ice. Meanwhile, an appropriate number of 1.5 ml Eppendorf tubes and 0.2 cm disposable cuvettes (Invitrogen) were also placed on ice to cool to 4°C. 80 µl of competent cells were added to the 1.5 ml tubes, followed by an appropriate amount of DNA, and mixed. Cuvettes were tapped to get the sample to the bottom, and then electroporated at the

following conditions: resistance set at 200 Ohms, capacitance set at 25 μ FD, volts set at 2.5 kV. After electroporation, 1 ml of SOC was immediately added to each cuvette. The mixture was then incubated at 37°C for 30 to 60 minutes. Dilutions were plated out on agar plates containing an appropriate antibiotic.

2.3 Genomic DNA extraction from adults or larvae

50 adult flies (or 3rd instar larvae) were frozen at -20°C, then homogenised in 500 μl of Solution A (0.1M Tris HCl, pH 9.0, 0.1M EDTA, pH 8.0, 1% SDS) using a Polytron (Kinematika). The homogenised solution was incubated at 70°C for 30 minutes, then 70 μl of 8 M potassium acetate was added. The mix was centrifuged twice at 13K, 4°C, 15 minutes each, to obtain a clear supernatant . 0.5 volumes of isopropanol was added and the DNA was then precipitated for 1 hour at -70°C. The DNA was pelleted at 13,000 rpm for 15 minutes at 4°C, then washed in 70% ethanol for 5 minutes and air dried. Genomic DNA was resuspended in 100 μl TE, extracted once with phenol:chloroform:isoamyl alcohol (25:24:1) at 13,000 rpm for 5 minutes, then once with chloroform, precipitated in 1/10th volume sodium acetate and 2.5 volumes ethanol for at least 1 hour at -70°C, centrifuged at 13,000 rpm at 4°C for 15 minutes, washed in 70% ethanol and resuspended in a final volume of 100 μl TE.

2.4 Single Embryo DNA Preparation for PCR

Single embryos of the desired genotype were collected in 0.5 ml tubes (1 per tube), using a Tungsten needle to pick up the embryos from a red-wine agar collection plate. Embryos were homogenised in 10 μl of 'Gloor & Engel's' buffer (10 mM Tris pH8.2, 1 mM EDTA, 25 mM NaCl plus 200 μg/ml of fresh Proteinase K [PCR grade from Boehringer Mannheim]), using a pipette tip. The embryos were then incubated at 37°C for 30 minutes, moved to 95°C for 2 minutes, then placed at 4°C for storage.

Using this preparation, I have found that 1 µl is sufficient for a 50 µl PCR reaction, although it may be possible to use less.

2.5 Plasmid DNA extraction

All small scale plasmid DNA extractions were performed using the UltraClean™ Plasmid Miniprep kit from MoBio. 5 ml cultures of *E. coli* were grown overnight at 37°C with shaking, 2 mls of which were then used for plasmid DNA extraction and the remainder used for re-innoculation of cultures or for making frozen glycerol stocks as required. Larger scale extractions of up to 50 mls were performed using either UltraClean™ Midi prep columns (MoBio) or a Qiagen MidiPrep kit, according to manufacturers instructions.

2.6 Agarose gel electrophoresis

Unless otherwise stated in the text, all agarose gels were made up of 1% SeaKem LE Agarose (BioWhittaker Molecular Applications) containing 0.3 µg/ml ethidium bromide, and were electrophoresed in 'Owl' electrophoresis tanks in 1 X TBE. Gel size - Mini (50 mls), Midi (100 mls) or Maxi (300 mls) - was dictated by the number of samples and/or degree of separation required.

2.7 Purification of DNA from agarose gels

Electrophoresis was performed in low-melt agarose gels (SeaPlaque low gelling temperature agarose, FMC BioProducts) containing 0.3 µg/ml ethidium bromide run in 1 X TAE buffer. After visualisation by UV irradiation, relevant bands were excised using a razor blade and placed into 1.5 ml Eppendorf tubes. Samples were melted at 65°C for 5 minutes, 1 ml of Wizard Minipreps DNA Purification Resin

(7 M Guanidine hydrochloride, Promega) was added and the samples were then transferred to a 2 ml syringe barrel inserted into a Wizard Purification column (Promega), and passed through by pushing gently on the syringe plunger.

The columns were washed with 2.5 ml of 80% isopropanol, then centrifuged for two minutes at 13,000 rpm to drain any remaining liquid. The column was placed into a fresh Eppendorf 1.5 ml tube and the purified DNA was eluted with 40 µl of hot TE by centrifuging at 13,000 rpm for 2 minutes.

2.8 RNA extraction from embryos and larvae

Total embryonic or larval RNA was prepared using the RNeasy RNA extraction kit from Qiagen. Larvae or embryos were collected, frozen in liquid nitrogen, and homogenised using a Polytron (Kinematika AG) in 300 µl of Lysis buffer equivalent (Buffer RLT) containing 1:100 volume of β-mercaptoethanol. Total RNA was then purified using the RNeasy columns according to the manufacturers instructions. Elution of RNA from the column was performed by spinning twice with 40 µl of RNAse-free dH_2O. Long term storage of total RNA was at -80°C.

2.9 Sequencing of DNA samples from plasmids or phage

Per reaction (prepared in a 0.5 ml microfuge tube, kept on ice at all times):

250 - 500 ng of template DNA
3.2 pmol of primer
8 µl of dRhodamine Terminator Cycle Sequencing Ready Reaction (PE Biosystems)
ddH_2O up to 20 µl

Reactions were performed in a Biometra PCR machine with the following program:

ramp to 96°C
96°C for 30 sec.
50°C for 15 sec.
60°C for 4 min.
---
cycle x 25
4°C hold

Sequencing reactions were then precipitated in the following manner:

2 µl of 3M Sodium acetate (pH 4.6-5) was added to each tube, followed by 50 µl of 95% ethanol. The tubes were vortexed to mix, placed on ice for 15 minutes, then spun at 13,000 rpm in a benchtop microfuge at 4°C for 30 minutes. Excess liquid was aspirated away, and the pellets were washed by adding 250µl of 70% ethanol and spinning as above for 5 minutes at room temperature. The supernatant was again aspirated away, and the pellets air dried completely by placing the tubes on the 37°C block with the lids open for 5-10 minutes. The dried pellets were then brought to the ICMB sequencing facility for loading onto a ABI prism sequencer.

2.10 PCR from adult *Drosophila* genomic DNA

All genomic DNA used was prepared by the method detailed in Chapter 2.3 above.

The reaction components used for 50 µl PCR from genomic DNA were:

Genomic template	50 ng
Primers	50 pmol
dNTPs	0.2 mM
Pwo polymerase	1.25 units
$MgSO_4$	1 - 2 mM (generally), supplied with Pwo polymerase
Reaction buffer	1 X, supplied with Pwo polymerase
dH_2O	up to 50 µl

Pwo polymerase was acquired from Boehringer Mannheim.

The standard PCR reaction was as follows:

95°C for 5 minutes

95°C for 30 seconds
55°C for 30 seconds
72°C for 30 seconds

cycle x 30

72°C for 10 minutes

2.11 RT-PCR from total RNA

RT-PCR was performed on total RNA isolated from embryos or larvae, using Qiagen Omniscript Reverse Transcriptase in a two-step reaction. Primers used were either random hexamers or primers specific to the gene of interest.

Per reaction

2 µl of 10 X Reaction buffer
2 µl of dNTP mix (5 mM each dNTP)
Primers (up to 10 µM, depending on optimisation)
1 µl of RNase inhibitor (from a 10 units/ µl stock)
1 µl Omniscript Reverse Transcriptase
Up to 2 µg of RNA template
RNase free dH_2O up to 20 µl

The reaction was allowed to proceed at 37°C for 1 hour, and was then stopped by heating at 93°C for 5 minutes, followed by immediate cooling on ice. PCR was then performed using this cDNA product as template, following the reaction conditions detailed in the section above, and the products were then visualised by electrophoreses on a 1% agarose gel.

2.12 Southern Blotting

This protocol was adapted from Church and Gilbert (1984); PNAS 81, 1991-1995).

The relevant DNA samples were first electrophoresed on an agarose gel and subsequently photographed beside a ruler on a Herolab UV Transilluminator (UVT-28M). This gel photograph was then used to determine the migration of the DNA in the gel by standard plotting of the molecular weight marker distances on logarithmic graph paper. Gels were acid depurinated in 0.25 M HCl for 20 minutes at room temperature, rinsed in dH_2O, then denatured by rinsing 2 X 15 minutes in 1X denaturation buffer (0.8 M NaCl, 0.4 N NaOH). Gels were then rinsed again in dH_20 and neutralized in 0.025 M $NaHPO_4$ for 3 X 10 minute washes.

Transfer of DNA to a Nytran nylon membrane (Schleicher and Schuell) was performed in 5 X SSPE (0.75M NaCl, 0.05M NaH_2PO_4, 0.006 M EDTA) overnight over sponges in a Pyrex tray. The membrane was subsequently rinsed in 5 X SSPE for 1 - 2 minutes to remove any adherent agarose and the DNA was UV-crosslinked to the membrane using a Strata-linker (Stratagene) at 1200 mJ.

Prior to prehybridisation the membranes were rinsed again briefly in 5X SSPE. The membranes were then incubated in prehybridisation buffer (0.5 M $NaHPO_4$, pH 7.2, 7% SDS, 0.001 M EDTA, 1% BSA) equilibrated to 65°C. Prehybridisation was performed at 65°C with rolling in sealed Hybaid bottles for 1 hour minimum. Fresh buffer (same composition as above) was used for hybridisation with 200 µl of appropriate probe added, at a specific activity of at least 1 x 10^6 counts per ml. Unless otherwise specified, all hybridisations were performed at 65°C overnight.

Membranes were washed post-hybridisation three times for 15 minutes at 65°C with Wash Buffer 1 (0.04M $NaHPO_4$, pH 7.2, 0.001M EDTA, 5% SDS, 0.5% BSA), then five times for 5 minutes at 65°C in Wash Buffer 2 (0.04 M $NaHPO_4$, pH 7.2, 1% SDS, 0.001 M EDTA). Membranes were briefly blotted between two pieces

of Whatman 3M paper, wrapped in cling-film and mounted on blotting paper with Stratagene orientation stickers. Autoradiography was at -80°C in an 8 X 10 inch cassette (Genetic Research Instrumentation Ltd.) with Kodak XAR-5 film. Films were developed using a Konica SRX-101A developer.

2.13 Northern Blotting

This protocol was adapted from Molecular Cloning: A Laboratory Manual/Second Edition, chapter 7, Maniatis et al.. (1989), Cold Spring Harbor Laboratory Press.

All solutions were made up with DEPC-treated dH_2O (RNase-free). Total RNA was prepared from third instar larvae and embryos using the RNeasy RNA extraction kit (Qiagen).

10 µg of total RNA from the relevant samples was loaded onto a 1% agarose gel containing 1 X formaldehyde gel running buffer (hereafter termed FA gel running buffer - 0.02 M MOPS (pH 7.0), 8 mM sodium acetate, 1 mM EDTA (pH 8.0)) and 2.2 M formaldehyde. Gels were cast in the fume hood and allowed to set for at least 30 minutes at room temperature, The gels were pre-run at 100V for 10 - 15 minutes before loading the samples.

RNA samples were prepared in sterile microfuge tubes as follows:

per 20 µl reaction	RNA	up to 4.5 µl
	5X FA gel-running buffer	2.0 µl
	formaldehyde	3.5 µl
	formamide	10.0 µl

(When amounts of RNA exceeded 4.5 µl, total sample size was increased to 50 µl and other reagents were adjusted accordingly.)

Samples were incubated at 65°C for 15 minutes, and then chilled on ice. 2 µl sterile FA gel loading buffer was added to the samples, which were then loaded on the pre-run gel. Molecular weight markers were loaded in the first lane (RNA ladder, 0.24 kb - 9.5 kb, GibcoBRL). The gel was submerged in 1 X FA-gel running buffer, and run at 100V for 3 hours, until the bromophenol blue had migrated approximately 2/3rds the way down the gel. Gels were not usually stained with Ethidium bromide, although that is an option at this stage, but rather were transferred to a nitrocellulose membrane immediately after electrophoresis.

Prior to transfer by capillary action, the agarose gel was soaked for 20 minutes in 0.05 M NaOH to partially hydrolyse the RNA. The gel was then rinsed 3 times for 5 minutes in dH_2O, and soaked for 30-40 minutes in transfer buffer (either 5 X SSPE or 20 X SSC have been used, with no detectable difference between the two). Transfer of RNA to a nylon membrane (Nytran, Schleicher and Schuell) was performed in a similar fashion to transfer of DNA in the 'Southern Blotting' section, i.e. by capillary activity with 5 X SSPE (or 20 X SSC) overnight over sponges in a Pyrex tray. The membranes were rinsed in transfer buffer for a 1 - 2 minutes to remove any adherent agarose and the RNA was subsequently UV-crosslinked to the membrane using a Strata-linker (Stratagene). The membrane was stained with methylene blue (0.04% in 0.5 M acetic acid (pH 5.2)) for 5 minutes, then rinsed several times with dH_2O to visualise the RNA (a characteristic doublet of ribosomal RNA should be clearly visible) and the markers. A photograph was taken with a ruler placed beside the marker lane, using a HeroLab Gel Documentation System. Membranes were stored at -20°C, or placed in pre-hybridisation buffer for immediate use.

Hybridisation of radioactive probes to RNA immobilised on a nitrocellulose membrane and autoradiography was performed in an identical fashion to the method described in the Southern Blotting section.

2.14 Random Primer ^{32}P-labeling

The HighPrime kit from Boehringer Mannheim was used for all random primer labelling.

Each labelling reaction was 25 µl total and set up in the following manner:

50-100 ng of DNA, 5 µl 5X buffer, and dH_2O up to 20 µl was added to a screw-cap tube. The mix was heated at 70°C for 5 minutes, then placed immediately on ice to prevent re-annealing of the DNA. 5 µl of High Prime mix was added, keeping the mix at 4°C at all times. This reaction mix was brought to the radioactive room and 50 µCi of ^{32}P-dCTP (Amersham) was added behind a perspex screen. The reaction tube was then incubated at 37°C for 15 minutes.

Unincorporated nucleotides were removed by spin chromatography. In spin columns (Bio-Spin Disposable Chromatography Columns, Bio-Rad) - 2 mls of G50 resin (5 g of G50 beads suspended in 50 mM Tris (pH 8.0), 100 mM NaCl, 10 mM EDTA (pH 8.0), 0.5% SDS) was spun for 4 minutes at 2000 rpm in a benchtop centrifuge. In a second spin, the column was equilibrated with 1 ml of stop solution (40 mM Tris (pH 8.0), 20 mM EDTA (pH 8.0), 0.5% SDS, 200 µg/ml salmon sperm DNA). Stop solution was also added to the labelling reaction (175 µl to a 25 µl reaction). The stopped reaction (200 µl total) was added to the column, and the tube was then rinsed with the same volume of stop solution and added to the column to make a total of 400 µl. The rinsed screw cap tube was placed in the bottom of a 15 ml snap-cap tube (Sarstedt) and the Bio-Rad column was then placed so that the reaction mix would elute back into the screw-cap tube. This arrangement was then spun again for 2 - 3 minutes to allow the stopped labelling reaction to elute into the screw-cap tube.

The cleaned reaction was mixed in the tube and 1/100 of the volume was taken out for a scintillation count (using a Packard Tri-Carb 2100TR Liquid Scintillation Analyzer). The reaction was roughly monitored for efficiency of incorporation by checking both the column and the incorporated counts by Geiger counter before an accurate count was taken by scintillation counting.

All probes were boiled for 5 minutes prior to adding to the hybridization buffer in a Southern or Northern blotting experiment.

2.15 Subcloning

Subcloning of DNA fragments into plasmid vectors was performed on several occasions, details of which are described in the text. What follows is a general protocol used for those experiments.

Restriction digestion of DNA

In general, restriction digests were performed in 1.5 ml Eppendorf tubes, using enzymes from New England Biolabs. Unless otherwise indicated, the 10 X reaction buffer provided with the enzyme was used. Digests were normally performed on the 37°C hot-block, and allowed to proceed for at least 2 hours. If required, the restriction enzyme activity was then inactivated by placing the tube at 65°C for 20 minutes.

Ligations

All ligations were performed using T4 DNA ligase from Promega, and the appropriate reaction buffer provided. Whenever possible, an insert:vector ratio of 3:1 was used. Ligations were allowed to proceed overnight at 16-18°C. In blunt-end ligations, purified vector was pretreated with Shrimp Alkaline Phosphatase (Amersham), according to the manufacturers instructions, in order to remove 3' phosphates and reduce background contamination of vector-only colonies.

Electroporation

Electroporation was performed using a BioRad electroporator at these conditions: resistance set at 200 Ohms, capacitance set at 25 μFD, volts set at 2.5 kV.

2.16 Preparation of Protein from Larval Extracts

30 wandering third instar larvae were taken from vials or bottles and placed in a dissecting dish containing 1X EBR. Excess food was rinsed off the larvae with a plastic pipette. Larvae were then transferred to an Eppendorf 2 ml tube and the excess EBR was removed with a yellow pipette tip. 300 μl of lysis EBR (1 X EBR, 10 mM EDTA, 10 mM DTT, 1:100 dilutions of the protease inhibitors PMSF, CLAP and Aprotinin), previously chilled on ice, was added and larvae were then homogenised for approximately 30 seconds- 1 minute with a Polytron homogenisor (Kinematica AG). 150 μl of 3X SDS-PAGE sample buffer plus 10 μl of 1M DTT (previously heated to 70°C) was added and the mixture immediately placed at 100°C for 10 minutes. A hole was pierced in the top of the tube to prevent pressure causing the cap to burst open. The heated sample was then spun for 2 minutes at 13,000 rpm in a benchtop microfuge (Heraeus Instruments 'Biofuge 13'). The supernatant was removed to fresh screw cap tube and either frozen at -20°C, or immediately prepared for loading on an SDS-PAGE gel.

In a 300 μl preparation of larval protein extract, I estimate that 15 μl is equivalent to 1 larva.

2.17 SDS-PAGE of Proteins

Two types of gel apparatus were used for electrophoresis of protein samples - Hoeffer Scientific Instruments 'Vertical Slab Gel Unit' rigs for large gels, and NuPage ready-made gels (Novex) for smaller gels - and the choice is indicated in the text where

relevant. This section only describes the set-up of larger SDS-PAGE gels. Novex mini-gels were set up and run to the manufacturers specifications.

Hoeffer Scientific Instruments 'Vertical Slab gel Unit' set up:

Two glass plates (16 cm X 18 cm) were washed with dH_2O, Decon (diluted 1:5 with dH_2O), dH_2O again, and finally rinsed with 100% ethanol and wiped dry with a paper towel. The glass plates were separated by 2 spacers, one at either end, and then clamped together with one end sealed with parafilm. Acrylamide gels were poured in between the glass plates from the top and allowed to set, the Resolving (Lower) gel first, followed by the Stacking (Upper) gel. The following tables describe the amounts of solutions used in a variety of final acrylamide percentages:

Resolving (Lower) Gel

Recipes for 1 - 1.5 mm thick gel (in bold text), or 1 - 0.75 mm thick gel. Lower buffer consists of 1.5 M Trizma base, pH 8.8. Acrylamide refers to a stock of 30% acrylamide:0.8% Bis-acrylamide (Severn Biotech Ltd.). AMPS is a 10% stock of Ammonium persulphate (Sigma).

	7.5%		*10%*		*12.5%*	
Lower buffer	**10ml**	5ml	**10ml**	5ml	**10ml**	5ml
Acrylamide	**10ml**	5ml	**13.3ml**	6.65ml	**16.7ml**	8.35ml
20% SDS	**200µl**	100µl	**200µl**	100µl	**200µl**	100µl
0.5 M EDTA	**80µl**	40µl	**80µl**	40µl	**80µl**	40µl
dH_2O	**19.72ml**	9.86ml	**16.42ml**	8.21ml	**13.02ml**	6.51ml
10% AMPS	**400µl**	200µl	**400µl**	200µl	**400µl**	200µl
TEMED	**40µl**	20µl	**40µl**	20µl	**40µl**	20µl

After pouring the gel, butanol saturated with 0.25 X lower buffer was layered over the top to help form an even interface between resolving and stacking gels. Resolving gels were allowed to polymerise for 15 to 20 minutes at room temperature. The butanol layer was then poured off, washed with dH_2O, and the stacking gel poured on top.

Stacking (Upper) gel

All stacking gels were made up in 10 mls containing:

Upper buffer	2.5 ml
acrylamide	1.33 ml
20% SDS	50 µl
0.5 M EDTA	20 µl
UREA to 8 M	4.8 g
H_20	to 10 ml
10% AMPS	100 µl
TEMED	10 µl

A plastic comb was placed at the top of the stacking gel to form the wells, and the gel was then allowed to polymerise for 15 minutes at room temperature. The polymerised gel slab was then fixed in position in the buffer tank, and 1X running buffer (25 mM Trizma base, 192 mM glycine, 1% SDS) was poured into the upper and lower buffer chambers. Protein samples containing 1X sample buffer (50 mM Trizma base, 2 mM EDTA, 2% SDS, 10% glycerol, 0.01% bromophenol blue in ethanol) and 100 mM DTT were boiled for 5 minutes, then loaded into the wells using a Hamilton syringe. 30 µl of a molecular weight marker (Protein Marker, Broad Range, New England Biolabs) was loaded in the first well. Gels were generally run at 55 V overnight at room temperature.

2.18 Transfer of SDS-PAGE gels

Proteins electrophoresed on SDS-PAGE gels were transferred to Protran nitrocellulose membrane (Schleicher and Schuell) in preparation for Western blotting. Prior to setting up for transfer, 4 L of Towbin transfer buffer was prepared (per litre: 800 mls dH_20, 3.025g Sigma 7-9 Tris, 14.425 g Sigma-Aldrich glycine, 200 mls methanol, 0.1% SDS - 4 litres of buffer was prepared first without SDS, 250 mls

decanted for use in soaking the Protran membrane, and 17.5 ml 20% SDS was then added to give a final concentration of 0.1%).

The blot was set-up within a cassette in a blotting tank (BioRad 'Trans-Blot') in the following fashion:

(- pole) - sponge - filter paper - gel - nitrocellulose - filter paper - sponge - **(+ pole)**

Blotting was performed at 55 volts at 4°C for 3 - 4 hours. The membrane was rinsed and subsequently stained with Ponceau-S (0.2% Ponceau-S in 3% TCA) for 5 minutes at room temperature with shaking. The Ponceau-S was rinsed off with water and the position of the molecular weight markers on the filter was marked unambiguously with a needle. The membrane was then either placed at 4°C for storage, or used immediately in a Western blot.

2.19 Western Blotting and Immunological Detection (ECL)

The membrane containing transferred proteins was placed in a plastic container and rinsed for 5 minutes with PBS-Tw (1 X PBS + 0.1% Tween 20), then blocked for 30 minutes -1 hour with Safeway dried skimmed milk (5% in PBS-Tw) at room temperature with shaking (40 ml for full gel). The membrane was then washed 2 x 3 minutes, 1 x 15 minutes, then 2 x 5 minutes with PBS-Tw (a minimum of 20 mls each wash).

Primary antibodies were incubated with the membrane in PBS-Tw for 60 minutes at room temperature, or overnight at 4°C (20 ml volume or less). The membrane was washed again - 2 x 3 minutes, 1 x 15 minutes, 2 x 5 minutes with PBS-Tw, before adding the appropriate HRP-conjugated secondary antibody, at a concentration of 1:10,000 diluted in PBS-Tw, for 60 minutes at room temperature. The final washes in PBS-Tw were 2 x 3 minutes, 1 x 15 minutes , 4 x 5 minutes.

Immunological detection of bands was performed using ECL reagents from Amersham:

To develop the blot, equal volumes of ECL reagents 1 and 2 were mixed (10 mls total for a full gel-sized membrane), then poured over the membrane which was placed in a plastic container. The mixture was allowed to sit for 1 minute and was then aspirated away. The nitrocellulose membrane was then placed face-down on a layer of cling-film, wrapped up, mounted on a piece of 3M Whatman filter paper, and placed in an autoradiography cassette. The mounted membrane was then exposed to Kodak XAR film in a dark room for a variety of times (usually 10 seconds, 30 seconds, and 1 minute), in order to detect any signal. Kodak XAR Films were developed in a Konica SRX-101A developer.

2.20 Protein expression in *E.coli*

Freshly transformed ER2566 bacterial expression cells were used for all expressed proteins.

50 ml overnight culture was grown at 37°C in LB plus 50 mg/ml ampicilin (amp). The following morning, 500 ml of LB + amp was inoculated with 5 - 7 mls of the overnight culture, and then grown at 37°C until it had obtained an OD600 of 0.8.

A 1 ml sample of this uninduced culture was taken, pelleted at 4000 rpm for 5 minutes in a benchtop microfuge, washed with 1 ml TEN (1 X TE + 100 mM NaCl), and then resuspended in 60 µl TE. 30 µl sample buffer and DTT were added immediately, and the mixture was then sonicated (approximately 1 second bursts for 30 seconds - 1 minute), and frozen at -20°C.

When the culture reached OD600 0.8, 1 mM IPTG (1 ml of a 500 mM stock) was added to induce expression of the recombinant protein. The cells were induced usually for 1 hour at least, although overnight induction was also used on occasion. A

further 1 ml aliquot of the induced culture was taken, and the cells were spun down and lysed as above.

The induced 500 ml culture was pelleted in 2 bottles, 250 mls in each, by spinning at 4000 rpm for 20 - 30 minutes at 4°C (Beckman JLA 10.500 rotor). The supernatant was then removed and poured back into the culture flask for subsequent autoclaving and disposal. Pellets were resuspended and pooled in 10 mls TEN (the combined volume for both pellets) in a 50 ml Falcon tube, then spun again at 4000 for 15-20 minutes at 4°C in benchtop centrifuge. The supernatant was then discarded and the tubes briefly inverted onto paper towels to drain completely. Pellets were frozen at -80°C for storage.

At this point, 10 µl aliquots of the uninduced and induced samples were run on SDS-PAGE to see if overexpression of the induced protein could be detected in the induced cell extracts.

2.21 Protein Purification using Ni-NTA beads (Batch Purification)

Frozen pellets of bacteria containing induced recombinant protein were thawed on ice for 10-20 minutes, with occasional vortexing. The pellets were weighed to determine the amount of Lysis buffer to be used (Total weight - [12 g for the tube] = pellet weight).

Pellets were lysed directly in their Falcon tubes with Lysis Buffer (8 M Urea, 5 mM Immidazole, pH 8.0) for 1 hour at room temp with moderate shaking (this was best done by attaching the tubes to a rotating platform), using 20 mls of Lysis Buffer per gram of pellet. After lysis the viscous solution was spun at 10,000 rpm for 20-30 minutes to pellet the cellular debris. The supernatant was collected, now termed the 'Cleared Lysate'. A 100 µl aliquot was then taken for analysis by SDS-PAGE.

Ni-NTA beads (Qiagen) were added to the Cleared Lysate (1 ml beads per 6 - 7 mls Cleared Lysate), and incubated for 1 hour at room temperature with shaking, as above. The beads were pelleted at 2000 rpm for 5 minutes in the benchtop centrifuge, and another 100 µl aliquot of the Flow Through was taken. The remaining Flow Through was discarded, or saved until the analysis was complete.

The beads were washed 3 times at room temperature with Wash Buffer (8 M Urea, 5 mM Immidazole, pH 6.3), on a shaker as above - twice with 10 mls, once with 5 mls. After the first 2 washes, the beads were spun down in benchtop centrifuge, a 100 µl aliquot was taken, then the rest was aspirated off. The 3rd wash was poured directly into a BioRad chromatography column and spun for 5 minutes at 2000 rpm. A 100 µl aliquot of the 3rd wash was taken, and the rest discarded.

Bound proteins were eluted from the beads by adding 0.5 mls Elution Buffer (either 8 M Urea, 5 mM Immidazole, pH 4.5 or 8M Urea, 500 mM Immidazole, pH 6.3) and spinning this through the BioRad column for 5 minutes at 2000 rpm directly into 1.5 ml Eppendorf. This was repeated for 5 or 6 elution fractions, and the beads then kept at 4°C afterwards, either for regeneration (see Qiagen protocol) or to strip off remaining bound protein by boiling in sample buffer. All fractions were stored at -20°C, and the various samples were analysed by SDS-PAGE, usually running 10 µl of Uninduced, Induced, Cleared Lysate and Flowthrough, 30 µl of each wash, and 50 µl of the Elution fractions.

2.22 Methanol/Chloroform precipitation of proteins

Per 100 µl of protein sample, the following was added:

400 µl Methanol
100 µl $CHCl_3$

300 µl dH_2O

The tube was vortexed after each step, and the final mix was then centrifuged for 2 minutes at 13,000 rpm in a benchtop microfuge. The upper phase was carefully removed (the protein lies at the interface) and 300 µl Methanol was added to the remaining protein fraction. The mix was again centrifuged for 2 minutes at 13,000 rpm, the supernatant was removed, and the pellet air-dried at room temperature. Proteins were resuspended in hot SDS-PAGE sample buffer.

2.23 Preparation of recombinant protein for injection into rabbits

Protein samples were electrophoresed on a preparative SDS-PAGE gel, i.e. a gel where all the sample is loaded into one large well, and run overnight as described previously. Gels were then rinsed 3 x 10 minutes in dH_2O, and stained with Aqueous Coomassie Blue (0.1% Coomassie Blue in Laemmli buffer [25 mM Trizma base, 192 mM Glycine]), for 60 minutes at room temperature with shaking, to visualise the band of recombinant protein. The gel was then destained for 3 X 10 minutes with Laemmli running buffer, and the desired band was excised using a razor blade. The band was cut into smaller strips, then ground to a fine powder using a ceramic mortar and pestle (Phillip Harris) which had been pre-chilled in the -80°C freezer and contained a small pool of liquid Nitrogen. Ground-up protein was placed into a 13 ml snap-cap tube and sent on dry ice to the Scottish Antibody Production Unit (SAPU) at Carluke Hospital, Lanarkshire, for injection into rabbits. All other aspects of antibody production were performed by SAPU.

2.24 DAPI staining of *Drosophila* neuroblast squashes

Third instar larvae were isolated from vials and washed in EBR in a dissecting dish to remove excess food. Individual larvae were then transferred to a new well containing EBR and the brain was dissected out by pulling the larva apart with forceps, and then dissecting away any surrounding tissue. Imaginal discs were also removed. Up to 5 brains were processed on one slide, so dissected brains were placed in a 3rd well of EBR until ready, but never for more than 10 minutes. The brains were then transferred with forceps to a well containing 0.5 X EBR to hypotonically swell the neuroblast cells, and then transferred to a 45% acetic acid drop (placed on a coverslip) to fix for 3 minutes. A clean polylysine-treated slide was placed on top of the cover slip, allowing it to be picked up. The brains were then squashed by pressing down on the inverted slide (placed between a folded Kim-Wipe) and immediately snap-frozen by dipping in liquid Nitrogen. The cover slip was breathed on to warm it, and then quickly flicked off with razor blade. The slide was placed into a Coplin jar containing PBS to rinse off any remaining fix, then transferred to a jar containing 0.1µg/ml DAPI stock in PBS + 0.05% TritonX-100 for 5-10 minutes. The slide was then washed by dipping into another jar containing PBS + 0.05% TritonX-100 (hereafter termed PBS-Tx) and dried on a Kim-Wipe. A coverslip was mounted using approximately 40 µl of Mowiol 4-88 (Calbiochem) in glycerol, and allowed to set for 30 minutes before viewing under the fluorescence microscope.

2.25 General protocol for antibody staining of larval brains

Unless otherwise specified, all immunofluorescence was observed using an Olympus AX-70 'Provis' fluorescence microscope, and digital images were captured using a cooled Charge Coupled Device (CCD) camera with Vysis QUIPS software on an Apple Macintosh 8600 PowerPC.

Third instar larvae were rinsed in EBR, brains were dissected as described in the section above, and were then hypotonically swollen for 3 minutes in 0.25X EBR. The brains were then fixed for 5 minutes in 4% paraformaldehyde (high quality from TAAB), 5% acetic acid, 0.1% TritonX-100 in 0.1725X EBR, by placing them in a drop on a siliconized coverslip. The coverslip was picked up using an inverted polylysine-treated slide, and the brains were squashed during the fix by pressing down repeatedly and very hard on the slide. Slides were dipped in liquid Nitrogen and the coverslips then flicked off as described above. The slide was placed immediately in PBS for 2 minutes, then permeablised for 3 X 10 minutes in PBS-Tx (PBS + 0.05% TritonX-100). Blocking was performed in 3% BSA in PBS for 1 hour at RT (normal goat serum has also been used - no difference was observed between the two blocking agents).

After blocking, the brains were washed for 5 minutes in PBS-Tx, then incubated overnight at 4°C in the primary antibody (or antibodies, if double or triple staining was being performed) diluted in PBS + 0.3% BSA. The slide was washed for 6 X 5 minutes in PBS-Tx, and incubated for 2 hours at room temperature in the appropriate secondary antibody diluted in PBS + 0.3% BSA. The slides were again washed for 6 X 5 minutes in PBS-Tx, and a further round of secondary antibody incubation was performed if more than one primary antibody had been used. The brains were also stained with DAPI (0.1 μg/ml) in PBS, in the second last wash. The slides were then drained and mounted in Mowiol, allowing 30 minutes for the Mowiol to set, and examined under the fluorescence microscope.

2.26 α-tubulin staining of larval brains

Three methods were used for fixation of *Drosophila* neuroblasts for detection of mitotic spindels by α-tubulin staining, as detailed in Chapter 3. In all cases, the α-tubulin antibody used was a mouse monoclonal from Sigma, at a dilution of 1:100.

Secondary antibody detection was as described in Chapter 2.25, using Alexa secondaries (Molecular Probes). These three methods are outlined below:

Formaldehyde fixation in NKHE buffer:

This method of fixation was performed in a similar manner to the general protocol described in Chapter 2.25 above, with the following modifications:

Brains were dissected in NKHE buffer (130 mM NaCl, 4.7 mM KCl, 10 mM HEPES, pH6.9, 5 mM EGTA) without hypotonic swelling. Fixing was performed on a siliconized coverslip in 4% PFA in NKHE buffer for 10-15 minutes. After the first 2 minutes in fix, the brains were squashed very hard onto a polylysine slide, and the squash repeated several times during the fix. Incubation of primary antibody(ies) was performed as in Chapter 2.25, in PBS-Tx + 0.3% BSA overnight at 4°C. Secondary antibodies were incubated in PBS-Tx + 0.3% BSA at 1:500 dilution for 2 hours at room temperature, or 1 hour at 37°C. DAPI was included in the second-last wash as described previously.

Methanol fixation

Brains were dissected in EBR without hypotonic swelling, then placed in a drop of 0.5% acetic acid in dH_2O on a siliconised coverslip and immediately squashed onto a polylysine slide. The coverslip was removed after freezing in liquid nitrogen as detailed above, and the slide then placed in Methanol + 5 mM EGTA at -20°C for 10 minutes. The brains were then washed 5 minutes in PBS at room temperature, permeabilised in PBS-Tx for 3 x 10 minutes, blocked for 1 hour at room temperature in PBS + 3% BSA, and washed again for 5 minutes in PBS. Incubation in primary antibody was overnight at 4°C in PBS-Tx. Washes, secondary antibody incubation and DAPI staining were performed as outlined in Chapter 2.25.

Bonaccorsi *et al.* fixation protocol

This protocol for analysis of mitotic spindles in Drosophila neuroblasts was adapted from Bonaccorsi et al. (2000), Nature Cell Biology 2, 54-56.

Brains were disected from 3rd instar larvae in EBR as detailed above, then fixed in 4% PFA in PBS for 30 minutes at room temperature in a dissecting dish. Following this, the brains were transferred to another well containing 45% acetic acid fro 3 minutes, then transferred to a drop of 60% acetic acid on a siliconised coverslip and squashed gently onto a polylysine slide. Coverslips were then removed after freezing in liquid nitrogen, and the slides placed in Ethanol at -20°C for 10 minutes. The brains were then permeabilised in PBS + 0.1% TritonX 100 for 10 minutes at room temperature, washed twice in PBS, and then blocked for 1 hour in PBS + 3% BSA. Primary and secondary antibody incubations, washes and DAPI staining were performed as described above.

2.27 TUNEL labelling of larval brains (Apotag kit)

In order to detect apoptotic nuclei, the Apotag kit (Appligene Oncor), which utilises TdT-mediated dUTP nick end labeling, was used to stain third larval instar brains. The following protocol, adapted from the manufacturers instructions, was used:

Third instar larval brains were dissected, hypotonically swollen and fixed as detailed in Chapter 2.25 above. The brains were then washed for 2 minutes in PBS, and 75 µl of Equilibration buffer was added per slide for 10-30 seconds. The buffer was drained off and 55 µl of working TdT enzyme solution was added for 1 hour at 37°C under a plastic coverslip. The slides were then washed in 35 ml Stop/Wash solution in a Coplin jar for 10-15 minutes.

For the subsequent immunodetection, a mouse anti-digoxigenin antibody (Boehringer) followed by an anti-mouse Alexa 488 secondary was used to detect the reaction rather than the supplied sheep anti-digoxigenin antibody-FITC conjugate, as

this allowed a stronger signal to be detected. Application of primary and secondary antibodies was identical to the above protocol for General Immunofluorescence of larval brains.

2.28 Whole mount staining of larval brains

Third instar larval brains were dissected in PBS, then fixed in 1 ml fixing solution (3.7% Formaldehyde, PEMS [0.2 M PIPES, 4 mM MgSO4, 2 mM EDTA, pH 6.9]) in a dissecting dish for 15 minutes at room temperature. After fixing, the brains were transferred to another well containing 1 ml of PBS-Tx (PBS + 0.1% TritonX 100). This wash was repeated twice, followed by a block of 1 hour in PBS-Tx + 3% BSA. The larval brains were then transferred to a new well containing primary antibody at the appropriate concentration, diluted in PBS-Tx, and the dish was placed on a rocking platform at 4°C overnight (if performing double or triple staining, all the primaries were incubated together). The next morning, the brains were washed 3 times in PBS-Tx, again by transferring to new wells for each wash, and then incubated in secondary antibody at the appropriate concentration diluted in PBS-Tx, for at least 1 hour at room temperature (again, all secondaries were incubated together if more than one was required). Finally, the brains were washed 3 times in PBS-Tx, stained with DAPI (0.1 μg/ml) diluted in PBS-Tx for 10 minutes at room temperature, washed again in PBS-Tx, and mounted on a clean slide in a drop of 80% glycerol or Mowiol. The mounting agent was allowed to sit for 15-20 minutes at room temperature before viewing the brains under the fluorescence microscope.

2.29 BrdU labelling of whole mount brains

This protocol was performed as per the protocol above, with the following modifications:

Larval brains were dissected in a drop of Schneiders *Drosophila* medium, then transferred to Schneiders medium plus 12 μg/ml of BrdU (Boehringer Mannheim) and incubated at room temperature for the required timepoint, as stated in the text. Brains were fixed for 15 minutes in 4% PFA in PBS, rinsed 3 X 5 minutes in PBS-Tx, and then blocked for 45 minutes - 1 hour in 3% BSA in PBS. Following the block, the brains were incubated in fresh 2N HCl for 45 minutes (to nick the DNA and allow subsequent detection of incorporated BrdU), rinsed 3 X 5 minutes in PBS only, and finally incubated in rat anti-BrdU antibody (1:2 dilution, Harlan Sera) overnight at 4°C. Further washes and secondary antibody (anti-rat Alexa 488, Molecular Probes) detection was performed as detailed in the section above.

2.30 Preparation of embryos for immunofluorescence

A collection cage containing the appropriate fly stock was set up for an overnight collection on red wine concentrate agar, with a dollop of wet yeast placed in the center. The following morning, the plate was removed and the embryos were rinsed into a microsieve with dH_2O, using a large paintbrush to brush the embryos into the sieve. The embryos were rinsed again in dH_2O to remove any adherent yeast, then dechorionated in fresh 1:1 [bleach:dH_2O] for 2-3 minutes. The bleach was rinsed off with dH_2O, and the embryos placed in 10 mls of 50% heptane, 3.7% formaldehyde in PBS to fix. A bottle setup (scintillation vial with microsieve placed over the neck, and then sealed with a cap) was used to fix the embryos for 15-20 minutes at room temperature with shaking (by taping the bottle to a rotating platform). After fixing, the formaldehyde (bottom layer) was removed, and 10 mls of cold methanol was added. The bottle was shaken very hard to devitillenise the embryos, which then sank to the bottom of the bottle and could be drawn off using a Pasteur pipette. The devitillinised embryos were placed into a fresh Eppendorf, washed twice with cold methanol, and then stored in 100% methanol at -20°C until required.

2.31 Antibody staining of *Drosophila* embryos

Adapted from Theurkauf and Heck chapter on Identification and Characterization of Mitotic Mutations in Drosophila, Methods in Cell Biology Vol. 61, pp317-346.

Stored embryos were rehydrated through a methanol series by transferring them through 100%, 75%, 50%, and 30% methanol in PBS, followed by 100% PBS and finally PBS + 0.1% TritonX-100. An appropriate amount of primary antibody was then added, diluted in PBS, and the embryos placed on a rotating wheel at 4°C overnight, or for 2 hours at room temperature. The embryos were rinsed 4 X 15 minutes in PBS-Tx before adding the appropriate secondary antibody, diluted in PBS, for 2 hours at room temperature. The embryos were washed again 3 X 15 minutes, stained with DAPI in PBS-Tx (0.1 μg/ml) for 5 minutes, then rinsed again in PBS-Tx for 15 minutes. In order to mount the embryos, they were allowed to settle, most of the wash solution was drawn off, and the remaining 100 - 200 μl containing the embryos was removed using a P1000 tip. The embryos were pipetted onto a clean slide and the excess PBS removed by capillary action using a Kim-Wipe. 40 μl of 80% glycerol was then added onto the embryos, and a coverslip was placed on top and allowed to set for 30 minutes before viewing under the fluorescence microscope.

2.32 Antibody staining of *Drosophila* cultured cells for RNAi

Drosophila S2 and Dmel2 cells were grown on Permanox Chamber Slides (Lab-Tek) for the timepoints indicated in the text. The cells were then spun at 4000 rpm in a benchtop centrifuge fitted with a slide-holder for 10 minutes at room temperature. Cells were fixed in the chambers using 4% PFA in PBS for 3 minutes. The separating chambers were then removed, and the cells were permeabilised by dipping the slide into 1% TritonX-100 in PBS for 1 minute, followed by 2 X 10

minute incubations in 0.05% TritonX-100 in PBS (this harsh permeabilisation allows better visualisation of the centrosomal antibody CP190, used in the RNAi experiment, without disrupting the other antibodies used). The cells were blocked for 1 hour in 3% BSA in PBS at room temperature, followed by a 5 minute wash in PBS-Tx. Incubation of the required primary antibodies (diluted in 0.3% BSA in PBS) was overnight at 4°C. The cells were then washed 6 X 5 minutes in PBS-Tx, followed by secondary antibody incubation for 1 hour at 37°C (each secondary antibody was incubated separately). Final washes were 6 X 5 minutes in PBS-Tx, with the second last wash containing 0.1 μg/ml DAPI, and the slides were mounted in Mowiol-glycerol.

2.33 DAPI staining of polytene chromosome preparations

Salivary glands were dissected from wandering 3rd instar larvae (previously fattened with wet yeast) in EBR and fixed in a drop of 45% acetic acid on a polylysine slide for 30 seconds. The glands were then transferred to a drop of lactic acid:dH_2O:glacial acetic acid (in a ratio of 1:2:3) with 5% glycerol on a siliconised coverslip for 4 - 5 minutes. Squashing of the salivary glands was performed by picking up the coverslip with a clean polylysine slide, and tapping on the inverted side. After subsequent freezing in liquid Nitrogen, the coverslip was flicked off with a razor blade, and the slide was then immersed in PBS for 2 minutes. To stain, the slide was incubated in PBS-Tx + 0.1 μg/ml DAPI for 5 minutes at room temperature. After a final rinse in PBS-Tx for 3 minutes, the glands were mounted in Mowiol-glycerol, allowed to set for 30 minutes, and viewed under the Olympus Provis fluorescence microscope.

2.34 Antibody staining of polytene chromosomes

Adapted from Whitfield et al.(1995), Journal of Cell Science 108, 3377-3387.

Salivary glands were dissected from wandering 3rd instar larvae in EBR, and fixed in 45% acetic acid, 3.7% PFA for 2 - 3 minutes on a siliconised coverslip. The chromosomes were then spread as detailed in the above section, by picking up with a polylysine slide and tapping on the inverse side. The coverslip was flicked off after freezing in liquid Nitrogen, and the slide then incubated for 5 minutes in PBS. After draining the slide, the primary antibody was incubated on the slide for 1 hour at room temperature, diluted appropriately in PBS + 3% BSA. Following the primary incubation, the slide was washed 5 X 5 minutes with PBS, followed by the secondary antibody incubation for 1 hour at room temperature, also diluted in PBS + 3% BSA. The slide was then washed 5 X 5 minutes in PBS again, the second last wash containing 0.1 μg/ml DAPI, and was mounted in Mowiol-glycerol. Stained chromosomes were visualised under the Olympus Provis fluorescence microscope.

2.35 LacZ staining of larval tissues

Wandering third instar larvae were isolated from vials, and tissues were dissected as described above. Dissected tissues were placed into a multi-well polystyrene plate, rinsed once with PBS, then fixed in 3.7% formaldehyde/0.1% glutaraldehyde in PBS for 10 minutes at room temperature. The tissues were rinsed 2 X 5 minutes in PBS followed by 1 X 5 minute rinse in PBS + 0.1% TX-100. Equilibration was in staining solution (10 mM NaH2PO4/ Na2HPO4 (pH 7.2), 150 mM NaCl, 1 mM MgCl2, 3.1 mM K_4 [$Fe^{II}(CN)_6$], 3.1 mM K_3 [$Fe^{III}(CN)_6$], 0.3% TritonX-100) for 2 - 3 minutes. The tissues were then transferred to staining solution containing 1/30 volume of 8% X-gal in DMF, and left to stain for as long as desired at 37°C.

Following staining, the tissues were rinsed twice with PBS + 0.1% TX-100, twice with PBS, then placed in 50% glycerol in PBS. The dish was incubated again at 37°C for a minimum of 2 hours, to dissolve the crystals of X-gal. Finally, the tissues

were mounted in 50% glycerol in PBS, and the coverslip was sealed with nail polish. Examination of stained tissues under appropriate magnification was performed using the Provis microscope, and photography was performed using Kodak Ektachrome 160 colour slide film, with an exposure series at 1/3 from +2 to -2.

2.36 Preparation of double stranded RNA from PCR templates

This protocol was kindly communicated to us by Tom Kaufman.

Template DNA was prepared by PCR, as detailed in Chapter 5, and was designed to incorporate a 5' T7 RNA polymerase binding site on either end. This dsDNA template was then purified using the MoBio PCR Clean-Up Kit, and used for RNA synthesis.

RNA synthesis from the PCR template was achieved using the MEGAshortscript T7 kit (Ambion), according to the manufacturers instructions with the following amendments:

Per reaction -
- 2 µl of 10X Reaction Buffer
- 2 µl each of ATP, CTP, GTP, UTP mixes
- 2 µl of enzyme mix
- 1 µg total of template DNA
- up to 20 µl with Nuclease-free dH_2O

This reaction was incubated at 37°C for 4 hours, followed by precipitation of the RNA by 1/10th volume sodium acetate, 2.5 volumes 100% ethanol. The pellets were air dried and resuspended in 40 µl of Nuclease-free dH_2O.

To prepare dsRNA, the resuspended pellets were heated to 65°C for 30 minutes, then placed in a 65°C water bath which was then allowed to cool slowly to room temperature. The concentration of dsRNA was checked by spectrophotometry, using the calculation that an OD260 of 1 = 45 µg/ml of dsRNA. An aliquot of dsRNA

was also electrophoresed on a 1% agarose gel. Finally, the dsRNA was stored at -20°C until required.

2.37 Injection of *Drosophila* embryos with plasmid DNA

(For the purpose of creating germline transformants.)

Preparation of embryos

A 30 minute collection of w^{1118} embryos was used for each injection cycle. The embryos were washed off the laying plate into a sieve with dH_2O, and dechorionated in fresh 50% bleach in dH_2O for 2-3 minutes. The sieve was then rinsed well with dH_2O and blotted dry with a paper towel. The embryos were transferred to an agar slice and lined up under a light microscope with their anterior ends pointing to the right, normally 40 - 50 embryos per agar slice. The embryos were then picked up using a coverslip with one end coated in heptane glue, so that the posterior ends were now facing away from the edge of the coverslip. The coverslip was attached to a slide by a drop of Halocarbon oil and placed in a drying chamber for 5 -10 minutes at room temperature to desiccate the embryos. After desiccation, the embryos were covered with a layer of heavy Halocarbon oil, series 700 (Halocarbon Products Company), and placed on the injecting apparatus for injection.

Preparation and injection of plasmid DNA

Constructs for injection were cloned into the pUAST transformation vector as described elsewhere. In preparation for injection, 500 ng of the construct was co-precipitated with 250 ng of pUCHS πΔ2-3 helper plasmid (hereafter termed Δ2-3) in a total volume of 20 µl by adding $1/10^{th}$ volume of 3 M Sodium acetate and 2 volumes of 100% Ethanol, incubating on ice for 10 - 15 minutes, spinning at 13,000 rpm at 4°C

for 10 minutes. The pellet was washed with 70% Ethanol, spun again at 13,000 rpm for 5 minutes, dried at room temperature, and finally resuspended in 10 µl dH_20. Prior to injection, 10 µl of 2X Injection Buffer (0.2 mM $NaPO_4$, 10 mM KCl, pH 7.8) was added.

A femtotip needle (Eppendorf) was loaded with 2 µl of co-precipitated pUAST-construct and Δ2-3 in 1 X Injection Buffer, using a microloader pipette tip (Eppendorf). Bubbles were avoided by loading the mix as close to the base of the needle as possible. The needle was fixed to the injecting apparatus in the 18°C constant temperature room, and focused so as to be level with the prepared embryos lined up on a sticky-coverslip (see procedure above). Only embryos earlier than stage 3 (i.e. pre-pole cell formation) were injected - older ones were destroyed by running through with the needle. After injecting, the coverslip was removed and placed in a small weighing boat. The embryos were covered with Halocarbon oil series 95, and left in the 18°C room to recover and hatch. Hatched larvae were harvested and placed in fresh vials of Dundee mix fly food, no more than 20 larvae per vial. Eclosed flies were then back-crossed to w^{1118} flies to test for transformants, as described in the text.

Chapter 3
Phenotypic characterisation of *l(3)IX-14*

Chapter 3 Summary

l(3)IX-14^{1} is a late larval lethal mutation which was generated in a chemical mutagenesis screen in 1971 (Shearn *et al.*, 1971). It was then further characterised first by Gatti and Baker in a study addressing late larval lethal mutants in *Drosophila*, then by a previous Ph.D. student in this laboratory, Sue Ann Krause. However, this earlier work went little further than determining the basic mitotic chromosome phenotypes described in the Introduction. I therefore initiated a more detailed phenotypic analysis of various aspects of this unusual mutation, with regard not only to chromosomal morphology but also investigating the state of other important cell division machinery. I found that some characteristic aspects of mitosis appear normal in *l(3)IX-14*^{1}, such as the phosphorylation of Histone H3 and the dissociation of nuclear lamins (both specific to mitosis). Nevertheless, there appeared to be an increase in the levels of apoptosis in mutant neuroblasts, and replication timing was also seen to be affected. Furthermore, a distinct increase in the ratio between the mitotic index of these cells and the numbers of P-H3 positive cells (i.e. marked for mitosis) suggested a cell cycle block earlier than metaphase (perhaps late G2). Examination of other cell division processes revealed that centrosome duplication and/or separation was defective, as was mitotic spindle formation in these mutants. This suggested that the *l(3)IX-14*^{1} gene product may be playing a role in more processes than was previously thought. Finally, investigation into the structure of endoreduplicated polytene chromosomes in *l(3)IX-14*^{1} showed these were also profoundly affected, as they were smaller than their wild type counterparts and had become structurally distorted and had lost their characteristic banding pattern. I showed however that although these chromosomes were severely affected in *l(3)IX-14*^{1}, they were still able to bind certain chromosome-associated

factors such as CP190. Thus it may be that the polytene chromosome phenotype reflects mainly a combination of replication and packaging defects, although this study does not further investigate these possibilities.

3.1 Histone H3 Phosphorylation of condensed mitotic chromosomes is normal in *l(3)IX-14^{1}* neuroblasts

l(3)IX-14^{1} neuroblasts have a distinct chromosome condensation defect, namely that of hypercondensed mitotic chromosomes that appear to have a halo of loosely condensed chromatin surrounding them (introduced in Chapter 1). I investigated whether this phenotype was due to improper phosphorylation of Histone H3, a well characterised event correlated with the commitment to mitosis in late G2 and chromosome condensation (Gurley et al., 1975; Hendzel et al., 1997; Van Hooser et al., 1999; Wei et al., 1999). Neuroblasts from wild type and *l(3)IX-14^{1}* homozygous third instar larvae were stained with a rabbit polyclonal antibody raised to the Serine-10 phosphorylated form of Histone H3 (Upstate Biotechnologies) - hereafter annotated as P-H3. This staining was performed on brains fixed in 4% PFA, 10% acetic acid to allow for good chromosome morphology (the 10% acetic acid allows the brains to be squashed to a monolayer more easily, and does not affect P-H3 staining of mitotic chromosomes). Figure 3.1 shows typical mitotic figures observed in wild type and *l(3)IX-14^{1}* homozygous neuroblasts. The mutant panels show the characteristic hypercondensed mitotic chromosome phenotype prevalent in *l(3)IX-14^{1}* homozygotes, and it can be seen that the entire chromosomes are stained apparently normally. Other late larval lethal *l(3)IX-14^{1}* alleles, i.e. *l(3)IX-14^{4Y7}* (also shown in Figure 3.1) and *l(3)IX-14^{eB}*, have identical phenotypes to the chemically induced *l(3)IX-14^{1}* allele and also have normal P-H3 staining. It appears therefore that phosphorylation of Histone H3 is not affected in *l(3)IX-14* mutants, and that this process is not linked to the aberrant phenotypes observed.

Figure 3.1 P-H3 staining of larval neuroblasts

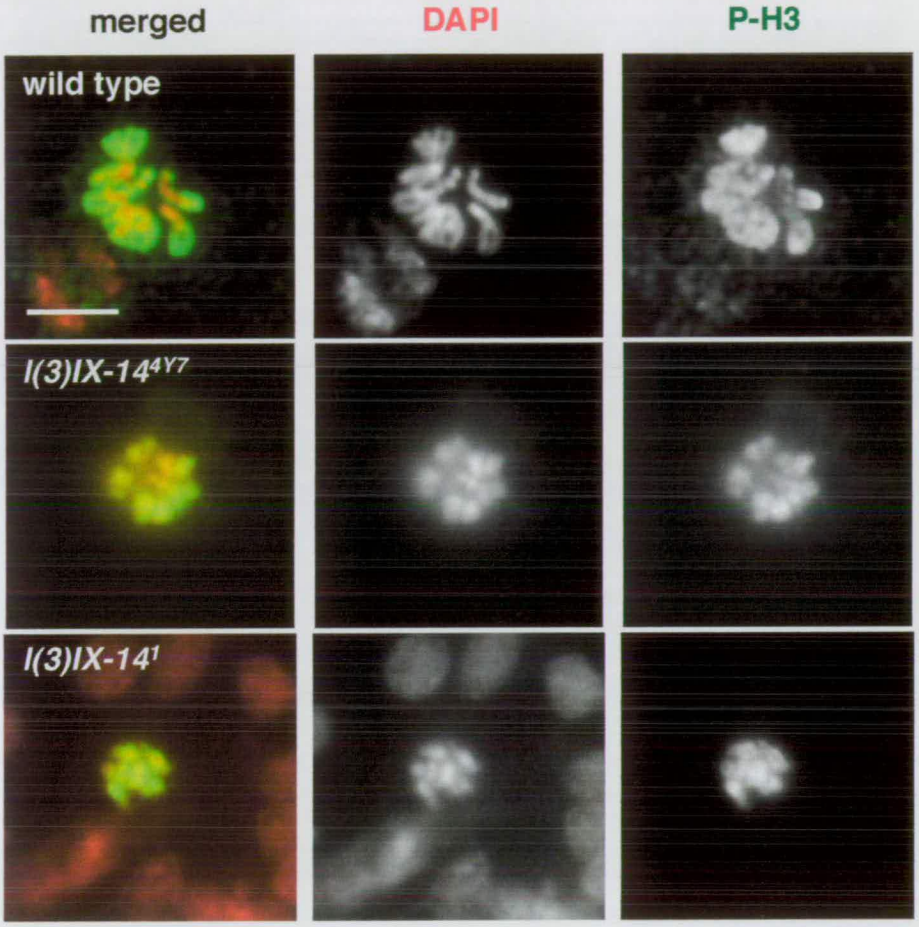

Figure 3.1 - Squashed preparation of 3rd instar brains from wild type, *l(3)IX-14* and *l(3)IX-14^{4Y7}* larvae. Brains were hypotonically swollen in 0.25X EBR, followed by fixation in 4% PFA, 10% acetic acid to allow for a better spread. Anti-phosphorylated Histone H3 (P-H3, rabbit polyclonal from Upstate Biotechnologies, 1:1000 dilution) staining is shown false-coloured in green, DAPI staining in red. Images were captured at 100X magnification. Scale bar = 2.5μm.

Figure 3.2 P-H3 staining of whole mount brains. 3rd instar larval brains from wild type and *l(3)IX-14*^{1} homozygotes were dissected and fixed in 4% PFA in PBS. The brains were then incubated in anti-P-H3 (1:1000) overnight at 4˚C, followed by a mouse anti-rabbit Alexa 594 secondary antibody. Images were captured at 40X magnification in the red (P-H3) channel only (scale bar = 200μm).

Figure 3.3 BrdU staining of whole mount brains. Dissected 3rd instar larval brains were labelled with 12 μg/ml BrdU for 2 hours at room temperature, nicked in 2 N HCl for 30 minutes, then fixed in 4% PFA in PBS. Staining with rat anti-BrdU was performed overnight at 4˚C, followed by a goat anti-rat Alexa 488 secondary. Panels A and C were captured at 40X magnification (scale bar = 200μm), panels B and D show the areas boxed in white at 100X magnification (scale bar = 10μm), both in the green channel only.

Figure 3.2 P-H3 staining of whole mount brains

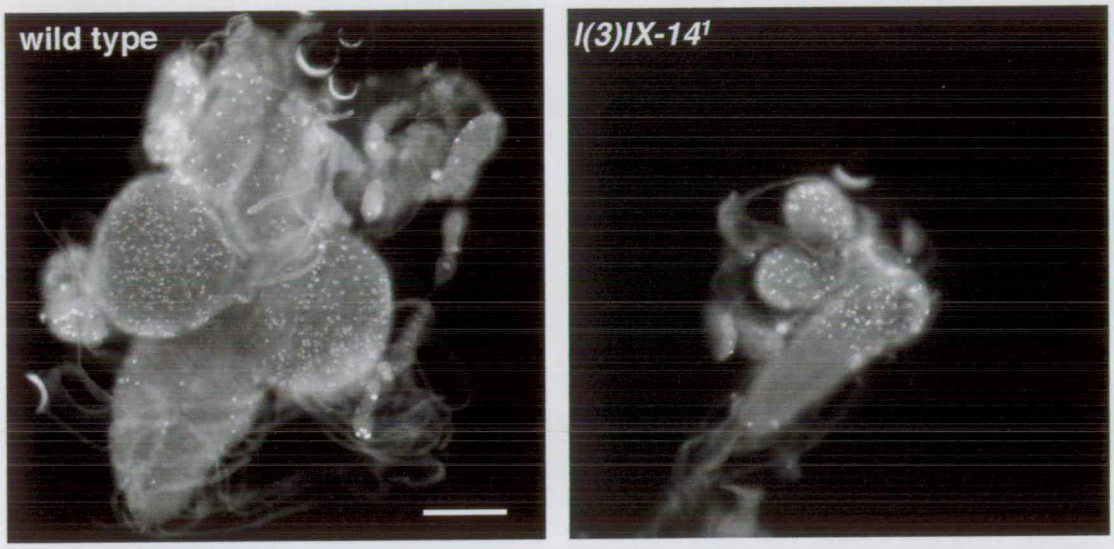

Figure 3.3 BrdU staining of whole mount brains

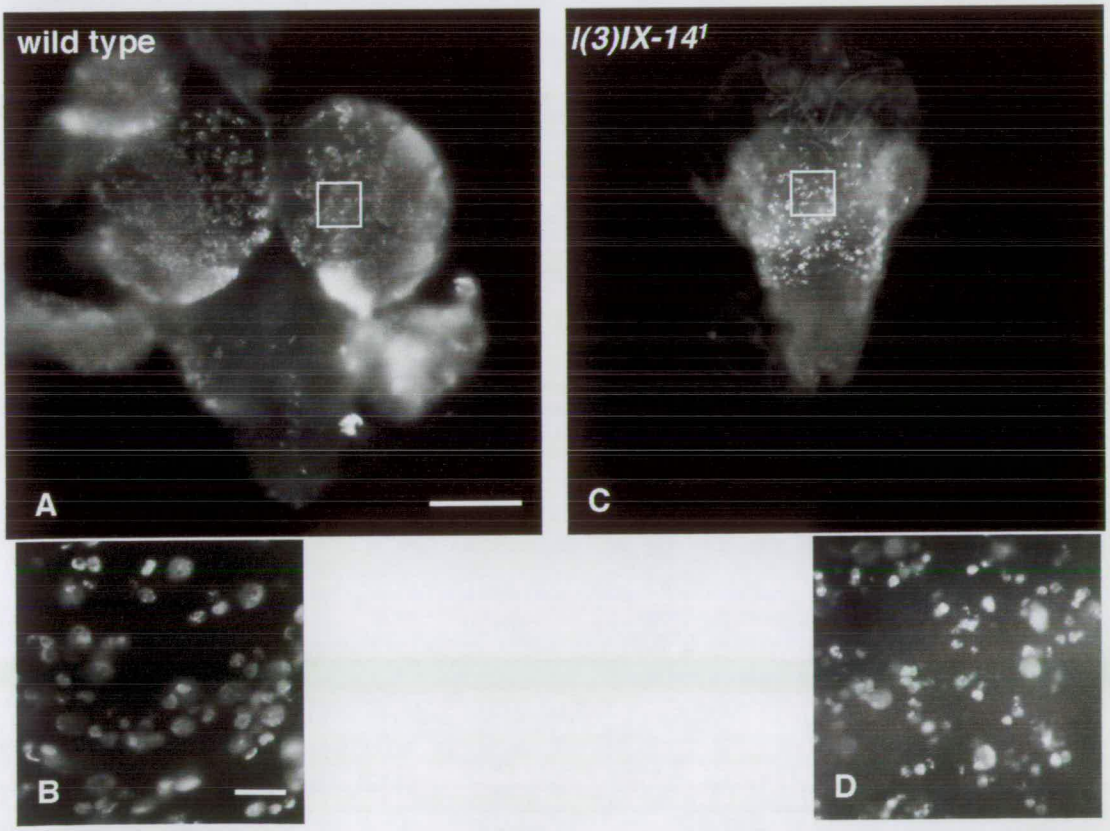

3.2 Comparison of Mitotic Index and Phosphorylated Histone H3 levels in wild type and *l(3)IX-14^1* homozygous neuroblasts

A previous study of *l(3)IX-14^1* by Gatti and Baker (1989) had reported that this mutant was characterised by a metaphase arrest. My observations of DAPI stained neuroblasts from *l(3)IX-14^1* homozygotes confirmed that very few anaphase figures are observed in 3rd instar larval brains from this mutant, consistent with a metaphase arrest. However, measurements of the Mitotic Index (M.I.) of mutant neuroblasts from third instar larvae, initially performed by Sue Ann Krause (Ph.D. thesis, 1999) but later repeated by myself (shown in Table 3.1), have shown that the M.I. of these cells is substantially lower than that of wild type, signifying that a metaphase arrest is not occurring.

An intriguing result obtained from the P-H3 staining of mutant neuroblast squashes and whole-mounts appears at first to be in contradiction to the observed low M.I. Whole mount staining of *l(3)IX-14^1* 3rd instar larval brains with anti P-H3 (see Figure 3.2) showed that *l(3)IX-14^1* brains appear to have obvious proliferation defects such as much-reduced size compared to wild type and missing imaginal discs. Nevertheless, it appeared that a substantial proportion of the mutant cells were P-H3 positive, relative to the smaller brain size.

In order to quantify this, I counted the number of P-H3 positive cells relative to the total number of DAPI stained nuclei in a range of brains from wild type and *l(3)IX-14^1* 3rd instar larvae. The results, shown in Table 3.1, indicate that the percentage of cells staining positive for P-H3 in *l(3)IX-14^1* mutants is relatively close to the number seen in wild type. When compared with the low M.I. (measured from the same slides, counting only in the DAPI channel) this result implies that *l(3)IX-14^1* may arrest or delay in late G2, with only a small proportion of these cells are able to continue on to a

state of mitotic chromosome condensation. Alternatively, a large fraction of these mutant cells may abort their attempts at cell division and exit mitosis prematurely without proceeding through anaphase, perhaps activating an apoptotic pathway (see Chapter 3.4).

Table 3.1

Comparison of various aspects of proliferation in wild type versus *l(3)IX-14^1* neuroblasts.

allele	Mitotic Index (%)	P-H3 positive (%)	Ratio P-H3 M.I.	BrdU positive (%)	Ratio BrdU M.I.	TUNEL positive (%)
wild type	0.75	1.7	2.3	14.6	19.5	0.28
l(3)IX-14^1	0.29	1.4	4.8	5.2	17.9	1.26

3.3 Replication defects in *l(3)IX-14^1* neuroblasts

I tested whether the proliferation defects observed in *l(3)IX-14^1* mutant neuroblasts were linked to a replication defect, by examining Bromodeoxyuridine (BrdU) incorporation. BrdU is a thymidine analogue that, once incorporated into DNA during replication, can be detected immunohistochemically. BrdU incorporation into larval neuroblasts can be accomplished in two ways, either by feeding the larvae on food containing BrdU, or by dissecting the brain and incubating it directly in a BrdU-containing solution. I originally attempted the feeding method, which has been proven to work well for other studies in this laboratory. However, whilst the wild type control larvae fed normally on the treated food, the *l(3)IX-14^1* homozygotes did not. No homozygotes appeared to have eaten after having been in the food overnight, as judged

by the absence of any food colouring in the gut. I therefore proceeded with the direct incubation of larval brains in a BrdU solution.

Figure 3.3 shows whole mounts of third instar brains from wild type and *l(3)IX-14*^{1} homozygous larvae after a 2 hour incubation in a 12 μg/ml solution of BrdU, and subsequently stained with a rat anti-BrdU monoclonal antibody. In the wild type brain in panel A, it can be seen that the proliferating zones of the optic lobes are extensively labelled, and a magnified image of that area (Panel B) shows that BrdU appears to be incorporated evenly in these cells. In comparison, the mutant figures shown in Panels C and D also show incorporation of the drug into similar areas as wild type. However, neither the pattern nor the extent of incorporation appears to mirror that of wild type, and the higher magnification panel clearly shows a range in the amount of incorporation, with many cells only appearing to have incorporated very small amounts of the drug. Since all the brains have been incubated in BrdU for the same length of time, and that incorporation levels in the mutant are substantially lower, there may be fewer cells replicating. Alternatively, perhaps the rate of progression through replication is slowed down. I therefore quantified the numbers of replicating cells in wild type compared to *l(3)IX-14*^{1} mutant brains. The brains were labelled by incubating in 12 μg/ml BrdU for 2 hours, making squashed preparations of the brains, and detecting incorporation by anti-BrdU staining. The number of BrdU-labelled cells was divided by the total number of cells counted to give the percentage of replicating cells. Images were taken from a range of 4 brains each from wild type and *l(3)IX-14*^{1} homozygotes. The results, presented alongside the M.I. and P-H3 results in Table 3.1, clearly show that replication in *l(3)IX-14*^{1} is occurring at much reduced levels. After 2 hours in BrdU, almost 15% of wild type cells have incorporated the marker, as opposed to only 5% in the mutants. However, the ratio of BrdU positive cells to the M.I. is similar in wild type and in *l(3)IX-14*^{1} mutants. This is again suggestive of a block or delay in the cell cycle at an earlier stage than mitosis, which may be producing the general proliferation defects observed in *l(3)IX-14* alleles.

3.4 TUNEL labelling shows an elevated level of apoptosis in *l(3)IX-14^{1}* homozygote brains

l(3)IX-14^{1} mitotic cells almost never undergo anaphase chromosome segregation, nor do I see a significant rise in polyploidy in *l(3)IX-14^{1}* which would imply that the mitotic chromosomes decondense and the cells enter another cell cycle. However, the results presented in Chapter 3.2 indicate that an almost normal level of P-H3 staining in these brains (relative to their decreased size). What then can account for the low M.I. observed? Since *l(3)IX-14^{1}* cells do not appear to arrest in mitosis, I hypothesised that they may instead be triggering an apoptotic pathway.

I tested for elevated levels of apoptosis in *l(3)IX-14^{1}* by TUNEL labelling of 3rd instar homozygous brains, compared to wild type brains, using the Apotag TUNEL labelling kit as described in the Methods section. Figure 3.4 shows a selection of typical apoptotic bodies observed in wild type and *l(3)IX-14^{1}* TUNEL labelled brains. Table 3.1 (see above section) shows that the number of apoptotic bodies observed in *l(3)IX-14^{1}* homozygotes in significantly higher than that observed in wild type brains. From this study I conclude therefore that *l(3)IX-14^{1}* cells commit to mitosis normally, as shown by the relatively normal frequency of P-H3 positive nuclei. The cells may then arrive at metaphase with improperly condensed chromosomes, and instead of triggering a mitotic arrest are directed into an apoptotic pathway, accounting for the low M.I. and high levels of TUNEL positive nuclei.

3.5 The nuclear lamina is dissociated normally in *l(3)IX-14^{1}* mitotic neuroblasts

In order to determine whether the nuclear envelope was disassembled normally in *l(3)IX-14^{1}* mutants, homozygous neuroblasts were stained with a mouse anti-lamin antibody and compared to wild type preparations. Figure 3.4 shows that anti-lamin

Figure 3.4 TUNEL staining of larval neuroblasts

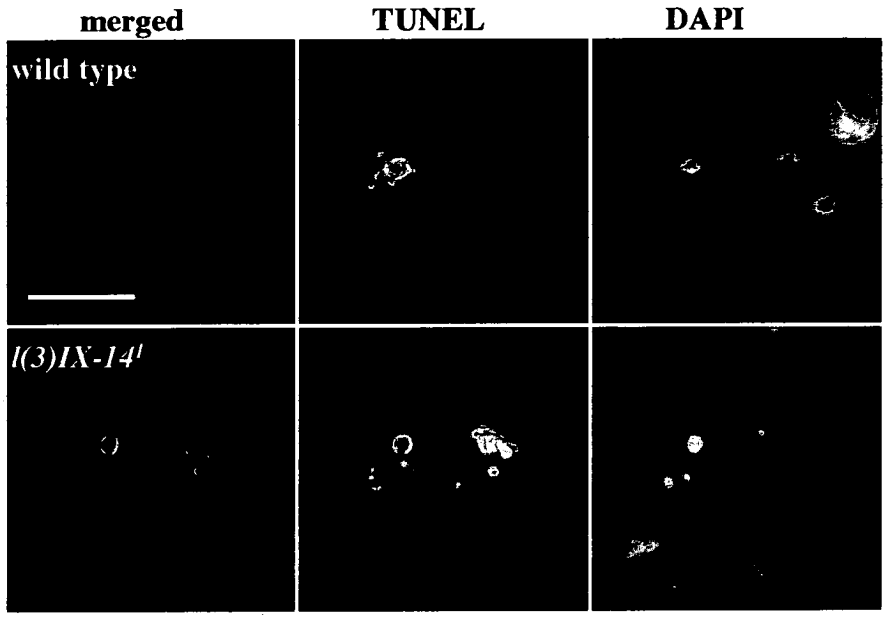

Figure 3.4 - TUNEL labelling of larval neuroblasts. Images show representative staining of apoptotic bodies in wild type and *l(3)IX-14*^{1} mutant neuroblasts. Squashed preparations of 3rd instar larval brains were fixed in 4% PFA, 10% acetic acid in PBS and TUNEL labelled using the Apotag kit from Appligene Oncor. TUNEL labelling was detected by incubation at 4°C overnight with a mouse anti-digoxigenin antibody, followed by a rabbit anti-mouse Alexa 488 secondary. Images were captured at 100X magnification, scale bar = 5μm.

Figure 3.5 anti-lamin staining of larval neuroblasts

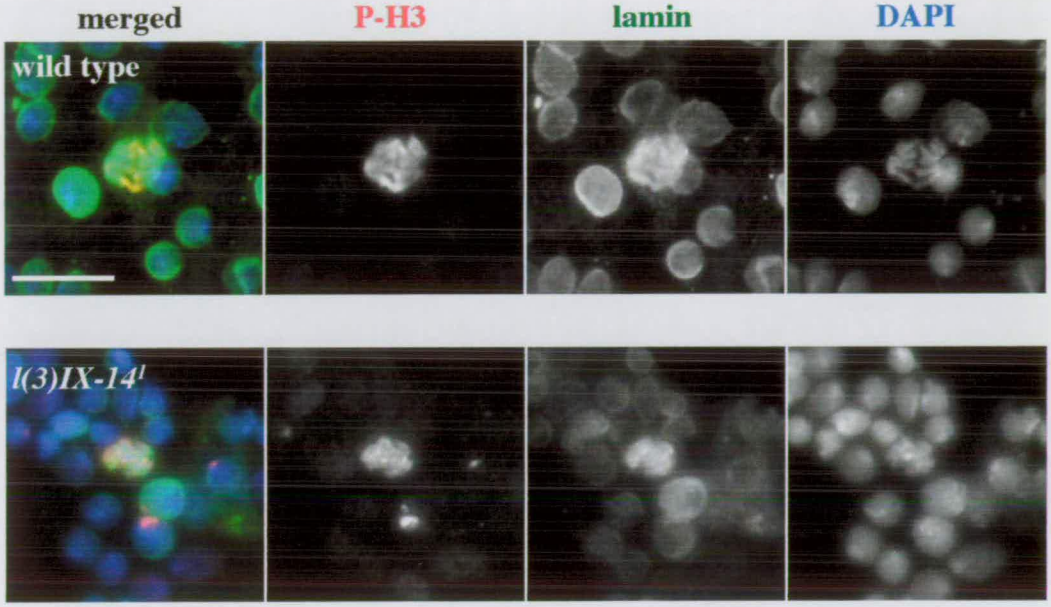

Figure 3.5 - Anti-lamin staining of larval neuroblasts. 3rd instar larval brains were fixed in 4% PFA, 10% acetic acid in PBS and incubated overnight at 4°C with rabbit anti-P-H3 and mouse anti-lamin antibodies, followed by secondary detection with goat anti-rabbit Alexa 594 and rabbit anti-mouse Alexa 488 antibodies respectively. Images are shown at 100X magnification, scale bar = 5μm.

staining in wild type cells surrounds the DAPI stained chromatin during interphase, and is then disassembled during mitosis. Incorrect nuclear envelope breakdown during mitosis could lead to the non-segregation phenotype observed in *l(3)IX-14^{1}*. However, the lower panel in figure 3.5 shows that lamin staining appears to emulate that seen in wild type preparations, and therefore can probably be regarded as normal in this mutant.

3.6 Mitotic spindles are abnormal in *l(3)IX-14^{1}* homozygous mutant brain squashes

Mitotic chromosome hypercondensation can occur as a result of mitotic arrest induced by microtubule-destabilising drugs such as nocodazole or colchicine which disrupt the mitotic spindle. These hypercondensed chromosome morphologies are not identical to the *l(3)IX-14^{1}* phenotype - they usually lack the halo of loosely condensed chromatin that causes the characteristic 'fuzziness' of *l(3)IX-14^{1}*. Nevertheless, spindle abnormalities may account for the hypercondensed aspects of the *l(3)IX-14^{1}* mutant chromosome phenotype. I therefore examined mitotic spindle morphology in *l(3)IX-14^{1}* homozygous versus wild type 3rd instar larval brains by staining with an anti α-tubulin mouse monoclonal antibody (Sigma) by a variety of fixation methods, in order to test which method was better at preserving MT spindles. The different fixation methods presented here correlate with those given in the Methods chapter 2.26.

Formaldehyde fixation in NKHE buffer

The preparations were prepared as described in the Methods and co-stained with P-H3 to allow easier identification of mitotic figures (hypotonic swelling which would improve chromosome morphology cannot be used as this disrupts spindles). The results of this fixation method are presented in Figures 3.6.

Figure 3.6 Anti-alpha-tubulin staining of neuroblasts (paraformaldehyde fixation). 3rd instar larval brains from wild type and *l(3)IX-14*^{1} homozygotes were dissected and fixed in 4% PFA in NKHE buffer for 10-15 minutes at room temperature, then incubated with P-H3 and alpha-tubulin antibodies as detailed in Figure 3.6.1. Images were captured at 100X magnification on the Olympus Provis microscope (scale bar = 5μm).

Figure 3.6 α-tubulin staining of neuroblasts (PFA fix)

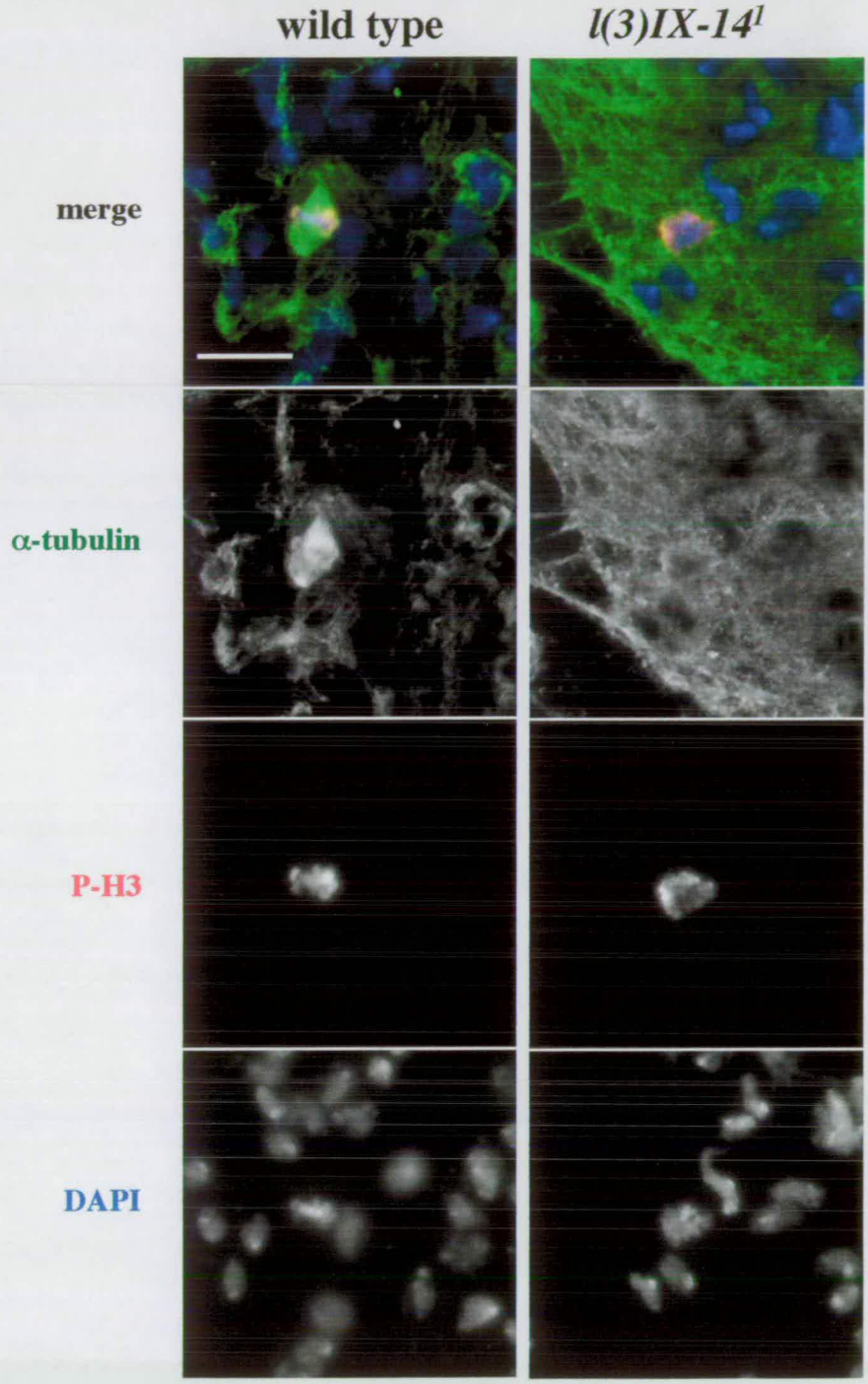

Mitotic spindles can be detected in the wild type squashes using this method of fixation, although the morphology of these spindles was often poor. Nevertheless, mitotic spindles are clearly apparent in the wild type panels (Figure 3.6, left panels). However, *l(3)IX-14*^{1} preparations appeared significantly different. I was unable to detect a correctly formed mitotic spindle in any cells that were P-H3 positive using this fixation method. There appears to be a dense and unorganised network of microtubules throughout the brain tissue. This lack of spindles is not due to reduced amounts of α-tubulin in *l(3)IX-14*^{1} homozygotes, as Western blotting has shown levels consistent with wild type (Figure 3.6B).

Methanol fixation

With the methanol fixation protocol, staining again with α-tubulin and P-H3, wild type spindles were also clearly visible. Visualisation of these figures through a Deltavision deconvolution microscope showed that these wild type spindles appeared flatter, possibly due to the squashing procedure (Figure 3.7, left panels), and may result from the physical squashing of the brains during this preparation. Once again, no obvious spindles were detected by this fixation method in *l(3)IX-14*^{1} mutants. Examination of these mutants using the deconvolution microscope did show a hint of spindle formation in a few P-H3 positive cells, although the morphology of these squashes prevents any definite conclusions. What can be concluded though is that if there are any rudimentary mitotic spindles forming in *l(3)IX-14*^{1} mutant cells they must be substantially weaker than those observed in wild type, which are not disrupted during the fixing and squashing procedure. The above fixation procedures are therefore presumably not capable of preserving any spindle morphology in the mutant brains.

Figure 3.7 Anti-alpha-tubulin staining of neuroblasts (methanol fixation). 3rd instar larval brains from wild type and *l(3)IX-14*^{1} homozygotes were dissected and squash-fixed in 5% acetic acid followed by incubation in 100% methanol + 5mM EGTA at -20°C for 10 minutes. The preparations were incubated with rabbit anti-P-H3 and mouse anti-alpha tubulin (Sigma) overnight at 4°C, followed by secondary antibody detection with Alexas 594 and 488 respectively, as detailed previously. Images were captured at 100X magnification using a Deltavision deconvolution microscope (scale bar = 5μm).

Figure 3.7 α-tubulin staining of neuroblasts (Methanol fix)

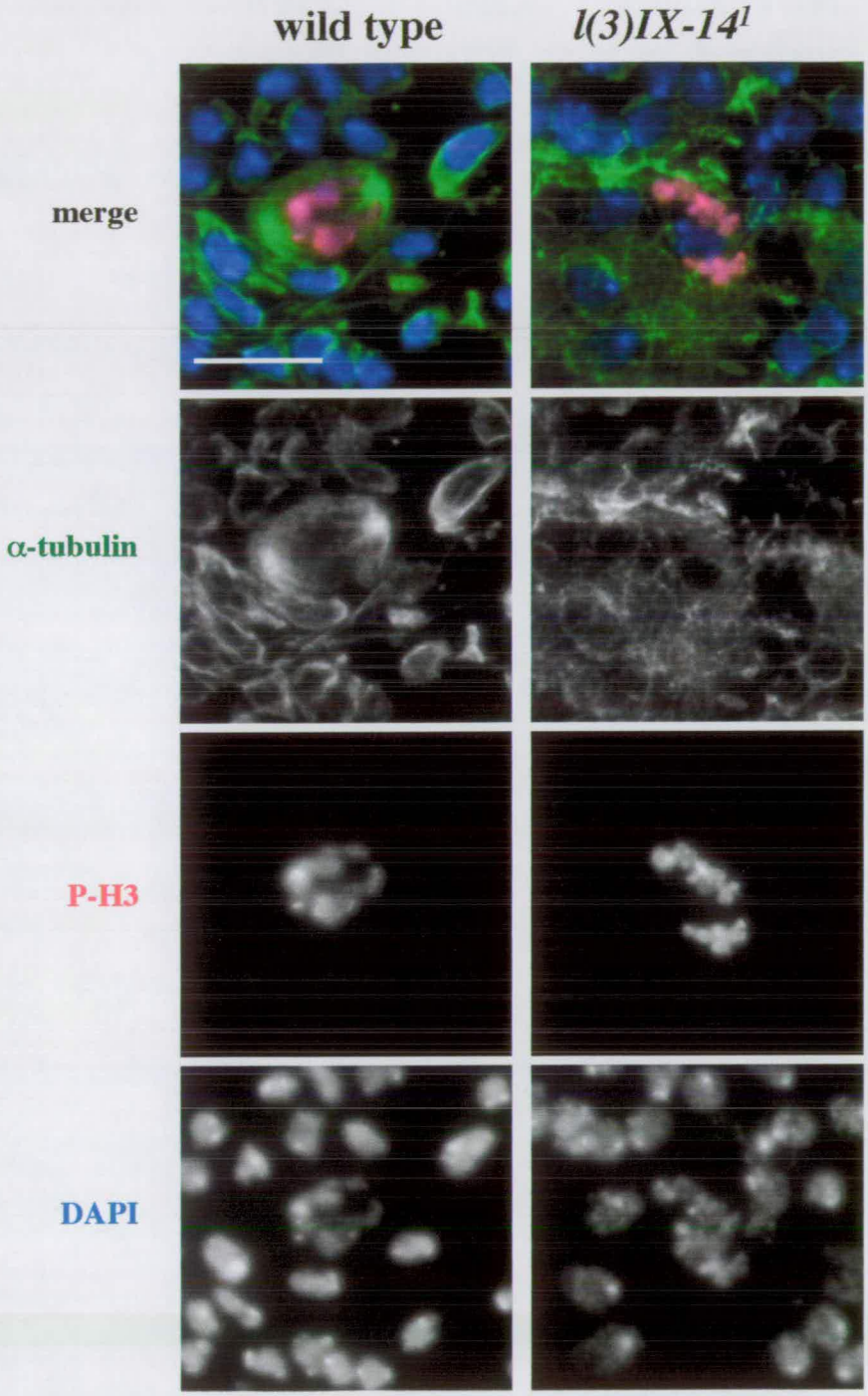

Bonaccorsi *et al.* fixation protocol

The final spindle fixation method used was adapted from a recent communication by Bonaccorsi *et al.* to Nature Cell Biology (Bonaccorsi et al., 2000), which used a longer fix in 4% PFA combined with a 45% acetic acid fix and a squash step in 60% acetic acid, followed by a post-fix in ethanol at -20°C. This protocol proved to be the most useful in studying mitotic spindles in larval neuroblasts, as the long fix seemed to be very effective in preserving MT morphology.

As can be seen in Figure 3.8, mitotic spindles were easily detectable in both wild type neuroblasts and the larger Ganglion Mother Cells (GMCs) (left and right panels respectively). In addition, the mitotic chromosome morphology is good in these fixed preparations, in comparison to the poor morphology in the previous two fixation protocols above, although the P-H3 staining in these figures was weak and appeared to be partially lost from the central chromosomal regions, probably an artefact of the fixation procedure. As the P-H3 staining was appearing faint and uneven, I therefore used CP190 (a centrosomal marker) in combination with α-tubulin to examine mitotic spindles with this protocol. The combination of mitotic-specific CP190 staining of centrosomes and the good chromosomal morphology provided by this protocol allowed for easy identification of mitotic figures.

Contrary to the results from the other fixation methods, mitotic spindles were observed in *l(3)IX-14^{1}* mutants using the Bonaccorsi protocol, albeit mostly abnormal ones. It appears therefore that the longer fix used in this protocol helps to preserve MT structure which may be weaker in the mutants. A range of phenotypes was observed in mutants, going from apparently normal bipolar spindles, to monopolar spindles, to completely disorganised spindles. A selection of these is presented in Figure 3.9. However, for the most part the mutant spindles appeared to have thicker bundles of MTs, compared to the finer structures observed in wild type, and it was noticed that many of the apparently bipolar mitotic spindles appeared asymmetrical in size. This suggests that although these bipolar mitotic spindles at fist appear almost normal, they

Figure 3.8 α-tubulin and CP190 staining of wild type brains

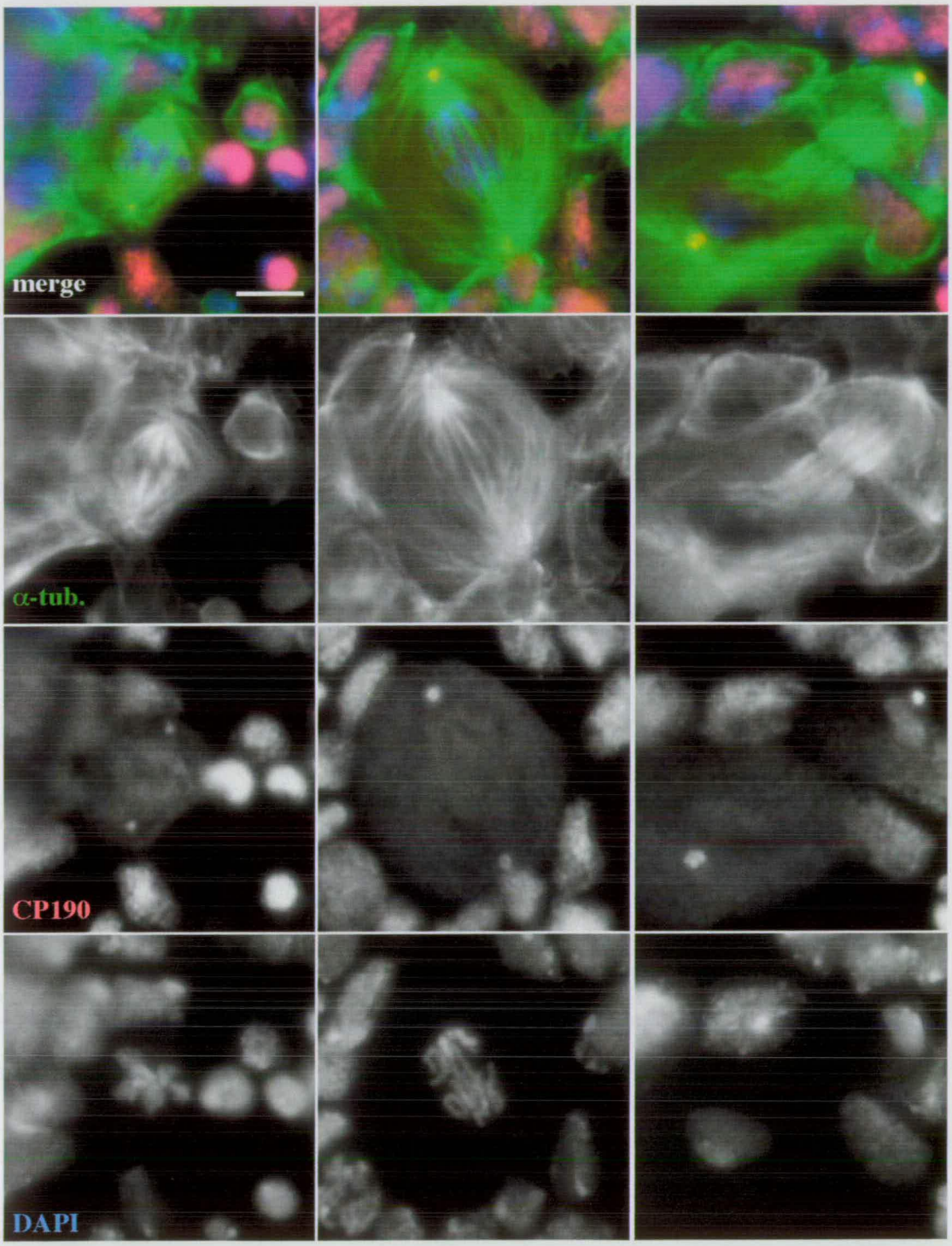

Figure 3.8 α-tubulin and CP190 staining of wild type brains using the Bonaccorsi et *al.* fixation method. Left panels show a neuroblast, middle and right panels show the larger ganglion mother cells. Images were taken at 100X magnification, scale bar = 5μm.

Figure 3.9A α-tubulin and CP190 staining of *l(3)IX-14*^{1} brains

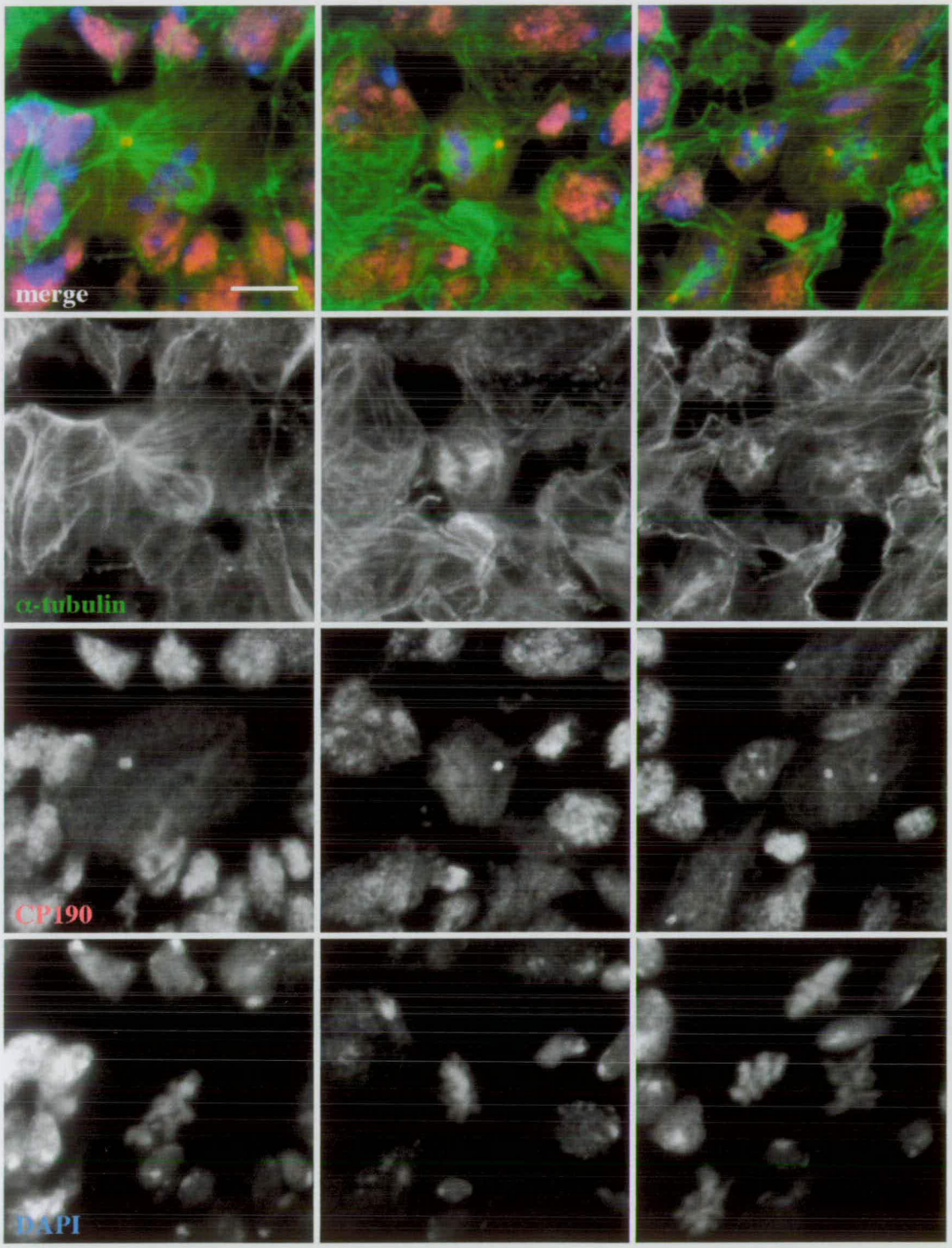

Figure 3.9A α-tubulin and CP190 staining of *l(3)IX-14*^{1} neuroblasts using the Bonaccorsi et *al.* fixation method. Images were taken at 100X magnification, scale bar = 5μm.

Figure 3.9B α-tubulin and CP190 staining of *l(3)IX-14*[1] brains

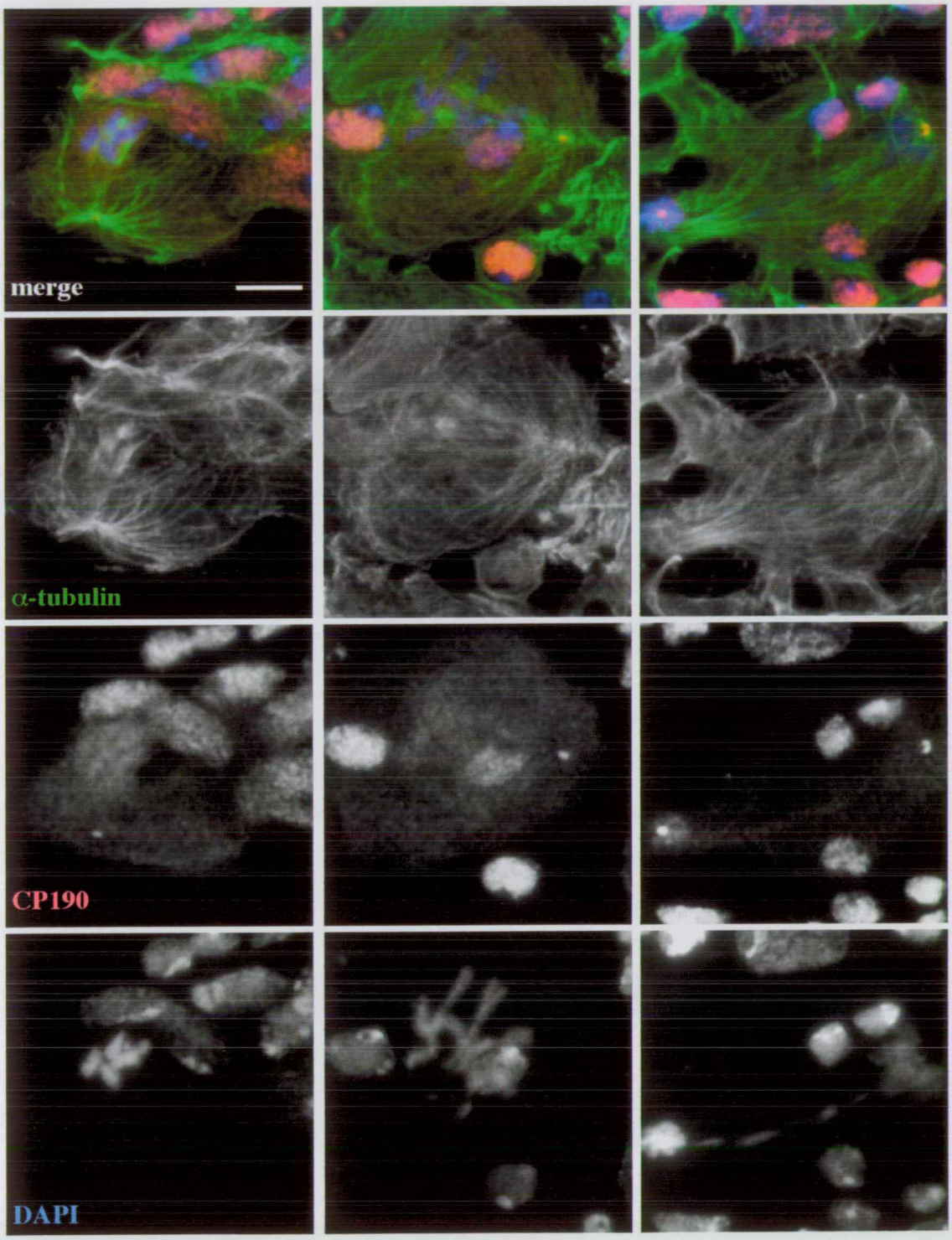

Figure 3.9B α-tubulin and CP190 staining of *l(3)IX-14*[1] ganglion mother cells using the Bonaccorsi et *al.* fixation method. Images were taken at 100X magnification, scale bar = 5μm.

Figure 3.10 Quantitation of *l(3)IX-14*^{1} spindle defects

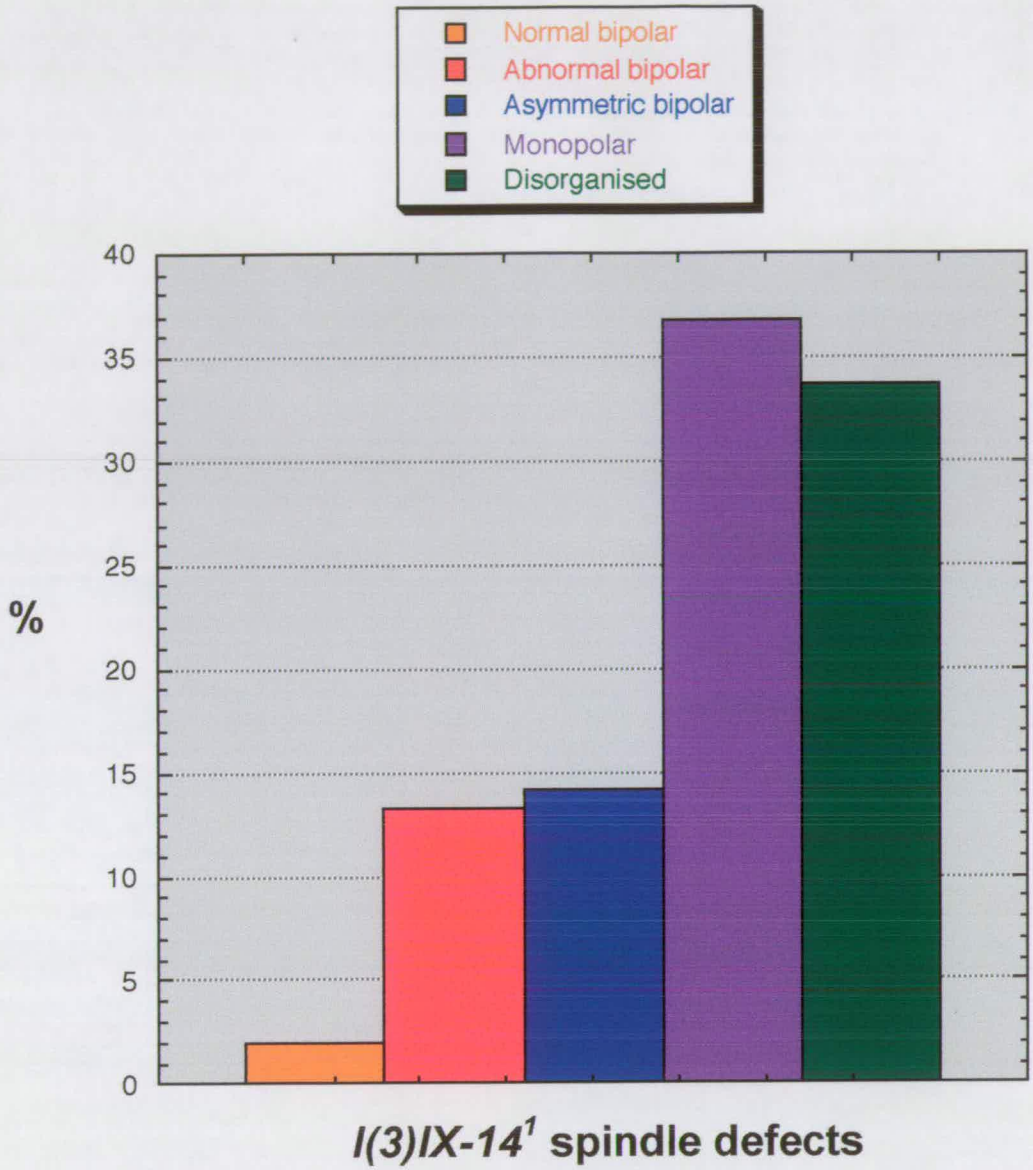

Figure 3.10 Quantitation of mitotic spindle defects in *l(3)IX-14*^{1} mitotic brains. Mitotic cells were scored on the basis of chromosome morphology and centrosomal staining by CP190 in brain squashes prepared by the Bonaccorsi protocol. Spindle morphology in wild type controls was >99% normal bipolar.

may in fact be defective and unable to actively segregate chromosomes. This is reflected in the absence of observed anaphase figures in these mutants. Additionally, the preponderance of monopolar and disorganised spindles would suggest that many cells are prevented from progressing into anaphase. The various phenotypes observed are quantified in Figure 3.10.

As CP190 was used as a co-stain in these figures, it was noticed that many mitotic figures in *l(3)IX-14^{1}* appeared to have only one centrosome (verified by focusing up and down through the focal plane to ensure that another centrosome was not simply out of view). Figures with monopolar spindles always had a single centrosome, whereas the apparently bipolar figures and disorganised spindles often (but not always) had two. I therefore proceeded to test whether centrosomal defects could correlate with the mitotic spindle defects observed here.

3.7 The centrosome cycle is affected in *l(3)IX-14^{1}* mutants

As mitotic spindles appear to be disrupted in *l(3)IX-14^{1}* homozygotes, I investigated whether this was related to a centrosome defect in these mutants. Centrosomes were detected in wild type and *l(3)IX-14^{1}* homozygous 3rd larval instar brain squashes using an anti-CP190 rabbit antibody (kindly provided by W. Whitfield, Dundee). Anti γ-tubulin (Sigma) was also tried originally, but gave such high background in brain squashes that it proved unusable.

In wild type neuroblasts, CP190 was clearly seen to stain paired centrosomes in metaphase and anaphase. CP190 proved useful as its staining pattern is nuclear in interphase, then centrosomal throughout mitosis. Figure 3.11 shows the staining pattern of the CP190 antigen in wild type neuroblasts, with a strong centrosomal signal appearing at the prometaphase/metaphase boundary (Panels C and D). From metaphase through to anaphase, the staining persists at the centrosomes with only a faint trace of

Figure 3.11 - CP190 staining of wild type neuroblasts. 3rd instar larval brains from wild type and *l(3)IX-14*^{1} homozygotes were dissected, fixed in 4% PFA + 10% acetic acid in PBS. A polyclonal rabbit CP190 antibody (Rb188) was incubated overnight at 4°C, followed by secondary antibody detection with Alexas 594. Images of the range of wild type phenotypes observed were captured at 100X magnification: DNA false-coloured in red, CP190 in green. Scale bar = 5μm.

Panel A : CP190 localisation on prometaphase chromosomes. *Panel B*: CP190 localisation on condensed chromosomes. *Panel C*: Cp190 localisation at duplicated centrosomes and on chromatin. *Panel D*: CP190 localisation at centrosomes only. *Panel E*: Anaphase figure showing CP190 localisation at centrosomes and partially on chromatin.

Figure 3.11 CP190 localisation on wild type neuroblasts

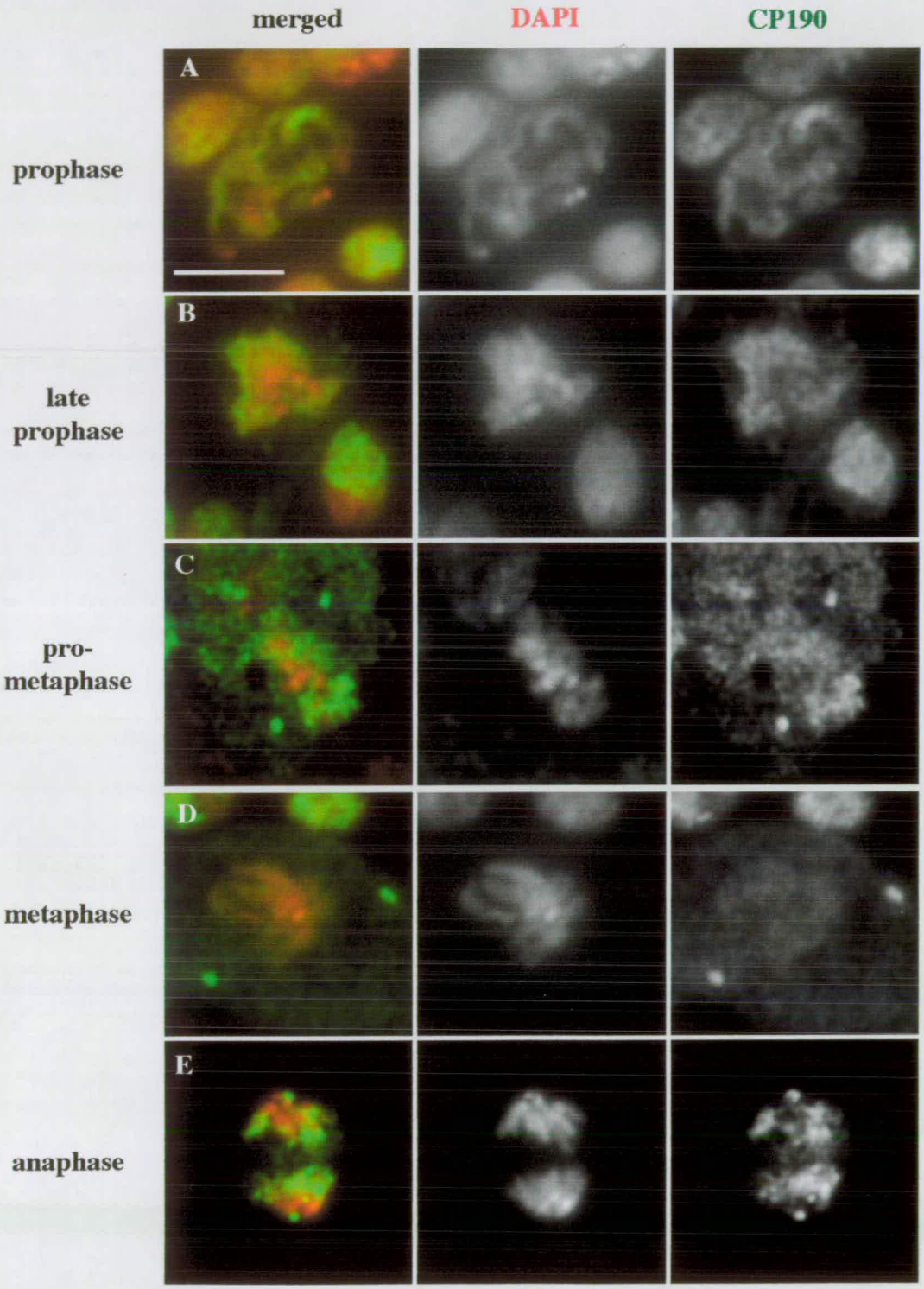

chromatin staining (Panel D), until the latter part of mitosis when staining once again appears on chromatin (Panel E).

Examination of *l(3)IX-14*^{1} homozygote neuroblasts proved to be extremely interesting. When stained with CP190 antisera, as shown in Figure 3.12, most mitotic figures did not appear to have two well separated centrosomes, compared with wild type cells of a similar stage (compare Figure 3.11, Panels C and D with Figure 3.12, Panels C through E). In the majority of *l(3)IX-14*^{1} mitotics, only one centrosomal spot was observed. In many cases, this centrosome appeared to have a slight dumbbell shape (Figure 3.12, Panels D and E), which may imply two unseparated centrosomes lying closely adjacent to one another. Overall, a range of phenotypes was identified in *l(3)IX-14*^{1} homozygotes, examples of which are shown in Figure 3.12, and quantified in Figure 3.13. It appears therefore that *l(3)IX-14*^{1} homozygotes have defects in centrosome replication and/or separation, as judged by the predominance of mitotic figures with only one identifiable centrosome. This may be an important contribution to the severe mitotic spindle defects manifest in *l(3)IX-14*^{1} homozygous neuroblasts, as duplicated centrosomes are needed to form the microtubule organising centres at opposite poles of the cell during mitosis.

Additionally, the *l(3)IX-14*^{1} homozygous mitotic chromosomes appear to have higher levels of staining by the CP190 antibody than in wild type. This may reflect another aspect of the altered mitotic chromosome structure that we have observed for the *l(3)IX-14* mutant. CP190 has a nuclear staining pattern during interphase and is also known to bind to polytene chromosomes at specific loci (Whitfield *et al.*, 1995). The observation of enhanced mitotic chromosome staining in *l(3)IX-14*^{1} may mean either that CP190 is staying attached to chromatin for longer than normal in *l(3)IX-14*^{1}, or that mitotic chromosome condensation is occurring earlier than normal before the bulk of CP190 has detached from the chromatin.

Figure 3.12 - CP190 staining of *l(3)IX-14^{1}* neuroblasts. Fixing and staining with Rb188 was performed as described in Figure 3.8.1. Images of the range of *l(3)IX-14^{1}* phenotypes observed were captured at 100X magnification: DNA false-coloured in red, CP190 in green. Scale bar = 5μm.

Panels A and B: CP190 localisation on prometaphase chromosomes. *Panel C*: CP190 localisation on condensed chromosomes. *Panels Dand E*: Hypercondensed mitotic chromosome figures showing CP190 staining both faintly on chromatin and strongly at an unseparated centrosome.

Figure 3.12 CP190 localisation on *l(3)IX-14*[1] neuroblasts

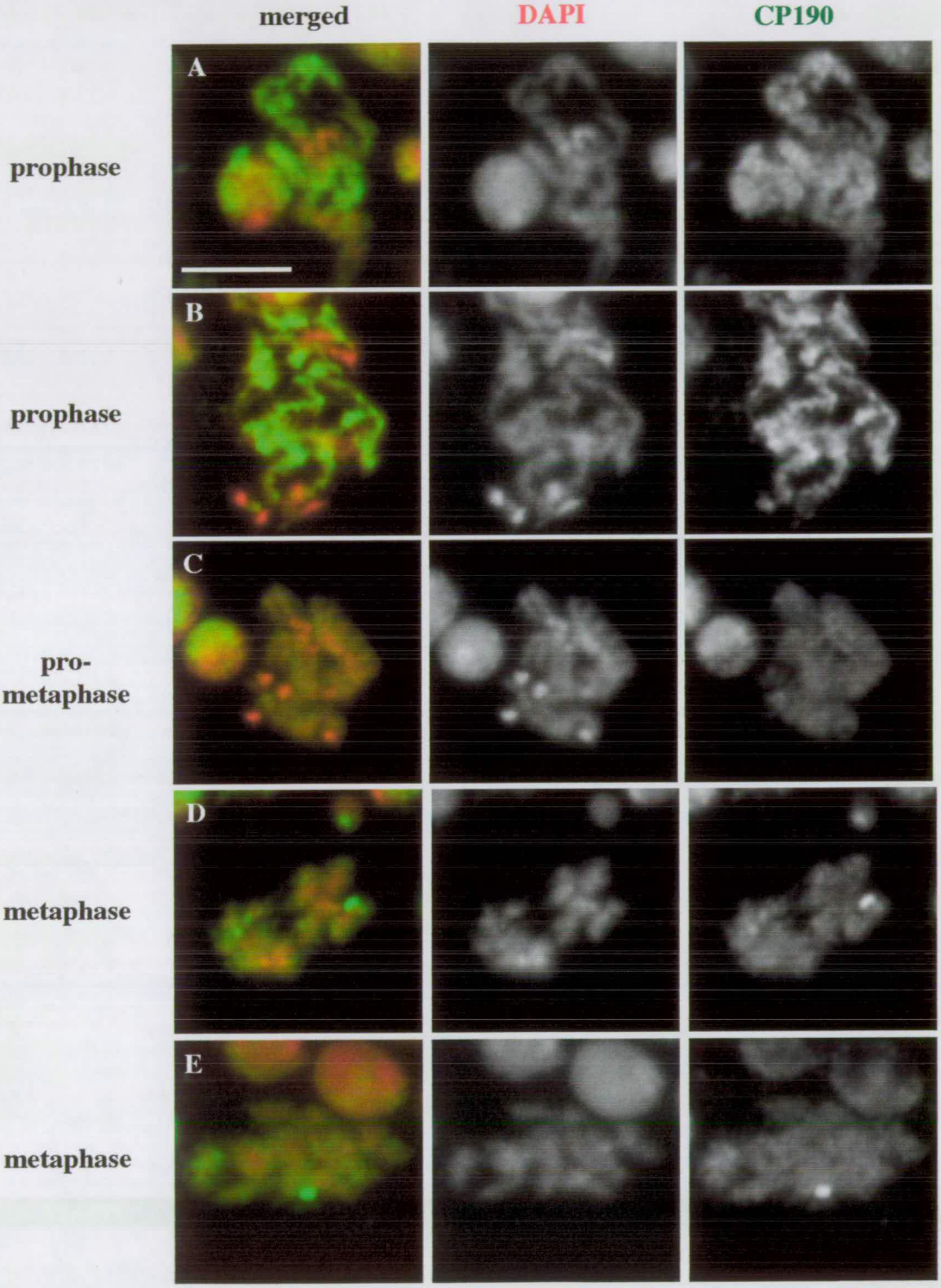

Figure 3.13

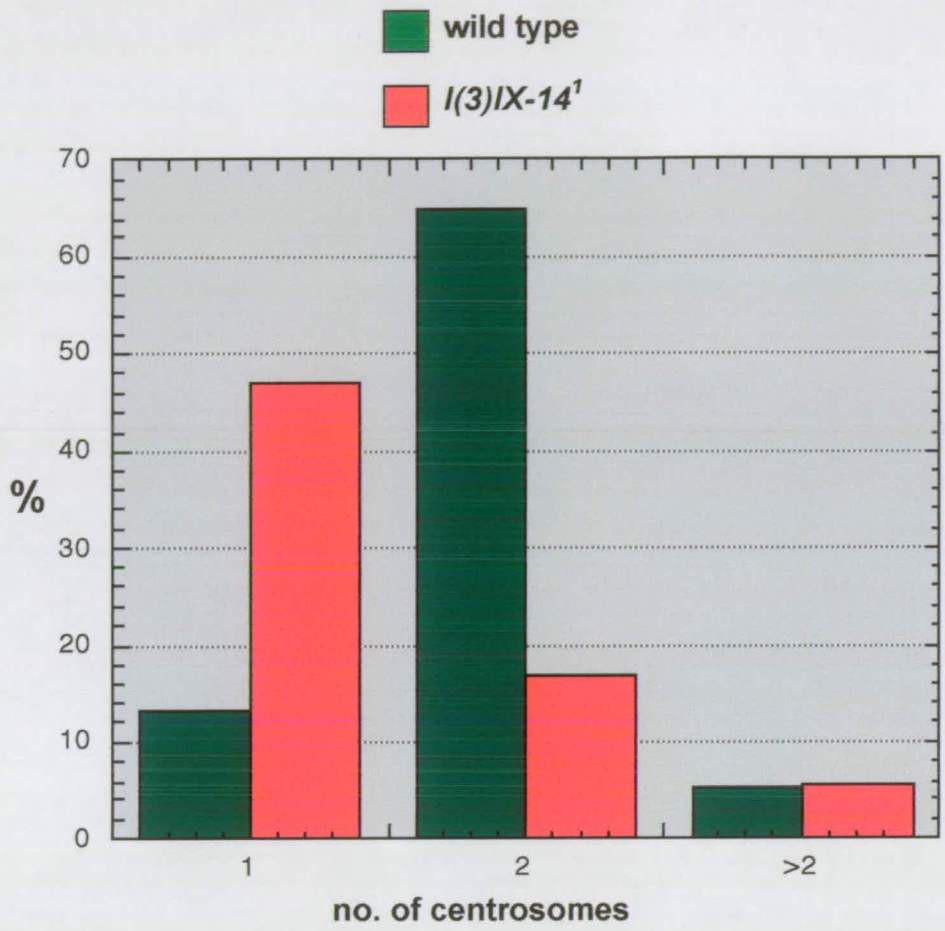

Allele	Mitotic cells counted
wild type	151
l(3)IX-14^{1}	108

Figure 3.13 Quantitation of centrosome number in wild type versus *l(3)IX-14*^{1} mitotic neuroblasts, as judged by CP190 staining.

3.8 Examination of the kinetochore components Bub1 and INCENP on *l(3)IX-14*^{1} mitotic chromosomes

Following the observation of defects in mitotic spindle assembly described above, I examined whether the checkpoint that monitors microtubule attachment to the kinetochore remained active on *l(3)IX-14*^{1} mutant chromosomes. This was performed using a rabbit polyclonal antibody raised against the *Drosophila* homologue of yeast Bub1 (kindly provided by Claudio Sunkel, Porto). This well characterised protein is known to localise to centromeres of mitotic chromosomes from prometaphase onwards until alignment at the metaphase plate, and serves to monitor the attachment of kinetochore microtubules. Bub1 then dissociates from the centromeres once the checkpoint conditions have been met. By examining *l(3)IX-14*^{1} neuroblasts for this protein, I was hoping to observe whether the Bub1 protein still localised to centromeres in the mutant, thus implying the checkpoint remained active. Wild type neuroblasts were stained in parallel as a control.

Figure 3.8.1 shows the results of Bub1 staining on wild type and *l(3)IX-14*^{1} neuroblasts. In wild type, Bub1 stains the centromeres of mitotic chromosomes (Figure 3.14A, top panels) until kinetochore MTs have attached, at which stage the staining becomes dispersed (Figure 3.14A, lower panels). However, in *l(3)IX-14*^{1} figures it can be seen that the Bub1 antibody consistently localises to the centromeres of mitotic chromosomes and no figures were observed where the staining became dispersed, indicating that the kinetochore attachment checkpoint remains active in this mutant. This correlates well with the mitotic spindle defects observed in Chapter 3.6 above, as it is unlikely that the disrupted spindles are able to form proper kinetochore attachments.

It was hoped that analysis of INCENP staining in the *l(3)IX-14*^{1} mutant may provide additional information about the mutant chromosomal figures. INCENP is a chromosomal passenger protein and has a dynamic localisation pattern in mitotic cells. It appears first along the chromosome arms, then progresses to the centromeres at

Figure 3.14 Bub1 staining on wild type and *l(3)IX-14*[1] neuroblasts

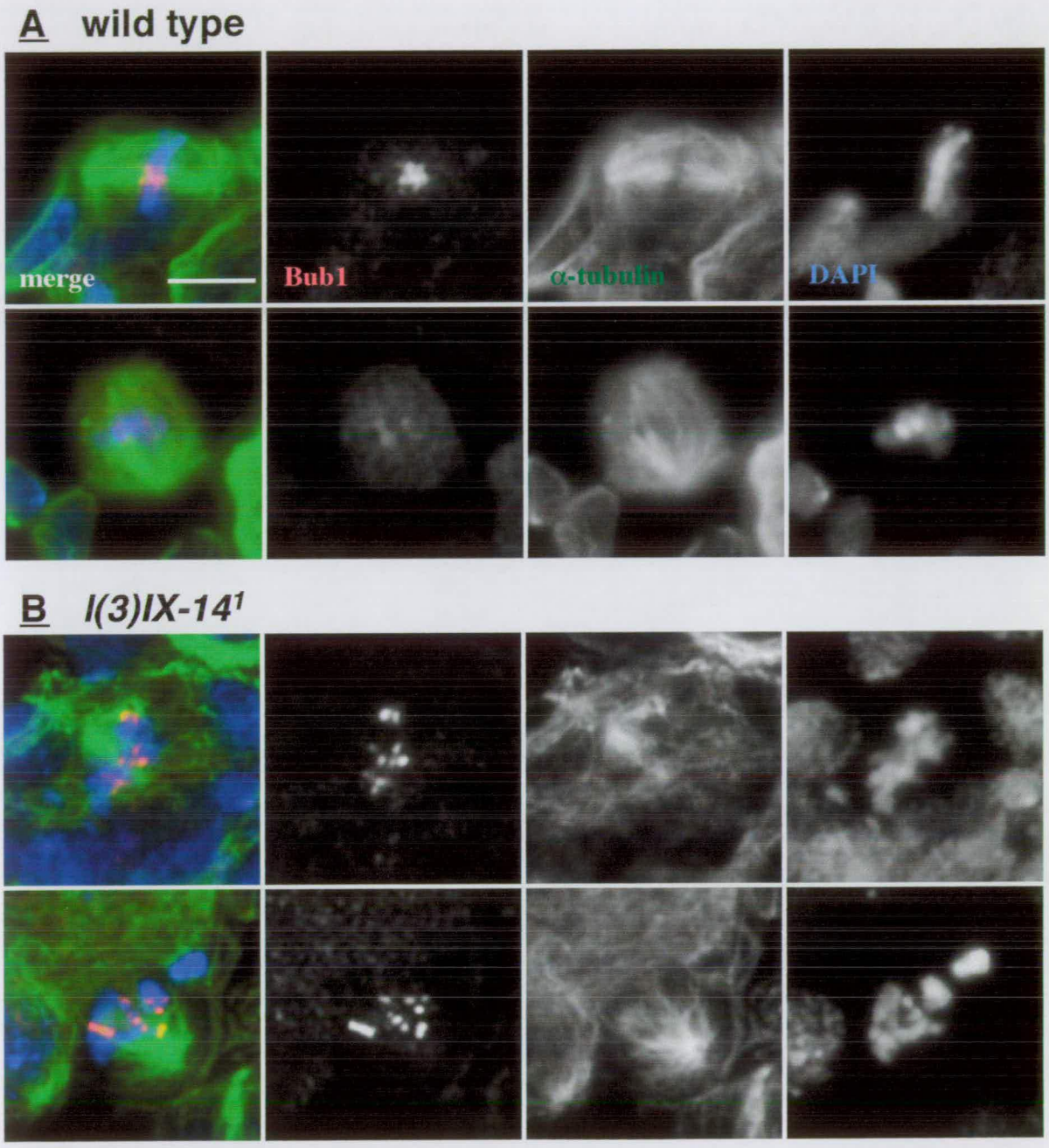

Figure 3.14 - Bub1 staining of wild type and *l(3)IX-14* neuroblasts, using the Bonaccorsi protocol. The rabbit Bub1 antibody is shown in red, microtubules in green and DNA in blue. Images were captured at 100X magnification, scale bar = 5 μm.

Figure 3.15 INCENP staining on wild type and *l(3)IX-14*[1] neuroblasts

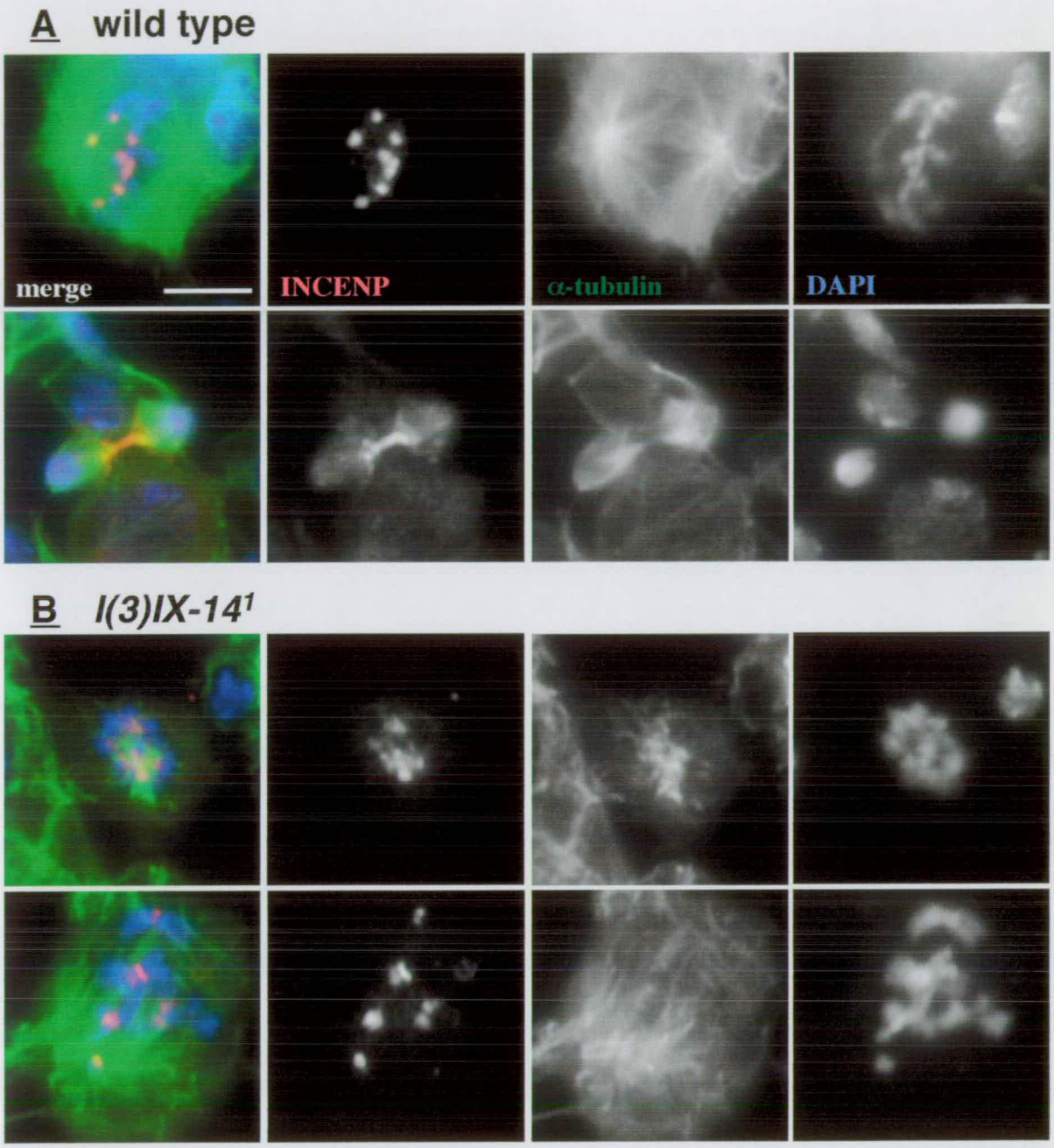

Figure 3.15 - INCENP staining of wild type and *l(3)IX-14* neuroblasts, using the Bonaccorsi protocol. INCENP staining is shown in red, microtubules in green and DNA in blue. Images were captured at 100X magnification, scale bar = 5 μm.

metaphase, and is finally deposited at the central spindle during anaphase (Earnshaw and Cooke, 1991). By examining INCENP staining on *l(3)IX-14*^{1} mitotic chromosomes, I was hoping to determine whether the mutant chromosomes were halting at a specific stage in mitosis. Figure 3.15A shows wild type staining with a rabbit INCENP antibody (obtained from W. Earnshaw), demonstrating the range of localisation described above. In *l(3)IX-14* ^{1} mitotic chromosomes however, staining of INCENP was only seen at the centromeres, not along chromosome arms, suggesting these figures are accumulating at metaphase (Figure 3.15B - both figures show disorganised spindle morphology typical of *l(3)IX-14*^{1}). As no anaphases are observed in this mutant the formation of a central spindle does not occur and one would therefore not expect to see INCENP staining of this structure. Indeed, all INCENP staining appeared to be on the mitotic chromosomes, demonstrating that these figures have not attempted to progress into anaphase.

3.9 Polytene chromosome architecture is severely affected in *l(3)IX-14*^{1} homozygous mutants

An intriguing aspect of the *l(3)IX-14*^{1} mutant phenotype, as noted in Part III of the Introduction, is that polytene as well as mitotic chromosomes are affected. Polytene chromosomes from salivary gland squashes of wild type third instar larvae have a characteristic banding pattern along the chromosome arms, and the centromeres of the endoreduplicated chromosomes are clustered at a structure termed the chromocenter (Figure 3.16, panel A). In 3rd instar *l(3)IX-14*^{1} homozygous larval polytene chromosomes this characteristic banding pattern is abolished and the chromosome arms themselves seem to be twisted and frayed (Figure 3.16, panel B). In many cases I was unable to identify an obvious chromocenter. Additionally, mutant polytene chromosomes are approximately 1/2 (or less) the size of those seen in wild type, although exactly how much smaller has not been quantified. This reduction in size may

Figure 3.16 DAPI stained polytene chromosomes

wild type

l(3)IX-14[1]

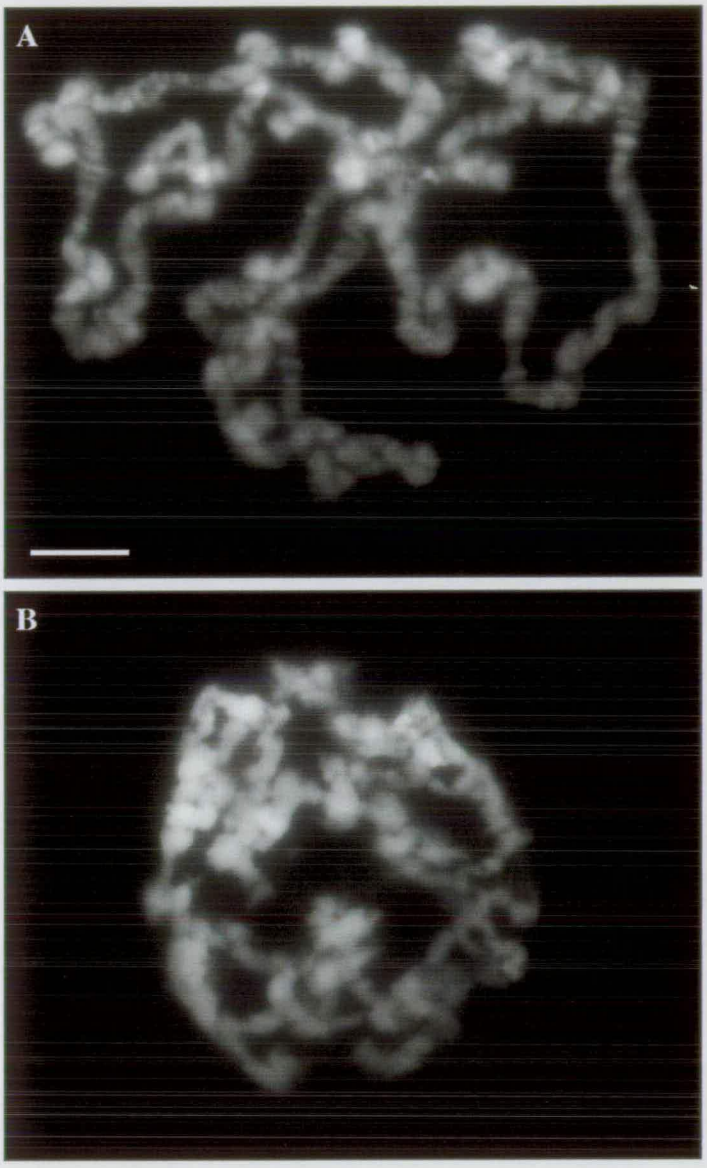

Figure 3.16 DAPI stained polytene chromosomes. Salivary glands from 3rd instar larvae were dissected and fixed in 45% acetic acid, then transfered to lactic acid:dH_2O:glacial acetic acid (in a ratio of 1:2:3) and stained with 0.1 μg/ml DAPI. Images were captured at 100X, scale bar = 10μm.

be due to under-replication as the data presented in Chapter 3.3 (summarised in Table 3.1) clearly show reduced BrdU incorporation in neuroblasts in the *l(3)IX-14*^{1} mutant.

In order to investigate the polytene chromosome phenotype further, I performed immunofluorescence on salivary gland squashes with a rabbit CP190 antibody, which is known to bind in a specific pattern to polytene chromosomes (Whitfield et al., 1995). This experiment was an attempt to determine whether factors that were known to bind to polytene chromosomes were affected by the aberrant morphology. Figure 3.17 shows the CP190 binding pattern in wild type polytene chromosomes - a characteristic banding pattern is produced that does not match the pattern of bands and interbands produced by DAPI staining, but is nevertheless specific and reproducible. The *l(3)IX-14*^{1} mutant polytene chromosomes stained with the same antibody are also shown in Figure 3.17, and it can be seen that in these mutants the characteristic banding pattern of CP190 is abolished. However, the chromosomes are still stained with the antibody, albeit in a non-specific manner. This result signifies that some chromosome-associated proteins remain bound to the mutant polytene chromosomes despite their structural abnormalities. It would be informative in the future to test whether known chromosomal structural components, such as topo II, HP-1 or BEAF-32 for example, are also still localised to these mutant chromosomes.

Figure 3.17 CP190 stained polytene chromosomes

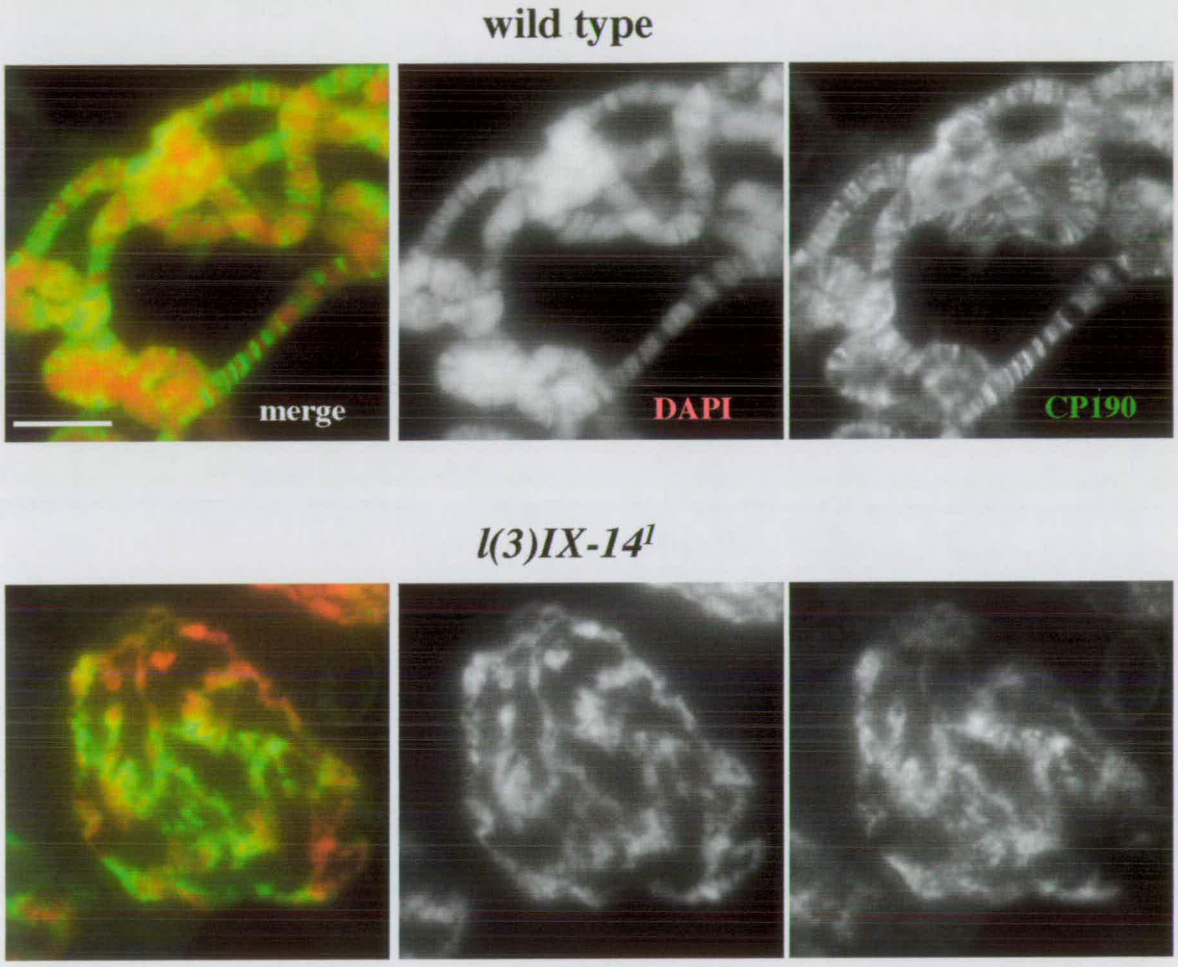

Figure 3.17 - CP190 stained polytene chromosomes. Salivary glands from 3rd instar larvae were dissected and fixed in 45% acetic acid in PBS, and incubated for 1 hour at room temperature in rabbit CP190 antibody (Rb188). Secondary detection was with Alexa 594, followed by staining with 0.1 μg/ml DAPI. Images are captured at 100X, scale bar = 5μm.

Chapter 4
Molecular analysis of *IX-14*

Chapter 4 summary

A candidate gene encoding *IX-14* mapping to 3R (85F10-F16) was cloned by identifying a *Drosophila* adult head library EST whose sequence overlapped with a ~700 bp fragment flanking the P insertion in *l(3)IX-14*^{4Y7}. This full length cDNA was 3.6 kb in length and contained an ORF of 2.1 kb coding for a 683 amino acid protein with homology to proteins in the M8 class of zinc-metalloproteases. The best characterised member of this family is the GP63 protein (also called Leishmanolysin) from the pathogen *Leishmania*, although homology stems mostly from the highly conserved zinc-metalloprotease motif and immediate surrounding regions. Strong evidence that this gene is responsible for the observed phenotypes in *l(3)IX-14* alleles came from Northern blot experiments which showed that the predicted 3.6 kb mRNA for this EST was missing in homozygous mutants. However, sequencing of the entire coding region of *IX-14* detected no lesions in the ORF, only base changes in the 5' UTR and upstream region that were shown to also be present in a different mutant line (*l(3)k43*, a mutant of DmORC2), and were therefore judged to be natural polymorphisms. The P insertion site was mapped to 40 bp upstream of the start of transcription, and precise excision had been previously shown to revert the mutant phenotype. Two imprecise excision events created the alleles *l(3)IX-14*^{eB} and *l(3)IX-14*^{eG}, which are late larval and embryonic lethal lines respectively. PCR analysis of this region allowed the further characterisation of these excision derivatives at the molecular level. The P insertion allele *l(3)IX-14*^{4Y7} was also used to analyse the expression of *IX-14*, utilising the *lacZ* reporter gene present in the P element. β-galactosidase staining of larval tissues revealed expression of *IX-14* in the proliferation zones of larval brains, but not in discs. Intriguingly, no expression was detected in

larval salivary glands either, even though *l(3)IX-14* alleles were shown to have severely disrupted polytene chromosomes.

Further characterisation of the upstream genomic region of *IX-14* prior to the release of the completed *Drosophila* scaffold genomic sequence discovered a novel gene approximately 900bp upstream and oriented in the opposite direction. This gene, designated *BNG*, was observed to have low homology to the mouse TAFI68 and human SL-1 transcription factors. This transcript may be embryonic only, based on three lines of evidence: 1) the existence of embryonic library ESTs for the gene, 2) the lack of a detectable transcript in Northern blots of larval RNA, and 3) the fact that the lesion created by *l(3)IX-14*^{eG} deletes this gene and that this line is embryonic lethal.

4.1 Cloning a putative cDNA for the *l(3)IX-14* gene

A fragment of genomic DNA flanking the insertion site of *l(3)IX-14*^{4Y7} was previously cloned by an inverse PCR strategy, shown in Fig. 4.1 (Alison Wilkie and Marie-Louise Loupart). After conducting a BLAST search using the sequence of this fragment against the *Drosophila melanogaster* EST database, I was able to identify two *Drosophila* GH (adult head) library ESTs that had 100% identity to a section of the cloned genomic fragment and appeared to be overlapping the fragment as shown in Figure 4.2. The ESTs GH12357 and GH12368 were obtained from Genome Systems (both cloned into the pOT2 plasmid vector) and were found to be 4.5 kb and 3.6 kb respectively. On analysis of the clones by sequencing, GH12357 appeared to be a chimeric clone as it contained sequence identical to *Drosophila melanogaster* mitochondrial DNA at its 3' end. This clone was therefore not used for further investigation. Sequencing of GH12368 showed that the 3.6 kb EST appeared to be a full length cDNA, containing a 2.1 kb ORF and long 5' and 3' UTRs, as shown in Figure 4.3.

Fig.4.1 Inverse PCR of genomic fragment flanking *l(3)IX-14*^{4Y7} P insertion

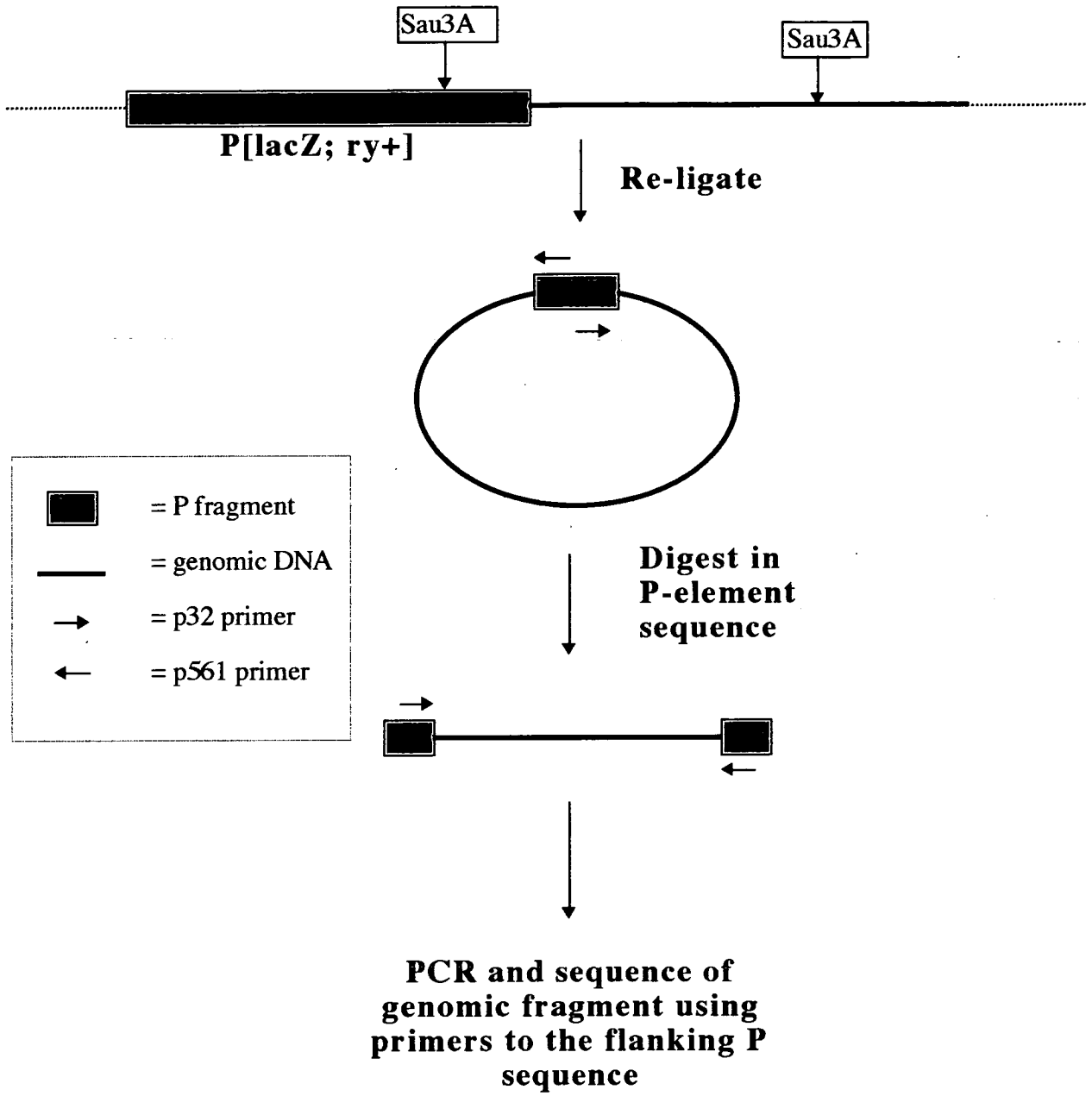

Figure 4.1 Diagrammatic representation of the inverse PCR cloning procedure. An approximately 700bp fragment of genomic DNA flanking the 5' end of the P element insertion in *l(3)IX-14*^{4Y7} was cloned by this method, and allowed the identification of 2 *Drosophila melanogaster* adult head library ESTs.

Figure 4.2 BLAST alignment of PCR fragment sequence vs. ESTs GH12357 and GH12368

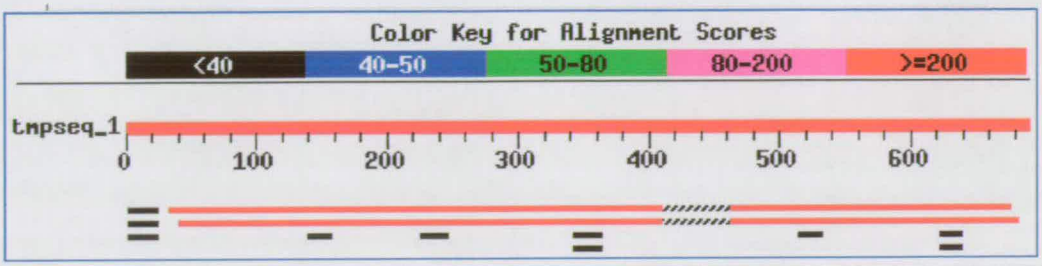

Sequences producing significant alignments:		Score (bits)	E Value
gb|AI134806.1|AI134806	GH12357.5prime GH Drosophila melanog...	702	0.0
gb|AI134814.1|AI134814	GH12368.5prime GH Drosophila melanog...	690	0.0

Figure 4.2 BLASTn output of the 700bp inverse PCR fragment sequence vs. the *Drosophila* EST database, showing high score matches to 2 adult head library ESTs. The EST sequences were nearly identical along the ~650bp overlapping portion with the inverse PCR product.

The predicted protein from the GH12368 clone (presented in 3-letter amino acid code above the open reading frame in Figure 4.3) was used to perform a BLASTp search against the nonredundant (nr) protein database on GenBank, and was discovered to have high homology (45% identity, 59% similarity over the length of the protein) with an uncharacterised predicted protein from the *C. elegans* genomic database, and loose homology (26% over 53 amino acids) to the GP63 (or Leishmanolysin) protein from the pathogen *Leishmania*, a protein from the M8 class of zinc-metalloproteases. Further analysis showed that main areas of homology between the GH12368 protein and *C.elegans* predicted proteins compared with GP63 homologues are centered around a zinc-metalloprotease motif (-H-E-X-X-H-), shown boxed in red in Figure 4.3. This motif has been well characterised in the cell-surface zinc-metalloprotease GP63 in the pathogen *Leishmania*, and it has been determined that the two Histidine residues coordinate the zinc ion that is required for the proteolysis reaction, whereas the Glutamic acid residue functions as the active site. On the strength of this homology, the protein encoded by GH12368 appears to be a novel zinc-metalloprotease loosely related to the M8 class of zinc-metalloproteases.

In addition to the predicted *C. elegans* homologue, subsequent BLAST searches with the GH12368 predicted protein using both BLASTp and tBLASTn algorithms have to date detected human, mouse and bovine EST homologues, and a predicted metalloprotease from the *Arabadopsis thaliana* genome sequencing project. An alignment of the various animal homologues detected so far is shown in Fig. 4.4 (the *Arabadopsis* homologue currently exists only as a fragmented series of contigs in the database and was therefore not included in the alignment). Intriguingly, there appear to be no homologues in the completed yeast or bacterial sequence databases. This leads me to conclude that the IX-14 protein may be exclusive to metazoan eukaryotes.

Further database searches using the predicted GH12368 protein against the SMART (Simple Modular Architecture Research Tool) database (version 3.1, (Schultz

Figure 4.3 cDNA sequence of *IX-14*. Sequence is shown in interleaved format, with the amino acid sequence corresponding to the ORF presented in 3 letter code. The predicted signal sequence is shown underlined in red, cAMP phosphorylation site underlined in green, tyrosine kinase phosphorylation sites underlined in yellow, protein kinase C phosphorylation sites underlined in light blue, zinc-metalloprotease motif boxed in red, and the polyadenylation signal underlined in black.

Figure 4.3 cDNA sequence of *IX-14*

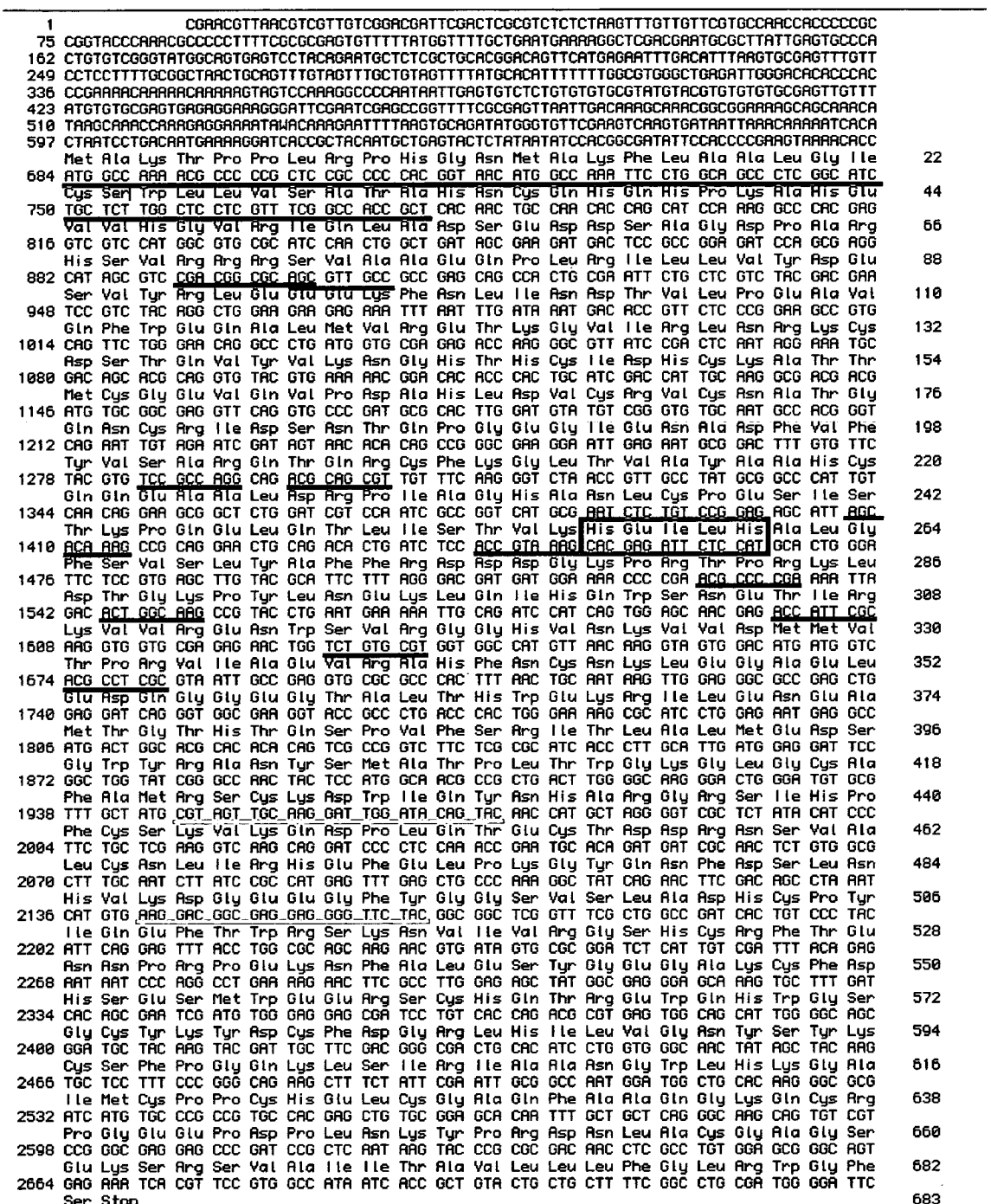

Figure 4.4 Clustal alignment of IX-14 animal homologues and the GP63 zinc metalloprotease from Leishmania, using the CLUSTAL algorithm contained in the Lasergene MegAlign program. *H. sapiens*, *M. musculus* and *B. bovis* sequences are conceptual translations of partial ESTs. Residues identical to the *D. melanogaster* IX-14 protein are shaded in grey. The HEXXH zinc metalloprotease motif is boxed in red.

Figure 4.4 Clustal alignment of *IX-14* homologues

et al., 2000)) have reveled a potential signal sequence at the N-terminal end of the protein (see Figure 4.3, underlined in red), although whether this sequence acts to target the protein to a cellular membrane is currently unknown. Finally, a search for motifs using the ProSite program on the ExPASY server predicted a cAMP phosphorylation site (underlined in light green), 2 Tyrosine kinase phosphorylation sites (underlined in purple), and 10 Protein kinase C phosphorylation sites (underlined in light blue), as well as the above mentioned zinc-metalloprotease motif (all shown on Figure 4.3).

4.2 Mapping the GH12368 EST

The *l(3)IX-14*^{1} mutation had previously been mapped to the region 85E10-F16 on the right arm of the 3rd chromosome, by a series of crosses to deficiency lines with known breakpoints (Sue Ann Krause, Ph.D. thesis, 1999). It was demonstrated that the *l(3)IX-14* mutation failed to complement the deficiency line Df(3R)by62, placing it in this region (Figure 4.5A). In order to demonstrate the putative *IX-14* cDNA clone also mapped within this region, and to further narrow down the map position I was able to demonstrate by Southern blotting using the GH12368 cDNA as a probe that this clone hybridised to P1 clone DS01918. In this experiment, a commercially available filter containing a gridded array of P1 clones (obtained from Genome Systems) was used. The grid coordinates of the hybridisation signal, an example of which is shown in Figure 4.5B, allowed the unambiguous identification of a particular P1 clone. It was then determined, by consulting the Berkeley Drosophila Genome Project (BDGP) web-page, that this clone had previously been mapped by *in situ* localisation to polytene chromosomes to position 85F10-F16. Subsequent analysis of the recently completed *Drosophila* genome has since shown that this mapping was correct.

Figure 4.5 Mapping the *l(3)IX-14*^{1} mutation

A

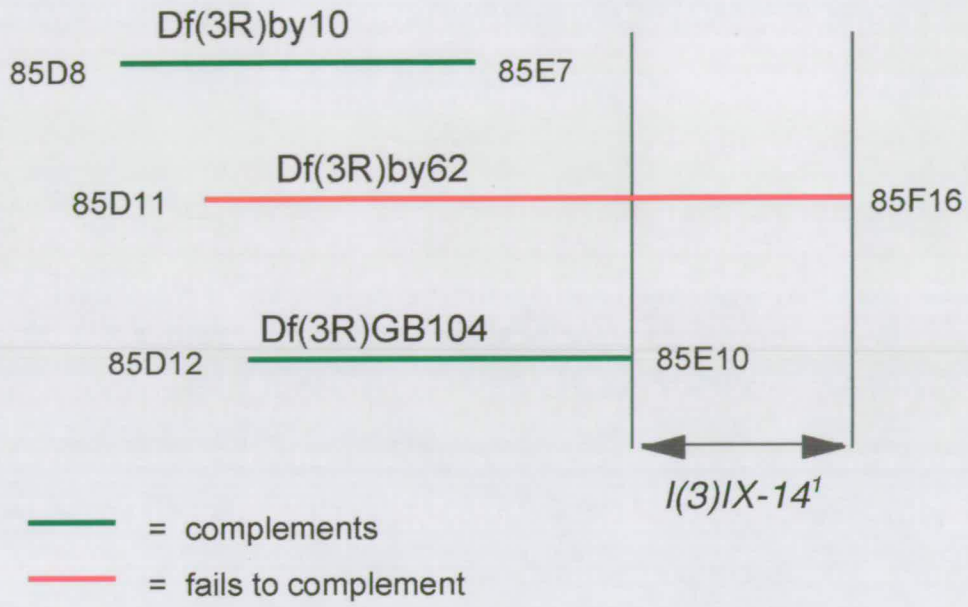

B

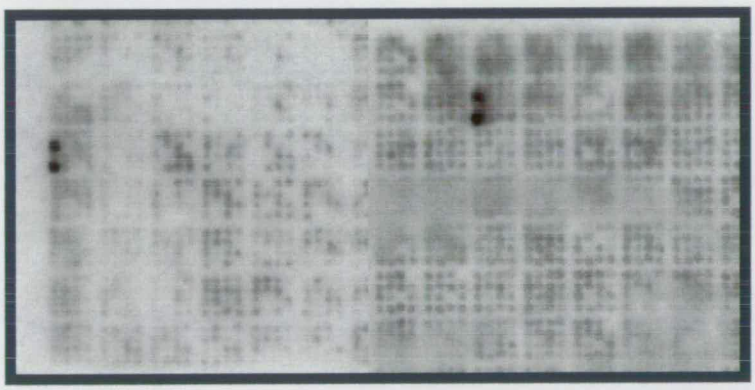

Figure 4.5 **A**) Mapping the *l(3)IX-14*^{1} mutation by complementation tests with deficiency lines. The ICR-170 induced *l(3)IX-14*^{1} mutation was mapped to the region 85E10-F16 by virute of failure to complement the deficiency line Df(3R)by62. **B**) Mapping the *IX-14* locus by Southern hybridiation to a gridded P1 array. The GH12368 EST corresponding to the *IX-14* gene was hybridised to a Genome Systems P1 filter, shown above. The P1 clones identified by this method were mapped independantly by the BDGP to region 85F10-F16 by *in situ* hybridisation to polytene chromosomes.

The placing of the putative *IX-14* cDNA on the right arm of the 3rd chromosome also provided evidence that previous reports of the *l(3)IX-14*^{1} mutation being allelic to the *ads* (*all discs small*) mutation were incorrect, as *ads* has been mapped to region 75C3-4 on the left arm of the 3rd chromosome. I have also performed complementation crosses with the *l(3)IX-14*^{1} and *l(3)IX-14*^{4Y7} lines to the *ry*^{100} line, which is listed as another allele of *ads* on FlyBase, and shown that they complement and are therefore not allelic. These details have been communicated to the FlyBase curators and an amendment has been placed under the entry for *l(3)IX-14*^{1}.

4.3 Northern blot analysis indicates GH12368 is the transcript responsible for the *l(3)IX-14*^{1} mutation

A Northern blot was performed with *Drosophila melanogaster* total RNA isolated from 3rd instar wandering larvae of wild type, *l(3)IX-14*^{1} heterozygotes and homozygotes, and *l(3)IX-14*^{4Y7} heterozygotes and homozygotes, using the GH12368 cDNA as a probe. The results showed that the expected mRNA size of 3.6 kb was detected (after 2 weeks exposure at -80°C) in wild type and both heterozygote lanes, but was absent (or greatly reduced beyond detectable levels) in both homozygote lanes (see Figure 4.6). All lanes appear nearly equally loaded, as judged by subsequent hybridisation with a probe to Ribosomal Protein (RP) 49. This result provides strong evidence that this cDNA encodes the gene responsible for the *l(3)IX-14*^{1} mutation since the GH12368 message is missing in homozygotes of both the original ICR-170 induced mutation and the P-element induced allele.

4.4 Characterisation of the *IX-14* genomic region:

Previous to the identification of the putative *IX-14* EST, and prior to the completed *Drosophila melanogaster* scaffold sequence released in March of 2000, 8 genomic phage clones were isolated from a *Drosophila melanogaster* genomic library

Figure 4.6 Northern blot analysis of GH12368

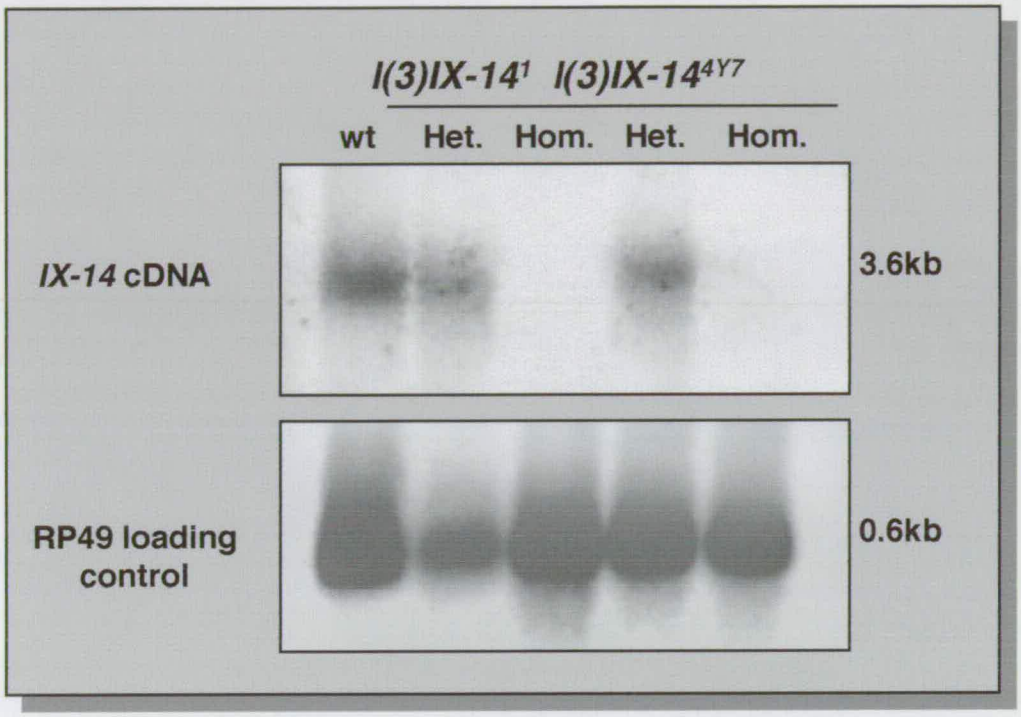

Figure 4.6 Northern blot analysis of the GH12368 EST. 3rd instar larva total RNA from wild type, *l(3)IX-14*^{1} homozygotes and heterozygotes, and *l(3)IX-14*^{4Y7} homozygotes and heterozygotes was probed with the GH1268 EST. The predicted message of 3.6 kb is absent in both homozygous mutant lines. RP49 is shown as a loading control.

by Alison Wilkie, an honours student in the laboratory (1997). This screen was performed with a view to using any larger genomic fragment that was obtained to probe a cDNA library - a classical route to cloning a putative gene. This route was abandoned once I was able to identify EST clones matching the sequence of the P-element flanking fragment (see Section 4.1). However, the genomic clones isolated from Alison Wilkie's screen did prove to be useful in characterising some of the *IX-14* genomic region.

The 8 genomic phage clones were identified by probing with the ~700 bp genomic fragment flanking the P-element *l(3)IX-14*^{4Y7} which was isolated by inverse PCR (described in section 4.1). Initial characterisation of these phage clones was carried out by various restriction digests, which demonstrated that several of the 8 clones were duplicates of each other. Further Southern blots of these digests (with the same probe used in the screen) identified smaller bands, which were to be sub-cloned and characterised further. However, after identifying the GH12368 cDNA clone, and subsequently checking that it also hybridised to the same fragments in these phage clones, I decided to use primers designed to the EST clone to sequence directly from the phage clones into the surrounding genomic region. I was able to demonstrate that two of the phage clones characterised, clones 6 and 10, contained the first 818 bp of the GH12368 EST, made up of 715 bp of 5' UTR and 103 bp of coding region. The downstream sequence to this did not match sequence to the λ clone arms, and was thus taken to be part of the first *IX-14* intron. This intron appeared to be large, since repeated attempts to PCR it using primers designed to various sections of coding region failed. I had also sequenced over 1 kb into Intron I from the phage clones, and sequence obtained from the phage arms did not match GH12368 cDNA sequence, so it appeared that the 3' ends of these phage clone inserts occur in this large first intron (see Figure 4.7A), and were thus of no use for examining the remaining downstream coding region of *IX-14*.

Figure 4.7 *IX-14* Genomic Region

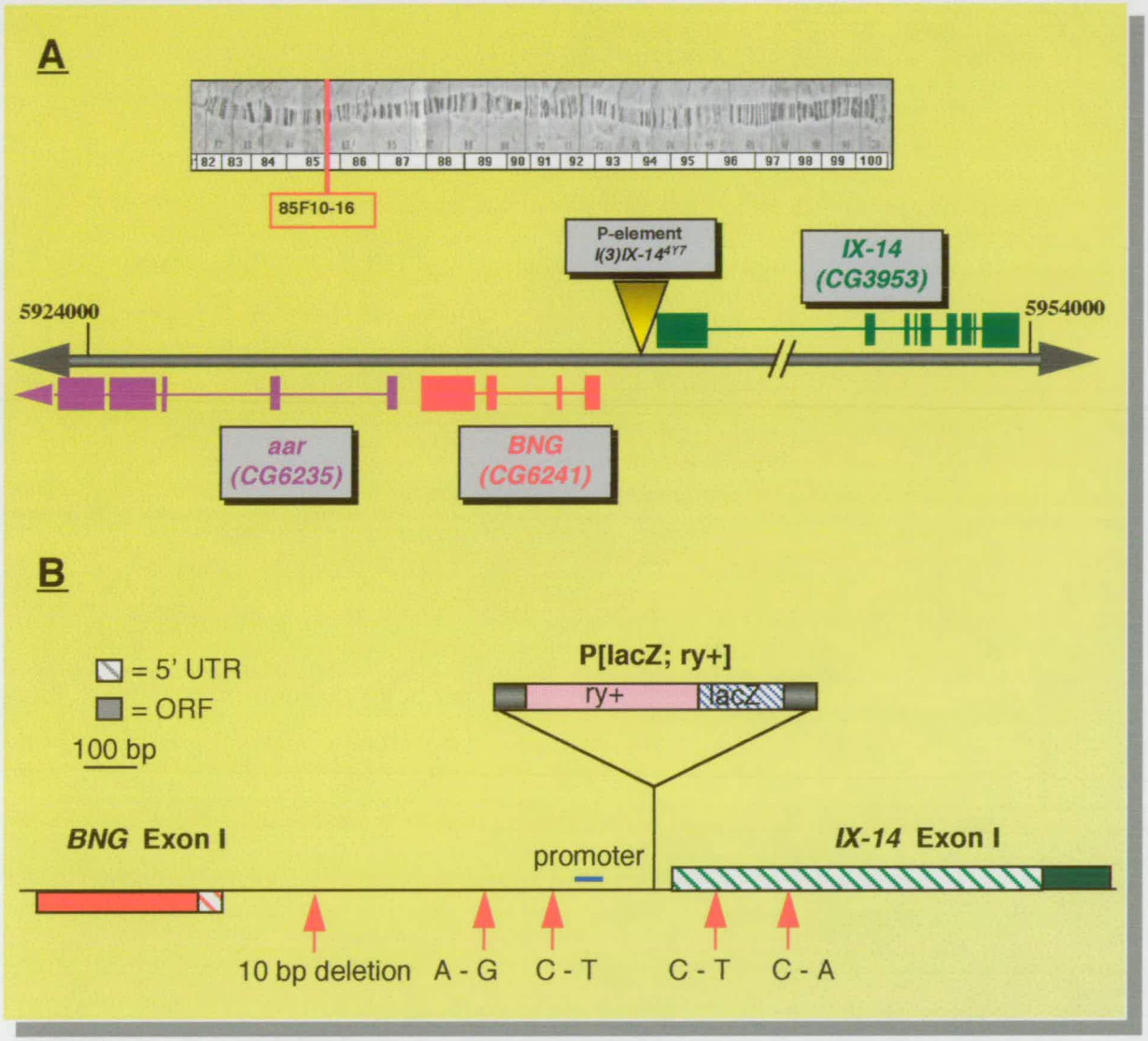

Figure 4.7 **A**) Schematic representation of the *IX-14* genomic region, showing the intron-exon structure of genes in the 85F16 region. The *IX-14* gene containing 9 exons is shown on the upper strand in green, neighbouring genes *BNG* and *aar* on the lower strand in red and purple respectively. The GadFly annotation for each gene is given in brackets, and the numbered divisions refer to the nucleotide positions on the annotated *Drosophila* scaffold sequence. The P element insertion in *l(3)IX-14*^{4Y7} is shown as a yellow triangle. **B**) Higher magnification of the genomic region surrounding the P element insertion site, showing the P orientation, a predicted promoter (blue line), and polymorphisms (red arrows) found between wild type, *l(3)IX-14* and *l(3)k43* sequences. The P element is not shown to scale.

The phage clones were more useful however for characterising the upstream genomic region of *IX-14*. A 6.9 kb XbaI product of clone 5, which had given a positive signal when probed with the 700 bp P-element flanking probe, had been sub-cloned and sequenced entirely. This sub-clone did not however contain any sequence matching the GH12368 EST, although it did contain several AT rich regions, as does the immediate upstream region of *IX-14*, which may account for the cross-hybridisation. On further investigation, it was observed that the first exon of a gene encoding the regulatory subunit of protein phosphatase 2A (responsible for the mutation *abnormal anaphase resolution* (*aar*)) was contained within this 6.9 kb region. I performed a complementation cross between *l(3)IX-14* mutant alleles and a P-element allele of *aar* (*l(3)P1532*) and established that they were not allelic - a similar complementation test had previously been performed by Mayer-Jaekel *et al.* (1993) with the same result.

Further sequencing along the phage insert from the 6.9 kb XbaI fragment towards the start of the *IX-14* region resulted in nearly 10 kb of contiguous double stranded sequence of this genomic region. Analysis of this sequence compared to the sequence of the P-element flanking fragment allowed me to establish the insertion site of the *l(3)IX-14*^{4Y7} P-element, 40 bp upstream of the start of transcription of *IX-14* (Figure 4.7B). Database searching revealed 4 nearby P insertions: *l(3)j9A5*, *EP0520*, *EP3111* and *EP3702*, as well as a predicted promoter sequence 140 bp upstream of the start of GH12368 (see Figure 4.7B). Significantly, when I compared this upstream genomic sequence to the 'others' EST database on GenBank by BLASTn, I was able to identify 2 *Drosophila* ESTs, LD35363 and LD45793, that were a 100% match to a region of this genomic sequence approximately 1 kb upstream of *IX-14*. These ESTs were ordered, sequenced completely, and shown to be full length cDNAs encoding a novel protein of 3302 bps (872 aa), with its first exon starting 843 bp upstream of *IX-14* on the opposite strand. BLAST searching with the predicted protein brought up no significant homologues, although there are weak similarities at the N-terminal end (less

than 20%, over a region of approximately 100 aa) with the human and mouse transcription factors SL-1 and TAFI68 respectively (see Figure 4.8). As this gene is novel, I temporarily designated it *BNG*, for "Brian's New Gene". The exon/intron structure of this gene, based on the cDNA sequence compared to the genomic region and from the GeneFinder prediction program (GeneFinder,) is shown in Figure 4.7A. Since the completion of the *Drosophila* genome, this predicted gene has been given the database identifier CG6241 and has been annotated as a putative transcription factor, presumably due to its weak similarity to SL1 and TAFI68.

The remaining downstream regions of *IX-14* were characterised by a combination of PCR from wild type genomic DNA using primers designed to cDNA sequence, and by comparison of the *IX-14* cDNA sequence to the completed *Drosophila* scaffold sequence as it became available. From the assembled scaffold sequence it was seen that Intron I was 8.7 kb in size, accounting for the inability to PCR it under the conditions used (described in chapter 2.10), although long-range PCR may possibly have been able to amplify this region. Assembly of the *IX-14* cDNA sequence onto the scaffold genome sequence shows that *IX-14* is composed of 9 exons, detailed in Figure 4.7A. Additionally, the completed *Drosophila* genome sequence verified the position of *IX-14* as mapped by S.A. Krause and myself to within the region 85F10-F16, and also verified the position and sequence of the two nearby upstream genes to *IX-14*, i.e. *BNG* (CG6241) and *aar*.

4.5 Northern blot of the CG6241 (BNG) transcript

The presence of another novel gene less than 1 kb away from the P element *l(3)IX-14*^{4Y7} insertion site raises the question of whether this gene is also affected by the insertion. Unfortunately no known mutations or insertions are known to reside within this novel gene, so a simple complementation cross was not possible. I therefore tested whether the CG6241 transcript was affected by Northern blot analysis.

Figure 4.8 Clustal alignment of BNG (CG6241) homologues

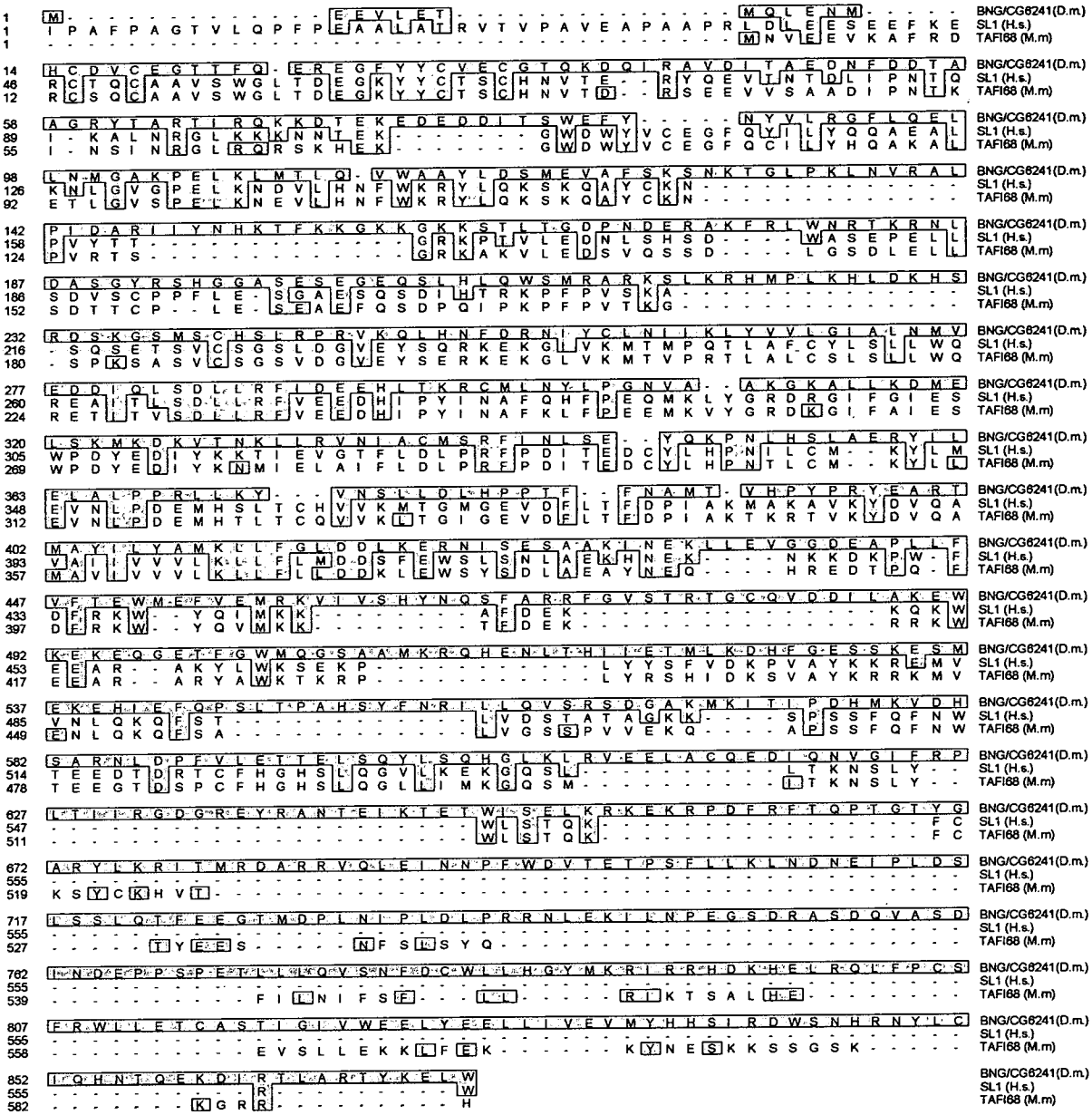

Figure 4.8 Clustal alignment of *D. melanogaster* BNG (CG6241) and its homologues TAFI68 (*M. musculus*) and SL-1 (*H. Sapiens*), using the MegAlign package (Lasergene). Residues matching BNG (CG6241) are boxed in light grey.

Section 4.3 shows that the *IX-14* transcipt appears to be absent in larval total RNA from *l(3)IX-14* homozygous alleles. However, I was unable to detect a signal in any lanes, including the wild type larval lane, for CG6241 when I blotted the same nitrocellulose filter with a probe prepared from the cDNA LD35363. As this cDNA is derived from an embryonic library, this may signify that this transcript is embryonic only, and not detectable in third instar larvae. A second blot was therefore performed including wild type embryonic total RNA, made from an overnight embryo collection. Analysis of this blot showed that an extremely faint band was detectable in the wild type embryo lane after 2 weeks but no detectable bands were present in any 3rd instar larval lane. I conclude from this that the CG6241 message is only expressed at extrememly low levels in embryos only.

4.6 Localisation of the *IX-14* transcript by β-galactosidase expression

The localisation of the *IX-14* transcript in larval brains was analysed in the *l(3)IX-14*^{4Y7} allele by virtue of the *lacZ* reporter gene contained within the P-element. The P appeared to be inserted 40 bp before the start of transcription of *IX-14*, and was shown (by PCR analysis, see Chapter 4.9) to be in the orientation 3'-5' relative to the *IX-14* gene. It was therefore a useful tool for this experiment as attempted transcription of the *IX-14* transcript in the P-element allele would result instead in the expression of the *lacZ* reporter gene, in turn detectable by β-galactosidase staining.

β-galactosidase staining was performed as detailed in chapter 2.35 on brains and salivary glands dissected from 3rd instar larvae of *4Y7* heterozygotes and homozygotes. Figure 4.9 shows that expression of *IX-14* in heterozygote brains appears to be concentrated in zones of proliferation in the optic lobes and ventral ganglion, consistent with a role for *IX-14* in mitotically dividing tissues. The neighbouring panel shows staining in a homozygous brain - it can be seen that the

Figure 4.9 β-galactosidase staining of *l(3)IX-14^{4Y7}* heterozygote and homozygote larval tissues

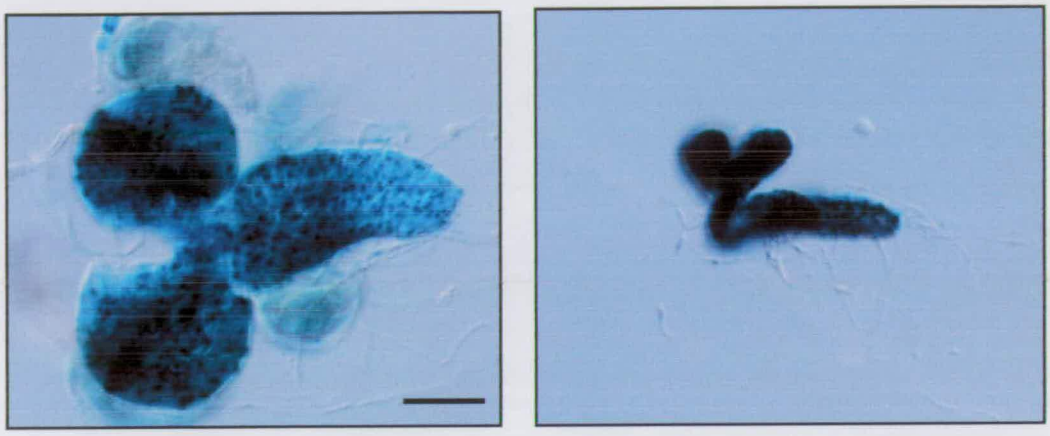

l(3)IX-14^{4Y7}/ TM6B

l(3)IX-14^{4Y7}/ *l(3)IX-14^{4Y7}*

Figure 4.9 β-galactosidase staining of *l(3)IX-14^{4Y7}* heterozygote and homozygote larval tissues. *IX-14* gene expression in larval tissues was monitored by utilising the lacZ marker gene present in the P element inserted in *l(3)IX-14^{4Y7}*. Expression of lacZ can clearly be seen in larval brains, in the proliferation zones of both heterozygotes and homozygotes in the optic lobes and ventral ganglion (scale bar = 200μm). In contrast, salivary gland staining showed no detectable expression of *IX-14* (data not shown).

brain is much less than half the size of the heterozygous brain, and that the staining appears much darker as there are two copies of the P-element present in each cell.

As *l(3)IX-14* alleles were observed to have a polytene chromosome phenotype (discussed in Chapter 3.9), I decided to perform salivary gland staining with the same technique to determine whether *IX-14* gene expression could be detected. β-galactosidase staining was carried out on salivary glands from both heterozygous and homozygous larvae from the *l(3)IX-14*^{4Y7} line. However, I was unable to detect any staining in either of these tissues (data not shown). A convenient control in this case was staining of brains from the same dissected larvae, which repeated the observations described above. Thus it seemed that *IX-14* is genuinely not expressed in salivary gland tissues, which may indicate that the polytene chromosome phenotypes observed may in fact be a downstream effect of the general proliferation defects seen in this mutant. However, a counter-argument is the fact that other mitotic mutants such as *l(3)k43* (a member of the ORC complex involved in initiation of replication) have apparently normal polytene chromosomes (Loupart *et al.*, 2000). Evidently more needs to be done to investigate this intriguing aspect of *l(3)IX-14* further.

4.7 Sequencing of *IX-14* coding and upstream regions from wild type and *l(3)IX-14*^{1} homozygous genomic DNA

In order to determine the lesion created by the ICR-170 mutagen in the original *l(3)IX-14*^{1} line, I undertook to sequence the entire coding region of the putative *IX-14* gene, as well as portions of upstream and intronic genomic regions, from wild type and homozygous mutant genomic DNA. This was achieved using primers designed to the known genomic sequence to amplify 1-2 kb fragments by PCR, then sequencing these PCR products directly. The amplified products were first electrophoresed on a 1% agarose gel to determine whether the product was a strong single band. Useable reactions were then purified of enzyme, buffers, dNTPs and primers by using the

MoBio PCR Clean-Up kit. Direct sequencing reactions were subsequently performed with the appropriate primers as described in chapter 2.9.

In total, I sequenced approximately 10 kb of genomic DNA from both wild type and *l(3)IX-14*^{1} homozygotes. The sequences were assembled into contigs using the LaserGene DNAStar software package, after removal of low quality sequence. The wild type and *l(3)IX-14*^{1} sequences were then compared to see if a lesion could be detected. Unfortunately, no base changes were observed in the *IX-14* coding region (repeated sequencing on both strands of questionable areas ruled out ambiguities due to poor quality sequence). As an additional safeguard, the contigs were also aligned against the finished *Drosophila* genome sequence as it became available for that region. Several base changes as well as one small insertion and one deletion were detected in the upstream genomic regions of *IX-14* and in the 5' UTR of this gene, shown in Figure 4.7B. However, these were ruled out as being the lesion responsible since the same changes were found in homozygous DNA taken from another lethal mutant in the laboratory, *l(3)k43*. It appears that these changes were thus natural polymorphisms that were present in various *Drosophila melanogaster* lines. As a precaution, the entire genomic region of the upstream gene CG6241 (or BNG) was also amplified and sequenced, but was not found to contain lesions either.

Since no lesion has been found in this coding region of the ICR-170 induced *l(3)IX-14*^{1} allele (even though this line fails to complement the P-element induced allele *l(3)IX-14*^{4Y7} which is known to be inserted 40 bp upstream of *IX-14*), I postulate that the lesion may be affecting an upstream regulatory sequence outside of the area examined in this study. I have shown that a disruption in the upstream region adjacent to the predicted promoter by the *l(3)IX-14*^{4Y7} P insertion abolishes any detectable mRNA message (Figure 4.6). I feel it is therefore not unreasonable that disruption of another regulatory region could cause a similar decrease in mRNA levels observed in the *l(3)IX-14*^{1} homozygous lane.

4.8 Verifying the P-element insertion site and orientation in *l(3)IX-14^{4Y7}*

In order to demonstrate that it was possible to amplify products by PCR using primers to the P element inverted repeat sequence (i.e. primer PF2) in combination with primers designed to the surrounding genomic region (see Figure 4.12), a series of PCR amplification reactions were performed on *l(3)IX-14^{4Y7}* homozygous genomic DNA and wild type DNA using the primer pairs shown in Table 4.1 below.

Table 4.1 Primer combinations used to verify the P-element insertion site

Allele	Upper Primer	Lower Primer	Product of expected size?
wild type	BPUP1	BPLW2	yes (1003 bp)
l(3)IX-14^{4Y7}	BPUP1	BPLW2	no product
wild type	PF2	Ex1-Int1.Lw	no product
l(3)IX-14^{4Y7}	PF2	Ex1-Int1.Lw	yes (1100 bp)

The results of these PCR reactions are shown in Table 4.1. It can be seen that as expected, the BPUP1/BPLW2 primer combination amplifies a product of 1003 bp in the wild type lane, but this product cannot be amplified under these conditions in the *l(3)IX-14^{4Y7}* line as the inserted P-element is too large to amplify. The other primer combinations give expected sizes and confirm the orientation of the P-element insertion as shown in Figure 4.7. Finally, the PF2/ Ex1-Int1.Lw product was purified and sequenced using the primers BPLW2 and Ex1-Int1.Lw and the P-element insertion site was verified as 40 bp upstream of the start of transcription of *IX-14* (Figure 4.10).

Figure 4.10 Sequencing the insertion site of the P element in *l(3)lX-14*^{4Y7}

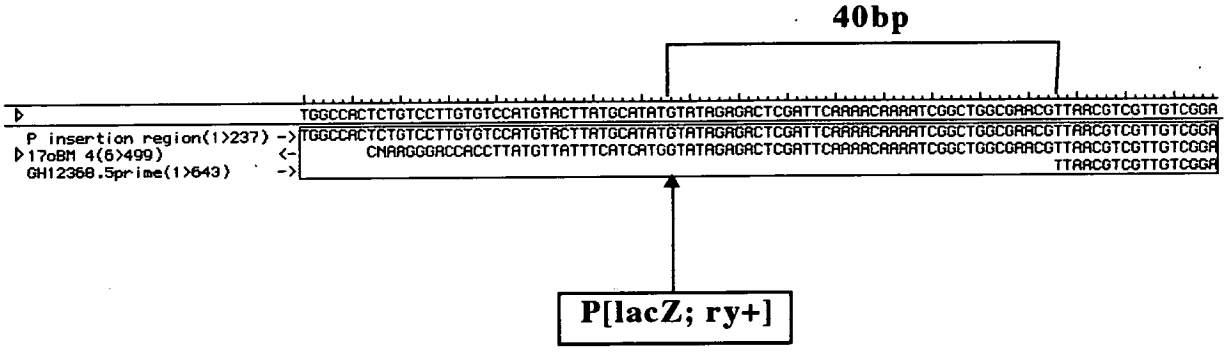

Figure 4.10 Determination of the P insertion site was performed by direct sequencing of the PF2/ Ex1-In1.Lw primer pair PCR product. Template DNA was first purified with the MoBio PCR Clean up kit. The nucleotides shown in red signify a mismatch with the concensus scaffold sequence for the region, and correspond the 5' terminal inverted repeat of the P element. The start of the GH12368 EST is shown for reference.

4.9 Mapping the P-element excision derivatives *l(3)IX-14^{eB}* and *l(3)IX-14^{eG}* by PCR analysis

A PCR-based strategy was used to define the lesions caused by the imprecise P-element excision events in *l(3)IX-14^{eB}* and *l(3)IX-14^{eG}*. I first set out to establish whether the 5' and 3' ends of the P-element were still present in these lines - both lines are *ry*, so at least some of the internal P[lacZ, ry+] sequence was missing. Similar PCR reactions to chapter 4.8 were performed, i.e. using the PF2 inverted repeat primer, to determine this. In addition, primer pairs upstream and downstream of the P-element insertion site were used to determine whether any genomic DNA was removed during the imprecise excision events. Figures 4.11A and B show the combinations used and the results obtained.

PCR was performed on genomic DNA prepared from 3rd instar homozygous larvae from the *l(3)IX-14^{eB}* line. It was shown that since the primer combination p32/BPLW2 could amplify a product of the correct size, then at least some of the 5' P-element sequence was still present. However, no combination using the PF2 inverted repeat primer was successful, indicating that the P-element inverted repeats must no longer be present. Additionally, I was unable to amplify across the insertion region using BPUP1/BPLW2, indicating that a sizable fragment of P-element does indeed remain. Genomic primer pairs upstream and downstream produce the correct product sizes, except combinations involving the primer BGEN2 which lies close (65 bp) upstream of the P-element insertion site. From these reactions it can be concluded that the imprecise excision event in *l(3)IX-14^{eB}* removed the P-element inverted repeats, some P-element sequence, and a small fragment (less than 100 bp) of genomic DNA flanking the 3' end of the P-element (see Figure 4.11C). Although this line is still late larval lethal, the homozygous larvae are sicker and very few attempt to crawl up the sides of the vial. This may indicate a shift to a slightly more severe defect in this line, perhaps due to the missing 3' flanking genomic fragment.

Figure 4.11 Mapping the P element excision derivitives of *l(3)IX-14*^{4Y7} by PCR. **A)** Diagram showing the genomic region surrounding the P element insertion site. Relevant primer sites are shown as light grey arrows on the upper or lower strands. **B)** Table of PCR results from the primer pairs shown in (A). **C)** Schematic representation of the structure of the genomic region in the P insertion line *l(3)IX-14*^{4Y7} and the 2 imprecise excision derivitives *l(3)IX-14*^{eB} and *l(3)IX-14*^{eG}. Deleted genomic regions are depicted in dashed lines.

Figure 4.11 Mapping the *l(3)IX-14^{4Y7}* excision derivatives by PCR

A

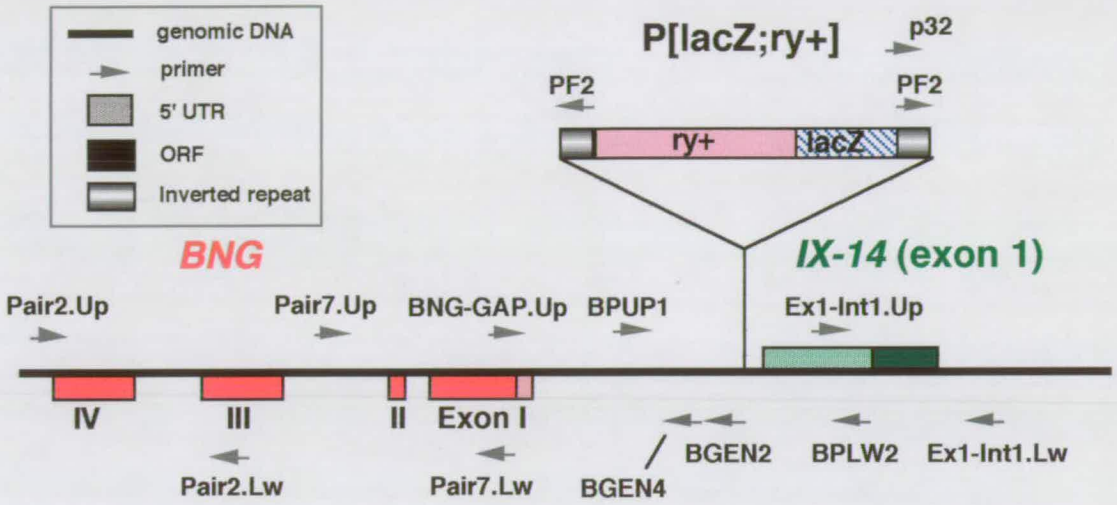

B

Primer pair	*l(3)IX-14^{4Y7}*	*l(3)IX-14^{eB}*	*l(3)IX-14^{eG}*
PF2 + BPLW2	+	+	-
p32 + BPLW2	+	+	-
Ex1-Int1.pair	+	+	+
BPUP1 + BPLW2	-	-	-
BGEN2 + BPUP1	+	-	-
BNG-GAP.Up + BGEN4	+	+	-
Pair7.Up + Lw	+	+	-
Pair2.Up + Lw	+	+	-

C

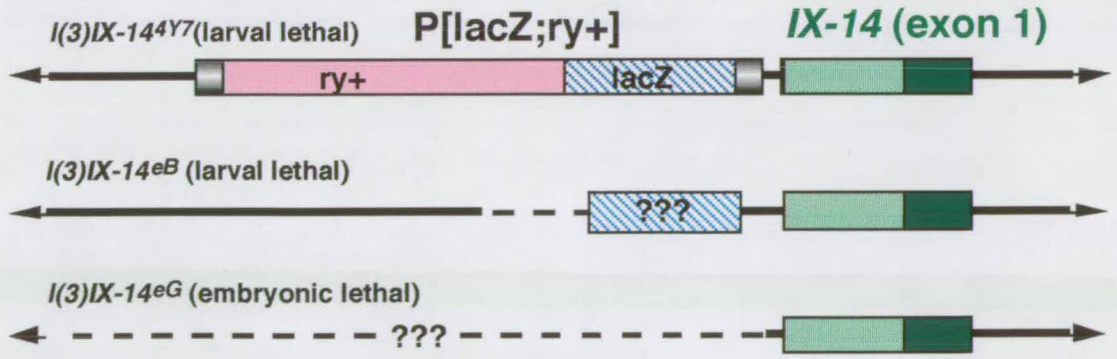

Analysis of the *l(3)IX-14^{eG}* line proved more difficult, as this was an embryonic lethal allele of *l(3)IX-14*. In order to obtain homozygous genomic DNA from this line, it was out-crossed to the Krüppel-GFP;TM3 balancer line (kindly provided by Tom Kornberg). Homozygous mutant embryos could then be selected by virtue of their lack of GFP fluorescence under UV light (heterozygotes and embryos homozygous for the balancer line proved easily detectable using this method). Genomic DNA was then prepared from single embryos by the method described in chapter 2.4 and used for further study. PCR analysis with DNA from these embryos showed that not only did the P element sequences appear to be missing, but also a substantial fragment of DNA flanking the 3' end of the P-element (i.e. some of the upstream 5' genomic sequence from *IX-14*) as no primer combinations used were able to amplify this region. However, I was able to use the primer combination of Ex1-Int1 upper and lower primers to amplify a product from the region 5' of the P-element. This result can be taken as a positive control therefore, as it shows that the genomic DNA prepared from single embryos by the method described was usable for PCR. The excision event in this line therefore seems to have excised not only the P-element, but a large (i.e. at least 4 - 5 kb, as yet I have not mapped exactly how large) portion of the genomic region flanking the 3' end of the P-element (see Figure 4.11C). An important point to note is that the coding region of the upstream gene CG6241 (a.k.a. *BNG*) is deleted by this excision. As *l(3)IX-14^{eG}* is an embryonic lethal allele, the deletion of CG6241 is presumably contributing to the severity of the phenotype in this line.

4.10 P-element mediated germline rescue of *l(3)IX-14*

I have obtained strong evidence to show that the novel metalloprotease gene we have designated *IX-14* is responsible for the intriguing mitotic and polytene chromosome phenotypes observed in the various alleles studied. In order to reinforce

this claim, I attempted to perform P-element mediated germline rescue of the *l(3)IX-14* mutation by inserting a wild type copy of the *IX-14* gene and demonstrate that it could restore viability (Spradling and Rubin, 1982). In order to achieve this I first cloned the full length *IX-14* cDNA into the pUAST transformation vector, as diagrammed in Figure 4.12, and verified the insertion by sequencing. I then attempted to create germline transformant lines of the w^{1118} strain with the *IX-14* cDNA integrated into the genome of the flies. This was done by direct injection of w^{1118} embryos with pUAST-*IX-14* into the posterior end of dechorionated embryos prior to pole-cell formation. A plasmid containing a transposase source (Δ2-3) was co-injected to facilitate integration of the rescue construct into the pole-cell genomic DNA. Any larvae that hatched from these injected embryos would be placed into a food vial, and any emerging adult flies would be back-crossed to w^{1118} virgins. Transformant flies would be detected in the progeny of these back-crosses as *white*$^{+}$ flies. Following identification of transformant lines, the insertion would be mapped as lines carrying the rescue construct on the X or 2nd chromosome would be used for the subsequent rescue steps.

This well established technique for creating *Drosophila* transformant lines would hopefully then allow me to create by a series of crosses a fly that was homozygous for the *l(3)IX-14*^{1} mutation on the 3rd chromosome, and that carried a copy of the copy of the rescue construct on the X or 2nd chromosome. As transcription of this construct would be dependent on Gal4 binding to the UAS sites located in the plasmid, a heat-shock inducible Gal4 driver (or other - many types exist) would also be required (Brand and Perrimon, 1993). Once this set of conditions had been met, heat shock induction of the Gal4 driver would hopefully induce transcription of the *IX-14* cDNA and act to rescue the lethality of the *l(3)IX-14*^{1} mutation.

Unfortunately, I was unable to complete this experiment due to the fact that despite injecting nearly 1000 embryos, I did not manage to obtain any transformant lines. The results of my injection attempts are summarised in Table 4.2 below. The survival rate of injected embryos, approximately 20%, is in agreement with results

Figure 4.12 Cloning the Full length *IX-14* EST into the pUAST transformation vector

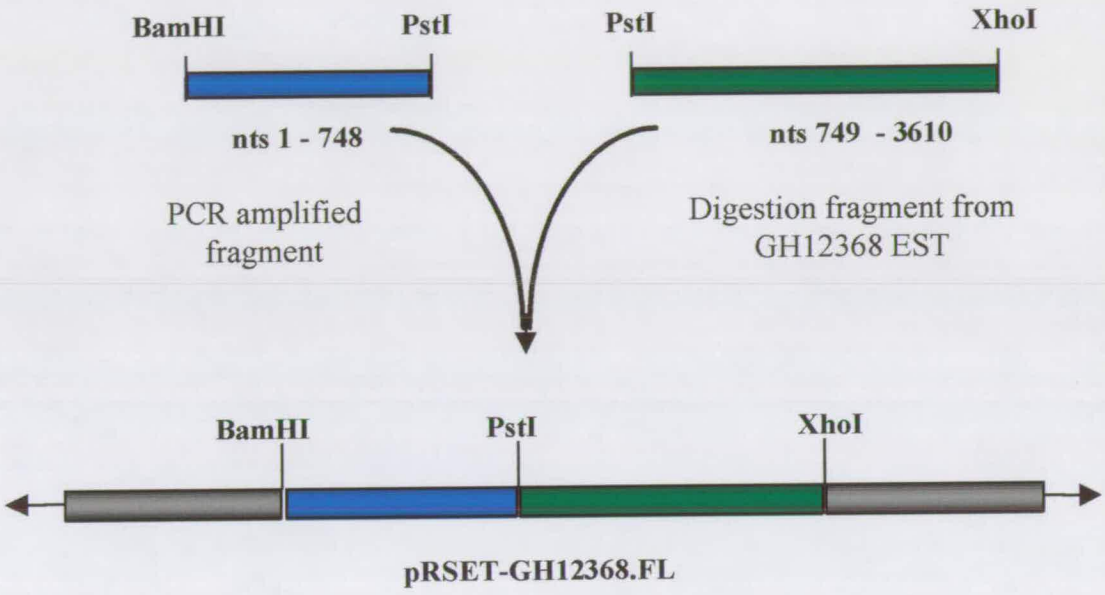

Figure 4.12 Cloning the Full length *IX-14* EST into the pUAST transformation vector. The Full length GH12368 EST was cloned in 2 fragments digested as shown above. The pUAST-GH12368.FL construct contained the entire *IX-14* ORF.

from previous experiments in this and other laboratories (Sharron Vass, personal communication). However, the number of surviving adults eclosing from these hatched larvae was lower than expected. This may therefore suggest that leaky expression of the rescue construct in any larvae that were transformants may be lethal, and that expression of *IX-14* may be very tightly regulated. As the *IX-14* gene is predicted to be a metalloprotease, it may well be the case that ectopic expression could cause lethality. An alternative explanation is that more DNA is required in the injection of w^{1118} embryos to increase the chances of a transformation event. This experiment will be repeated and these possibilities explored in subsequent work to be performed as part of my Wellcome Trust Prize Fellowship as outlined in Chapter 7.

Table 4.2 Summary of *l(3)IX-14* rescue experiment

Number of injected embryos	Number of hatched larvae	Number of eclosed flies	Number of single-pair matings	Number of sterile flies	Total number of progeny scored	Number of transformant lines
837	165 (19.7%)	79 (9.4%)	79	11	4231	0

Chapter 5
Production of IX-14 antibodies

5.1 Design of protein expression constructs for recombinant IX-14 protein

In order to further investigate the role of the IX-14 protein in the cell, I expressed a recombinant form of IX-14 in bacteria and injected it into rabbits for the purpose of raising antibodies. Using the sequence from the GH12368 plasmid (see Chapter 4), I was able to clone three fragments of IX-14 into the bacterial expression vector pRSET-B. These expression constructs comprised of the full length protein (683 aa), the N-terminal 138 aa, and the C-terminal 283 aa. Figure 5.1 diagrams the cloning of these constructs, and 5.2 diagrams the resulting fusion proteins.

The entire *IX-14* cDNA required the ligation of a 5' BamHI/ PstI fragment and a 3' PstI/ XhoI fragment simultaneously in order to clone it into pRSET-B, as there were no convenient restriction enzyme sites flanking the cDNA that did not also cut internally. However, as there was an upstream stop codon close to the first ATG of *IX-14*, I designed a PCR primer that would change this codon to an Alanine residue. The primer also contained a BamHI site at its 5' end for cloning purposes. After amplifying this modified 5' fragment from GH12368 cDNA plasmid by PCR, the product was purified and digested with the appropriate enzymes in preparation for cloning. Figure 5.1 diagrams this cloning procedure in more detail.

The N-terminal construct was created by digestion of pRSET-GH12368FL with EcoRI, gel purifying the vector plus remaining reduced insert, and allowing it to religate, creating a plasmid containing nucleotides 1 to 243 of the *IX-14* ORF. The C-terminal construct was created in a similar fashion, this time by restriction digestion of the FL construct using BamHI to remove the first 1341 nucleotides of the ORF, and subsequent re-ligation of the plasmid. All three recombinant forms of IX-14 were

Figure 5.1 Cloning the *IX-14* expression constructs into the pRSET vector

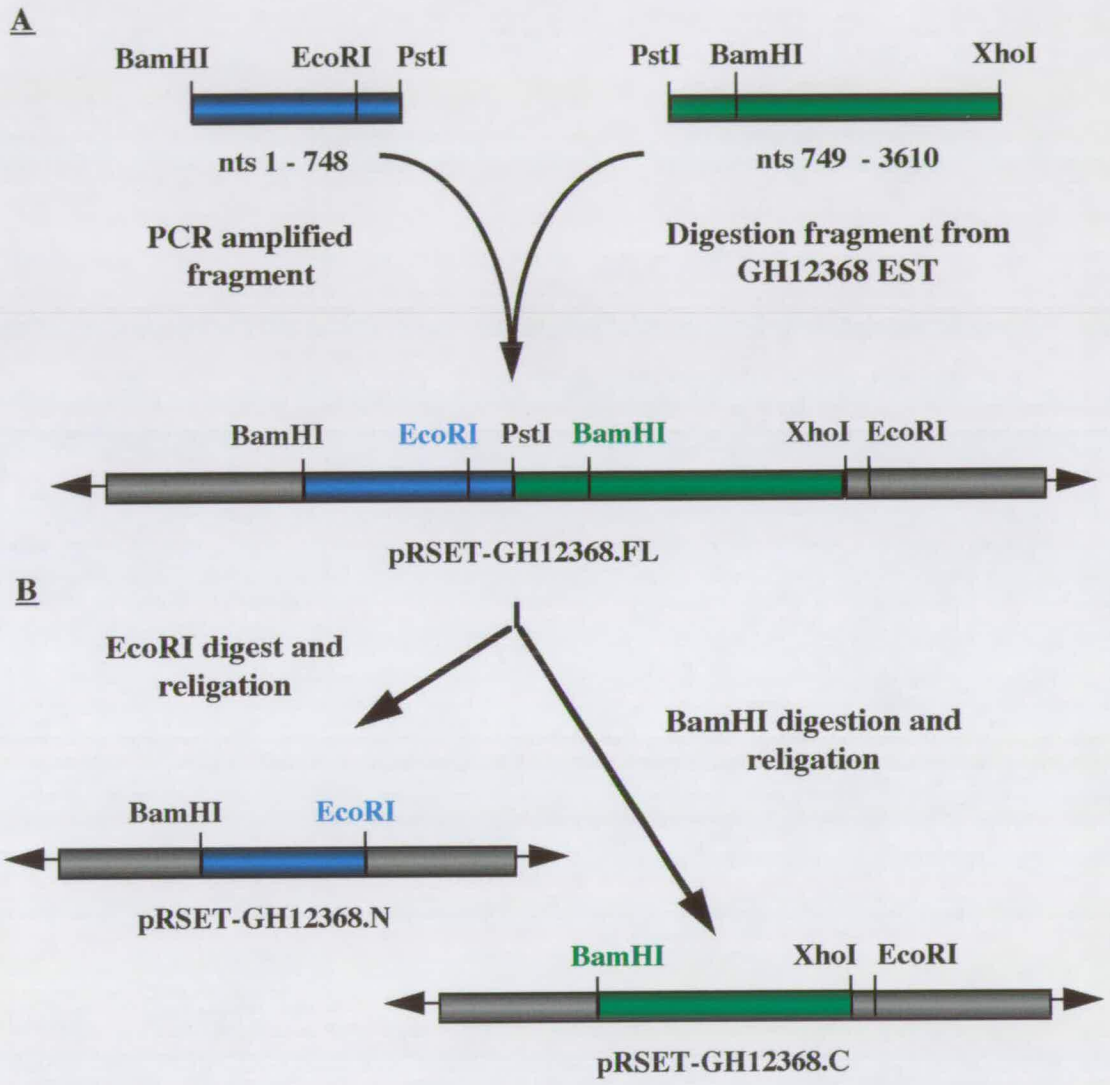

Figure 5.1 A) Cloning the Full length *IX-14* ORF into the pRSET transformation vector. The Full length GH12368 ORF was cloned in 2 fragments as shown above (5' fragment in blue, 3' fragment in green, vector sequence in grey), resulting in the pRSET-GH12368.FL construct. **B)** Construction of pRSET-GH12368.N and pRSET-GH12368.C.

verified by sequencing. Originally, all 3 recombinant forms were to be expressed. However, as detailed in Chapter 5.2, I was only able to express the C-terminal form in transformed bacteria, so ultimately only this recombinant protein was used for injection.

5.2 Expression and purification of a C-terminal portion of IX-14

For expression of the recombinant form of IX-14, the above constructs were transformed by electroporation into ER2566 bacterial expression cells (BL-21 and BL-21 LysS cells were also tried, but more success was achieved using ER2566 cells). The transformed bacteria were grown in LB containing 50 μg/ml ampicillin and expression was induced by adding 1 mM IPTG (see Materials and Methods for details). Aliquots of uninduced and induced bacterial extracts were electrophoresed by SDS-PAGE and stained with Coomassie Brilliant Blue to detect any overexpression. However, I was unable to detect any overexpression of the desired construct in the induced fractions.

Other conditions of induction were attempted, such as increasing the amount of IPTG, or growing the cells at 30°C, but these had no noticeable affect. It may be that overexpression of this recombinant protein is toxic to bacterial cells. It was therefore decided to proceed to purification of the recombinant protein via Nickel-Agarose beads, in order to determine whether any expression of the recombinant protein was occurring at all. Pellets of expressed culture were lysed and the Qiagen Ni-Agarose beads were subsequently added (see Materials and Methods). Elution of proteins bound to the beads was performed using either 5 mM Immidazole/ pH 4.5, or 500 mM Immidazole/ pH 8. Analysis of the elution fractions by SDS-PAGE, alongside the bacterial lysate and wash fractions, showed that for the C-terminal construct, the predicted 28 kDa protein was eluted off cleanly from the beads (Figure 5.3). Several

Figure 5.2 Design of expression constructs

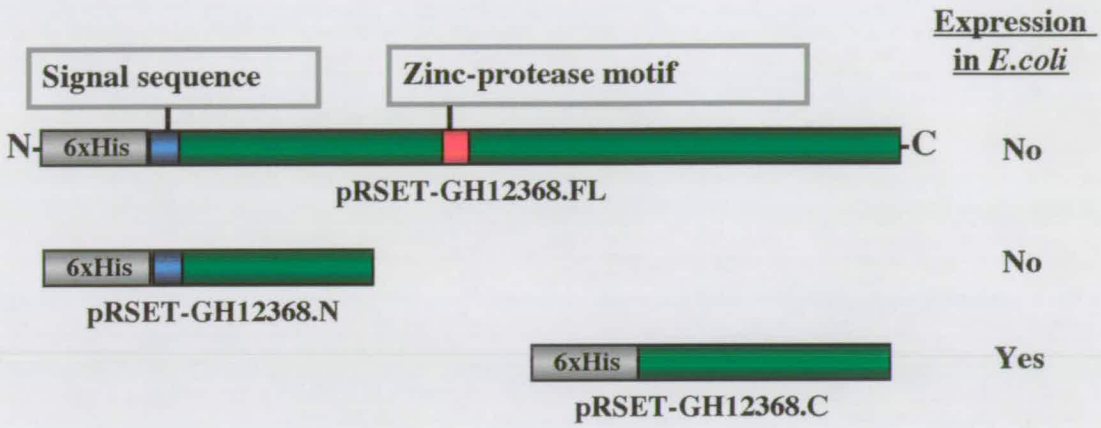

Figure 5.3 Purification of 6 His-tagged C-terminal fusion protein

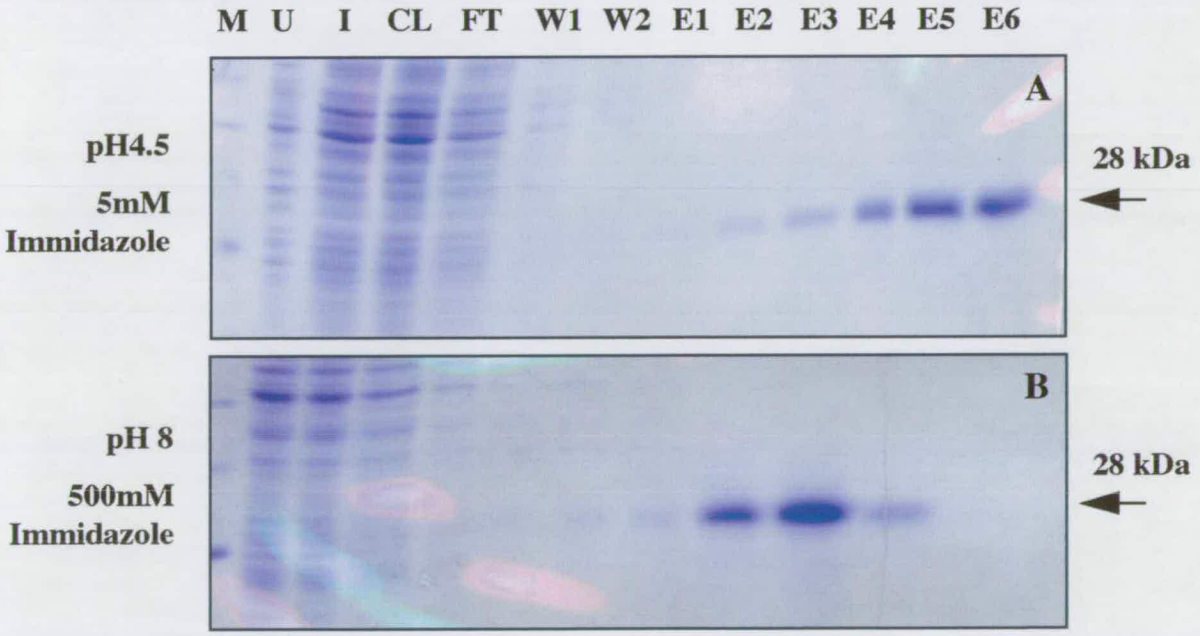

Figure 5.3 Purification of His-tagged fusion protein. Samples were electrophoresed by SDS-PAGE on a 12% acrylamide gel. Two different elution conditions (A and B) are shown. M = marker, U = uninduced, I = induced, CL = cleared lysate, FT = flow through, W = wash, E = elution.

pellets of expressed protein needed to be processed and the elution fractions pooled and methanol-chloroform precipitated for injection into rabbits. The precipitated protein was excised from an aqueous stained acrylamide gel, ground up under liquid nitrogen, and sent to the Scottish Antibody Production Unit (SAPU) at Carluke Hospital, Lanarkshire, who were contracted to perform all animal handling. We received 5 bleeds from each of 3 rabbits (R738, R747, and R759) for the production of this C-terminal IX-14 antibody, and the testing of these is described below.

5.3 Western blots of rabbit sera on embryonic and larval extracts

A total of 5 bleeds were received from each of 3 rabbits; R738, R747 and R759. Each of these bleeds was characterised as they arrived by Western blot analysis of embryonic protein samples (see Figure 5.4 for example), and subsequently against larval extracts. Unfortunately, none of these bleeds produced a strong single band signal at the expected molecular weight size for IX-14 (71 kDa). All immune sera produced several background bands which appear to be amplified versions of bands seen in the pre-immune sera.

Given that no strong characteristic bands were observed in wild type embryonic protein extracts, I blotted extract prepared from wild type versus *l(3)IX-14*^{1} homozygous mutant larvae, in order to establish whether any of the bands were reduced or absent in the mutants. This would provide stronger evidence that the correct protein was being recognised by these antibodies, despite the large amount of background. Figure 5.5 shows a blot of larval protein extract comparing wild type versus *l(3)IX-14*^{1} homozygous mutants. It can be seen that a faint band in the range of the predicted size of IX-14 does appear to be reduced in the mutant lanes. However, since the amount of background bands is so high, it is difficult to make any firm conclusions from these blots.

Figure 5.4 Western blot of wild type embryonic protein extract with IX-14 C-terminal antibodies

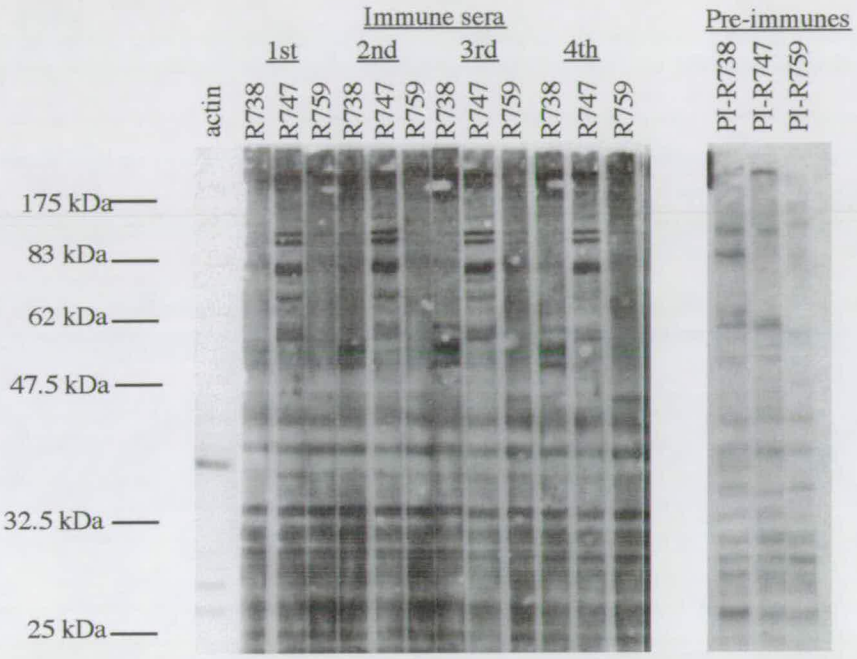

Figure 5.4 -Western blot detection of IX-14 C-terminal antibodies on embryonic protein extract. Bleeds 1 through 4 from rabbits R738, R747 and R759 were used at a 1:1000 dilution. Pre-immunes from the same animals are shown blotted against the same protein extract. Rabbit anti-actin has been used as a control, at 1:1000 dilution.

Figure 5.5 Western blot of wild type and *l(3)IX-14*^{1} larval protein extract with IX-14 C-terminal antibodies

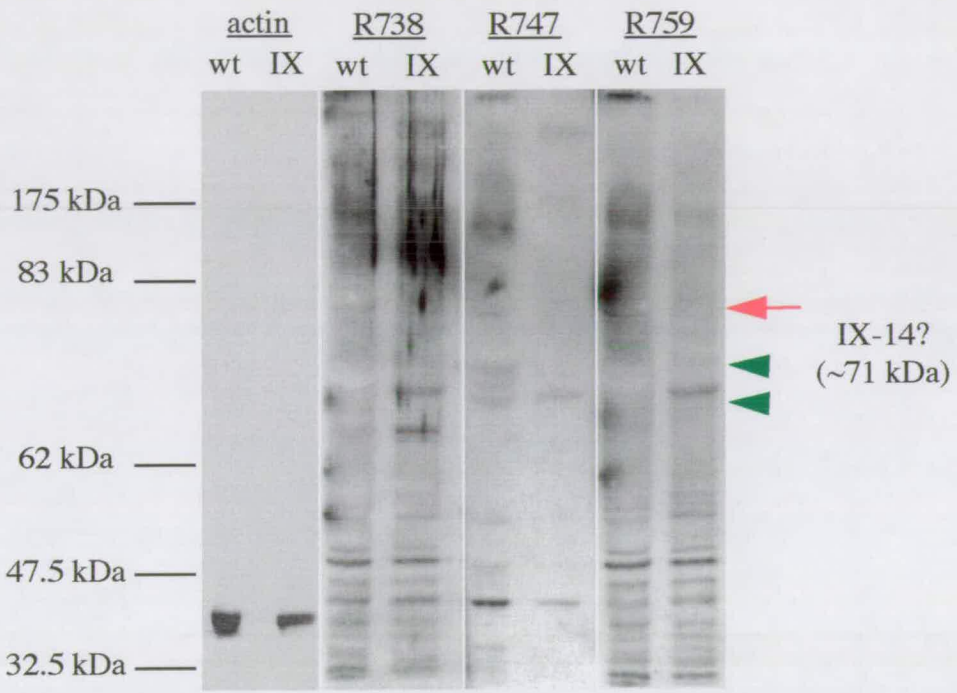

Figure 5.5 Western blot detection of IX-14 C-terminal antibodies on larval protein extract. Bleed 4 from rabbits R738, R747 and R759 were used at a 1:1000 dilution. Rabbit anti-actin (1:500 dilution) was used as a loading control. The red arrow points to a faint band present in all 3 rabbit immune sera in the wild type lanes that cannot be detected in *l(3)IX-14*^{1} extract. Green arrowheads also point to bands missing in the mutant extract, but these are only detectable with R747 serum.

Following the difficulty to convincingly determine whether these antibodies are recognising the IX-14 protein by Western blot analysis, I tested whether they would at least recognise the fusion protein that they were raised against. Figure 5.6 shows a Western blot of protein samples from transformed bacteria expressing the fusion protein, and the purified protein itself. It can be seen that the 28 kDa fusion protein band is recognised by the C-terminal antibody R759. Both R738 and R747 also gave the same result, verifying that these antibodies were indeed raised to the correct fusion protein.

5.4 Immunofluoresence studies on embryos and larval neuroblasts

Despite the lack of an obvious band by Western blotting, I decided to test whether the antibodies I raised to the C-terminal portion of IX-14 were able to detect cellular protein by immunofluoresence. I tested all bleeds of R738, R747 and R759 on both embryos and 3rd instar larval neuroblast squashes, versus their corresponding pre-immune sera.

Figure 5.7 shows staining of wild type embryos with immune sera from R759, which appears to stain interphase nuclei. This nuclear staining is distinct in interphase cells but becomes dispersed during mitosis, and is not seen in the pre-immune serum from the same animal. Closer examination of mitotic figures reveals that the dispersed staining in mitotic cells appears to be excluded from the condensed chromosomes (right panels in Figure 5.7). As this pattern of staining was not seen in pre-immune serum I postulate that this nuclear staining pattern may reflect the localisation of the IX-14 protein in embryos. Immune sera from R747 gave identical results to R759. However, immune sera from rabbit R738 did not show this nuclear localisation, only a honey-comb cytoplasmic pattern seen also in R738 pre-immune serum.

Figure 5.6 Detection of pRSET-GH12368.C fusion protein by R759 antisera

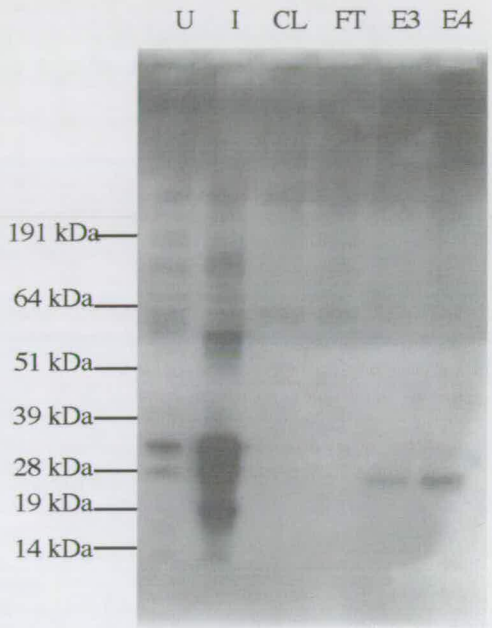

Figure 5.6 - Detection of pRSET-GH12368.C fusion protein by R759 antibody. Samples of Uninduced (U) and Induced (I) ER2566 cells, Cleared Lysate (CL), Flow Through (FT), and Elutions from fractions E3 and E4 of the pH 4.5, 5mM Immidazole purification (see Figure 5.3 for Coomassie) were blotted with R759 1st bleed. The 28 kDa pRSET-GH12368.C protein is detected in the two Elution fractions E3 and E4. The R738 and R747 immune sera also detect the purified 28 kDa fusion protein.

Figure 5.7 IX-14 C-terminus antibody staining on wild type embryos

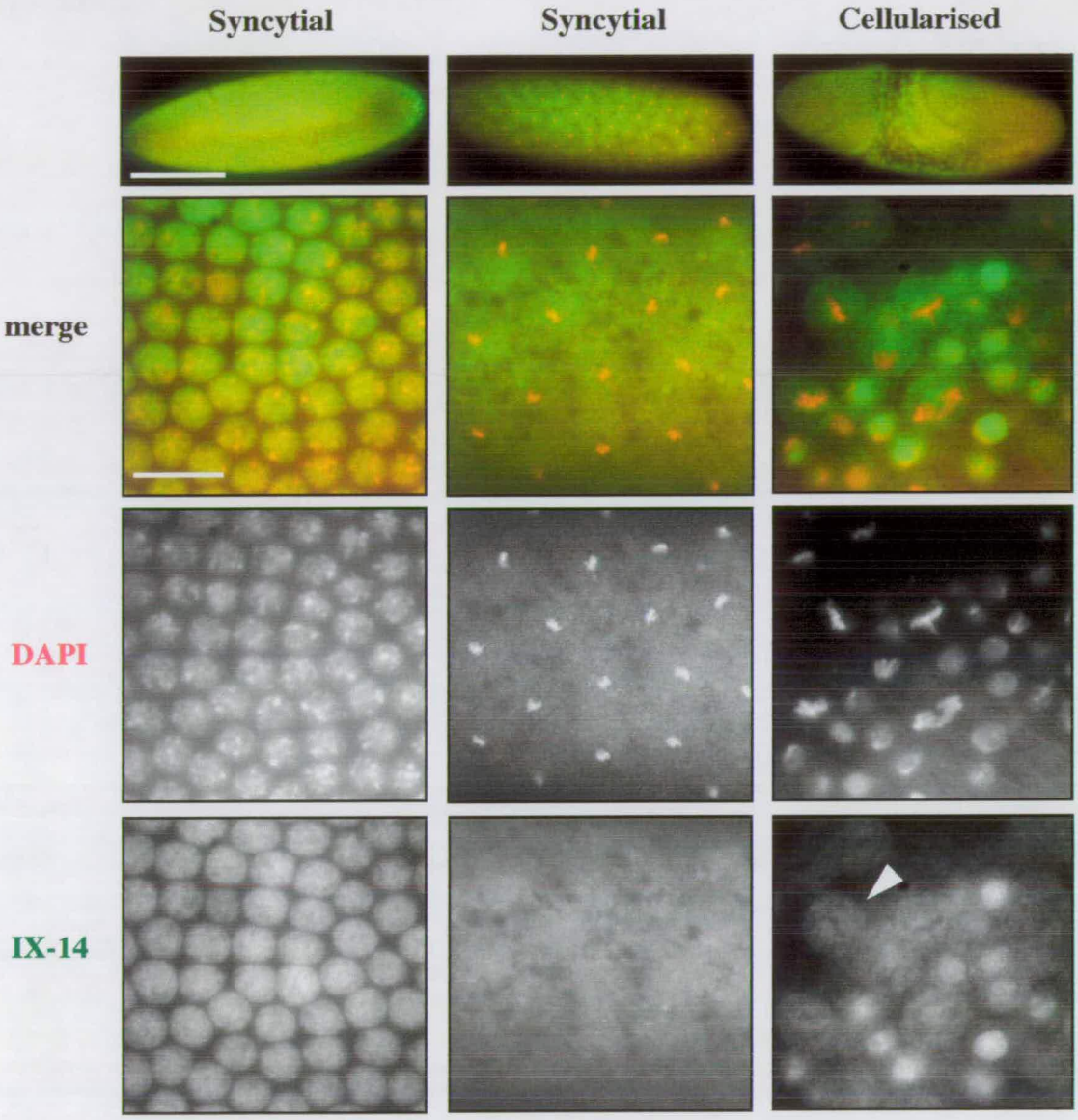

Figure 5.7 Wild type embryos stained with IX-14 C-terminus antibody (R759, bleed 4). Interphase staining is nuclear (left panels), mitotic staining is dispersed (middle and right panels) and appears to be excluded from chromatin (right panels, arrowhead). Top row shows whole embryo images taken at 20X (scale bar = 200μm), all other panels are at 100X (scale bar = 5μm).

The staining pattern of these immune sera on 3rd instar larval neuroblasts was very similar to that seen in embryos. Figure 5.8 shows examples of wild type and *l(3)IX-14*^{1} neuroblasts stained with R759 sera (4th bleed, 1:500 dilution). Interphase staining of nuclei can clearly be seen in both cases, as in embryos, and this staining then becomes dispersed in metaphase (arrowheads). Immune sera from R747 gave an identical staining pattern to R759, although as in embryos the R738 sera staining appeared identical to the corresponding background from the pre-immune sera for that rabbit.

It appears then that the IX-14 protein may have a nuclear localisation in the cell throughout interphase. This may correlate well with a role for IX-14 in the initiation stages of mitosis, as suggested by the Immunofluorescence results on the mutant larval brains (see Chapter 3 and Discussion Chapter 7). A caveat is that since these antibodies were raised to the C-terminal end of the protein, the observed localisation, if real, may not hold true for the entire protein. It has been shown that many proteases are cleaved to become active, usually at their N-termini. Antibodies raised to the N-terminus of IX-14 may therefore give a different localisation.

However, due to the lack of a strong signal by Western blot analysis on larval and embryonic tissues, and the high level of background in the immune sera, it cannot presently be determined that these antibodies are recognising only the IX-14 gene product. The immunofluorescence studies using the R759 and R747 sera however do give convincing nuclear staining in embryos and larval neuroblasts, not seen in the corresponding preimmune sera. Although one would expect reduced staining of IX-14 in 3rd instar homozygous mutant larvae, there are possible reasons why this is not seen to be the case here. Maternal contribution and a long protein half-life may contribute to the apparent IX-14 signal observed in these mutants, although at the late 3rd instar stage one would normally expect most maternal contribution to have been depleted. This depletion may be reflected in the patchy staining often seen in mutant brains with these sera. In addition, the high background observed with these sera by

Figure 5.8 IX-14 C-terminus antibody staining on wild type and *l(3)IX-14* neuroblasts

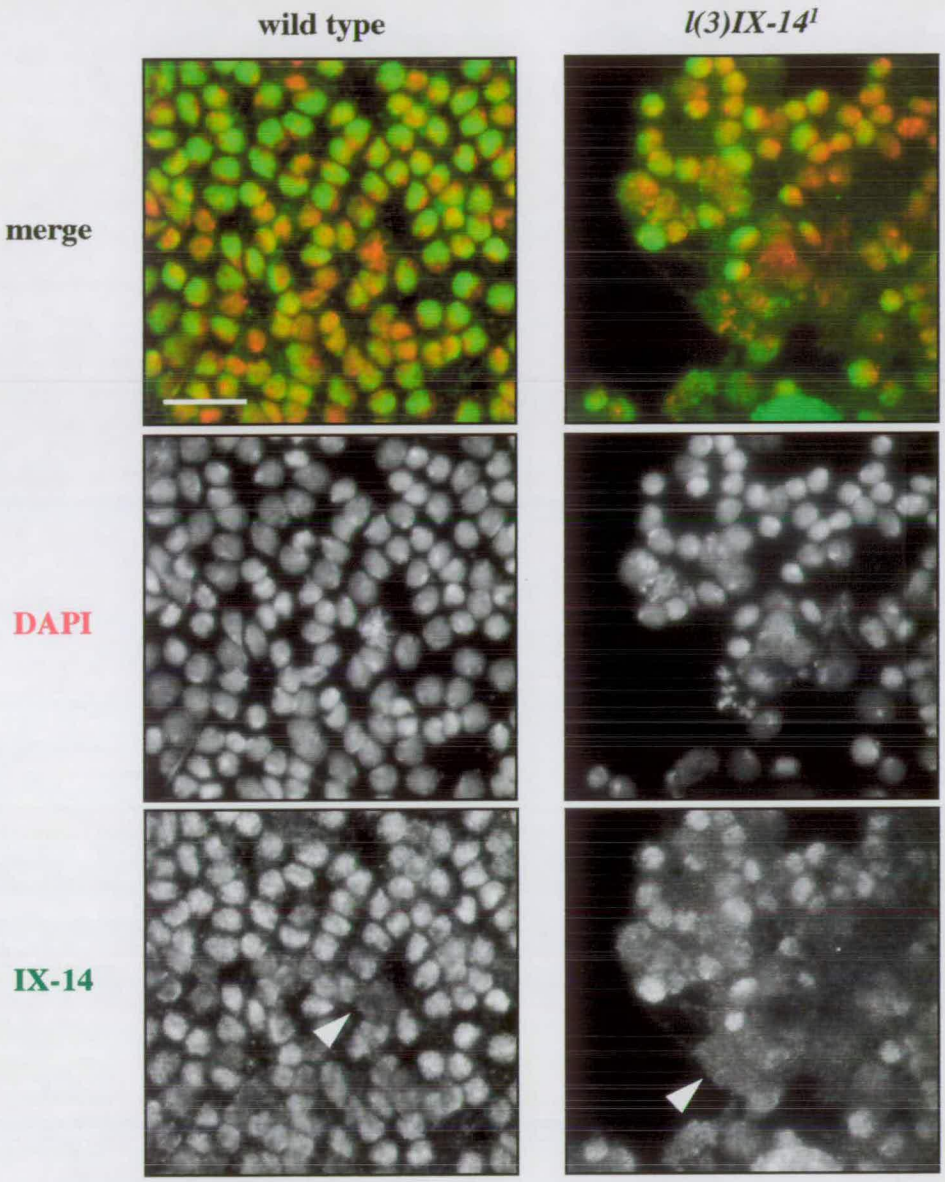

Figure 5.8 Wild type 3rd instar neuroblasts stained with IX-14 C-terminus antibody (R759, bleed 4, 1:500 dilution). A nuclear staining pattern is detected in interphase cells from both wild type and *l(3)IX-14*^{1} homozygous larvae, although the staining often appears more patchy in mutant brains. This nuclear staining is dispersed in mitotic figures (arrowheads). Squashes are shown at 100X magnification, scale bar = 5μm.

Western blotting of embronic and larval protein extracts may be a contributing factor.

The results from these IX-14 C-terminal antibodies therefore require further verification. I aim to address many of the issues raised here during the course of my Wellcome Trust Fellowship (see Chapter 7). Firstly, affinity purification of these antibodies against the fusion protein expressed in bacteria may help to decrease background and should allow cleaner Western blotting and immunofluorescence. Secondly, new antibodies will be raised to the full-length IX-14 protein, which should also help to confirm the observed localisation in embryos and neuroblasts. Lastly, by creation of a GFP-IX-14 construct would allow visualisation of IX-14 in live tissue, and provide independant verification of the immunofluorescence results.

Chapter 6
RNAi on *Drosophila* tissue culture cells

6.1 Background to dsRNA-mediated interference of gene function

First discovered and subsequently used extensively in *C. elegans*, dsRNA-mediated interference (RNAi) is a novel method for creating specific null mutations by selectively destroying mRNA for a targeted gene. One only needs to refer to the systematic efforts to knock out all predicted ORFs on the 1st and 3rd chromosomes of *C. elegans* to appreciate the extensive usage of the technique (Fraser et al., 2000; Gonczy et al., 2000). This targeting is sequence specific and relies on the homology between the dsRNA product introduced into the cell and its mRNA target. Beyond this however, little is known about the precise mechanisms of the process, although current theory suggests that the dsRNA may be converted to smaller fragments which would guide unknown endogenous cellular destruction mechanisms to the mRNA in question (Yang et al., 2000; Zamore et al., 2000).

Following its success in *C. elegans*, the RNAi methodology made the jump to *Drosophila*, and until recently has relied upon the physical injection of dsRNA into early embryos. Several publications have demonstrated the power of this technique, e.g. (Quinn et al., 2000; Denef et al., 2000; Wei et al., 2000). However, embryos can be a technically difficult tool to use in RNAi experiments due to the need to physically inject the desired construct, and can be limited in its ability to address particular questions in cell biology. This problem has recently been overcome by the successful introduction of RNAi in *Drosophila* tissue culture cells such as the S2 and Dmel2 lines (Clemens et al., 2000). The benefits are immediately obvious - one only needs to serum-starve cells and soak them in dsRNA for 1 hour to initiate the effect. A

monolayer of cells can then be centrifuged easily onto adhesive slides and stained immunohistochemically. In parallel, protein extract can be made from an aliquot of cells from the same timepoint and blotted for the protein in question to ascertain efficacy.

Despite the currently low number of publications stemming from this method, the number of groups (including our own) who have successfully applied it to a variety of cell cycle genes is growing steadily. I therefore decided to initiate a study of the effect of IX-14 RNAi in *Drosophila* tissue culture cells, with the view that it might provide an independent verification of the striking phenotypes I have observed in the *l(3)IX-14* larval mutants (discussed in Chapter 3), and indeed may provide important additional information as to the function of the IX-14 protein.

6.2 Design and preparation of template DNA

This protocol we have used was received from the Kaufman laboratory and is based on the methods described in Clemens et al. (2000). Briefly, a ~700bp PCR product designed to a region of the gene of interest is used as a template for the dsRNA reaction. The primers used to amplify this product were modified to include a T7 polymerase binding site at their 5' ends (described in Materials chapter), thus providing a built-in recognition site for the T7 polymerase on either strand of the template fragment. After transcription of sense and antisense RNA from this template, the RNA would be heated to 65°C and allowed to anneal into a double stranded form. This dsRNA would then be incubated with *Drosophila* cultured cells to initiate the RNAi experiment.

I used two different primer pairs designed to the GH12368 EST (i.e. the *IX-14* cDNA, see Chapter 4.1) to amplify the templates: primers T7BMC01/T7BMC09 to amplify template 'A' (650 bp) and T7BMC04/T7BMC07 to amplify template 'B' (800 bp) (sequences given in Materials section). These primer pairs were chosen on the

basis that template 'A' would include the first ATG of the message, and that template 'B' would encompass the -H-E-X-X-H- zinc-metalloprotease motif further along in the sequence (see Figure 6.1A) (although there is currently no information on whether the efficiency of the dsRNA-mediated degradation of the mRNA message is enhanced by including the ATG). The 5' ends of these primers included the T7 binding site as detailed above, and a standard PCR reaction was performed on the GH12368 EST cloned into pOT2 (based on Methods Chapter 2.10). The results of these two reactions are shown in Figure 6.1B. The volumes of 5 identical reactions for each primer pair were pooled and purified using the MoBio PCR Clean-up Kit. Preparation of dsRNA from these templates was performed using the MEGAshortscript T7 kit (as described in Methods Chapter 2.36) and resulted in approximately 10 mg/ml of dsRNA from both templates. Electrophoresed samples of resulting dsRNA are shown in Figure 6.1B.

6.3 RNAi experimental details

Two sets of RNAi experiments were performed on two different *Drosophila melanogaster* cell lines, S2 and Dmel2 cultured cells, as detailed in Table 6.1. The first set of experiments were designed to test which cell line would give an observable phenotype with dsRNA from template 'A', which covered the *IX-14* ATG. The second set of experiments was designed to test *a)* whether the results in the S2 line from Experiment 1 were repeatable, and *b)* whether a different RNAi template to the same gene could achieve the same results.

1 X 10^6 cells were induced to take up dsRNA by incubating them in Serum-free Expression medium (Sigma) together with 15 μg of dsRNA for 1 hour at room temperature. Cells were prepared in parallel for immunofluorescence by growing them on Permanox chamber slides (Lab-Tek) for the duration of the experiment, and Western blot analysis by growing them in 6-well plates and preparing protein extract

Figure 6. 1 Design of RNAi primer pairs

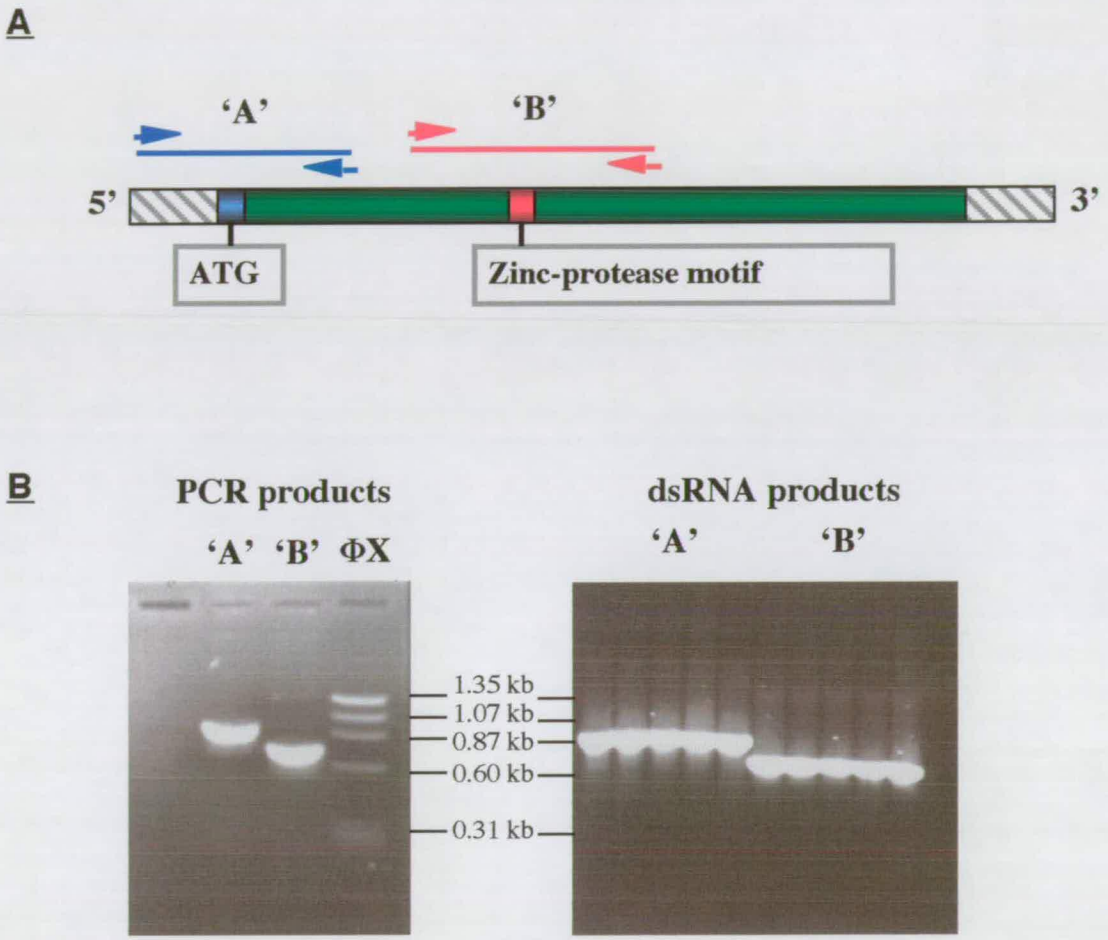

Figure 6. 1 **A)** Design of RNAi primer pairs. Two primer pairs were designed to the *IX-14* cDNA sequence, A (650 bp) which spans the ATG and B (800 bp) which spans the predicted zinc-metalloprotease motif, shown in blue and red above respectively. Grey shaded areas represent 5' and 3' UTRs, solid green bar designates the ORF.

B) Gel electrophoresis of 'A' and'B' primer pair PCR and dsRNA products produced from those templates. ΦX digested with HaeIII was used as a molecular weight marker.

from specific timepoints. Protein extracts were prepared in a similar manner to that described in Chapter 2.16, i.e. in Lysis EBR + SDS-PAGE buffer containing DTT. The extracts were sonicated for approximately 1 second bursts for 30 seconds, and boiled for 3 minutes before being stored at -20°C until needed. Slides for each timepoint were prepared by spinning for 10 minutes at 4000 rpm to help the cells adhere to the slide, fixing the cells in 4% PFA in PBS for 3 minutes followed by normal permeabilisation, blocking and incubation steps for the relevant antisera used (see Methods Chapter 2.32).

For each experiment, 7 timepoints were taken starting at Time 0 (i.e. before addition of dsRNA), then once every 24 hours until 144 hours. Previous attempts had shown that RNAi of other proteins involved in cell cycle events required a minimum of 48 - 72 hours before any phenotypes were observed (Mar Carmena, Victor Simossis, Sharron Vass, personal communication), although this cannot be regarded as a general guideline.

Table 6.1

	Experiment 1		**Experiment 2**	
Cells used	**S 2**	**Dmel2**	**S 2**	**S 2**
Template used	Template 'A'	Template 'A'	Template 'A'	Template 'B'
Phenotype observed?	Yes	No	Yes	Yes
Antibodies Set 1	P-H3 CP190 DAPI	P-H3 CP190 DAPI	P-H3 CP190 DAPI	P-H3 CP190 DAPI
Set 2	P-H3 α-tubulin DAPI	P-H3 α-tubulin DAPI	P-H3 α-tubulin DAPI	P-H3 α-tubulin DAPI

6.4 Western blot of RNAi timepoints

The equivalent of 3 X 10^5 cells from all timepoints were electrophoresed on Novex minigels and transferred to nitrocellulose filters. The filters were then blotted with the 5th bleed of R759 serum, raised to the C-terminal third of the *IX-14* protein (see Chapter 6 for details). Figure 6.2 shows the results of this blot. Unfortunately, as the rabbit antibodies that I currently possess (see Chapter 5) do not give a strong signal on Western blots, I was unable to detect a band corresponding to the *IX-14* product on these filters. It is therefore impossible for me to say whether *IX-14* protein levels have been significantly reduced in this RNAi experiment. I therefore decided that the judgement on the success of this experiment at this time would have to be made using phenotypic analysis alone, comparing dsRNA treated cells to control cells from the same timepoints.

6.5 Immunofluorescence of RNAi cells

For the first RNAi attempt, two sets of both S2 and Dmel2 cells with and without dsRNA treatment (i.e. 4 slides per timepoint) were grown directly on Permanox chamber slides as detailed in 6.3 above. At each timepoint, the relevant slide would be centrifuged at 4000 rpm for 10 minutes to adhere cells in suspension, and fixed with 4% PFA for 3 minutes. I then incubated each set of cells with the antibodies listed in Table 6.1 above. The immunofluorescence reagents were chosen based on the previously observed phenotypes of the *l(3)IX-14* mutation in larval brains (described in Chapter 3) i.e. that of hypercondensed mitotic chromosomes (seen by DAPI and P-H3 staining), unseparated/unreplicated centrosomes (CP190 staining), and misformed mitotic spindles (α-tubulin staining).

From examination of the slides from various timepoints in Experiment 1, I observed that obvious mutant phenotypes were only apparent in the S2 cultured cells. I

Figure 6.2 Western blot of RNAi timepoints

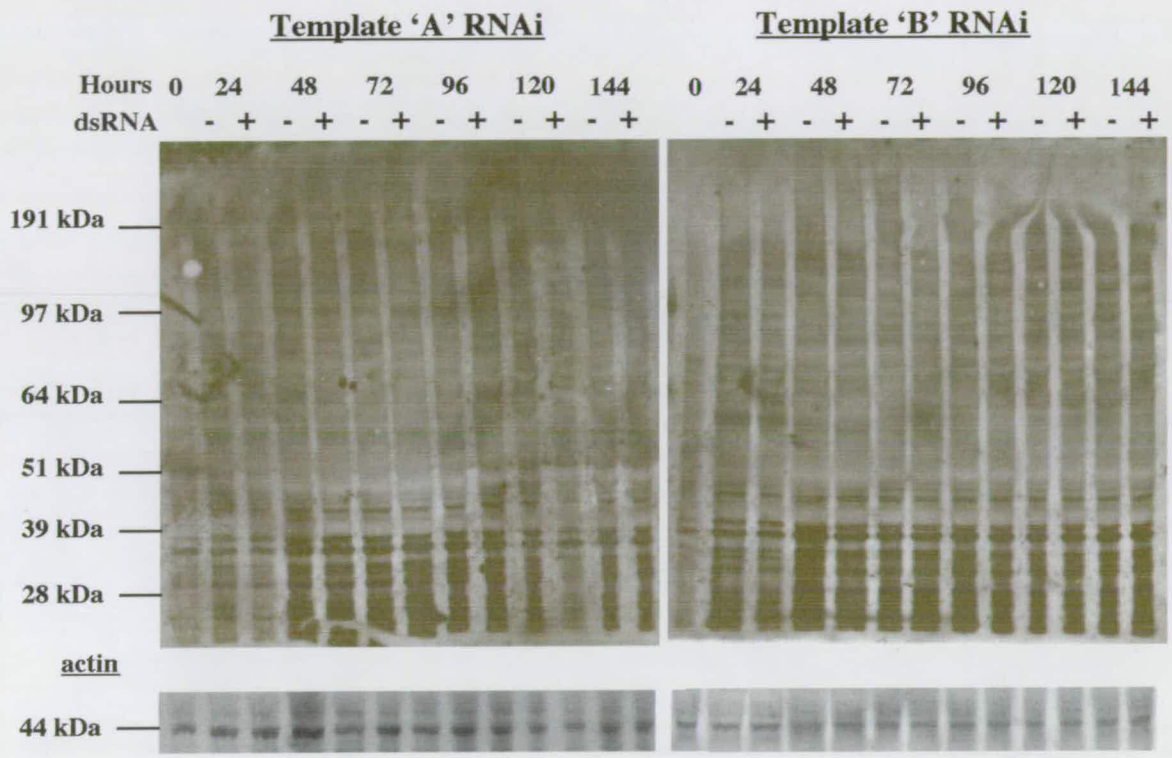

Figure 6.2 Western blot of RNAi timepoints. Nitrocellulose filters containing cell protein extracts from the indicated timepoints were probed with the *IX-14* C-terminal antibody R759 (5th bleed). The blots were then stripped and blotted with rabbit anti-actin as a loading control (lower panels).

therefore concentrated on this cell line for the phenotypic examinations in Experiment 1, and in the design of Experiment 2, where 2 different dsRNA templates (i.e. *IX-14* templates 'A' and 'B')were used to treat the same cell line. In contrast to the control images shown in Figures 6.3 and 6.5, samples treated with *IX-14* dsRNA started to show a mutant phenotype from 72 hours onwards (Figures 6.4 and 6.6) . At a low frequency (approximately 5% of mitotics), I was able to detect similar phenotypes to those previously observed in the *l(3)IX-14* larval alleles mentioned above, although many of the surrounding cells looked normal. From the cell density counts at each timepoint, the cells seemed to be proliferating normally (see Table 6.2 and Figure 6.7). Figures 6.4 and 6.6 show a selection of panels highlighting the main phenotypes observed. As these are not hypotonically swollen cells, the chromatin phenotype is harder to resolve. However, it can be clearly seen that both centrosome and spindle defects are apparent after 72 hours. Many cells apparently have only one centrosome (seen in Figure 6.4, left column) or possibly paired centrosomes that have not separated (middle and right columns), in comparison to the control cells from the same timepoint that always have clearly separated centrosomes at this stage of the cell cycle. A caveat to bear in mind is that both S2 and Dmel2 cells have a background of polyploidy, and this can influence the number of centrosomes observed. However, when aberrant numbers of centrosomes are observed in control cells, it is always an increase in number that is observed, not a decrease to a single centrosome during mitosis as observed in the dsRNA treated cells. It is reasonable therefore that the reduced number of centrosomes seen in dsRNA treated cells can indeed be attributed to the interference effect of the *IX-14* dsRNA.

The second main phenotype observed is that of disrupted or misformed mitotic spindles. In control cells, mitotic chromosomes that are congressing or have aligned on the metaphase plate are always accompanied by a clearly defined mitotic spindle (see Figure 6.5). In the dsRNA affected S2 cells however, this clear mitotic spindle is not

Figure 6.3 Untreated *Drosophila* S2 cultured cells stained with CP190, P-H3 and DAPI.

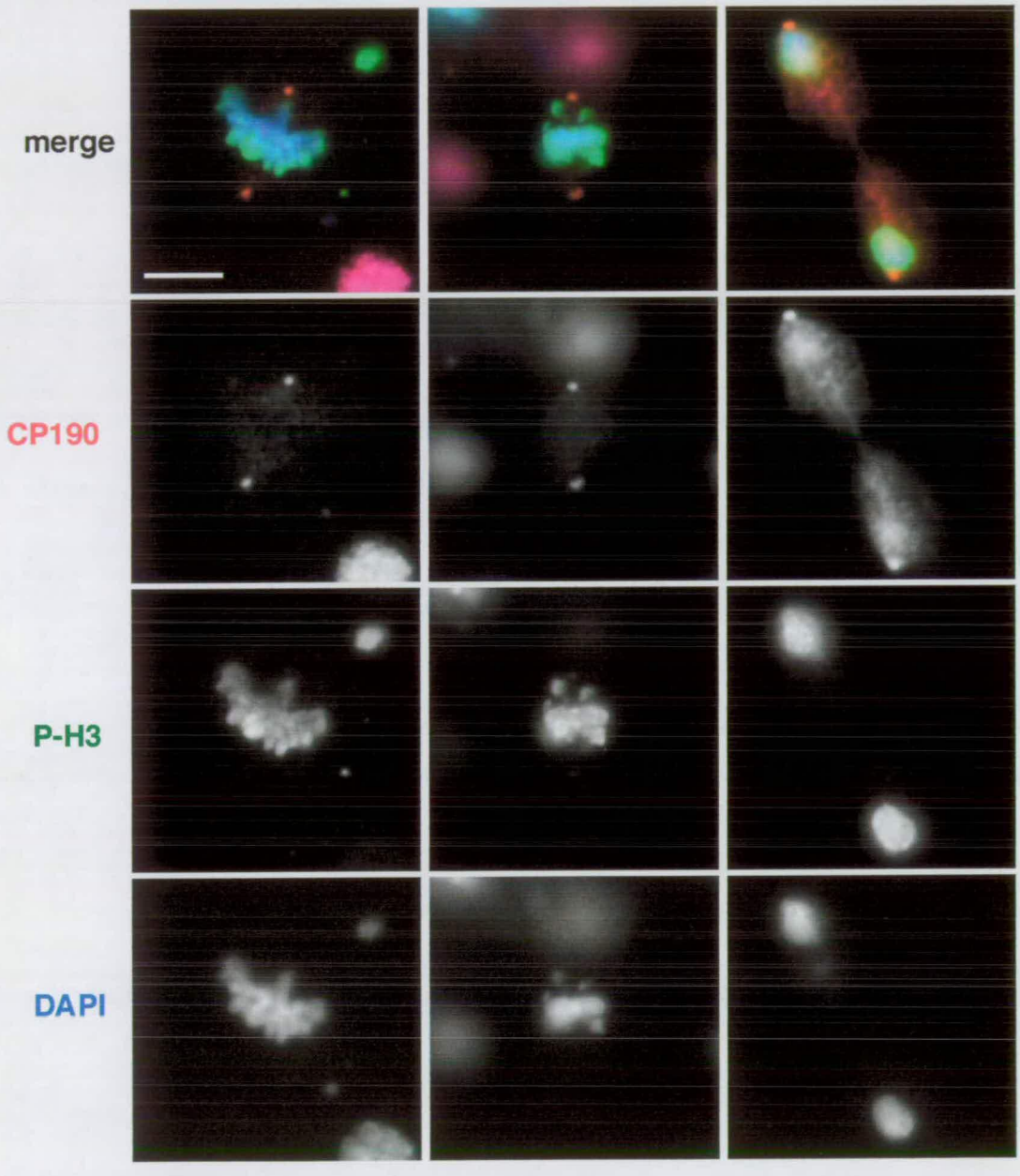

Figure 6.3 CP190, P-H3 and DAPI staining of untreated *Drosophila* S2 cells. Images were taken at 100X magnification, scale bar = 5μm.

Figure 6.4 dsRNA-treated *Drosophila* S2 cultured cells stained with CP190, P-H3 and DAPI.

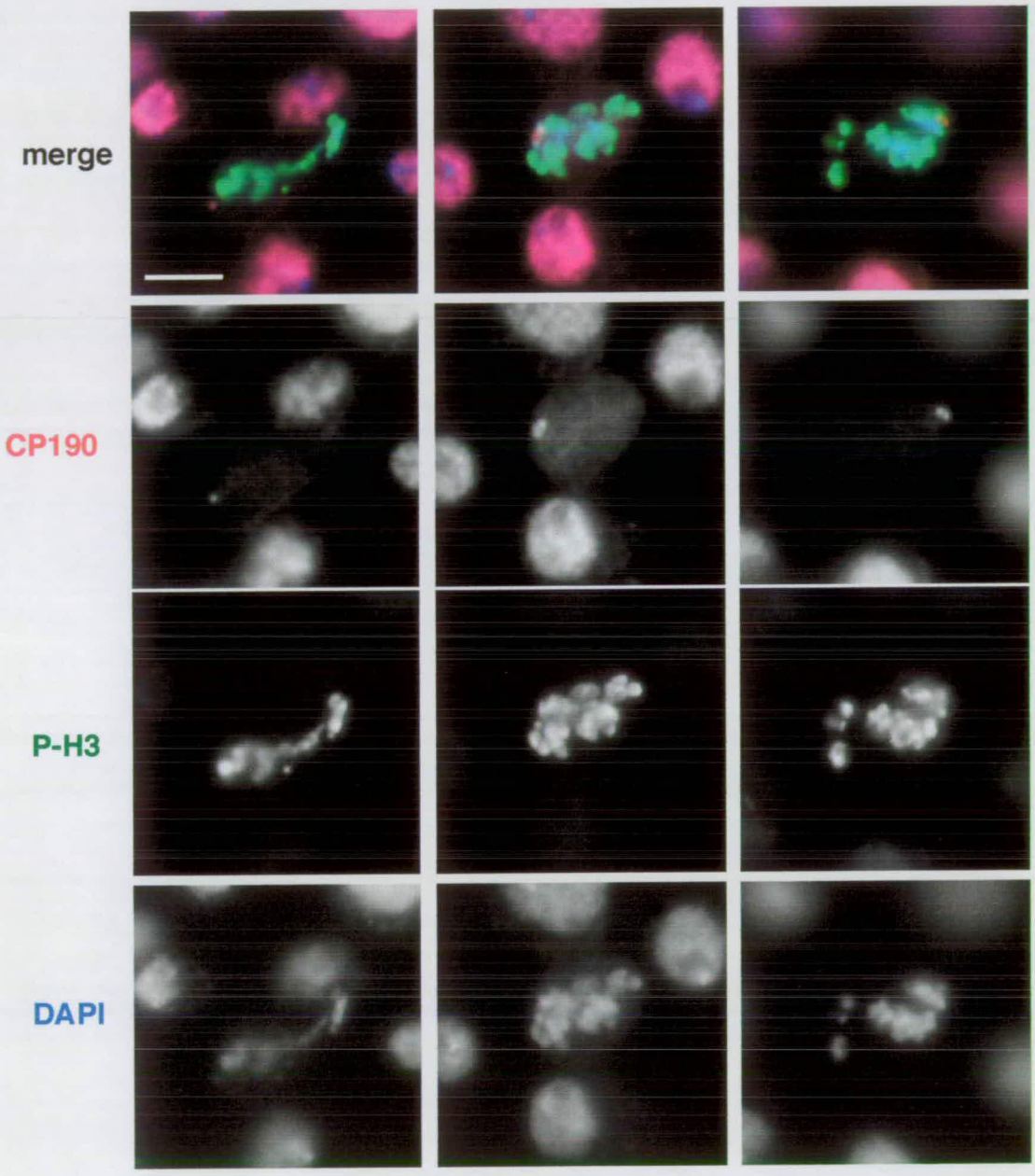

Figure 6.4 CP190, P-H3 and DAPI staining of dsRNA-treated *Drosophila* S2 cells. Images were taken at 100X magnification, scale bar = 5μm.

seen. Occasionally there are hints of monopolar or rudimentary spindles (Figure 6.6, left and right columns respectively). Figure 6.6, middle column shows what may be a bipolar spindle, but even this is clearly abnormal in comparison to the control spindles shown in Figure 6.5, and examination of the chromosomes in this figure shows they appear hypercondensed and are scattered across the spindle. These phenotypes correlate well with what I have observed in mutant larval brain squashes, where bipolar mitotic spindles are only observed at a low frequency, and most mitotic figures show either malformed monopolar or severely disorganised spindles accompanied by hypercondensed mitotic chromosomes (see Chapter 3).

As mentioned above, the mutant phenotypes reported here were only apparent in S2 cultured cells at a low frequency, approximately 5% of mitotic cells. This may be due to several reasons: incomplete penetration of the dsRNA effect due to unequal exposure or uptake of the dsRNA treatment, low turnover of the target protein or possibly delayed cell division in mutant cells . As a consequence, 'healthy' cells (i.e. those that did not take up dsRNA) would out-compete RNAi'd cells in the same dish, and thus reduce considerably the fraction of dsRNA affected cells observed. It may also be the case that if a protein has a low turnover rate, some recovery from the dsRNA treatment might occur before any effect is seen. It must be stressed that this technique is extremely new in its application to *Drosophila* tissue culture cells - no doubt further studies will help to explain the low penetrance observed here.

Important points to consider from this experiment are: 1) the phenotypes that were observed (albeit at a low frequency) match those observed in the *l(3)IX-14* larval lethal alleles and have not been observed in control cells (i.e. where no dsRNA was added). This indicates that the effect was specific to the *IX-14* gene. 2) RNAi experiments on other *Drosophila* genes involved in the cell cycle, such as INCENP, Aurora B kinase, Poly, Scc1 and Orc2 have different phenotypes to IX-14 RNAi (Mar Carmena, Victor Simossis, Sharron Vass, personal communication), again showing

Figure 6.5 Untreated *Drosophila* S2 cultured cells stained with α-tubulin, P-H3 and DAPI.

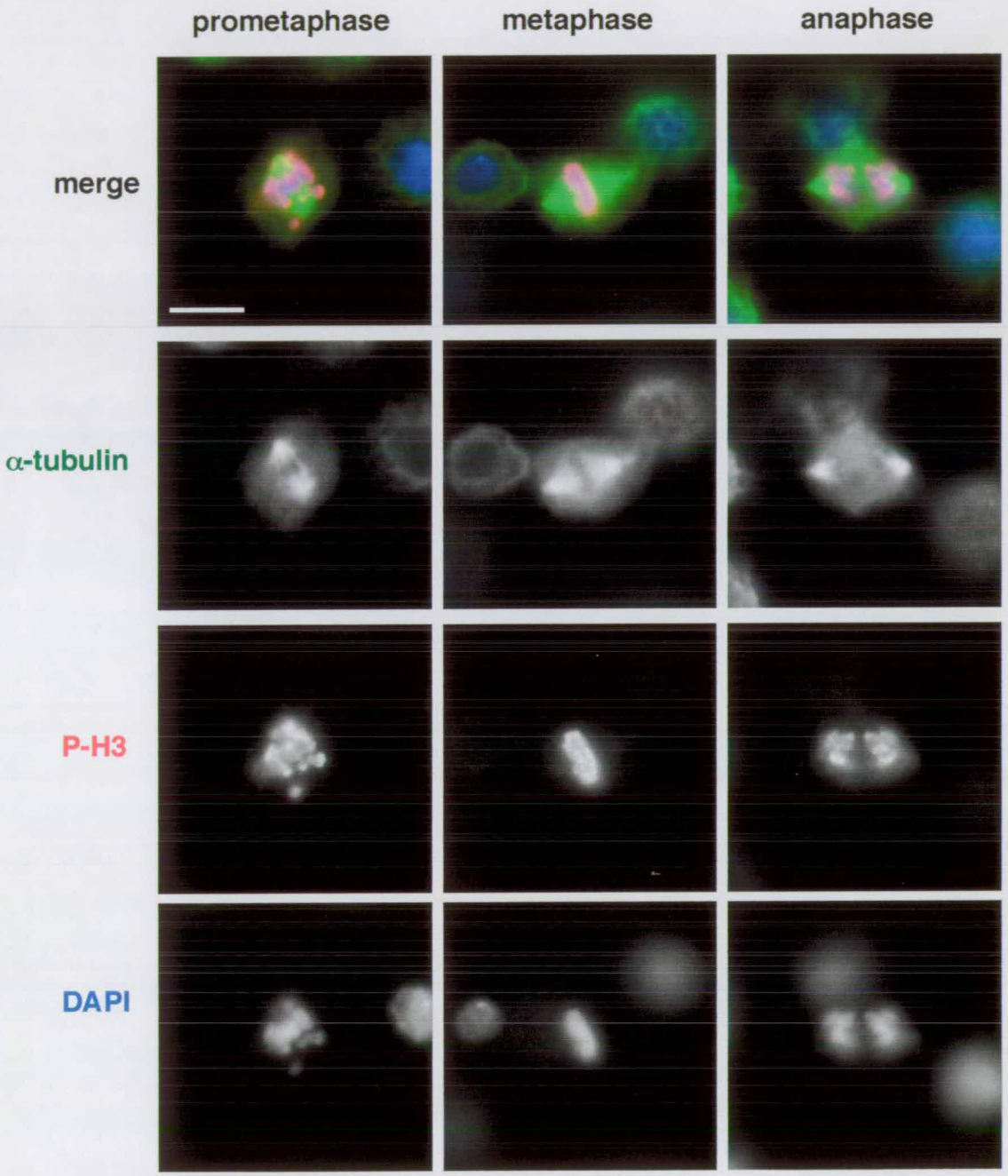

Figure 6.5 α-tubulin, P-H3 and DAPI staining of untreated *Drosophila* S2 cells. Images were taken at 100X magnification, scale bar = 5μm.

Figure 6.7 Graphs of cell counts during RNAi experiments

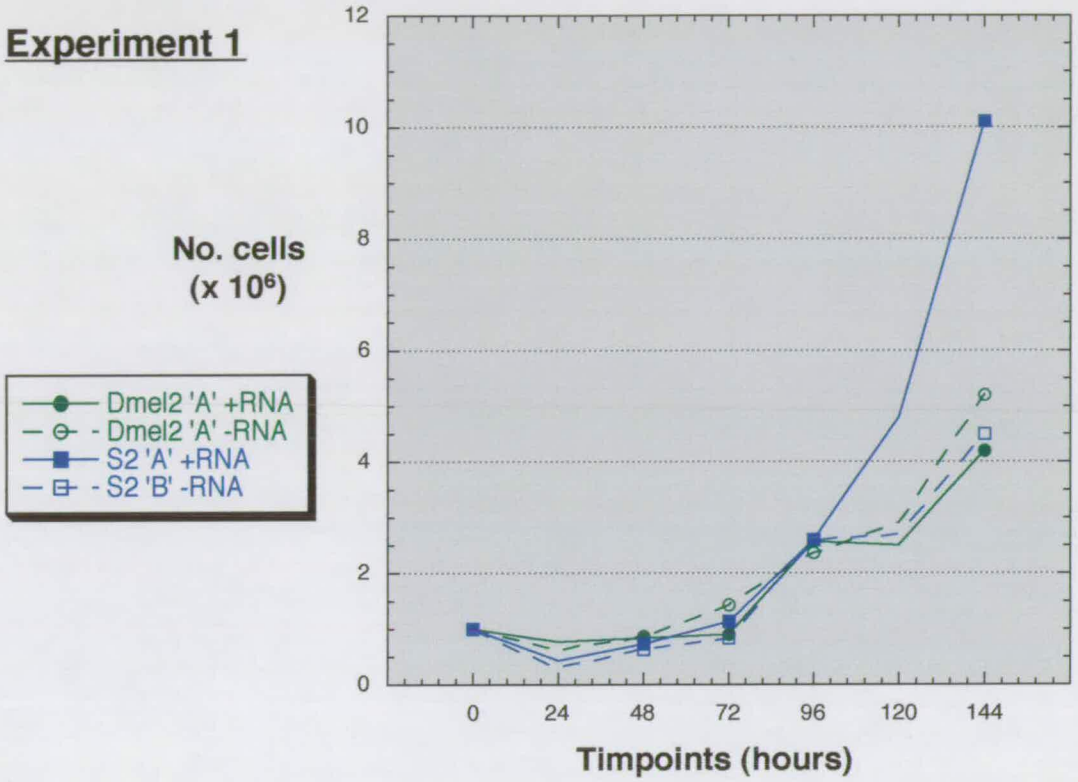

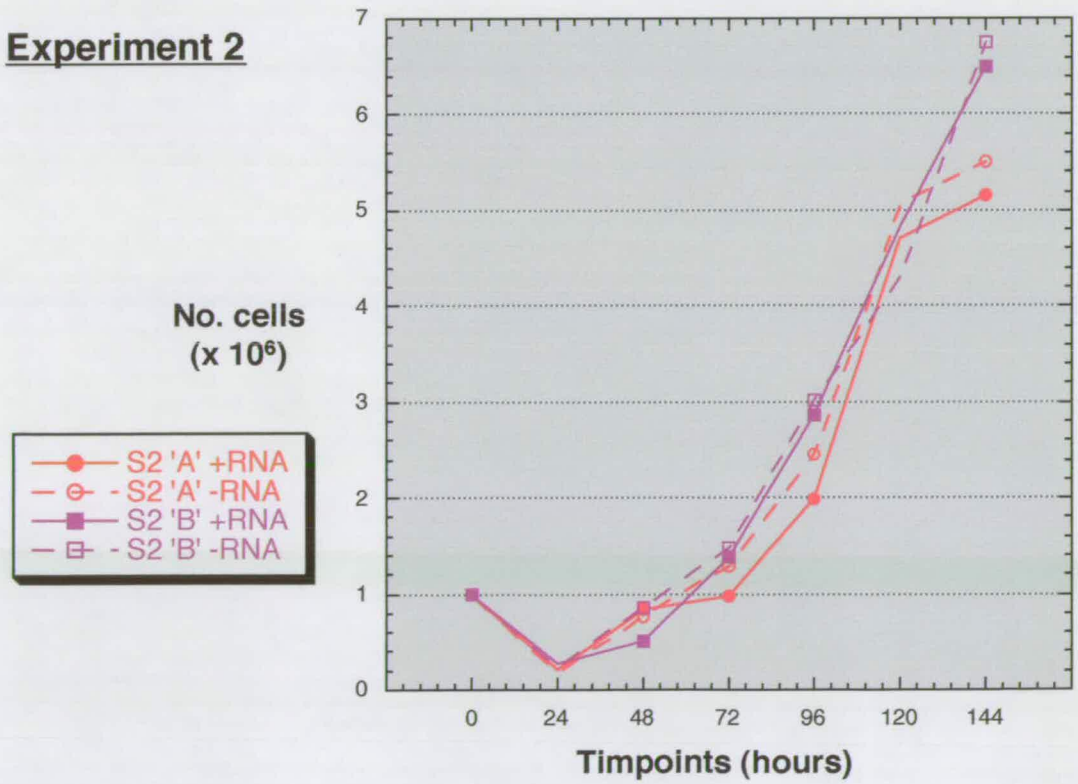

underlining the gene specific effects. 3) RNAi experiments using a control dsRNA construct made from random human intronic DNA give no observable phenotype (Mar Carmena and Richard Adams, personal communication). This shows that the effects seen are not a consequence of random-sequence dsRNA on *Drosophila* cells, but rather are sequence-specific.

I conclude therefore that the effect of IX-14 RNAi was specific to S2 cultured cells incubated with dsRNA and that the *IX-14* mRNA was specifically targeted, resulting in similar phenotypes to the ICR-170 and P-element induced alleles *l(3)IX-14*^{1} and *l(3)IX-14*^{4Y7}. This provides further evidence that the novel zinc-metalloprotease encoded by *IX-14* is responsible for the observed phenotypes in these alleles.

Table 6.2 Record of cell counts during RNAi experiments

Experiment 1	**Dmel2 'A' + RNA**	**Dmel2 'A' - RNA**	**S2 'A' + RNA**	**S2 'A' - RNA**
24h	7.8×10^5	6.4×10^5	4.3×10^5	3.1×10^5
48h	8.5×10^5	8.7×10^5	7.3×10^5	6.2×10^5
72h	9.1×10^5	1.45×10^6	1.14×10^6	8.4×10^5
96h	2.58×10^6	2.37×10^6	2.6×10^6	2.6×10^6
120h	2.5×10^6	2.9×10^6	4.8×10^6	2.7×10^6
144h	4.2×10^6	5.2×10^6	1.1×10^7	4.5×10^6

Experiment 2	**S2 'A' + RNA**	**S2 'A' - RNA**	**S2 'B' + RNA**	**S2 'B' - RNA**
24h	2.2×10^5	1.8×10^5	2.7×10^5	2.3×10^5
48h	8.4×10^5	7.5×10^5	5.1×10^5	8.6×10^5
72h	9.8×10^5	1.29×10^6	1.38×10^6	1.47×10^6
96h	1.98×10^6	2.46×10^6	2.85×10^6	3.01×10^6
120h	4.7×10^6	5.05×10^6	4.83×10^6	4.3×10^6
144h	5.15×10^6	5.50×10^6	6.5×10^6	6.75×10^6

Chapter 7
Discussion and Conclusions

IX-14 affects many cell division processes

My Ph.D. thesis has focused on the molecular and phenotypic characterisation of the *Drosophila melanogaster* late larval lethal mutant *l(3)IX-14*^{1} and its various alleles. I originally approached this mutant as one affecting mitotic chromosome architecture, based on the results of previous work performed in our labaratory (see Introduction Part III). These results showed that the predominant chromosomal defect in *l(3)IX-14*^{1} was one of hypercondensed mitotic chromosomes with a halo of poorly condensed chromatin, and a secondary defect (at a low frequency) of poorly condensed chromosomes. I have since discovered during the course of my Ph.D. that there appear to be profound defects in several aspects of the cell cycle machinery. From the phenotypic analyses detailed in Chapter 3, I have noted effects on the following:

1) Structure of mitotic and polytene chromosomes. By staining of 3rd larval instar neuroblast squashes with DAPI, I was able to confirm the hypercondensed mitotic chromosome phenotype previously observed. I also examined polytene chromosomes from *l(3)IX-14* mutants and showed that their morphology is significantly disrupted.

2) Cell cycle progression. By immunofluoresence studies using anti Phosphorylated Histone-H3 (P-H3) antibodies, I observed that the mitosis-specific phosphorylation of mitotic chromatin appeared normal in this mutant. Additionally, the ratio of the number of cells staining positive for P-H3 (i.e. committed to mitosis) to the M.I. was comparable in homozygous mutants to that in wild type, despite the much lower M.I.

seen in the mutant. This indicated a problem in cell cycle progression between G2 and M phases. Equally striking was the reduced number of mutant cells in 3rd instar brains that were in S phase as judged by BrdU incorporation, compared to wild type. This indicated a reduced ability in these mutants to enter or proceed through S phase. The consequences of these two cell cycle defects may result in the increased levels of apoptosis observed by TUNEL labeling in *l(3)IX-14^{1}*.

3) The centrosome cycle and formation of bipolar mitotic spindles. Immunofluoresence staining of larval neuroblasts with the centrosomal marker CP190 (which stains centrosomes exclusively in mitosis) provided evidence that the cell division machinery was disrupted in *l(3)IX-14^{1}* mutants. Homozygous mutants were shown to predominantly have only one centrosome during mitosis, whereas wild type mitotic cells normally have two. Leading on from this, staining with anti α-tubulin antibodies demonstrated that *l(3)IX-14^{1}* mutants have a range of severely disrupted mitotic spindle phenotypes. These include spindles that were either bipolar but asymmetric, monopolar, or in many cases completely disrupted. These spindle apparatus defects would help to explain the lack of any observed anaphase figures in this mutant.

It appears therefore that the *l(3)IX-14^{1}* mutation affects more than just the formation of mitotic chromosomes. Rather, it seems to be having a severe affect on progression through the cell cycle, and on the machinery of cell division. The process of eukaryotic cell division is complex and, not surprisingly, many of its components are interlinked. The emerging question to address is whether IX-14 acts in a specific role on a limited subset of the mitotic apparatus, or whether it plays a general upstream role in controlling these many processes?

It is possible that the protein may be required for centrosome duplication, as the number of cells with single centrosomes in *l(3)IX-14^{1}* mitotics is disproportionately high (see Chapter 3.8). Improperly replicated or separated centrosomes would help

explain another main phenotype, that of misformed mitotic spindles. Chapter 3.7 shows that the mitotic spindles observed in the *l(3)IX-14*^{1} mutant range from almost normal bipolar spindles (even in the presence of a single pole), to monopolar spindles to cases where no organised spindle can be detected. The IX-14 RNAi studies in Chapter 6 also provide further evidence corroborating these centrosome and spindle defects. These spindle disruptions may well be a by-product of the centrosome-cycle defect, as two opposite poles are normally required to form a bipolar spindle. I believe that many of the bipolar spindles that have been observed where only one centrosome is present can be accounted for by the nucleation of microtubules from the chromosomes themselves, a phenomenon recently documented in *Drosophila* neuroblasts by Bonaccorsi *et al.* (2000).

While a role in the centrosome cycle would explain many of the *l(3)IX-14*^{1} phenotypes, there remain two problems with this hypothesis:

a) First, why are no anaphases seen in *l(3)IX-14*^{1}? If some bipolar spindles are able to form, why are they not functional in segregating chromosomes? Almost normal-looking bipolar spindles were observed by Bonaccorsi *et al.* in the background of the *asterless* mutant in *Drosophila* (which abolishes centrosome formation), and they observed chromosome segregation taking place. Furthermore, if cells are unable to undergo anaphase due to centrosome and spindle defects, why is the observed mitotic index in *l(3)IX-14*^{1} significantly lower than wild type, and not higher as one would expect, i.e. why is there no metaphase arrest? A partial explanation may be that these mutant cells proceed into an apoptotic pathway as soon as a problem arises. This idea is supported by the data presented in Chapter 3.4, which shows that an elevated level of apoptosis is indeed occurring in the mutant brains.

b) The second problem comes from the mitotic chromosome morphology in *l(3)IX-14*^{1} mutants. If the mitotic spindle is disrupted by treatment with depolymerising drugs, for example nocodazole or colchicine, the mitotic chromosome morphology observed is one of hypercondensation of the chromosome arms into what

resembles short, tightly formed chromosomes. However, although a characteristic phenotype of *l(3)IX-14*^{1} alleles is the hypercondensation of mitotic chromosomes along their length, one also observes what appears to be a 'fuzziness' to the arms, reminiscent of a halo of loosely condensed chromatin, something that is not seen with drug treatment or in other spindle defect mutants. This implies that the timing or machinery of final mitotic chromosome condensation in *l(3)IX-14*^{1} may be faulty - chromosomes may not have been properly condensed to begin with, and then became hypercondensed when the mitotic spindle morphology broke down. Alternatively, it may imply that IX-14 is playing a secondary role in the maintenance of chromosome structure.

The crucial alternative to consider is that IX-14 is playing a more general role in cell proliferation, upstream of the cell division events that display these defects, as suggested by the model in Figure 7.1. The P-H3 and BrdU labeling experiments performed in Chapters 3.2 and 3.3 clearly indicate that although replication is affected in the *l(3)IX-14*^{1} mutants, the number of cells committed to mitosis as judged by P-H3 staining is close to wild type. A delay in replication could have drastic consequences to the cell - if mitotic chromosome condensation were to proceed too early, it may result in the chromosome morphology defects (although it is worth noting that the *l(3)IX-14*^{1} phenotype is not similar to mutations in known replication factors such as RFC4 or ORC2, both investigated in our laboratory).and could lead to cell death. However, from the ratio of M.I. versus the number of P-H3 positive cells in *l(3)IX-14*^{1}, it appears that the primary defect in these mutants may be late in G2, near the G2-M phase boundary. The number of cells committed to mitosis in G2 remains at near-normal levels, but the number of cells with condensed mitotic chromosomes is less than half that of wild type. Furthermore, no anaphases are seen in *l(3)IX-14*^{1} mutants, indicating that the few cells that do progress into mitosis reach metaphase but cannot continue and seem to abort the cell cycle. It seems likely therefore that the phenotypic

Figure 7.1 Possible cell-cycle roles for IX-14

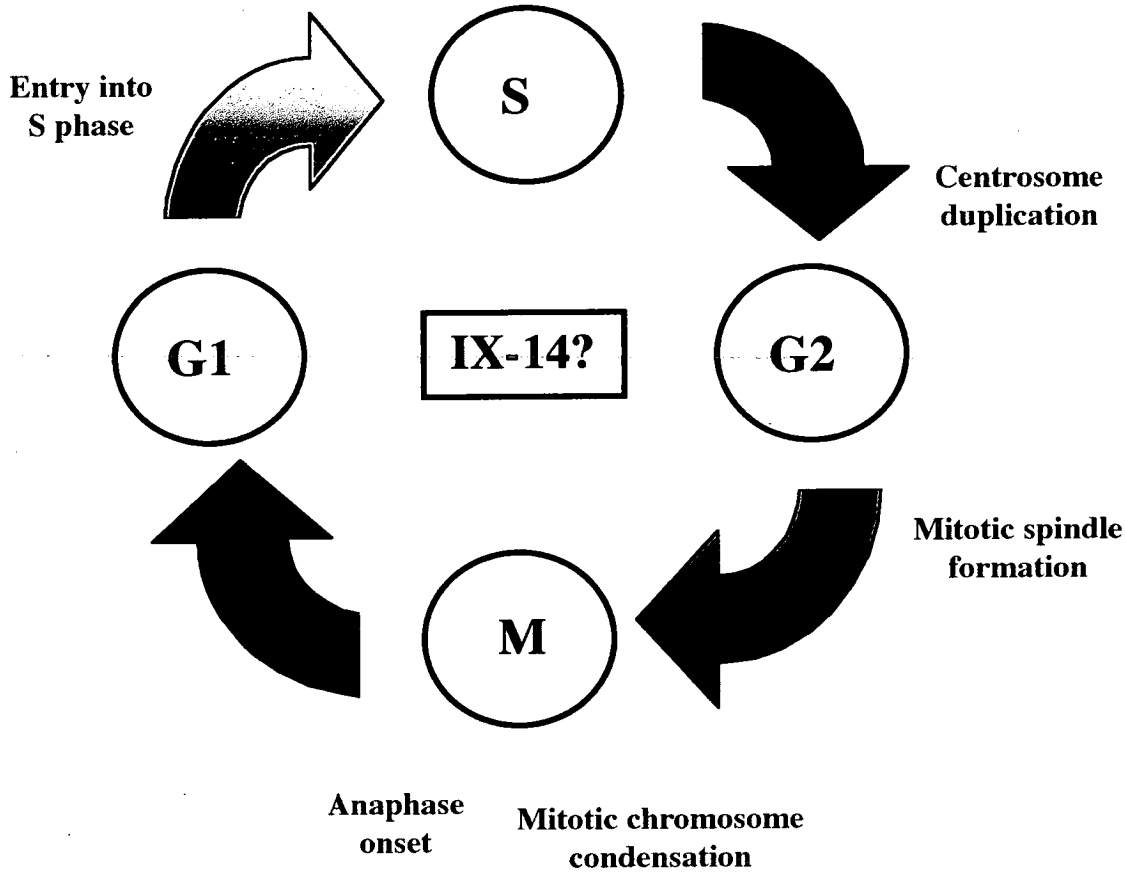

Figure 7.1 Possible cell-cycle roles for IX-14. The model presented above summarises the processes that appear to aberrant in the *l(3)IX-14* mutation, and suggests that the IX-14 protease may have multiple roles in controlling these processes at various stages of the cell cycle (grey text). Alternatively, disruption of a single event controlled by IX-14, such as the G2-M phase transition, may cause the other defects as a downstream effect.

observations I have made with regard to the cell division machinery may be downstream effects of a general problem prior to the onset of M phase.

How are these defective processes having an effect on polytene chromosome structure? Polytene chromosomes undergo multiple rounds of endoreduplication, but do not undergo mitosis and thus mitosis-specific events should not affect them. Indeed, other mitotic mutants (*l(3)k43* for example) appear to have normal polytene chromosomes (Loupart *et al.*, 2000). The profound defects on polytene chromosome structure in *l(3)IX-14*^{1} mutants may be explained by the replication defects suggested by the BrdU labeling experiments, i.e. incomplete or defective replication resulting in chromatin condensation problems. *l(3)IX-14*^{1} polytene chromosomes also appear to be less than half the size of their wild type counterparts, which also suggests a replication problem, although a quantitation of polyploidy has not been performed.

A novel role for zinc-metalloproteases?

The most striking feature of the molecular analysis I performed on the *l(3)IX-14*^{1} alleles is that the putative gene responsible appears to be a novel zinc-metalloprotease. Although attempts to perform germline-mediated rescue of the *l(3)IX-14*^{1} mutation using this gene remain incomplete, strong evidence that this is the right gene was provided by the Northern blot analysis shown in Chapter 4.3 and the gene-specific RNAi evidence from Chapter 6.

IX-14 was identified as a zinc-protease based on its amino acid sequence homology to the GP63 (Leishmanolysin) protein, a member of the M8 family of proteases. This homology sprang mainly from the conserved zinc-protease motif of '-H-E-X-X-H-'. I identified IX-14 homologues in other organisms that seem to have higher overall homology, especially the *C. elegans* predicted protein Y43F4A.1, with 45% identity and 59% similarity over the full length of the protein. It appears that IX-14 is present in higher eukaryotes, but not in prokaryotes or yeasts. Is this novel

protein only required for cell division in multicellular organisms? *Leishmania* is a single cell macrophage-parasite, but I believe that the homology to the GP63 protein purely reflects the predicted zinc-protease function of IX-14 as the two protein sequences are only similar around this motif (see alignment in Figure 4.1.4). GP63 is present in *Leishmania* as a cell-surface metalloprotease that is required for its parasitic activity. It is expressed in high quantities on the cell membrane and is believed to aid invasion of the macrophages by the parasite. It has been extensively studied due to its pathogenic role in the disease Leishmaniasis, and much work has focused on the protease activity of GP63. This work has been helpful for designing future experiments to test the putative metalloprotease activity of IX-14 itself, as presented in the Future Work section below. Another type of metalloprotease also being extensively studied are the matrix metalloproteases, as they have become implicated in tissue remodeling (Ishizuya-Oka et al., 2000) and various forms of cancer (Imanishi et al., 2000; Uria and Lopez-Otin, 2000). Matrix metalloproteases are extracellular, and have been shown to act in some cancers to digest the surrounding extra-cellular matrix and aid the process of metastasis (Ellerbroek and Stack, 1999; Horikawa et al., 2000; Johansson et al., 2000).

What relationship could these protease activities have with the eukaryotic cell cycle? To date there is only limited evidence to suggest a role for metalloprotease activity in this context where inhibitors of metalloprotease activity were seen to suppress proliferation of endothelial cells (Sang et al., 2000). It would seem therefore that the effects of the predicted metalloprotease IX-14 on the various aspects of cell division in *Drosophila* is essentially novel, and may belong to a previously undiscovered pathway of control for these processes. What role this may be will depend on what progress can be made in determining a substrate for the IX-14 protease (plans to address this question are presented in Future Work below). Perhaps, as the MI:P-H3 ratio suggests, IX-14 is required at the G2-M phase boundary to control entry into mitosis or is required to satisfy a checkpoint and allow metaphase to

proceed? Alternatively, as suggested by some of my immunofluoresence results on chromosomes, centrosomes and the mitotic spindle, IX-14 may be directly responsible for one or more of the cell division processes such as centrosome duplication or in the control of chromosome condensation. What is certain is that the IX-14 protein is vital, as loss of it results in lethality. Given its striking phenotypes and the novel aspect of a putative zinc-metalloprotease involvement, there is no doubt that studies will continue on this fascinating protein.

Future Work

In the final year of my Wellcome Trust Prize Studentship Ph.D., I applied for and was awarded a Wellcome Trust Prize Fellowship for a period of two years in which to continue work on the IX-14 protein. I wrote this Fellowship with regard to analysing the putative zinc-metalloprotease activity predicted by the sequence of the protein and to searching for possible interactors or substrates of this novel protein. What follows are the basic proposals included in that grant application.

Does the IX-14 gene product exhibit protease activity?

In order to test for protease activity of IX-14 I intend to employ a strategy to detect general protease activity by using commercially available kits such as the Quanticleave Protease Assay (Pierce), which uses an extremely sensitive casein-based assay to determine protease activity in various pH and temperature profiles. This could be performed using either purified IX-14 protein (which would have to be in the native state), or by using an *in vitro* transcription/translation system to produce the protein. The latter would be preferable since overexpression of the His-tagged full length protein has previously been shown to be difficult to achieve (see Chapter 5). Another possibility is a simple assay involving a polyacrylamide gel soaked in gelatin, often used in a variety of systems as a substrate in protease assays (Alfieri et al., 2000;

Chakrabarti et al., 2000; Hower et al., 2000). The IX-14 protein would be electrophoresed in the gel and subsequent detection should reveal a blank band corresponding to the area of protease activity present. If at a later stage I have been successful in identifying a substrate for IX-14 (see below) there may be the opportunity to use more specific protease assays, using chromogenic or fluorogenic substrates tailored to the substrate in question.

The zinc-metalloprotease domain present in IX-14 is a perfect match to the consensus motif of '-H-E-X-X-H-' present in the M8 family of zinc-metalloproteases, which included the GP63 protein. This motif has been well characterised by mutational analysis of the conserved Histidines and the Glutamate residues (Macdonald et al., 1995; McGwire and Chang, 1996; McMaster et al., 1994), and it has been determined that both Histidine residues are essential for coordinating the zinc ion, whereas the Glutamate residue is absolutely required for catalytic activity. With these results in mind, I aim to demonstrate that this motif is required for catalytic activity in IX-14 by site-directed mutagenesis of the conserved motif in a similar manner to the references quoted above.

Identifying a substrate for IX-14

Knowledge of a substrate for the IX-14 metalloprotease would be extremely helpful in studying its activity in the assays described above, and may also help to place more specifically this protease activity in the context of the cell cycle and chromosome condensation. Ideally, knowledge of the substrate would allow us to initiate new areas of research, depending on how much is known about it.

I aim to use the yeast 2-hybrid system to identify possible substrates. Using the zinc-metalloprotease motif mutated form of IX-14 mentioned above may help reduce the background of false positives in this case. Since there is likely to be high affinity between IX-14 and its substrate due to its enzymatic activity, mutation of the active

residue should increase the chances of isolating a *bona fide* interactor. This idea has been successfully used in identifying novel substrates of caspase 3 (Kamada et al., 1998).

Investigation of IX-14 homologues

Finally, there is scope to follow up the identification of IX-14 homologues in other systems, in particular in the nematode *C. elegans* and in mammals. We are currently in collaboration with Mark Roth in the Fred Hutchison Center of Cancer Research in Seattle to knock-out the *C. elegans* homologue of IX-14 by RNAi, which will hopefully mirror my own RNAi results on *Drosophila* cultured cells. Analysis of the mammalian homologues should be particularly useful. We are currently sequencing the human and mouse EST clones homologous to IX-14, and plan to raise antibodies to the relevant proteins. We would be able to use the wealth of tissue culture techniques available for these systems, such as the ability to synchronise populations of cells, and make full use of the superior morphology of mammalian cells. I intend to use either antibodies generated *de novo* or a GFP tagged version of IX-14 to study localisation of the protein in these systems. Finally, using other systems would give us access to more powerful biochemistry techniques such as immunoprecipitation from cell extracts, which would complement our 2-hybrid assay efforts to identify proteins interacting with IX-14.

References

Abrieu, A., Brassac, T., Galas, S., Fisher, D., Labbé, J.-C., and Dorée, M. (1998). The polo-like kinase Plx1 is a component of the MPF amplification loop at the G2/M phase transition of the cell cycle in *Xenopus* eggs., J. Cell Sci. *111*, 1751-1757.

Adachi, Y., Käs, E., and Laemmli, U. K. (1989). Preferential Cooperative Binding of DNA Topoisomerase II to Scaffold Attachment Regions., EMBO *13*, 3997-4006.

Adachi, Y., Luke, M., and Laemmli, U. K. (1991). Chromosome Assembly In Vitro: Topoisomerase II is Required for Condensation, Cell *64*, 137-148.

Adams, R. R., Wheatley, S. P., Gouldsworthy, A. M., Kandels-Lewis, S. E., Carmena, M., Smythe, C., Gerloff, D. L., and Earnshaw, W. C. (2000). INCENP binds the Aurora-related kinase AIRK2 and is required to target it to chromosomes, the central spindle and cleavage furrow., Curr. Biol. *10*, 1075-1078.

Adolph, K. W., Cheng, S. M., Paulson, J. R., and Laemmli, U. K. (1977). Isolation of a protein scaffold from mitotic HeLa cell chromosomes, Proc. Nat. Acc. Sci. USA *74*, 4937-4941.

Alfieri, S. C., Correia, C. E., Motegi, S. A., and Pral, E. M. (2000). Proteinase activities in total extracts and in medium conditioned by *Acanthamoeba polyphaga* trophozoites., J Parasitol *Apr;86(2)*, 220-7.

Akhmedov, A. T., Gross, B., and Jessberger, R. (1999). Mammalian SMC3 C-terminal and Coiled-coil Protein Domains Specifically Bind Palindromic DNA, Do Not Block DNA Ends, and Prevent DNA Bending., J. Biol. Chem. *274*, 38216-38224.

Andersen, S. S. L. (2000). Spindle assembly and the art of regulating microtubule dynamics by MAPs and Stathmin/Op18., Trends Cell Biol. *10*, 261-267.

Antonio, C., Ferby, I., Wilhelm, H., Jones, M., Karsenti, E., Nebreda, A. R., and Vernos, I. (2000). Xkid, a Chromokinesin Required for Chromosome Alignment on the Metaphase Plate, Cell *102*, 425-435.

Archer, J., and Solomon, F. (1994). The molecular biology of intermediate filaments., Int Rev Cytol *134*, 243-279.

Basto, R., Gomes, R., and Karess, R. E. (2000). Rough Deal and Zw10 are required for the metaphase checkpoint in *Drosophila.*, Nature Cell Biol. *2*, 939-943.

Belmont, L. D., and Mitchison, T. J. (1996). Identification of a protein that interacts with tubulin dimers and increases the catastrophe rate of microtubules., Cell *84*, 623-631.

Bhat, M. A., Philp, A. V., Glover, D. M., and Bellen, H. J. (1996). Chromatid segregation at anaphase requires the barren product, a novel chromosome associated protein that interacts with topoisomerase II., Cell *87*, 1103-1114.

Blat, Y., and Kleckner, N. (1999). Cohesins bind to preferential sites along yeast chromosome III, with differential regulation along arms versus the centric region., Cell *98*, 249-259.

Bobinnec, Y., Khodjakov, A., Mir, L. M., Rieder, C. L., Edde, B., and Bornens, M. (1998). Centriole disassembly *in vivo* and its effect on centrosome structure and function in vertebrate cells, J. Cell Biol. *143*, 1575-1589.

Bonaccorsi, S., Giansanti, M. G., and Gatti, M. (2000). Spindle assembly in *Drosophila* neuroblasts and ganglion mother cells, Nature Cell Biology *2*, 54 - 56.

Bradbury, E. M. (1992). Reversible histone modifications and the chromosome cell cycle., Bioessays *14*, 9-16.

Brand, A. H., and Perrimon, N. (1993). Targeted gene expression as a means of altering cell fates and generating dominant phenotypes., Development *118*, 401-415.

Chakrabarti, S. K., Matsumura, N., and Ranu, R. S. (2000). Purification and characterization of an extracellular alkaline serine protease from Aspergillus terreus (IJIRA 6.2)., Curr.. Microbiol. *Apr;40(4)*, 239-44.

Chan, G. K., Jablonski, S. A., Starr, D. A., Goldberg, M., and Yen, T. J. (2000). Human Zw10 and ROD are mitotic checkpoint proteins that bind to kinetochores., Nature Cell Biol. *2*, 944-947.

Chuang, P.-T., Albertson, D. G., and Meyer, B. J. (1994). DPY-27: A chromosome condensation protein homolog that regulates C. elegans dosage compensation through association with the X chromosome., Cell *79*, 459-474.

Ciosk, R., Zachariae, W., Michaelis, C., Shevchenko, A., Mann, M., and Nasmyth, K. (1998). An ESP1/PDS1 complex regulates loss of sister chromatid cohesion at the metaphase to anaphase transition in yeast., Cell *93*, 1067-1076.

Clemens, J. C., Worby, C. A., Simonson-Leff, N., Muda, M., Maehama, T., Hemmings, B. A., and Dixon, J. E. (2000). Use of double-stranded RNA interference in *Drosophila* cell lines to dissect signal transduction pathways., Proc Nat Acad. Sci USA *97*, 6499-6503.

Cobbe, N., and Heck, M. M. S. (2000). SMCs in the World of Chromosome Biology - From Prokaryotes to Higher Eukaryotes., J. Struct. Biol. *129*, 123-143.

Collas, P., K., L. G., and Tasken, K. (1999). The A-kinase-Anchoring Protein AKAP95 Is a Multivalent Protein with a Key Role in Chromatin Condensation at Mitosis, J. Cell Biol. *147*, 1167-1179.

Cooke, C. A., Bernat, R. L., and Earnshaw, W. C. (1990). CENP-B: A major human centromere protein located beneath the kinetochore., J. Cell Biol. *109*, 1475-1488.

Craig, J. M., Earnshaw, W. C., and Vagnarelli, P. (1999). Mammalian Centromeres: DNA Sequence, Protein Composition, and Role in Cell Cycle Progression., Exp. Cell Res. *246*, 249-262.

Cutts, S. M., Fowler, K. J., Kile, B. T., Hii, L. L., O'Dowd, R. A., Hudson, D. F., Saffery, R., Kalitsis, P., Earle, E., and Choo, K. H. (1999). Defective chromosome segregation, microtubule bundling and nuclear bridging in inner centromere protein gene (Incenp)-disrupted mice., Hum Mol Genet *8*, 1145-1155.

de Saint Phalle, B., and Sullivan, W. (1998). Spindle assembly and mitosis without centrosomes in parthenogenetic *Sciara* embryos., J. Cell Biol. *141*, 1383-1391.

Denef, N., Neubuser, D., Perez, L., and Cohen, S. M. (2000). Hedgehog induces opposite changes in turnover and subcellular localization of patched and smoothened., Cell *102*, 521-531.

Dictenberg, J. B., Zimmerman, W., Sparks, C. A., Young, A., Vidair, C., Zheng, Y., Carrington, W., Fay, F. S., and Doxsey, S. J. (1998). Pericentrin and gamma-tubulin form a protein complex and are organized into a novel lattice at the centrosome., J. Cell Biol. *141*, 163-174.

Downes, C. S., Mullinger, A. M., and Johnson, R. T. (1991). Inhibitors of DNA topoisomerase II prevent chromatid separation in mammalian cells but do not prevent exit from mitosis., Proc Nat Acad Sci USA *88*, 8895-8899.

Doxsey, S. J., Stein, P., Evans, L., Calarco, P., and Kirschner, M. (1994). Pericentrin, a highly conserved protein of centrosomes involved in microtubule organization., Cell *76*, 639-650.

Dutcher, S. K., and Trabuco, E. C. (1998). The UNI3 gene is required for assembly of basal bodies of *Chlamydomonas* and encodes d-tubulin, a new member of the tubulin superfamily, Mol. Biol. Cell *9*, 1293-1308.

Earnshaw, W. E., Halligan, B., Cooke, C. A., Heck, M. M. S., and Liu, L. F. (1985). Topoisomerase II is a structural component of mitotic chromosome scaffolds, J. Cell Biol. *100*, 1706-1715.

Earnshaw, W. E., and Heck, M. M. S. (1985). Localization of topoisomerase II in mitotic chromosomes., J. Cell Biol. *100*, 1716-1725.

Flemming, W. (1879). Arch Mikrosk Ana *18*, 151.

Ellerbroek, S. M., and Stack, M. S. (1999). Membrane associated matrix metalloproteinases in metastasis, BioEssays *21*, 940-949.

Fukagawa, T., and Brown, W. R. A. (1997). Efficient conditional mutation of the vertebrate CENP-C gene., Hum Mol Genet *6*, 2301-2308.

Fraser, A. G., Kamath, R. S., Zipperlen, P., Martinez-Campos, M., Sohrmann, M., and Ahringer, J. (2000). Functional genomic analysis of *C. elegans* chromosome I by systematic RNA interference., Nature *408*, 325-330.

Fuller, S., Gowen, B., Reinsch, S., Sawyer, A., Buendia, B., Wepf, R., and Karsenti, E. (1995). The core of the mammalian centriole contains g-tubulin, Curr.. Biol. *5*, 1384-1393.

Funabiki, H., and Murray, A. M. (2000). The *Xenopus* Chromokinesin Xkid Is Essential for Metaphase Chromosome Alignment and Must Be Degraded to Allow Anaphase Chromosome Movement, Cell *102*, 411-424.

Gasser, S. M. (1992). Functional Aspects of Chromosome Organization: Scaffold Attachment Regions and Their Ligands, Adv. Mol. Cell Biol. *4*, 75-101.

Gasser, S. M., Laroche, T., Falquet, J., Boy de la Tour, E., and Laemmli, U. K. (1986). Metaphase chromosome structure. Involvement of topoisomerase II., J. Mol. Biol. *188*, 613-629.

GeneFinder dot.imgen.bcm.tmc.edu:9331/gene-finder/gf.html.

Girard, F., Bello, B., Laemmli, U. K., and Gehring, W. J. (1998). *In vivo* analysis of scaffold-associated regions in *Drosophila*: a synthetic high-affinity SAR binding protein suppresses position effect variegation, EMBO J *17*, 2079-2085.

Glover, D. M., Hagan, I. M., and Tavares, A. M. (1998). Polo-like kinases: a team that plays throughout mitosis, Genes Dev. *12*, 3777-3787.

Gonczy, P., Echeverri, G., Oegema, K., Coulson, A., Jones, S. J., Copley, R. R., Duperon, J., Oegema, J., Brehm, M., Cassin, E., *et al.* (2000). Functional genomic analysis of cell division in *C. elegans* using RNAi of genes on chromosome III., Nature *408*, 331-336.

Gould, R. R., and Borisy, G. G. (1977). The pericentriolar material in Chinese hamster ovary cells nucleates microtubule formation., J. Cell Biol. *73*, 601-615.

Guacci, V., Koshland, D., and Strunnikov, A. (1997). A Direct Link between Sister Chromatid Cohesion and Chromosome Condensation Revealed through the Analysis of *MCD1* in *S. cerevisiae*, Cell *91*, 47-57.

Guacci, V., Yamamoto, A., Strunnikov, A., Kingsbury, J., Hogan, E., Meluh, P., and Koshland, D. (1993). Structure and function of chromosomes in mitosis of budding yeast, Cold Spring Harbour Symp Quant Biol. *58*, 677-685.

Gurley, L. R., Walters, R. A., and Tobey, R. A. (1975). Sequential phosphorylation of histone subfractions in the Chinese hamster cell cycle., J. Biol. Chem. *250*, 3936-3944.

Hardwick, K. G. (1998). The spindle checkpoint., Trends Genet. *14*, 1-4.

Heck, M. M. S. (1997). Condensins, Cohesins and Chromosome Architecture: How to Make and Break a Mitotic Chromosome, Cell *91*, 5-8.

Hendzel, M. J., Wei, Y., Mancini, M. A., Van Hooser, A., Ranalli, T., Brinkley, B. R., Bazett-Jones, D. P., and Allis, C. D. (1997). Mitosis-specific phosphorylation of histone H3 initiates primarily within pericentromeric heterochromatin during G2 and spreads in an ordered fashion coincident with mitotic chromosome condensation., Chromosoma *106*, 348-360.

Hinchcliffe, E. H., Li, C., Thompson, E. A., Maller, J. L., and Sluder, G. (1999). Requirement of Cdk2-cyclin E activity for repeated centrosome reproduction in *Xenopus* egg extracts, Science *283*, 851-854.

Hirano, T. (1998). SMC protein complexes and higher-order chromosome dynamics., Curr.. Op. Cell Biol. *10*, 317-322.

Hirano, T., Kobayashi, R., and Hirano, M. (1997). Condensins, Chromosome Condensation Protein Complexes Containing XCAP-C, XCAP-E and a Xenopus Homolog of the *Drosophila* Barren Protein, Cell *89*, 511-521.

Hirano, T., and Mitchison, T. J. (1993). Topoisomerase II does not play a scaffolding role in the organization of mitotic chromosomes assembled in *Xenopus* egg extracts., J. Cell Biol. *120*, 601-612.

Hirano, T., and Mitchison, T. J. (1994). A Heterodimeric Coiled-Coil Protein Required for Mitotic Chromosome Condensation *In Vitro*, Cell *79*, 449-458.

Holm, C., Goto, T., Wang, J. C., and Botstein, D. (1985). DNA topoisomerase II is required at the time of mitosis in yeast., Cell *41*, 553-563.

Horikawa, T., Yoshizaki, T., Sheen, T. S., Lee, S. Y., and Furukawa, M. (2000). Association of latent membrane protein 1 and matrix metalloproteinase 9 with metastasis in nasopharyngeal carcinoma., Cancer *89*, 715-723.

Hower, C. D., Dassow, M. S., Kajdacsy-Balla, A., Seabrook, G. R., Jean-Claude, J., Towne, J. B., and Cambria, R. A. (2000). Metalloproteinase levels are decreased in symptomatic carotid plaques., J. Surg. Res. *Feb;88(2)*, 155-9.

Hudson, D. F., Fowler, K. J., Earle, E., Saffery, R., Kalitsis, P., Trowell, H., Hill, J., Wreford, N. G., de Kretser, D. M., Cancilla, M. R., *et al.* (1998). Centromere protein B null mice are mitotically and meiotically normal but have lower body and testis weights., J. Cell Biol. *141*, 309-319.

Imanishi, Y., Fujii, M., Tokumaru, Y., Tomita, T., Kanke, M., Kanzaki, J., Kameyama, K., Otani, Y., and Sato, H. (2000). Clinical significance of expression of membrane type 1 matrix metalloproteinase and matrix metalloproteinase-2 in human head and neck squamous cell carcinoma., Hum. Pathol. *31*, 895-904.

Ishizuya-Oka, A., Li, Q., Amano, T., Damjanovski, S., Ueda, S., and Shi, Y. B. (2000). Requirement for matrix metalloproteinase stromelysin-3 in cell migration and apoptosis during tissue remodeling in *Xenopus laevis*., J. Cell Biol. *150*, 1177-1188.

Janssen, S., Durussel, T., and Laemmli, U. K. (2000). Chromatin Opening of DNA Satellites by Targetted Sequence-Specific Drugs., Mol. Cell. *6*, 999-1011.

Jantsch-Plunger, V., Gonczy, P., Romano, A., Schnabel, H., Hamill, D., Schnabel, R., Hyman, A. A., and Glotzer, M. (2000). CYK-4: A Rho Family GTPase Activating Protein (GAP) Required for Central Spindle Formation and Cytokinesis, J. Cell Biol. *149*, 1391-1404.

Jessberger, R., Frei, C., and Gasser, S. M. (1998). Chromosome dynamics: the SMC protein family., Curr.. Opin. Genet. Dev. *8*, 254-259.

Johansson, N., Ahonen, M., and Kahari, V. M. (2000). Matrix metalloproteases in tumour invasion., Cell. Mol. Life Sci. *57*, 16-24.

Kalitsis, P., Fowler, K. J., Earle, E., Hill, J., and Choo, K. H. (1998). Targeted disruption of mouse centromere protein C gene leads to mitotic disarray and early embryo death., Proc. Nat. Acc. Sci. USA *95*, 1136-1141.

Kamada, S., Kusano, H., Fujita, H., Ohtsu, M., Koya, R. C., Kuzumaki, N., and Tsujimoto, Y. (1998). A cloning method for caspase substrates that uses the yeast two-hybrid system: Cloning of the antiapoptotic gene gelsolin., Proc. Nat. Acc. Sci. USA. *95*, 8532-8537.

Kapoor, M., Montes de Oca Luna, R., Lozano, G., Cummings, C., Brinkley, B. R., and May, G. S. (1997). The CENP-B gene is not essential in mice., Mol. Biol. Cell *8*, 267a.

Kimura, K., and Hirano, T. (1997). ATP-Dependent Positive Supercoiling of DNA by 13S Condensin: A Biochemical Implication for Chromosome Condensation, Cell *90*, 625-634.

Kimura, K., Rybenkov, V. V., Crisona, N. J., Hirano, T., and Cozzarelli, N. R. (1999). 13S condensin actively reconfigures DNA by introducing global positive writhe: implications for chromosome condensation., Cell *98*, 239-248.

King, J. M., Hays, T. S., and Nicklas, R. B. (2000). Dynein Is a Transient Kinetochore Component Whose Binding Is Regulated by Microtubule Attachment, Not Tension., J. Cell Biol. *151*, 739-748.

Koshland, D., and Strunnikov, A. (1996). Mitotic Chromosome Condensation, Ann. Rev. Cell Dev. Biol. *12*, 305-333.

Kumagi, A., and Dunphy, W. (1996). Purification and molecular cloning of Plx1, a Cdc25-regulatory kinase from *Xenopus* egg extracts., Science *273*, 1377-1380.

Lacey, K. R., Jackson, P. K., and Stearns, T. (1999). Cyclin-dependent kinase control of centrosome duplication, Proc. Nat. Acc. Sci. USA. *96*, 2817-2822.

Laemmli, U. K., Käs, E., Poljak, L., and Adachi, Y. (1992). Scaffold-associated regions: cis-acting determinants of chromatin structural loops and functional domains, Curr.. Op. Genet. Dev. *2*, 275-285.

Lewis, C. D., and Laemmli, U. K. (1982). Higher Order Metaphase Chromosome Structure: Evidence for Metalloprotein Interactions, Cell *29*, 171-181.

Losada, A., Hirano, M., and Hirano, T. (1998). Identification of *Xenopus* SMC protein complexes required for sister chromatid cohesion., Genes Dev. *12*, 1986-1997.

Loupart, M.-L., Krause, S. A., and Heck, M. M. S. (2000). *Drosophila ORC2* mutants link replication timing, checkpoint control, and mitotic chromosome architecture, (manuscript in preparation).

Macdonald, M. H., Morrison, C. J., and McMaster, W. R. (1995). Analysis of the active site and activation mechanism of the Leishmania surface metalloprotease GP63., Biochem Biophys Acta *1253(2)*, 199-207.

Machado, C., and Andrew, D. J. (2000). D-Titin. A giant protein with dual roles in chromosomes and muscles., J. Cell Biol. *151*, 639-652.

Machado, C., Sunkel, C. E., and Andrew, D. J. (1998). Human autoantibodies reveal titin as a chromosomal protein., J. Cell Biol. *141*, 321-333.

Mackay, A. M., Ainzstein, A. M., Eckley, D. M., and Earnshaw, W. C. (1998). A dominant mutant of inner centromere protein (INCENP), a chromosomal protein, disrupts prometaphase congression and cytokinesis., J. Cell Biol. *140*, 991-1002.

Maney, T., Hunter, A. W., Wagenbach, M., and Wordeman, L. (1998). Mitotic centromere-associated kinesin is important for anaphase chromosome segregation., J. Cell Biol. *142*, 787-801.

Marklund, U., Larsson, N., Gradin, H. M., Brattsand, G., and Gullberg, M. (1996). Oncoprotein 18 is a phosphorylation-responsive regulator of microtubule dynamics., EMBO *15*, 5290-5298.

Mayer-Jaekel, R. E., Ohkura, H., Gomes, R., Sunkel, C. E., Baumgartner, S., Hemmings, B. A., and Glover, D. M. (1993). The 55 kd regulatory subunit of *Drosophila* protein phosphatase 2A is required for anaphase., Cell *72*, 621-633.

McGhee, J., and Felsenfeld, G. (1980). Nucleosome structure., Ann Rev Biochem *49*, 1115-1156.

McGwire, B. S., and Chang, K. P. (1996). Postranslational regulation of a Leishmania HEXXH metalloprotease (gp63). The effects of site-specific mutagenesis of catalytic, zinc binding, N-glycosylation, and glycosyl phosphatidylinositol addition sites on N-terminal end cleavage, intracellular stability, and extracellular exit., J. Biol. Chem. *271(14)*, 7903-9.

McMaster, W. R., Morrison, C. J., and Joshi, P. B. (1994). Mutational and functional analysis of the Leishmania surface metalloproteinase GP63: similarities to matrix metalloproteinases., Parasitology *108*, Suppl: S29-36.

McNeill, P. A., and Berns, M. W. (1981). Chromosome behavior after laser microirradiation of a single kinetochore in mitotic PtK2 cells., J. Cell Biol. *88*, 543.

Megee, P. C., Mistrot, C., Guacci, V., and Koshland, D. (1999). The centromeric sister chromatid cohesion site directs Mcd1p binding to adjacent sequences., Mol Cell *4*, 445-450.

Melby, T. E., Ciampaglio, C. N., Briscoe, G., and Erickson, H. P. (1998). The symmetrical structure of structural maintenance of chromosomes (SMC) and MukB proteins: long, antiparallel coiled coils, folded at a flexible hinge., J. Cell Biol. *142*, 1595-1604.

Merdes, A., Heald, R., Samejima, K., Earnshaw, W. C., and Cleveland, D. W. (2000). Formation of Spindle Poles by Dynein/Dynactin-dependent Transport of NuMA., J. Cell Biol. *149*, 851-861.

Merdes, A., Ramyar, K., Vechio, J. D., and Cleveland, D. W. (1996). A complex of NuMA and cytoplasmic dynein is essential for mitotic spindle assembly., Cell *87*, 447-458.

Michaelis, C., Ciosk, R., and Nasmyth, K. (1997). Cohesins: Chromosomal Proteins that Prevent Premature Separation of Sister Chromatids, Cell *91*, 35-45.

Mirkovitch, J., Mirault, M.-E., and Laemmli, U. K. (1984). Organization of the higher-order chromatin loop: specific DNA attachment sites on nuclear scaffold, Cell *39*.

Moir, R. D., Spann, T. P., Lopez-Soler, R. I., Yoon, M., Goldman, A. E., Khuon, S., and Goldman, R. D. (2000). Review: the dynamics of nuclear lamins during the cell cycle - relationship between structure and function., J. Struct. Biol. *129*, 324-334.

Moritz, M., Braunfeld, M. B., Sedat, J. W., Alberts, B., and Agard, D. A. (1995). Microtubule nucleation by g-tubulin-containing rings in the centrosome., Nature *378*, 638-640.

Mueller, R. D., Yasuda, H., Hatch, C. L., Bonner, W. M., and Bradbury, E. M. (1985). Identification of ubiquitinated histones 2A and 2B in *Physarum polycephalum*. Disappearance of these proteins at metaphase and reappearance at anaphase., J. Biol. Chem. *260*, 5147-5153.

Murray, A. M., and Szostak, J. W. (1985). Chromosome segregation in mitosis and meiosis., Annu Rev Cell Biol. *1*, 239-315.

Nasmyth, K., Peters, J.-M., and Uhlmann, F. (2000). Splitting the Chromosome: Cutting the Ties That Bind Sister Chromatids, Science *288*, 1379-1384.

Nurse, P. (1990). Universal control mechanism regulating onset of M phase., Nature *344*, 503-508.

Oakley, C. E., and Oakley, B. R. (1989). Identification of gamma tubulin, a new member of the tubulin superfamily encoded by mipA gene of *Aspergillus nidulans*., Nature *338*, 662-664.

Ohba, T., Nakamura, M., Nishitani, T., and Nishimoto, T. (1999). Self-Organisation of Microtubule Asters Induced in Xenopus Egg Extracts by GTP-Bound Ran., Science *284*, 1356-1358.

Paulson, J. R., and Laemmli, U. k. (1977). The Structure of Histone-Depleted Metaphase Chromosomes, Cell *12*, 817-828.

Paulson, J. R., and Langmore, J. P. (1989). Low Angle X-Ray Diffraction Studies of HeLa Metaphase Chromosomes: Effects of Histone Phosphorylation and Chromosome Isolations Procedure., J. Cell Biol. *96*, 1132-1137.

Perez-Castro, A. V., Shamanski, F. L., Meneses, J. J., Lovato, T. L., Vogel, K. G., Moyzis, R. K., and Pederesen, R. (1998). Centromeric protein B null mice are viable with no apparent abnormalities., Dev Biol. *201*, 135-143.

Peterson, C. (1994). The SMC family: Novel Proteins for Chromosome Condensation?, Cell *79*, 389-392.

Pfaar, C. M., Coue, M., Grisson, P. M., Hays, T. S., Porter, M. E., and McIntosh, J. R. (1990). Cytoplasmic dynein is localized to kinetochores during mitosis., Nature *345*, 263-265.

Qian, Y.-W., Erikson, E., Li, C., and Maller, J. (1998). Activated polo-like kinase Plx1 is required at multiple points during mitosis in Xenopus laevis., Mol. Cell Biol. *18*, 4262-4271.

Quinn, L. M., Dorstyn, L., Mills, K., Colussi, P. A., Chen, P., Coombe, M., Abrams, J., Kumar, S., and Richardson, H. (2000). An essential role for the caspase dronc in developmentally programmed cell death in *Drosophila*., J. Biol. Chem. *275*, 40416-40424.

Richmond, T. J., Finch, J. T., Rushton, B., Rhodes, D., and Klug, A. (1984). Structure of the nucleosome core particle at 7Å resolution., Nature *311*, 532-537.

Rieder, C. L., and Salmon, E. D. (1994). Motile kinetochores and polar ejection forces dictate chromosome position on the vertebrate mitotic spindle., J. Cell Biol. *124*, 223-233.

Rieder, C. L., and Salmon, E. D. (1998). The vertebrate cell kinetochore and its roles during mitosis., Trends Cell Biol. *8*, 310-318.

Robinson, J. T., Wojcik, E. J., Sanders, M. A., McGrail, M., and Hays, T. S. (1999). Cytoplasmic dynein is required for the nuclear attachment and migration of centrosomes during mitosis in *Drosophila*., J. Cell Biol. *146*, 597-608.

Ruiz, F., Beisson, J., Rossier, J., and Dupuis-Willams, P. (1999). Gamma-tubulin is necessary for basal body duplication in *Paramecium*, Curr.. Biol. *9*, 43-46.

Saitoh, H., Tomkiel, J. E., Cooke, C. A., Ratrie, H. R., Maurer, M., Rothfield, N. F., and Earnshaw, W. C. (1992). CENP-C, an autoantigen in scleroderma, is a component of the human inner kinetochore plate., Cell *70*, 115-125.

Saitoh, N., Goldberg, I., and Earnshaw, W. E. (1995). The SMC proteins and the coming of age of the chromosome scaffold hypothesis, BioEssays *17*, 759-766.

Saitoh, N., Goldberg, I., Wood, E., and Earnshaw, W. E. (1994). ScII: An Abundant Chromosome Scaffold Protein Is a Member of a Family of Putative ATPases with an Unusual Predicted Tertiary Structure, J. Cell Biol. *127*, 303-318.

Saitoh, Y., and Laemmli, U. K. (1994). Metaphase chromosome structure: bands arise from a differential folding path of the highly AT-rich scaffold., Cell *76*, 609-622.

Saka, Y., Sutani, T., Yamashita, Y., Saitoh, S., Takeuchi, M., Nakaseko, Y., and Yanagida, M. (1994). Fission yeast cut3 and cut14, members of the ubiquitous protein family, are required for chromosome condensation and segregation in mitosis. EMBO *13*, 4938-4952.

Sang, Q. X., Jia, M. C., Schwartz, M. A., Jaye, M. C., Kleinman, H. K., Ghaffari, M. A., and Luo, Y. L. (2000). New Thiol and sulfodiimine metalloproteinase inhibitors and their effect on human microvascular endothelial cell growth., Biochem. Biophys. Res. Commun. *274*, 780-786.

Savoian, M. S., Goldberg, M., and Rieder, C. L. (2000). The rate of poleward chromosome motion is attenuated in *Drosophila zw10* and *rod* mutants., Nature Cell Biol. *2*, 948-952.

Schaar, B. T., Chan, G. K. T., Maddox, P., Salmon, E. D., and Yen, T. J. (1997). CENP-E function at kinetochores is essential for chromosome alignment., J. Cell Biol. *139*, 1373-1382.

Schultz, J., Copley, R. R., Doerks, T., Ponting, C. P., and Bork, P. (2000). SMART: A Web-based tool for the study of genetically mobile domains., Nucleic Acids Research *28*, 231-234.

Shearn, A., Rice, T., Garen, A., Gehring, W. (1971). Imaginal disc abnormalities in lethal mutants of *Drosophila*., Proc Nat Acc Sci *68*, 2594-2598.

Shirayama, M., Tóth, A., Gálová, M., and Nasmyth, K. (1999). APC^{Cdc20} promotes exit from mitosis by destroying the anaphase inhibitor Pds1 and cyclin Clb5, Nature *402*, 203-207.

Smirnova, E. A., and Bajer, A. S. (1992). Spindle poles in higher plant meiosis., Cell Motil. Cytoskelet. *23*, 1-7.

Spradling, A. C., and Rubin, G. M. (1982). Transposition of cloned P elements into *Drosophila* germ line chromosomes., Science *218*, 341-347.

Starr, D. A., Willams, B. C., Hays, T. S., and Goldberg, M. (1998). ZW10 helps recruit dynactin and dynein to the kinetochore., J. Cell Biol. *142*, 763-774.

Steffensen, S., Coelho, P., Cobbe, N., Vass, S., Costa, M., Hassan, B., Propenko, S. N., Bellen, H., Heck, M. M. S., and Sunkel, C. E. (2000). A role for *Drosophila* SMC4 in the resolution of sister chromatids in mitosis., Submitted.

Steuer, E. R., Wordeman, L., Schroer, T. A., and Sheetz, M. P. (1990). Localization of cytoplasmic dynein to mitotic spindles and kinetochores., Nature *345*, 266-268.

Strick, R., and Laemmli, U. K. (1995). SAR's are cis DNA elements of chromosome dynamics: synthesis of a SAR repressor protein., Cell *83*, 1137-1148.

Strunnikov, A. V., Larionov, V. L., and Koshland, D. (1993). SMC1: an essential yeast gene encoding a putative head-rod-tail protein is required for nuclear division and defines a new ubiquitous protein family., J. Cell Biol. *123*, 1635-1648.

Taagepera, S., Rao, P. N., Drake, F. H., and Gorbsky, G. J. (1993). DNA topoisomerase IIa is the major chromosome protein recognized by the mitotic phosphoprotein antibody MPM-2., Proc. Nat. Acc. Sci. USA *90*, 8407-8411.

Tanaka, T., Cosma, M. P., Wirth, K., and Nasmyth, K. (1999). Identification of Cohesin Association Sites at Centromeres and along Chromosome Arms, Cell *98*, 847-858.

Theurkauf, W. E., and Hawley, R. S. (1992). Meiotic spindle assembly in *Drosophila* females: behaviour of nonexchange chromosomes and the effects of mutations in the nod kinesin-like protein., J. Cell Biol. *102*, 1679-1687.

Thrower, D. A., Jordan, M. A., Schaar, B. T., Yen, T. J., and Wilson, L. (1995). Mitotic HeLa cells contain a CENP-E-associated minus end-directed microtubule motor., EMBO *14*, 918-926.

Tomkiel, J. E., Cooke, C. A., Saitoh, H., Bernat, R. L., and Earnshaw, W. C. (1994). CENP-C is required for maintaining proper kinetochore size and for a timely transition into anaphase., J. Cell Biol. *125*, 531-545.

Uemura, T., Ohkura, H., Adachi, Y., Morino, K., and Shiozaki, K. (1987). DNA topoisomerase II is required for condensation and separation of mitotic chromosomes in S. pombe., Cell *50*, 917-925.

Uemura, T., and Yanagida, M. (1984). Isolation of type I and II DNA topoisomerase mutants from fission yeast: single and double mutants show different phenotypes in cell growth and chromatin organization., EMBO *3*, 1737-1744.

Uemura, T., and Yanagida, M. (1986). Mitotic spindle pulls but fails to separate chromosomes in type II DNA topoisomerase mutants: uncoordinated mitosis., EMBO *5*, 1003-1010.

Uria, J. A., and Lopez-Otin, C. (2000). Matrilysin-2, a new matrix metalloproteinase expressed in human tumors and showing the minimal domain organization required for secretion, latency, and activity., Cancer Res. *60*, 4745-4751.

Vafa, O., and Sullivan, K. F. (1997). Chromatin containing CENP-A and alpha-satellite DNA is a major component of the inner kinetochore plate., Curr.. Biol. *7*, 897-900.

Vaisberg, E. A., Koonce, M. P., and McIntosh, J. R. (1993). Cytoplasmic dynein plays a role in mammalian mitotic spindle formation., J. Cell Biol. *123*, 849-858.

Walker, J. E., Sarste, M., Runswick, M. J., and Gay, N. J. (1982). Distantly related sequences in the a- and b-subunits of ATP synthase, myosin, kinases and other ATP-requiring enzymes and a common nucleotide binding fold., EMBO *1*, 945-951.

Warburton, P. E., Cooke, C., Bourassa, S., Vafa, O., Sullivan, B. A., Stetten, G., Gimelli, G., Warburton, D., Tyler-Smith, C., Sullivan, K. F., *et al.* (1997). Immunolocalisation of CENP-A suggests a distinct nucleosome structure at the inner kinetochore plate of active centromeres., Curr.. Biol. *7*, 901-904.

Wei, Q., Marchler, G., Edington, K., Karsch-Mizrachi, I., and Paterson, B. M. (2000). RNA interference demonstrates a role for nautilus in the myogenic conversion of schneider cells by daughterless., Dev. Biol. *96*, 1451-1456.

Wei, Y., Yu, L., Bowen, J., Gorovsky, M. A., and Allis, C. D. (1999). Phosphorylation of Histone H3 is Required for Proper Chromosome Condensation and Segregation, Cell *97*, 99-109.

Whitfield, W. G. F., Chaplain, M. A., Oegema, K., Parry, H., and Glover, D. M. (1995). The 190 kDa centrosome-associated protein of Drosophila melanogaster contains four zinc finger motifs and binds to specific sites on polytene chromosomes, J. Cell Sci. *108*, 3377-3387.

Wood, K. W., Sakowicz, R., Goldstein, L. S. B., and Cleveland, D. W. (1997). CENP-E is a plus-end directed kinetochore motor required for metaphase chromosome alignment., Cell *91*, 357-366.

Wordeman, L., Earnshaw, W. C., and Bernat, R. L. (1996). Involvement of the CENP antigens in anchoring dynein to the mitotic kinetochore., Chromosoma *104*, 551-560.

Wordeman, L., and Mitchison, T. J. (1995). Identification and partial characterization of mitotic centromere-associated kinesin, a kinesin-related protein that associates with centromeres during mitosis., J. Cell Biol. *128*, 95-105.

Yao, X., Abrieu, A., Zheng, Y., Sullivan, K., and Cleveland, D. W. (2000). CENP-E forms a link between attachment of spindle microtubules to kinetochores and the mitotic checkpoint, Nature Cell Biol. *2*, 484-491.

Yang, D., Lu, H., and Erickson, J. W. (2000). Evidence that processed small dsRNAs may mediate sequence-specific mRNA degradation during RNAi in Drosophila embryos., Curr.. Biol. *10*, 1191-1200.

Yen, T. J., Compton, D. A., Earnshaw, W. C., and Cleveland, D. W. (1991). CENP-E, a human centromere associated protein released from chromosomes at the onset of anaphase., EMBO *10*, 1245-1254.

Zamore, P. D., Tuschl, T., Sharp, P. A., and Bartel, D. P. (2000). RNAi: double-stranded RNA directs the ATP-dependent cleavage of mRNA at 21 to 23 nucleotide intervals., Cell *101*, 25-33.

Zheng, Y., Wong, M. L., Alberts, B., and Mitchison, T. J. (1995). Nucleation of microtubule assembly by a gamma-tubulin-containing ring complex., Nature *378*, 578-583.